

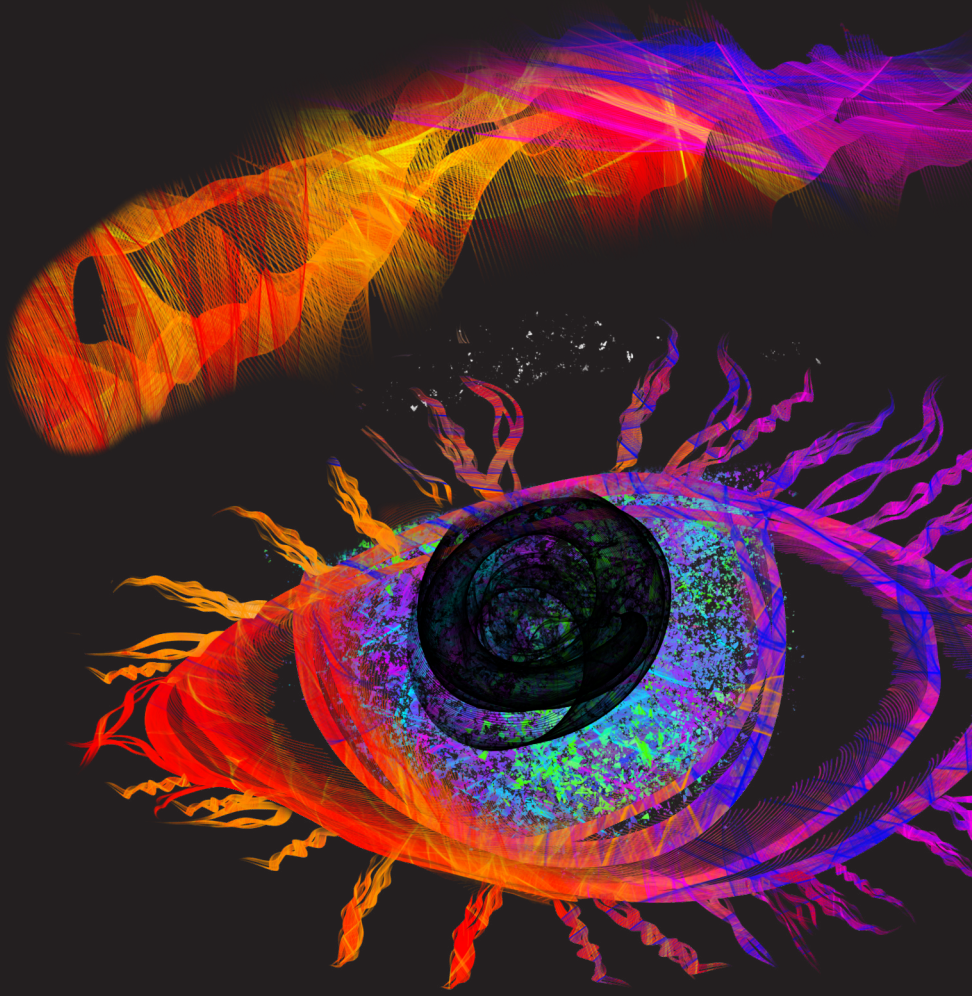
## PDF hosted at the Radboud Repository of the Radboud University Nijmegen

The following full text is a publisher's version.

For additional information about this publication click this link.

<http://hdl.handle.net/2066/201895>

Please be advised that this information was generated on 2019-06-02 and may be subject to change.



# INSIGHTS INTO EYS-ASSOCIATED RETINAL DYSTROPHIES

FROM DISEASE SPECTRUM TOWARDS GENETIC THERAPY

MURIËL MESSCHAERT



# **Insights into *EYS*-associated retinal dystrophies**

From disease spectrum towards genetic therapy

**Muriël Messchaert**

## **Colophon**

The work presented in this thesis was carried out within the Department of Human Genetics, Donders Institute for Brain, Cognition and Behaviour, Radboud university medical center, Nijmegen, The Netherlands.

The printing of this thesis was financially supported by the Radboud University Nijmegen.

© **Muriël Messchaert, 2019**

Printed by: Proefschriftmaken.nl

Designed by: SVDH Media | [www.svdhmedia.nl](http://www.svdhmedia.nl)

ISBN: 978-94-6380-257-4

# **Insights into *EYS*-associated retinal dystrophies**

From disease spectrum towards genetic therapy

## **Proefschrift**

ter verkrijging van de graad van doctor  
aan de Radboud Universiteit Nijmegen  
op gezag van de rector magnificus prof. dr. J.H.J.M. van Krieken,  
volgens besluit van het college van decanen  
in het openbaar te verdedigen op donderdag 11 april 2019  
om 12.30 uur precies

door

## **Muriël Messchaert**

geboren op 15 juni 1989  
te Delden

**Promotoren**

Dr. Rob W.J. Collin

Prof. dr. Frans P.M. Cremers

**Manuscriptcommissie**

Prof. dr. J.G.J. Hoenderop

Prof. dr. D. Sharon (Hadassah Medical Center, Jerusalem, Israël)

Dr. A.M.G. Pasmooij (Universitair Medisch Centrum Groningen)

**Paranimfen**

Lonneke Duijkers

Michael Kwint

## Table of contents

<b>List of abbreviations</b>		6
<b>Chapter 1</b>	General introduction	9
<b>Chapter 2</b>	<i>EYS</i> mutation update: <i>In silico</i> assessment of 271 reported and 26 novel variants in patients with retinitis pigmentosa	35
<b>Chapter 3</b>	Extending the spectrum of <i>EYS</i> -associated retinal disease to macular dystrophy	63
<b>Chapter 4</b>	Eyes shut homolog is important for the maintenance of photoreceptor morphology and visual function in zebrafish	91
<b>Chapter 5</b>	Development of <i>EYS</i> microgenes as a potential therapy for <i>EYS</i> -associated retinal dystrophies	125
<b>Chapter 6</b>	Human derived photoreceptor-like cells as a model to identify and correct the mechanism underlying <i>EYS</i> -associated retinal dystrophies	145
<b>Chapter 7</b>	General discussion	171
<b>Summary</b>		189
<b>Samenvatting</b>		193
<b>Curriculum Vitae</b>		197
<b>Dankwoord</b>		201
<b>Donders Graduate School for Cognitive Neuroscience</b>		204
<b>Data management</b>		205

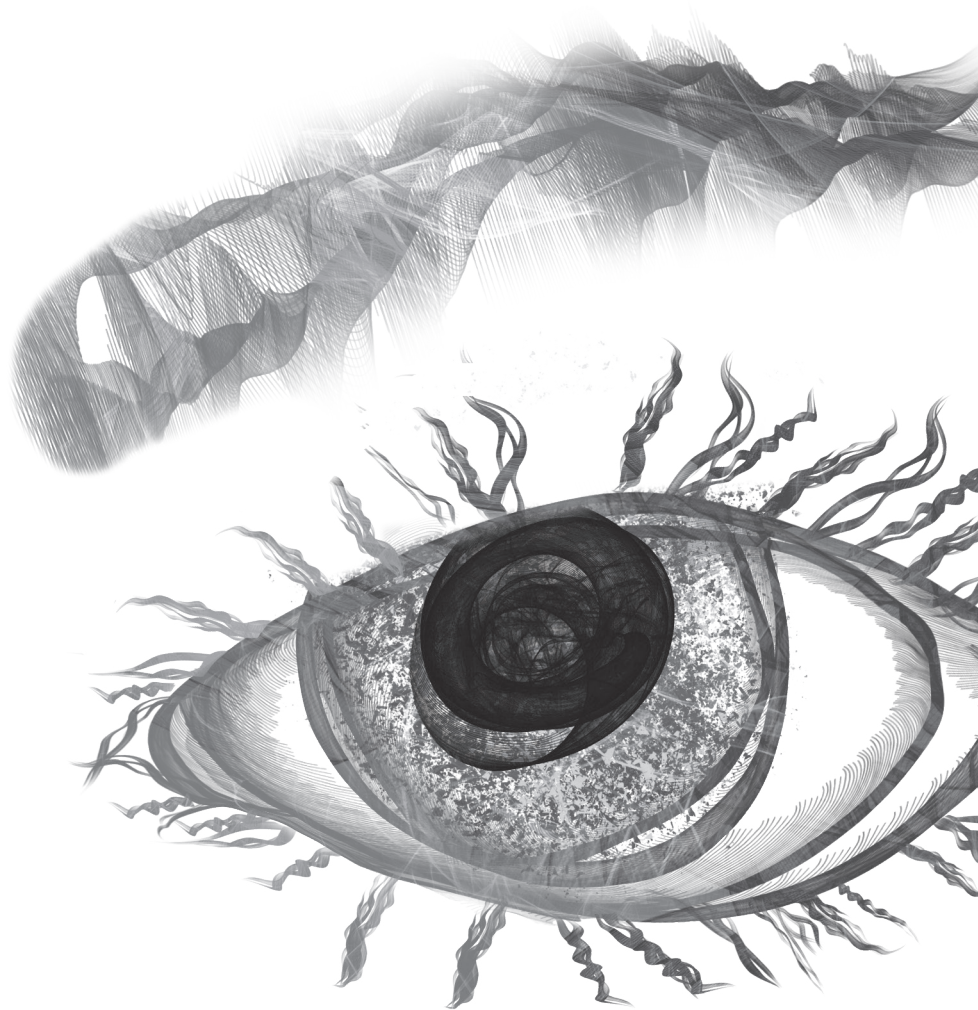


## List of abbreviations

*	stop codon
2D	two-dimensional
3D	three-dimensional
aa	amino acid
AAV	adeno-associated virus
ACMG	American College of Medical Genetics and Genomics
ad	autosomal dominant
AON	antisense oligonucleotide
ar	autosomal recessive
arRP	autosomal recessive retinitis pigmentosa
BB	basal body
BCVA	best-corrected visual acuity
BODIPY	boron-dipyrromethene
bp	base pair
CADD	combined annotation dependent depletion
Cas9	CRISPR associated protein 9
CC	connecting cilium
CD	cone dystrophy
cDNA	complementary deoxyribonucleic acid
cGMP	cyclic guanosine monophosphate
CRD	cone-rod dystrophy
CRISPR	clustered regularly interspaced short palindromic repeats
CRX	cone-rod homeobox
del	deletion
DMD	Duchenne muscular dystrophy
DNA	deoxyribonucleic acid
dpf	days post fertilization
EGF	epidermal growth factor
ERG	electroretinography
ESC	embryonic stem cell
EYS	eyes shut homolog
ExAC	exome aggregation consortium
FAF	fundus autofluorescence
FDA	US Food and Drug Administration
ffERG	full-field electroretinography
GMP	guanosine monophosphate
gRNA	guide RNA
HDR	homology-directed repair
IHC	immunohistochemistry

INL	inner nuclear layer
ins	insertion
iPSC	induced pluripotent stem cell
IS	inner segment
IRD	inherited retinal disease
kb	kilobase
kDa	kilodalton
LamG	laminin A G-like
LCA	Leber congenital amaurosis
LOVD	Leiden Open source Variant Database
mFERG	multifocal electroretinography
MIP	molecular inversion probe
mpf	months post fertilization
mRNA	messenger ribonucleic acid
NHEJ	non-homologous end joining
NR	neuroretina
ONL	outer nuclear layer
OS	outer segment
PCR	polymerase chain reaction
PR	photoreceptor
RNA	ribonucleic acid
RP	retinitis pigmentosa
RPE	retinal pigment epithelium
SD-OCT	spectral domain optical coherence tomography
SEM	standard error of the mean
spam	spacemaker
TALEN	transcription activator-like effector nuclease
VF	visual field
Vmax	maximum velocity
VMR	visual motor response
ZFN	zinc finger nuclease

# Chapter 1



# **General introduction**

## 1.1 The eye

The eye is a sensory organ that is responsible for capturing and processing visual information. The eye can be divided into an anterior part and a posterior part. The anterior part of the eye consists of the cornea, anterior chamber, conjunctiva, pupil, ciliary body and lens. The posterior part of the eye is formed by the vitreous body, choroid, retina and optic nerve. Light enters the eye via the pupil and goes through the cornea and the lens to the back of the eye where it reaches the retina. Here, light is converted into an electrical signal that leaves the eye via the optic nerve to visual centers in the brain (Figure 1.1).

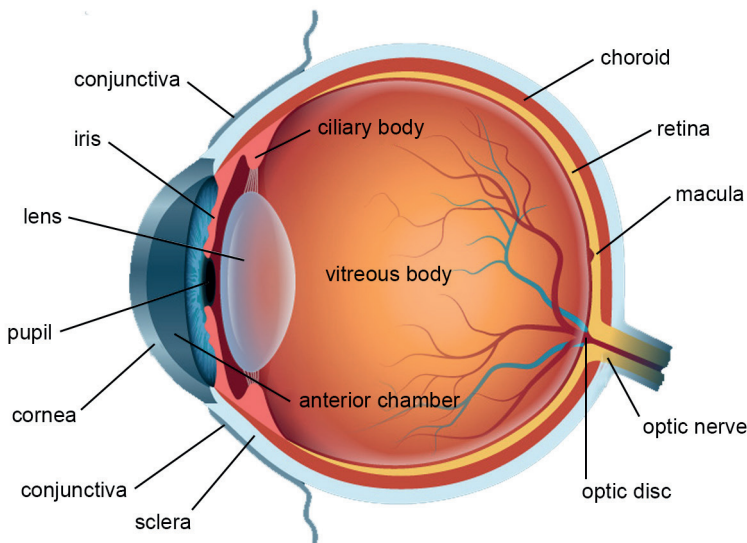


**Figure 1.1. Anatomy of the eye.**

The anterior segment of the eye contains the cornea, conjunctiva, pupil, ciliary body and lens. The posterior segment consists of the vitreous body, retina, choroid and optic nerve.

## 1.2 Anatomy of the retina

The retina, that lines the inner surface of the eye, is a layered structure with highly specialized cells that together are responsible for converting light into an electrical signal. Basically, the retina consists of an outer pigmented layer and an inner layer, which is called the neural retina. The retina is composed of ten primary layers that are formed by multiple different cell types (Figure 1.2).

The most posterior layer of the retina is formed by a monolayer of pigmented cells, called the **retinal pigment epithelium (RPE)**. The RPE separates the neural retina from the choroid, and is involved in the transport of nourishing components from the choroid to the neural retina. Furthermore, the RPE supports the adjacent photoreceptor cells, such that they can function properly. Most importantly, RPE cells play an important role in

phagocytosis of the photoreceptor outer segment disks.<sup>1,2</sup> The **photoreceptor cell layer** is the outer most layer of the neural retina and consists of the outer segments of rod and cone photoreceptor cells. The third layer is the **external limiting membrane**, also called outer limiting membrane, which is made of adherens junction and tight junction proteins, and serves to support the maintenance of the retinal structure through mechanical strength.<sup>3,4</sup> The cell bodies of the photoreceptor cells are forming the **outer nuclear layer**. Cone pedicles or rod spherules form synapses with the dendrites of bipolar cells and processes of horizontal cells in the **outer plexiform layer**. The synaptic interactions that take place in the outer plexiform layer play a role in increasing contrast and thereby enhancing the ability to detect objects.<sup>5</sup> The sixth layer contains cell bodies of the amacrine, bipolar and horizontal cells, and is called the **inner nuclear layer**. Bipolar cells receive synaptic input from the photoreceptor cells and transmit this to the ganglion cells. Two types of bipolar cells can be distinguished: on-center bipolar cells and off-center bipolar cells. Photoreceptors are depolarized in the dark and release glutamate, which activates off-center bipolar cells. Light triggers the release of glutamate by the photoreceptor cells, thereby activating on-center bipolar cells.<sup>6</sup> Horizontal cells are laterally oriented neurons, which integrate and regulate the information from photoreceptor cells. In the **inner plexiform layer**, axons of the bipolar cells connect with the dendrites of ganglion cells. Amacrine cells form the connection between bipolar cells and ganglion cells. The **ganglion cell layer** is the eighth layer of the retina and contains cell bodies of ganglion cells and some displaced amacrine cells. The axons of the ganglion cells form the next layer: the **nerve fibre layer**. The axons of the ganglion cells are collected in a bundle of fibres by the optic nerve. Ganglion cells collect information from amacrine cells and bipolar cells and transfer this to the optic nerve, via which the electrical signal is sent to the brain. Finally, the tenth layer, closest to the vitreous body and called the **inner limiting membrane**, is composed of astrocytes and terminations of the Müller cells. Astrocytes originate from the brain and enter the retina along the developing optic nerve. They are important for the maintenance of the blood-retina barrier, form nutritive service to the neurons, and play a role in ionic homeostasis.<sup>7,8</sup> The major role of Müller cells is to give structural and functional support to other retinal cells. They regulate uptake of neurotransmitters, are involved in phagocytosis of neural debris, control homeostasis by taking up extracellular  $K^+$ , and play a role in the storage and breakdown of glycogen.<sup>9,10</sup> In addition, Müller cells play a role in the recycling of chromophore in the alternative retinal cycle that involves cones.<sup>11</sup>

### 1.3 Photoreceptor cells

There are two types of light-sensitive photoreceptors, namely **rods** and **cones**. Humans have approximately 130 million photoreceptor cells, with twenty times more rods than cones.<sup>12</sup> Rods are mainly located in the mid-periphery of the retina and are stimulated by dim light, whereas cones are stimulated by bright light. Therefore, rods are responsible

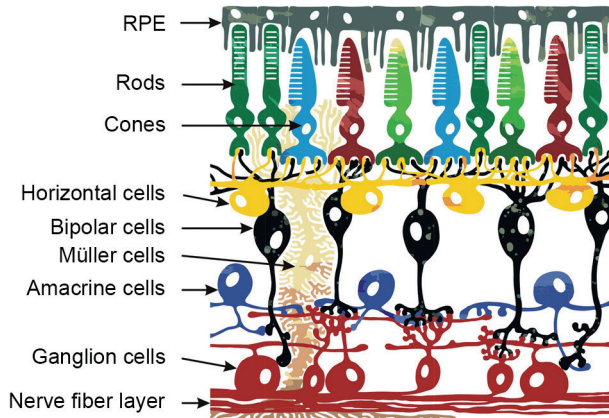


**Figure 1.2. Anatomy of the retina.**

The retina is a multi-layered structure composed of different cell types: retinal pigment epithelium (RPE), photoreceptor cells (rods and cones), horizontal cells, bipolar cells, Müller cells, amacrine cells and ganglion cells. All together, these cells are responsible for converting light into an electrical signal that goes to the brain. This picture was kindly provided by Rozan Vrooman.

for peripheral vision and vision under dim light conditions, whereas cones are mainly responsible for central vision, colour vision and allow high visual acuity.<sup>12,13</sup> In the human retina, three cone subtypes can be distinguished: S-, M- and L-cones or blue, green and red cones respectively. The S-cones are dispersed through the entire retina, whereas the M- and L-cones cluster in the fovea. The S-cones are sensitive to supra-frequency photons ( $\lambda_{\max} \sim 415\text{--}430$  nm), the M-cones to middle-frequency photons ( $\lambda_{\max} \sim 530\text{--}537$  nm), and the L-cones to low-frequency photons ( $\lambda_{\max} \sim 555\text{--}565$  nm).<sup>14</sup> The center of the human retina contains an area enriched with cone photoreceptors, called the fovea, which has the highest visual acuity of the retina.<sup>15,16</sup> Both rods and cones have an outer and inner segment, a cell body that contains the nucleus, and a synaptic end (Figure 1.3).<sup>17</sup> The outer segment of the photoreceptor is in direct contact with RPE cells, while the synapses of the photoreceptors are connected to bipolar cells, horizontal cells and amacrine cells. The inner segment is the place where protein synthesis occurs and the outer segment is responsible for the actual phototransduction, i.e. capturing photons and producing electrical responses. The inner segment is linked to the outer segment by the connecting cilium (CC), a microtubule-based structure that is important for transport of proteins from the inner segment to the outer segment. The outer segment consists of disks that are formed by invaginations of the plasma membrane.<sup>13</sup> Outer segments therefore have a high density of membranes that contain visual pigments responsible for capturing light. The outer segment disks are constantly renewed. Around 10% of the photoreceptor disks are shed and phagocytized by the RPE every day. Simultaneously, new membrane disks

are formed and replaced at the base of the outer segment, maintaining photoreceptor function and homeostasis.<sup>18,19</sup>

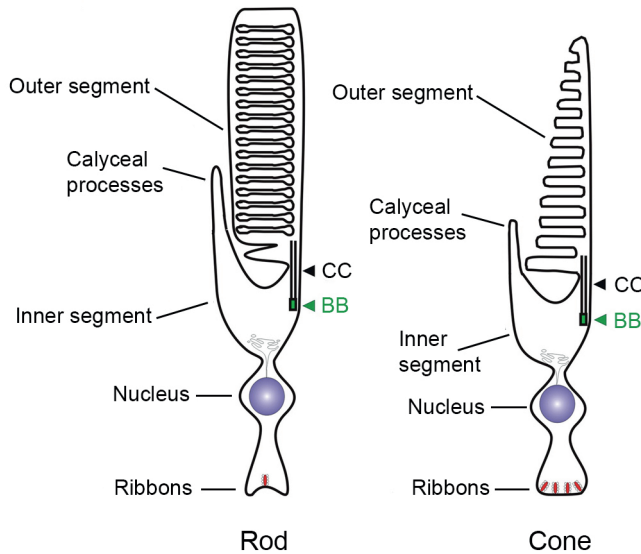


**Figure 1.3. Schematic representation of the photoreceptor cells.**

Both rod (left panel) and cone (right panel) photoreceptor cells are composed of an outer segment, a cell body that contains the nucleus, and an inner segment. The inner segment is connected with the outer segment by the connecting cilium (CC). BB: basal body of the connecting cilium. Adapted from Slijkerman et al.<sup>20</sup>

### 1.3.1 The phototransduction cascade

Phototransduction takes place in the outer segment of the photoreceptor cells. In rods, the phototransduction cascade is initiated by rhodopsin. Basically, the absorption of light by rhodopsin activates a G-protein cascade that results in an electrical signal at the plasma membrane of the rod photoreceptor.<sup>21</sup> Rhodopsin consists of two components, a light-sensitive G-protein coupled receptor called opsin and a chromophore, 11-*cis*-retinal.<sup>22</sup> When a photon is absorbed by the photoreceptor cell, the chromophore isomerizes from 11-*cis*-retinal to all-*trans*-retinal, which in turn changes rhodopsin to its active state.<sup>23</sup> Activated rhodopsin catalyses the exchange of GDP for GTP, thereby activating the G-protein transducin.<sup>12</sup> The  $\alpha$ -subunit of transducin dissociates and then activates cGMP-phosphodiesterase, which in turn hydrolyses cGMP in the cytoplasm. In response to decreased cGMP concentrations, cGMP-gated ion channels in the plasma membrane will close. This leads to hyperpolarisation of the cells and a decrease in the release of the neurotransmitter glutamate to the synapse with the bipolar cells.<sup>23</sup> Glutamate activated



bipolar cells transfer the signal to the ganglion cells, which in turn transfer the signal in the form of action potentials via the optic nerve to visual centers in the brain.

## 1.4 Inherited retinal diseases

Inherited retinal diseases (IRDs) are a group of blinding disorders generally characterized by a progressive degeneration of retinal cells. They affect approximately 1 in 2,000 individuals worldwide.<sup>24</sup> IRDs are genetically heterogeneous and have been associated with mutations in more than 250 genes (RetNet <http://www.sph.uth.tmc.edu/Retnet>). The large majority of IRDs are monogenic disorders, and are caused by mutations in genes that are expressed in photoreceptor cells or RPE cells. IRDs can follow all modes of Mendelian inheritance, i.e. autosomal dominant (ad), autosomal recessive (ar) and X-linked, and can be divided into different subtypes with varying clinical hallmarks, degree of progression, and age of onset. A few examples of digenic inheritance have been reported.<sup>25,26</sup> The distinction between different forms of IRDs can be very subtle, due to overlap in clinical symptoms and genetic causes. Retinal diseases can either present as a clinical phenotype restricted to the eye (non-syndromic IRD), or manifest together with other disorders located elsewhere in the body (syndromic IRD). Usher syndrome, Joubert syndrome and Bardet-Biedl syndrome are examples of syndromic types of IRD. Non-syndromic IRDs can be further divided in subgroups based on the disease progression and region of the retina that is affected. Progressive conditions affecting exclusively the central retina (macula), leading to central vision loss, are known as macular dystrophies, of which Stargardt disease is the most common form. Progressive conditions that affect the retina more widely can be classified based on the type of photoreceptor that initially degenerates. In cone dystrophy (CD) or cone-rod dystrophy (CRD), the cones are first affected, leading to a decrease of visual acuity and blind/blurry spots in the center of the visual field. In contrast, in rod-cone dystrophies, the rods are first affected, which initially leads to night blindness and subsequently peripheral vision loss. The most common example is retinitis pigmentosa (RP). The clinical hallmarks of RP will be described in more detail in the next section. The most severe form of IRD is Leber congenital amaurosis (LCA), affecting both photoreceptor cell types and/or the RPE and Müller cells, with a very early age of onset (1 year) and leading to complete blindness.<sup>27</sup>

### 1.4.1 Retinitis pigmentosa

Retinitis pigmentosa is a retinal disorder characterized by progressive degeneration of photoreceptor cells. The prevalence of RP is approximately 1 in 4,000 individuals worldwide and, like other IRDs, the disease can be inherited in an autosomal dominant, autosomal recessive, or X-linked manner.<sup>28,29</sup> In most RP cases, there is initial degeneration of rods followed by degeneration of cones.<sup>30</sup> Retinitis pigmentosa mainly affects rods, however, in advanced stages of RP cones are also affected due to the co-dependence of rods and cones. In addition, rods secrete an inactive thioredoxin, rod-derived cone viability factor

(RdCVF), that protects cones from degeneration.<sup>31,32</sup> There is a high variability in the clinical manifestation of RP; some patients suffer from vision loss in childhood whereas others do not have symptoms until (late) adulthood. The majority of the patients show a classic pattern of symptoms, namely night blindness in adolescence followed by loss of mid-peripheral vision in young adulthood. When the disease progresses, patients develop tunnel vision and finally lose central vision around the age of 60 years. In early stages of disease, a clinical diagnosis is difficult to establish, especially when there is no family history of RP. In later stages of RP, a clinical diagnosis is possible by fundus examination that shows the presence of pigmented deposits, narrowing of the arterioles, and a waxy pallor of the optic disc.<sup>28</sup> Visual field constriction or tunnel vision can be shown using visual field measurements. This test is often used to classify the severity of the disease, and to monitor progression, since it can quantitatively show photoreceptor degeneration as well as the degree of functional impairment. Other detailed ophthalmic examinations include fundus autofluorescence, full-field (ff) or multi-focal (mf) electroretinography (ERG), and spectral-domain or swept-source optical coherence tomography.<sup>33</sup>

### 1.5 Eyes shut homolog

Retinitis pigmentosa is both genetically and clinically heterogeneous, with 62 causal genes identified for autosomal recessive RP (arRP) to date (RetNet, <https://www.sph.uth.tmc.edu/RetNet/>). Mutations in **Eyes shut homolog (EYS)** account for approximately 5-10% of all arRP cases in the European population and are the leading cause of arRP in the Japanese population.<sup>34,35</sup> The *EYS* gene consists of 44 exons, whereby exon 42 is alternatively spliced and does not reside in most of the *EYS* transcripts. Depending on its splicing, *EYS* encodes for a 3,165 or 3,144 amino acids long EYS protein which is predominantly expressed in the retina.<sup>36,37</sup> Eyes shut homolog consists of 28 epidermal growth factor (EGF)-like domains and five laminin A G-like (LamG) domains (Figure 1.4), which are conserved among different species. An EGF domain is defined by the presence of six cysteine residues that are able to form disulfide bonds, and form two beta-sheets connected to each other by a loop. It has been described that EGF domains are important for intracellular signaling and cell adhesion.<sup>38</sup> The LamG domain is found in many different proteins and is, as seen for *EYS*, often located at the C-terminus. Proteins harboring LamG domains can have a wide variety of functions, such as cell adhesion, migration and signalling.<sup>39</sup>

The *Drosophila* ortholog of *EYS*, also known as spam or spacemaker, is located in the inter-rhabdomere space of the compound eye of the fly. Here, it is shown to play a major role in proper formation of the inter-rhabdomere lumen, since in *eyes* mutant flies, the inter-rhabdomere space was completely absent.<sup>40</sup> In zebrafish, it was recently shown that *eyes* localizes near the photoreceptor connecting cilium.<sup>41</sup> Furthermore, *eyes* knock-out zebrafish models show degeneration of the retinal architecture and visual impairment.<sup>41,42</sup>

Since *EYS* is specifically expressed in the retina, and supported by the fact that *Eys* is absent from several rodent species,<sup>36</sup> still very little is known about the exact function of *EYS* and the pathogenic mechanism underlying *EYS*-associated RP.

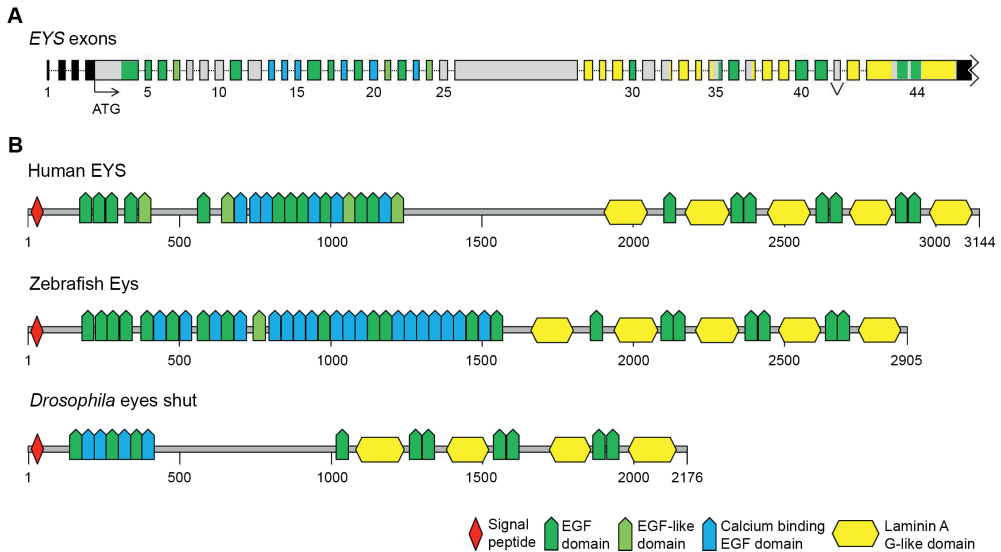


**Figure 1.4. Exonic structure and protein domain structure of eyes shut homolog (*EYS*).**

(A) *Eyes shut homolog* consists of 44 exons of which exon 42 is alternatively spliced. (B) Protein domain structure of *EYS* and its orthologs in *Drosophila* and zebrafish. Note the conservation of the order of EGF-like and laminin A G-like domains between the different species.

## 1.6 Models for IRDs

### 1.6.1 Animal models for IRDs

The role of animal models in the IRD field has not only been shown to be important for understanding the pathogenic mechanisms underlying the disease, but also in the development of novel therapies.

The **zebrafish** retina is morphologically similar compared to the human retina, meaning that all major cell and tissue layers that can be found in humans are also found in zebrafish. The zebrafish retina contains four cone subtypes which by far outnumber the rod photoreceptors.<sup>20</sup> Their cones are sensitive to the same three color wavelengths as cones in humans and, in addition, a fourth UV-sensitive cone is present. Other advantages of the zebrafish as a model are: they produce a large number of offspring, have relatively short generation time, and are easy genetically modified. However, a drawback of the zebrafish is its capacity to regenerate the retina after damage.<sup>43</sup>

Rodents are nocturnal animals and therefore their retina is specialized for night activity. The retina of **mouse and rat** contains sensitive rods and cones that are not evenly distributed over the retina and it does not contain a cone-rich area.<sup>20</sup> In general, rodents are a good model to study IRDs, because of their genetic similarity to human and there are some naturally occurring retinal degeneration models described. However, *Eys* is not present in mouse and rat,<sup>36</sup> which excludes it for the use as a research model for this particular gene. Since the **pig** is a diurnal animal, its retina is cone-rich with the highest density of cones in the central retina. This makes the pig a good model to study retinal dystrophies in which cones are affected. Disadvantages of using pig as a research model are the poorly annotated genome and the large space needed for housing. To overcome the latter, mini-pigs are widely used.

The **dog** retina is rod-dominated in most parts of the retina, but it does contain an area in the center of the retina that is cone-rich. Like for mice, many naturally occurring dog models have been identified and used for research. For example, in dogs with an *RPE65* mutation, gene therapy successfully restored vision.<sup>44</sup> Drawbacks of using dog as a model for IRDs are housing, long regeneration time, and ethical aspects.

### 1.6.2 Cellular models for IRDs

Vertebrate animal models all have their limitations in their use as a model for IRDs, such as their evolutionary distance from humans, differences in retinal morphology compared to humans, and, for large animal models, slow reproduction rate and high costs for housing. In addition, there are ethical issues surrounding the use of animal models for IRDs. Therefore, the search for alternatives is increasing. Over the last few years, technological development resulted in the ability to differentiate human derived **induced pluripotent stem cells (iPSCs)**<sup>45</sup> into retinal cells,<sup>46</sup> which makes it possible to study retinal degeneration *in vitro*. Since these cells contain the exact same genetic code as in the human subjects, specific consequences of mutations can be studied in these cells. Using gene editing techniques, the effect of correcting genetic defects can be studied in these cells as well. Developing disease models via differentiation of human-derived iPSCs involves several key elements: selection of the somatic cell type, a reprogramming strategy and choice of the differentiation protocol.

While selecting the somatic cell type for iPSC generation, it is important to take into account that these cells have epigenetic memory. This might influence the differentiation of iPSCs towards a lineage different than its origin.<sup>47</sup> Most reported cellular RP models use dermal fibroblasts as somatic cell type source. In addition, some studies showed that RPE and photoreceptors can also be generated from keratinocytes<sup>48</sup> or T-lymphocytes.<sup>49</sup> Blood cells are a convenient source for the generation of iPSCs, since it is less invasive to get them and the source is almost unlimited.<sup>50</sup> Another advantage of blood-derived human iPSCs is that they are identical to human embryonic stem cells with respect to morphology, DNA methylation, expression of surface antigens and transcription factors

associated with pluripotency, and their differentiation capacity.<sup>51</sup> Another somatic cell source is urine, which can be collected noninvasively and at multiple timepoints without any risks.<sup>52</sup> Besides the above mentioned somatic cell sources, adipose tissue, periodontal ligament, pancreatic islet beta cells, and mesenchymal stromal cells (wisdom teeth) are also reported suitable for reprogramming cells into iPSCs.<sup>53-56</sup>

For studying RP, there are models using a single cell type approach and models that are more mimicking the complete multi-layered retinal structure. In the single cell type approach, photoreceptors or RPE cells are generated from iPSCs in **two-dimensional (2D)** cultures. For this, specific signaling molecules are added to the culture medium and often this is combined with the use of matrices on which the cells are cultured.<sup>57-59</sup> It is easier to obtain RPE cells from iPSCs compared to photoreceptors. This can partly be explained by the tendency of iPSCs to differentiate towards ectoderm upon fibroblast growth factor withdrawal.<sup>60</sup>

The group of Takahashi was the first that successfully differentiated iPSCs derived from RP patients with mutations in *RP1*, *RP9*, *PRPH2* or *RHO* towards photoreceptor-like cells.<sup>57,61</sup> These cells expressed photoreceptor-specific markers, such as recoverin and rhodopsin. In addition, they showed a decrease in rod viability and increase in endoplasmic reticulum stress markers, similar to what is observed in RP patients.

A big advantage of the 2D cultures is that molecular events can be studied in a homogeneous cell population, as in case of RPE cells, which can be manually selected, excised and enriched. In case of other retinal cell types, the drawback is that the generated, not well-organized, cell layers often contain a mixture of different cell types.<sup>48,62</sup>

In addition to the generation of 2D culture models, different groups have shown that it is also possible to differentiate iPSCs into **three-dimensional (3D)** retinal structures. Nakano et al. were the first who described that pluripotent cells have the self-organizing capacity to form organoids.<sup>63</sup> Several other groups adapted this approach and, with small changes in the differentiation strategy, in some cases even photoreceptor outer segments could be generated.<sup>64-66</sup> It is amazing that spheres of iPSCs can differentiate into perfectly organized 3D retinal organoids containing layered retinal cells: photoreceptors, ganglion cells, Müller cells, horizontal cells, amacrine cells and bipolar cells. These organoids or optic cups can serve as a powerful tool to study retinal development and disease mechanisms. Furthermore, it might also be a potential therapeutic tool for cell and organ replacement. An example of a step towards clinical application is the study by Wiley et al.<sup>67</sup> They generated iPSCs from a large RP cohort according to Good Manufacturing Practice (GMP) by establishing common criteria for cellular identity and sterility. All iPSC lines were able to differentiate into 3D organoids and did not induce tumor formation after injection into mice. Phillips et al. modeled *VXS2*-associated microphthalmia, by comparing optic cups from a patient and a healthy person.<sup>68</sup> Patient-derived cells showed a delay in photoreceptor maturation, which was rescued by expression of exogenous *VSX2* early in the differentiation process. Human derived optic cups were also used to study gene

expression levels of *REEP6* and identified the presence of a retina-specific isoform. Disruption of this specific isoform in rod photoreceptors can cause retinal disease.<sup>69</sup> Parfitt et al. generated optic cups from iPSCs derived from an LCA patient with an intronic mutation in *CEP290*, that encodes a protein expressed in the connecting cilium. They showed that a pseudoexon was more prominently present in the mRNA of optic cups compared to fibroblasts. Expression of the full length *CEP290* was restored by blocking aberrant splicing, which in turn restored cilia function.<sup>70</sup>

These examples show that the use of optic cups is a good tool to mimic retinal development and disease. However, the generation of these 3D retinal organoids remains very challenging. The production process takes at least several months and it is highly dependent on manual manipulation and subjective selective criteria at initial stages. In addition, there can be high variability among different iPSC lines.<sup>71</sup>

### 1.6.3 Genetic modifications of IRD models

Homologous recombination is a mechanism naturally used by cells to repair double-stranded breaks in the DNA. However, it can also be used to introduce DNA into the genome of a host cell, for instance embryonic stem cells. For this, two flanking homologous arms are used to facilitate a targeted way of integration. With this method, DNA up to several kilobases (kb) can be introduced or exchanged.<sup>72</sup> Homologous recombination can also be used to generate knock-out or knock-in animals. Since the homology arms are sequence specific, the ability of targeting some loci is very low.

One of the first approaches of targeted gene modifications made use of zinc fingers, peptides that can recognize and bind 3 base pair DNA motifs. These zinc fingers can be fused with the endonuclease enzyme *FokI*, creating a zinc finger nuclease (ZFN) complex which can mediate targeted DNA cleavage. The cleaved DNA ends will be repaired by the cellular non-homologous end-joining (NHEJ) pathway, whereby sometimes mutations such as insertions and/or deletions are introduced.<sup>73</sup> Critical for the use of ZFNs is the nucleotide specificity, since off-target effects can interfere with the phenotype of interest. Furthermore, targeting options with this technique are limited to its DNA restriction motifs. To increase the restriction possibilities, a transcription activator-like (TAL) effector DNA-binding domain can be fused to a general cleavage domain. Hereby, a wide range of possible restriction motifs is estimated to be present once in every 35 base pairs of DNA.<sup>73</sup> When a TAL effector is combined with a nuclease, resulting in so-called transcription activator-like effector nucleases (TALEN), DNA can be cut at specific locations. It has been shown that TALEN are suitable for gene editing in zebrafish, mouse, rat or human derived embryonic stem cells and induced pluripotent stem cells.<sup>74-77</sup>

It has been recently discovered that prokaryotic immune components known as clustered regularly interspaced short palindromic repeats (CRISPR) and CRISPR-associated nucleases such as Cas9 are also able to mediate genome editing in mammalian cells.<sup>78-80</sup> The Cas9 nuclease cleaves double-stranded DNA at a specific target in the genome using guide

RNAs (gRNA). These double-strand breaks are repaired by either the NHEJ pathway or by the homology-directed repair (HDR) pathway. In case no template is present, insertions and/or deletions will be introduced when using NHEJ. The HDR pathway allows precise genome editing using a donor DNA template for repair. The CRISPR/Cas9 system has been adapted for efficient use in cells as well as a wide variety of organisms, including zebrafish, mouse, rat, pig, sheep and human.<sup>81-83</sup> The most important advantages of the use of CRISPR/Cas9 over other genome editing strategies are its efficiency and simplicity. The system can be easily adjusted by changing the gRNA sequence to any DNA sequence of interest, which makes that target options are enormous.

## 1.7 Therapeutic strategies for IRDs

Currently, there is no therapy available for RP patients that has been proven to prevent the development or progression of the disease or can restore visual function. Drugs currently used in the treatment of RP are focused on slowing down the progression of the disease or target secondary complications. Research for new therapies, such as gene therapy, cell therapy and prosthesis, are ongoing.<sup>17,84</sup>

### 1.7.1 Gene therapy

The retina is an accessible and immune-privileged structure, which makes it a suitable target for **gene therapy**.<sup>17</sup> Here, we will discuss gene replacement or augmentation therapy, meaning the replacement of a mutated gene that causes disease with a healthy copy of the gene or cDNA (Figure 1.5A). Due to the genetic heterogeneity of IRDs, including RP, it is not possible to design a common gene therapy for all genetic subtypes. Therefore, different therapeutic strategies are required depending on the causal gene, type of mutation and pattern of inheritance. For instance, recessive and X-linked mutations are more susceptible for gene augmentation therapy, because it leads to absence of the protein or to production of a null protein. In these cases, gene replacement or augmentation therapy could overcome the disease symptoms.

Currently, the two main approaches for delivery of therapeutic transgenes to the target cell type in the retina are viral or non-viral.<sup>85</sup> Viral vectors are mostly used in studies on gene therapy for RP, such as adeno-associated virus (AAV), adenovirus and lentivirus. The standard way of delivering viral vectors to the retina is via subretinal injection. The advantage of adenovirus and lentivirus is that they have large packaging capacity, up to 37 kb and 8 kb, respectively.<sup>86</sup> However, they are not very efficient in targeting retinal cells, partly due to their large size. The most commonly used viral vectors for pre-clinical and clinical studies are AAVs, since they are easy to manipulate and safe. There are different AAV subtypes, of which AAV2/5, AAV2/7, AAV2/8 and AAV2/9 have been shown to efficiently target both photoreceptors and RPE cells.<sup>87-90</sup> A huge drawback of the use of AAVs is their low packaging load of maximum 4.7 kb.<sup>86</sup> Liposomes, polymers, polypeptides and nanoparticles are examples of non-viral vectors. They have some advantages over viral

vectors, such as high packaging load, low immunogenicity and large scale production.<sup>91</sup> Of course the use of non-viral vectors also has drawbacks, such as lack of long-term gene expression, degradation and inefficient transport into the cell.<sup>84,86</sup>

Successful clinical trials for inherited retinal dystrophy have first been reported for *RPE65*-related LCA. Mutations in *RPE65* account for approximately 6% of all the LCA cases.<sup>27</sup> From 2008, results have been reported for three phase 1 clinical trials of AAV-mediated *RPE65* gene therapy for LCA (ClinicalTrials.gov identifiers: NCT00643747, NCT00481546, NCT00516477). In 2017, the results of a phase 3 clinical trial using LUXTURNA™ (voretigene neparvovec, AAV2-hRPE65v2) for the treatment of patients with vision loss due to bi-allelic *RPE65*-associated IRD were published by Spark Therapeutics Inc. (NCT00999609). The read-out was the 1-year improvement of multi-luminance mobility testing (MLMT) scores, which measures functional vision at specific light levels. The MLMT change score was significantly higher in the treated group versus the control group. No adverse events or immune responses were reported. LUXTURNA™ was recently approved by the US Food and Drug Administration (FDA), for the treatment of visual impairment due to *RPE65* mutations.

### 1.7.2 Gene therapy for RP

To date, several studies reported the successful use of gene therapy in animal models, resulting in delayed progress of RP or restored vision. For instance, the delivery of AAV vectors to replace mutated *CNGB1* or *MERTK* in animal models of arRP showed the restoration of protein expression and ERG activities, respectively.<sup>92,93</sup> Two other studies reported restored and preserved photoreceptors in murine and canine models of X-linked RP after gene therapy using an AAV loaded with the *RPGR* gene.<sup>94,95</sup> The promising results of these preclinical studies establish a scientific basis for application in human subjects. Currently, phase 1/2 clinical trials to treat *RLBP1*-, *PDE6B*-, *RPGR*-, or *MERTK*-associated RP with gene therapy are ongoing (ClinicalTrials.gov identifiers: NCT03374657, NCT03328130, NCT03116113, NCT03316560, NCT03252847, NCT01482195). These studies all involve subretinal injection of an AAV-vector containing a copy of the wild-type gene of interest.

### 1.7.3 Microgene therapy

As described above, the most commonly used way of delivering therapeutic transgenes is via AAV vectors. As mentioned before, one of the most important drawbacks of AAV is the limiting cargo capacity of approximately 4.7 kb. For large genes, for which the cDNA size exceeds 4.7 kb such as *EYS*, packaging the complete cDNA into an AAV is not possible and other strategies are required. To overcome this problem, the use of **microgenes** might be a possible solution (Figure 1.5B). A microgene is a smaller version of the gene of interest, containing the most important functional domains. This idea, amongst others, is based on the fact that in other species, smaller version of the same gene are still functional. For example, *EYS* orthologs in *Drosophila* and zebrafish are smaller than human *EYS* with



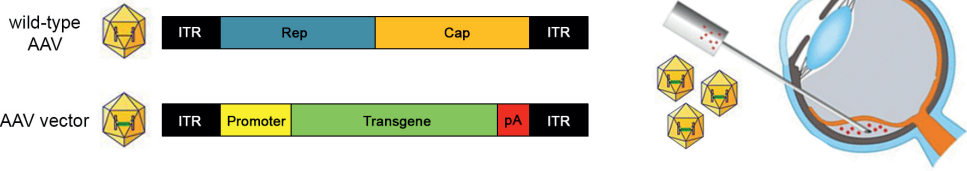
less EGF-like or LamG domains, but still maintain proper function (Figure 1.4). A study by Zhang et al. reported the delivery of a *miniCEP290* gene into a mouse model of LCA. Mice injected with *miniCEP290* significantly improved photoreceptor morphology, survival and function compared to control injected mice.<sup>96</sup> The potential of the microgene strategy has also been shown in studies outside the IRD field. Duchenne muscular dystrophy (DMD) is caused by mutations in the *DMD* gene, encoding the dystrophin protein. Several studies showed that AAV-mediated *micro-dystrophin* expression in different mutant mouse models with DMD lead to a milder form of muscle disease.<sup>97-99</sup> A study by Chen et al. showed that a type VII collagen microgene construct retained the function and characteristics of full length type VII collagen *in vitro*. Dystrophic epidermolysis bullosa (DEB) keratinocytes treated with the VII collagen microgene could produce a population of phenotypically corrected DEB cells, which showed the same characteristics as normal human keratinocytes.<sup>100</sup>

#### 1.7.4 Antisense oligonucleotide therapy

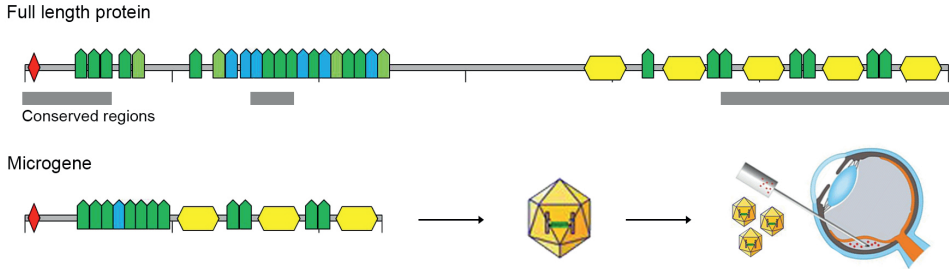
Another therapeutic strategy for IRDs that has emerged over the last years is the use of **antisense oligonucleotides (AONs)**.<sup>70,101-106</sup> These are small DNA or RNA molecules that are complementary to the pre-mRNA region of interest. Binding of AONs to their target can result in modulation of pre-mRNA splicing or degradation of the target transcript, depending on their chemistry. Redirection of pre-mRNA splicing is a commonly used application of AONs. As a consequence of the binding of AONs to their target, splice-regulating factors are no longer able to bind, and changes in splicing can occur.<sup>107</sup> In this way, AONs can be used to block mutations or regulatory sequences within the pre-mRNA, which eventually will induce inclusion or skipping of exons, block the recognition of pseudo-exons, or influence alternative splicing. For example, exons in which many different disease-causing mutations are found can be skipped using AONs to remove the mutations from the gene (Figure 1.5C). Two requirements for skipping regular exons as a potential therapy are that the skipping of the respective exon results in an in-frame transcript and that the exon does not encode a crucial domain for the structure or function of the protein.

In the first example of the successful use of AONs for IRD, AONs were used to target a deep-intronic variant in *CEP290* (c.2991+1655A>G) that leads to LCA.<sup>108</sup> This mutation creates a new splice donor site in intron 26, leading to the insertion of a pseudo-exon, resulting in a frameshift and premature termination of protein synthesis.<sup>108</sup> In patient-derived lymphoblastoid cells or fibroblasts, insertion of this pseudo-exon could be prevented by the administration of AONs targeting the pseudo-exon region.<sup>102,103</sup> Parfitt et al. treated patient-derived optic cups with AONs, which blocked aberrant splicing and restored expression of full length CEP290, leading to normal trafficking of ciliary proteins.<sup>70</sup> Intraocular injections of AONs to a humanized transgenic mouse model, in which part of the human *CEP290* gene (including the deep-intronic mutation) was inserted into the

**A Gene therapy**



**B Microgene therapy**



**C Antisense oligonucleotides**

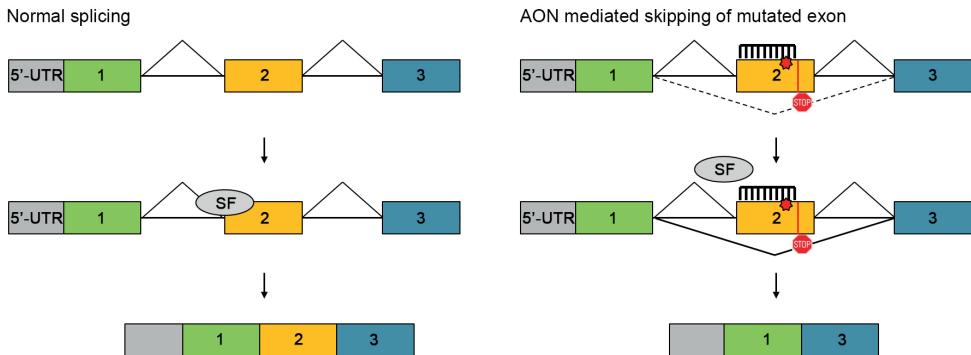


**Figure 1.5. Therapeutic approaches for inherited retinal diseases.**

(A) Gene therapy replaces the mutated gene with a healthy copy of the gene. Adeno-associated virus (AAV) vectors are most commonly used for retinal delivery. ITR: inverted terminal repeats; pA: PolyA tail. (B) Microgene therapy: the delivery of smaller versions of the gene of interest, containing the most important functional domains. (C) Antisense oligonucleotides (AONs) mediated correction of mRNA. SF: splice factors.

mouse *Cep290* gene, resulted in a significant decrease of aberrant *Cep290* transcripts.<sup>104,109</sup> Recently, Albert et al. successfully used AONs for the rescue of splice defects in photoreceptor precursor cells caused by two neighboring deep-intronic mutations in *ABCA4*.<sup>110</sup> Proof-of-concept studies for the use of AONs to correct splicing were also published for two other deep-intronic mutations, one in *USH2A* (c.7595-2144A>G) and one in *OPA1* (c.610+364G>A).<sup>105,111</sup> These studies demonstrate the potential of AON-based splice correction for IRDs.

Besides targeting deep-intronic variants, AONs can also be used for the skipping of regular exons that contain frameshift mutations. Exon skipping is currently one of the most promising therapeutic tools for DMD, and a successful first-in-man trial has recently completed. For DMD, AONs have been designed for numerous exons or combination of exons (double exon skipping).<sup>112</sup> Cysteine altering missense mutations in *NOTCH3* cause cerebral autosomal dominant arteriopathy with subcortical infarcts and leukoencephalopathy, or CADASIL, a hereditary cerebral small vessel disease. Rutten et al. used AON-mediated exon skipping to accomplish *NOTCH3* cysteine correction.<sup>113</sup>

In addition, AONs have also been developed for the inclusion of exons. Spinal muscular atrophy (SMA) is a neuromuscular disorder caused by mutations in the *SMN1* gene. In humans, a second gene, *SMN2*, is present which is identical to *SMN1* apart from five nucleotides. One of these changes, a C to T substitution in exon 7, is critical and leads to skipping of exon 7 in 90% of the produced mRNA, which in turn leads to a non-functional protein. As a therapy for SMA, an AON was designed to target the inhibitory intron splicing silencer N1, thereby promoting exon 7 inclusion in *SMN2* leading to the production of functional protein.<sup>114</sup>

### 1.7.5 Other therapeutic approaches

When RPE cells or photoreceptors are still intact, gene therapy seems to be a promising strategy. However, gene therapy is not an option when RPE cells or photoreceptors are fully degenerated, and alternative therapeutic strategies need to be employed. With *stem cell transplantation*, the patient receives healthy stem cells that can start to develop into normal retinal cells. So far, the most promising sources of cells for human retinal transplantation are embryonic stem cells (ESC) and iPSCs.<sup>46,115,116</sup> In more advanced stages of retinal degeneration, *optogenetics* is a promising therapeutic approach to restore vision. Optogenetics is a type of gene therapy, that renders light responsiveness to surviving retinal cells, such as cones, bipolar cells and ganglion cells that are not photosensitive anymore by their own.<sup>117</sup> *Retinal prosthesis* will be the optional therapy to treat patients without any functional photoreceptors. These devices will trigger neural activity in the remaining cells in the retina. The therapeutic approaches mentioned in this section will not be further discussed in this thesis.

## 1.8 Aim and outline of this thesis

The aim of this thesis is to unravel the pathogenic mechanism underlying *EYS*-associated retinitis pigmentosa, which will serve as the basis for the development of therapeutic approaches for the disease.

**Chapter 2** provides an overview of all the 271 reported and 26 novel *EYS* variant in patients with retinitis pigmentosa. All these variants were classified according to their pathogenicity using the ACMG guidelines. In addition, future prospects on how to experimentally assess the true causality of *EYS* variants are discussed in this chapter.

**Chapter 3** describes the spectrum of retinal disease and the course of visual function in a cohort of 30 patients carrying biallelic *EYS* variants. Intriguingly, two siblings that were diagnosed with macular dystrophy were found to carry compound heterozygous *EYS* variants: c.1299+5\_1299+8del and c.6050G>T. In addition, we show that the c.1299+5\_1299+8del variant affects splicing using an *in vitro* minigene splice assay.

In **Chapter 4**, we report the identification of *ey*s in zebrafish and the generation of a zebrafish *ey*s knock-out model using CRISPR/Cas9 technology to be able to study the function of *Eys*. This chapter shows that *Eys* is important for maintenance of photoreceptor morphology and visual function in zebrafish.

**Chapter 5** presents the development and *in vitro* testing of three different *EYS* microgenes that can be used as a potential therapeutic approach for the treatment of *EYS*-associated retinal dystrophies. We show that two out of three *EYS* microgenes encode stable microgene proteins.

In **Chapter 6**, AONs were designed for skipping *EYS* exon 26 as a therapeutic approach for retinal dystrophy caused by mutations in this exon. Patient-derived iPSCs were differentiated towards photoreceptor cells to test this approach in a cellular model. We observed downregulation of pluripotency markers in differentiated cells, whereas some retinal genes were upregulated, although expression levels were quite low. Furthermore, we show that *EYS* without exon 26 encodes a stable protein and that a combination of two AONs targeting exon 26 are able to skip the complete exon, supporting the therapeutic potential of AON-mediated skipping of this exon.

**Chapter 7** provides the general discussion of this thesis. We highlight our main findings and discuss future directions and challenges for the development of therapeutic approaches for *EYS*-associated retinal dystrophies.

## 1.9 References

1. Sparrow JR, Hicks D, Hamel CP. (2010) The retinal pigment epithelium in health and disease. *Curr Mol Med*; **10**: 802-823.
2. Strauss O. (2005) The retinal pigment epithelium in visual function. *Physiol Rev*; **85**: 845-881.
3. Omri S, Omri B, Savoldelli M, Jonet L, Thillaye-Goldenberg B, Thuret G, Gain P, Jeanny JC, Crisanti P, Behar-Cohen F. (2010) The outer limiting membrane (OLM) revisited: clinical implications. *Clin Ophthalmol*; **4**: 183-195.
4. Bunt-Milam AH, Saari JC, Klock IB, Garwin GG. (1985) Zonulae adherentes pore size in the external limiting membrane of the rabbit retina. *Invest Ophthalmol Vis Sci*; **26**: 1377-1380.
5. Kolb H. Outer Plexiform Layer. In: Kolb H, Fernandez E, Nelson R, eds. *Webvision: The Organization of the Retina and Visual System*. Salt Lake City (UT) 1995.
6. Nelson R, Connaughton V. Bipolar Cell Pathways in the Vertebrate Retina. In: Kolb H, Fernandez E, Nelson R, eds. *Webvision: The Organization of the Retina and Visual System*. Salt Lake City (UT) 1995.
7. Bussow H. (1980) The astrocytes in the retina and optic nerve head of mammals: a special glia for the ganglion cell axons. *Cell Tissue Res*; **206**: 367-378.
8. Vecino E, Rodriguez FD, Ruzafa N, Pereiro X, Sharma SC. (2016) Glia-neuron interactions in the mammalian retina. *Prog Retin Eye Res*; **51**: 1-40.
9. Bejarano-Escobar R, Sanchez-Calderon H, Otero-Arenas J, Martin-Partido G, Francisco-Morcillo J. (2017) Muller glia and phagocytosis of cell debris in retinal tissue. *J Anat*; **231**: 471-483.
10. Kolb H. Glial Cells of the Retina. In: Kolb H, Fernandez E, Nelson R, eds. *Webvision: The Organization of the Retina and Visual System*. Salt Lake City (UT) 1995.
11. Wang JS, Kefalov VJ. (2011) The cone-specific visual cycle. *Prog Retin Eye Res*; **30**: 115-128.
12. Sung CH, Chuang JZ. (2010) The cell biology of vision. *J Cell Biol*; **190**: 953-963.
13. Pearing JN, Salinas RY, Baker SA, Arshavsky VY. (2013) Protein sorting, targeting and trafficking in photoreceptor cells. *Prog Retin Eye Res*; **36**: 24-51.
14. Mustafi D, Engel AH, Palczewski K. (2009) Structure of cone photoreceptors. *Prog Retin Eye Res*; **28**: 289-302.
15. Mehri A. (2017) Non-extensive distribution of human eye photoreceptors. *J Theor Biol*; **419**: 305-309.
16. Curcio CA, Sloan KR, Kalina RE, Hendrickson AE. (1990) Human photoreceptor topography. *J Comp Neurol*; **292**: 497-523.
17. Dias MF, Joo K, Kemp JA, Fialho SL, da Silva Cunha A, Jr., Woo SJ, Kwon YJ. (2017) Molecular genetics and emerging therapies for retinitis pigmentosa: Basic research and clinical perspectives. *Prog Retin Eye Res*; **63**: 107-131.
18. Matsumoto B, Defoe DM, Besharse JC. (1987) Membrane turnover in rod photoreceptors: ensheathment and phagocytosis of outer segment distal tips by pseudopodia of the retinal pigment epithelium. *Proc R Soc Lond B Biol Sci*; **230**: 339-354.
19. van Soest S, Westerveld A, de Jong PT, Bleeker-Wagemakers EM, Bergen AA. (1999) Retinitis pigmentosa: defined from a molecular point of view. *Surv Ophthalmol*; **43**: 321-334.

20. Slijkerman RW, Song F, Astuti GD, Huynen MA, van Wijk E, Stieger K, Collin RW. (2015) The pros and cons of vertebrate animal models for functional and therapeutic research on inherited retinal dystrophies. *Prog Retin Eye Res*; **48**: 137-159.
21. Baylor DA, Burns ME. (1998) Control of rhodopsin activity in vision. *Eye (Lond)*; **12**: 521-525.
22. Hargrave PA. (2001) Rhodopsin structure, function, and topography the Friedenwald lecture. *Invest Ophthalmol Vis Sci*; **42**: 3-9.
23. Kefalov VJ. (2012) Rod and cone visual pigments and phototransduction through pharmacological, genetic, and physiological approaches. *J Biol Chem*; **287**: 1635-1641.
24. Sohocki MM, Daiger SP, Bowne SJ, Rodriguez JA, Northrup H, Heckenlively JR, Birch DG, Mintz-Hittner H, Ruiz RS, Lewis RA, et al. (2001) Prevalence of mutations causing retinitis pigmentosa and other inherited retinopathies. *Hum Mutat*; **17**: 42-51.
25. Dryja TP, Hahn LB, Kajiwarra K, Berson EL. (1997) Dominant and digenic mutations in the peripherin/RDS and ROM1 genes in retinitis pigmentosa. *Invest Ophthalmol Vis Sci*; **38**: 1972-1982.
26. Kajiwarra K, Berson EL, Dryja TP. (1994) Digenic retinitis pigmentosa due to mutations at the unlinked peripherin/RDS and ROM1 loci. *Science*; **264**: 1604-1608.
27. den Hollander AI, Roepman R, Koenekoop RK, Cremers FP. (2008) Leber congenital amaurosis: genes, proteins and disease mechanisms. *Prog Retin Eye Res*; **27**: 391-419.
28. Hartong DT, Berson EL, Dryja TP. (2006) Retinitis pigmentosa. *Lancet*; **368**: 1795-1809.
29. Verbakel SK, van Huet RAC, Boon CJF, den Hollander AI, Collin RWJ, Klaver CCW, Hoyng CB, Roepman R, Klevering BJ. (2018) Non-syndromic retinitis pigmentosa. *Prog Retin Eye Res*.
30. Hamel C. (2006) Retinitis pigmentosa. *Orphanet J Rare Dis*; **1**: 40.
31. Ait-Ali N, Fridlich R, Millet-Puel G, Clerin E, Delalande F, Jaillard C, Blond F, Perrocheau L, Reichman S, Byrne LC, et al. (2015) Rod-derived cone viability factor promotes cone survival by stimulating aerobic glycolysis. *Cell*; **161**: 817-832.
32. Leveillard T, Sahel JA. (2010) Rod-derived cone viability factor for treating blinding diseases: from clinic to redox signaling. *Sci Transl Med*; **2**: 26ps16.
33. Chang S, Vaccarella L, Olatunji S, Cebulla C, Christoforidis J. (2011) Diagnostic challenges in retinitis pigmentosa: genotypic multiplicity and phenotypic variability. *Curr Genomics*; **12**: 267-275.
34. Littink KW, van den Born LI, Koenekoop RK, Collin RW, Zonneveld MN, Blokland EA, Khan H, Theelen T, Hoyng CB, Cremers FP, et al. (2010) Mutations in the EYS gene account for approximately 5% of autosomal recessive retinitis pigmentosa and cause a fairly homogeneous phenotype. *Ophthalmology*; **117**: 2026-2033.
35. Iwanami M, Oshikawa M, Nishida T, Nakadomari S, Kato S. (2012) High prevalence of mutations in the EYS gene in Japanese patients with autosomal recessive retinitis pigmentosa. *Invest Ophthalmol Vis Sci*; **53**: 1033-1040.
36. Abd El-Aziz MM, Barragan I, O'Driscoll CA, Goodstadt L, Prigmore E, Borrego S, Mena M, Pieras JI, El-Ashry MF, Safieh LA, et al. (2008) EYS, encoding an ortholog of Drosophila spacemaker, is mutated in autosomal recessive retinitis pigmentosa. *Nat Genet*; **40**: 1285-1287.

37. Collin RW, Littink KW, Klevering BJ, van den Born LI, Koenekoop RK, Zonneveld MN, Blokland EA, Strom TM, Hoyng CB, den Hollander AI, et al. (2008) Identification of a 2 Mb human ortholog of *Drosophila* eyes shut/spacemaker that is mutated in patients with retinitis pigmentosa. *Am J Hum Genet*; **83**: 594-603.
38. Wouters MA, Rigoutsos I, Chu CK, Feng LL, Sparrow DB, Dunwoodie SL. (2005) Evolution of distinct EGF domains with specific functions. *Protein Sci*; **14**: 1091-1103.
39. Tisi D, Talts JF, Timpl R, Hohenester E. (2000) Structure of the C-terminal laminin G-like domain pair of the laminin alpha2 chain harbouring binding sites for alpha-dystroglycan and heparin. *EMBO J*; **19**: 1432-1440.
40. Husain N, Pellikka M, Hong H, Klimentova T, Choe KM, Clandinin TR, Tepass U. (2006) The agrin/perlecan-related protein eyes shut is essential for epithelial lumen formation in the *Drosophila* retina. *Dev Cell*; **11**: 483-493.
41. Yu M, Liu Y, Li J, Natale BN, Cao S, Wang D, Amack JD, Hu H. (2016) Eyes shut homolog is required for maintaining the ciliary pocket and survival of photoreceptors in zebrafish. *Biol Open*; **5**: 1662-1673.
42. Lu Z, Hu X, Liu F, Soares DC, Liu X, Yu S, Gao M, Han S, Qin Y, Li C, et al. (2017) Ablation of EYS in zebrafish causes mislocalisation of outer segment proteins, F-actin disruption and cone-rod dystrophy. *Sci Rep*; **7**: 46098.
43. Goldman D. (2014) Muller glial cell reprogramming and retina regeneration. *Nat Rev Neurosci*; **15**: 431-442.
44. Mowat FM, Breuwer AR, Bartoe JT, Annear MJ, Zhang Z, Smith AJ, Bainbridge JW, Petersen-Jones SM, Ali RR. (2013) RPE65 gene therapy slows cone loss in Rpe65-deficient dogs. *Gene Ther*; **20**: 545-555.
45. Takahashi K, Yamanaka S. (2006) Induction of pluripotent stem cells from mouse embryonic and adult fibroblast cultures by defined factors. *Cell*; **126**: 663-676.
46. Wiley LA, Burnight ER, Songstad AE, Drack AV, Mullins RF, Stone EM, Tucker BA. (2015) Patient-specific induced pluripotent stem cells (iPSCs) for the study and treatment of retinal degenerative diseases. *Prog Retin Eye Res*; **44**: 15-35.
47. Hu Q, Friedrich AM, Johnson LV, Clegg DO. (2010) Memory in induced pluripotent stem cells: reprogrammed human retinal-pigmented epithelial cells show tendency for spontaneous redifferentiation. *Stem Cells*; **28**: 1981-1991.
48. Tucker BA, Mullins RF, Streb LM, Anfinson K, Eyestone ME, Kaalberg E, Riker MJ, Drack AV, Braun TA, Stone EM. (2013) Patient-specific iPSC-derived photoreceptor precursor cells as a means to investigate retinitis pigmentosa. *Elife*; **2**: e00824.
49. Phillips MJ, Wallace KA, Dickerson SJ, Miller MJ, Verhoeven AD, Martin JM, Wright LS, Shen W, Capowski EE, Percin EF, et al. (2012) Blood-derived human iPSC cells generate optic vesicle-like structures with the capacity to form retinal laminae and develop synapses. *Invest Ophthalmol Vis Sci*; **53**: 2007-2019.

50. Gu H, Huang X, Xu J, Song L, Liu S, Zhang XB, Yuan W, Li Y. (2018) Optimizing the method for generation of integration-free induced pluripotent stem cells from human peripheral blood. *Stem Cell Res Ther*; **9**: 163.
51. Loh YH, Agarwal S, Park IH, Urbach A, Huo H, Heffner GC, Kim K, Miller JD, Ng K, Daley GQ. (2009) Generation of induced pluripotent stem cells from human blood. *Blood*; **113**: 5476-5479.
52. Li G, Xie B, He L, Zhou T, Gao G, Liu S, Pan G, Ge J, Peng F, Zhong X. (2018) Generation of Retinal Organoids with Mature Rods and Cones from Urine-Derived Human Induced Pluripotent Stem Cells. *Stem Cells Int*; **2018**: 4968658.
53. Bacakova L, Zarubova J, Travnickova M, Musilkova J, Pajorova J, Slepicka P, Kasalkova NS, Svorcik V, Kolska Z, Motarjemi H, et al. (2018) Stem cells: their source, potency and use in regenerative therapies with focus on adipose-derived stem cells - a review. *Biotechnol Adv*; **36**: 1111-1126.
54. Wada N, Wang B, Lin NH, Laslett AL, Gronthos S, Bartold PM. (2011) Induced pluripotent stem cell lines derived from human gingival fibroblasts and periodontal ligament fibroblasts. *J Periodontal Res*; **46**: 438-447.
55. Bar-Nur O, Russ HA, Efrat S, Benvenisty N. (2011) Epigenetic memory and preferential lineage-specific differentiation in induced pluripotent stem cells derived from human pancreatic islet beta cells. *Cell Stem Cell*; **9**: 17-23.
56. Oda Y, Yoshimura Y, Ohnishi H, Tadokoro M, Katsube Y, Sasao M, Kubo Y, Hattori K, Saito S, Horimoto K, et al. (2010) Induction of pluripotent stem cells from human third molar mesenchymal stromal cells. *J Biol Chem*; **285**: 29270-29278.
57. Jin ZB, Okamoto S, Osakada F, Homma K, Assawachananont J, Hiram Y, Iwata T, Takahashi M. (2011) Modeling retinal degeneration using patient-specific induced pluripotent stem cells. *PLoS One*; **6**: e17084.
58. Zhou S, Flamier A, Abdouh M, Tetreault N, Barabino A, Wadhwa S, Bernier G. (2015) Differentiation of human embryonic stem cells into cone photoreceptors through simultaneous inhibition of BMP, TGFbeta and Wnt signaling. *Development*; **142**: 3294-3306.
59. Yoshida T, Ozawa Y, Suzuki K, Yuki K, Ohyama M, Akamatsu W, Matsuzaki Y, Shimmura S, Mitani K, Tsubota K, et al. (2014) The use of induced pluripotent stem cells to reveal pathogenic gene mutations and explore treatments for retinitis pigmentosa. *Mol Brain*; **7**: 45.
60. Salasoo A, Feustel TC, Shiffrin RM. (1985) Memory codes and episodes in models of word identification: a reply to Johnston, van Santen, and Hale. *J Exp Psychol Gen*; **114**: 509-513.
61. Jin ZB, Okamoto S, Xiang P, Takahashi M. (2012) Integration-free induced pluripotent stem cells derived from retinitis pigmentosa patient for disease modeling. *Stem Cells Transl Med*; **1**: 503-509.
62. Osakada F, Jin ZB, Hiram Y, Ikeda H, Danjyo T, Watanabe K, Sasai Y, Takahashi M. (2009) In vitro differentiation of retinal cells from human pluripotent stem cells by small-molecule induction. *J Cell Sci*; **122**: 3169-3179.
63. Nakano T, Ando S, Takata N, Kawada M, Muguruma K, Sekiguchi K, Saito K, Yonemura S, Eiraku M, Sasai Y. (2012) Self-formation of optic cups and storable stratified neural retina from human ESCs. *Cell Stem Cell*; **10**: 771-785.



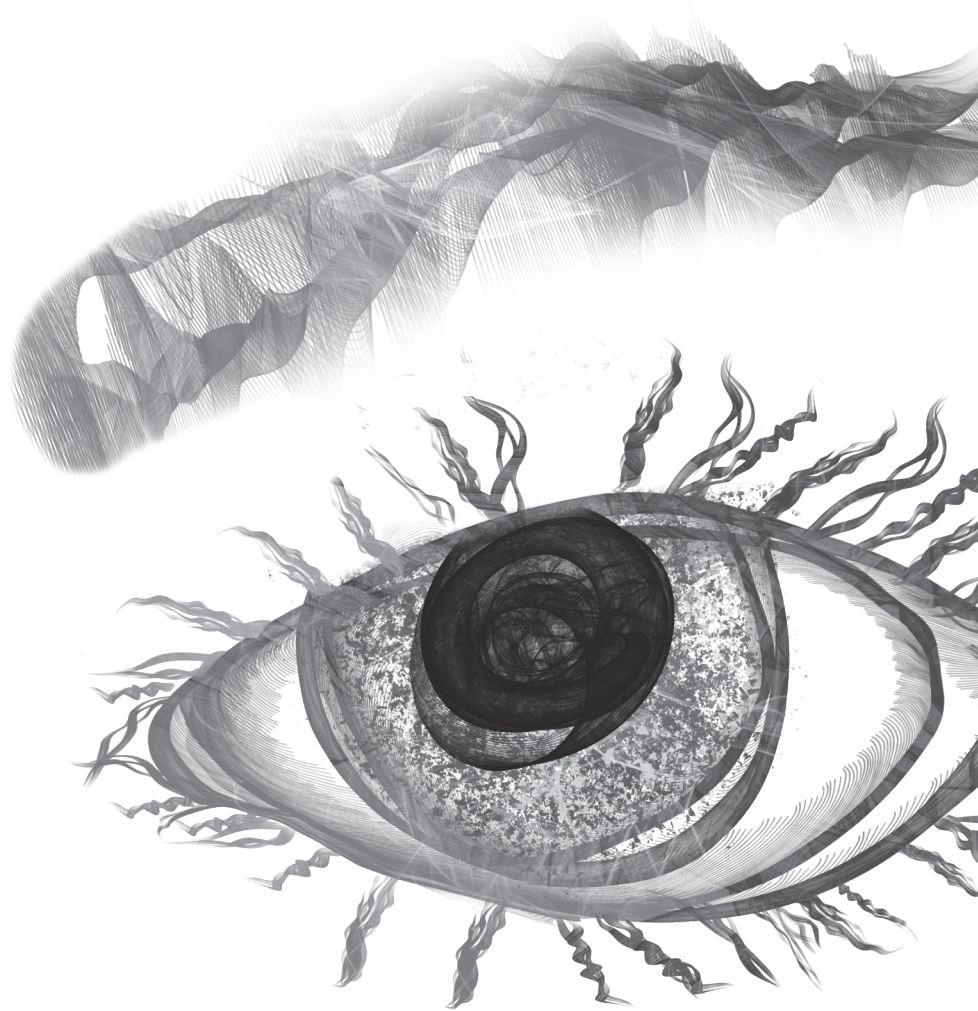
64. Zhong X, Gutierrez C, Xue T, Hampton C, Vergara MN, Cao LH, Peters A, Park TS, Zambidis ET, Meyer JS, et al. (2014) Generation of three-dimensional retinal tissue with functional photoreceptors from human iPSCs. *Nat Commun*; **5**: 4047.
65. Gonzalez-Cordero A, Kruczek K, Naeem A, Fernando M, Kloc M, Ribeiro J, Goh D, Duran Y, Blackford SJI, Abelleira-Hervas L, et al. (2017) Recapitulation of Human Retinal Development from Human Pluripotent Stem Cells Generates Transplantable Populations of Cone Photoreceptors. *Stem Cell Reports*; **9**: 820-837.
66. Wahlin KJ, Maruotti JA, Sripathi SR, Ball J, Angueyra JM, Kim C, Grebe R, Li W, Jones BW, Zack DJ. (2017) Photoreceptor Outer Segment-like Structures in Long-Term 3D Retinas from Human Pluripotent Stem Cells. *Sci Rep*; **7**: 766.
67. Wiley LA, Burnight ER, DeLuca AP, Anfinson KR, Cranston CM, Kaalberg EE, Penticoff JA, Affatigato LM, Mullins RF, Stone EM, et al. (2016) cGMP production of patient-specific iPSCs and photoreceptor precursor cells to treat retinal degenerative blindness. *Sci Rep*; **6**: 30742.
68. Phillips MJ, Perez ET, Martin JM, Reshel ST, Wallace KA, Capowski EE, Singh R, Wright LS, Clark EM, Barney PM, et al. (2014) Modeling human retinal development with patient-specific induced pluripotent stem cells reveals multiple roles for visual system homeobox 2. *Stem Cells*; **32**: 1480-1492.
69. Arno G, Agrawal SA, Eblimit A, Bellingham J, Xu M, Wang F, Chakarova C, Parfitt DA, Lane A, Burgoyne T, et al. (2016) Mutations in REEP6 Cause Autosomal-Recessive Retinitis Pigmentosa. *Am J Hum Genet*; **99**: 1305-1315.
70. Parfitt DA, Lane A, Ramsden CM, Carr AJ, Munro PM, Jovanovic K, Schwarz N, Kanuga N, Muthiah MN, Hull S, et al. (2016) Identification and Correction of Mechanisms Underlying Inherited Blindness in Human iPSC-Derived Optic Cups. *Cell Stem Cell*; **18**: 769-781.
71. Kytala A, Moraghebi R, Valensisi C, Kettunen J, Andrus C, Pasumarthy KK, Nakanishi M, Nishimura K, Ohtaka M, Weltner J, et al. (2016) Genetic Variability Overrides the Impact of Parental Cell Type and Determines iPSC Differentiation Potential. *Stem Cell Reports*; **6**: 200-212.
72. Hoshijima K, Jurynek MJ, Grunwald DJ. (2016) Precise genome editing by homologous recombination. *Methods Cell Biol*; **135**: 121-147.
73. Sander JD, Cade L, Khayter C, Reyon D, Peterson RT, Joung JK, Yeh JR. (2011) Targeted gene disruption in somatic zebrafish cells using engineered TALENs. *Nat Biotechnol*; **29**: 697-698.
74. Huang P, Xiao A, Zhou M, Zhu Z, Lin S, Zhang B. (2011) Heritable gene targeting in zebrafish using customized TALENs. *Nat Biotechnol*; **29**: 699-700.
75. Tesson L, Usal C, Menoret S, Leung E, Niles BJ, Remy S, Santiago Y, Vincent AI, Meng X, Zhang L, et al. (2011) Knockout rats generated by embryo microinjection of TALENs. *Nat Biotechnol*; **29**: 695-696.
76. Davies B, Davies G, Preece C, Puliyadi R, Szumska D, Bhattacharya S. (2013) Site specific mutation of the *Zic2* locus by microinjection of TALEN mRNA in mouse CD1, C3H and C57BL/6J oocytes. *PLoS One*; **8**: e60216.

77. Hockemeyer D, Wang H, Kiani S, Lai CS, Gao Q, Cassady JP, Cost GJ, Zhang L, Santiago Y, Miller JC, et al. (2011) Genetic engineering of human pluripotent cells using TALE nucleases. *Nat Biotechnol*; **29**: 731-734.
78. Jinek M, East A, Cheng A, Lin S, Ma E, Doudna J. (2013) RNA-programmed genome editing in human cells. *Elife*; **2**: e00471.
79. Mali P, Yang L, Esvelt KM, Aach J, Guell M, DiCarlo JE, Norville JE, Church GM. (2013) RNA-guided human genome engineering via Cas9. *Science*; **339**: 823-826.
80. Cong L, Ran FA, Cox D, Lin S, Barretto R, Habib N, Hsu PD, Wu X, Jiang W, Marraffini LA, et al. (2013) Multiplex genome engineering using CRISPR/Cas systems. *Science*; **339**: 819-823.
81. Sander JD, Joung JK. (2014) CRISPR-Cas systems for editing, regulating and targeting genomes. *Nat Biotechnol*; **32**: 347-355.
82. Whitworth KM, Lee K, Benne JA, Beaton BP, Spate LD, Murphy SL, Samuel MS, Mao J, O'Gorman C, Walters EM, et al. (2014) Use of the CRISPR/Cas9 system to produce genetically engineered pigs from in vitro-derived oocytes and embryos. *Biol Reprod*; **91**: 78.
83. Wu Y, Zhou H, Fan X, Zhang Y, Zhang M, Wang Y, Xie Z, Bai M, Yin Q, Liang D, et al. (2015) Correction of a genetic disease by CRISPR-Cas9-mediated gene editing in mouse spermatogonial stem cells. *Cell Res*; **25**: 67-79.
84. Dalkara D, Goureau O, Marazova K, Sahel JA. (2016) Let There Be Light: Gene and Cell Therapy for Blindness. *Hum Gene Ther*; **27**: 134-147.
85. Lipinski DM, Thake M, MacLaren RE. (2013) Clinical applications of retinal gene therapy. *Prog Retin Eye Res*; **32**: 22-47.
86. Trapani I, Puppo A, Auricchio A. (2014) Vector platforms for gene therapy of inherited retinopathies. *Prog Retin Eye Res*; **43**: 108-128.
87. Auricchio A, Kobinger G, Anand V, Hildinger M, O'Connor E, Maguire AM, Wilson JM, Bennett J. (2001) Exchange of surface proteins impacts on viral vector cellular specificity and transduction characteristics: the retina as a model. *Hum Mol Genet*; **10**: 3075-3081.
88. Allocca M, Mussolino C, Garcia-Hoyos M, Sanges D, Iodice C, Petrillo M, Vandenberghe LH, Wilson JM, Marigo V, Surace EM, et al. (2007) Novel adeno-associated virus serotypes efficiently transduce murine photoreceptors. *J Virol*; **81**: 11372-11380.
89. Lotery AJ, Yang GS, Mullins RF, Russell SR, Schmidt M, Stone EM, Lindbloom JD, Chiorini JA, Kotin RM, Davidson BL. (2003) Adeno-associated virus type 5: transduction efficiency and cell-type specificity in the primate retina. *Hum Gene Ther*; **14**: 1663-1671.
90. Leberherz C, Maguire A, Tang W, Bennett J, Wilson JM. (2008) Novel AAV serotypes for improved ocular gene transfer. *J Gene Med*; **10**: 375-382.
91. Charbel Issa P, MacLaren RE. (2012) Non-viral retinal gene therapy: a review. *Clin Exp Ophthalmol*; **40**: 39-47.
92. Conlon TJ, Deng WT, Erger K, Cossette T, Pang JJ, Ryals R, Clement N, Cleaver B, McDoom I, Boye SE, et al. (2013) Preclinical potency and safety studies of an AAV2-mediated gene therapy vector for the treatment of MERTK associated retinitis pigmentosa. *Hum Gene Ther Clin Dev*; **24**: 23-28.

93. Koch S, Sothilingam V, Garcia Garrido M, Tanimoto N, Becirovic E, Koch F, Seide C, Beck SC, Seeliger MW, Biel M, et al. (2012) Gene therapy restores vision and delays degeneration in the CNGB1(-/-) mouse model of retinitis pigmentosa. *Hum Mol Genet*; **21**: 4486-4496.
94. Beltran WA, Cideciyan AV, Lewin AS, Iwabe S, Khanna H, Sumaroka A, Chiodo VA, Fajardo DS, Roman AJ, Deng WT, et al. (2012) Gene therapy rescues photoreceptor blindness in dogs and paves the way for treating human X-linked retinitis pigmentosa. *Proc Natl Acad Sci U S A*; **109**: 2132-2137.
95. Pawlyk BS, Bulgakov OV, Sun X, Adamian M, Shu X, Smith AJ, Berson EL, Ali RR, Khani S, Wright AF, et al. (2016) Photoreceptor rescue by an abbreviated human RPGR gene in a murine model of X-linked retinitis pigmentosa. *Gene Ther*; **23**: 196-204.
96. Zhang W, Li L, Su Q, Gao G, Khanna H. (2018) Gene Therapy Using a miniCEP290 Fragment Delays Photoreceptor Degeneration in a Mouse Model of Leber Congenital Amaurosis. *Hum Gene Ther*; **29**: 42-50.
97. Liu M, Yue Y, Harper SQ, Grange RW, Chamberlain JS, Duan D. (2005) Adeno-associated virus-mediated microdystrophin expression protects young mdx muscle from contraction-induced injury. *Mol Ther*; **11**: 245-256.
98. Yue Y, Li Z, Harper SQ, Davisson RL, Chamberlain JS, Duan D. (2003) Microdystrophin gene therapy of cardiomyopathy restores dystrophin-glycoprotein complex and improves sarcolemma integrity in the mdx mouse heart. *Circulation*; **108**: 1626-1632.
99. Duan D. (2006) Challenges and opportunities in dystrophin-deficient cardiomyopathy gene therapy. *Hum Mol Genet*; **15 Spec No 2**: R253-261.
100. Chen M, O'Toole EA, Muellenhoff M, Medina E, Kasahara N, Woodley DT. (2000) Development and characterization of a recombinant truncated type VII collagen "minigene". Implication for gene therapy of dystrophic epidermolysis bullosa. *J Biol Chem*; **275**: 24429-24435.
101. Duijkers L, van den Born LI, Neidhardt J, Bax NM, Pierrache LHM, Klevering BJ, Collin RWJ, Garanto A. (2018) Antisense Oligonucleotide-Based Splicing Correction in Individuals with Leber Congenital Amaurosis due to Compound Heterozygosity for the c.2991+1655A>G Mutation in CEP290. *Int J Mol Sci*; **19**.
102. Collin RW, den Hollander AI, van der Velde-Visser SD, Bennicelli J, Bennett J, Cremers FP. (2012) Antisense Oligonucleotide (AON)-based Therapy for Leber Congenital Amaurosis Caused by a Frequent Mutation in CEP290. *Mol Ther Nucleic Acids*; **1**: e14.
103. Gerard X, Perrault I, Hanein S, Silva E, Bigot K, Defoort-Delhemmes S, Rio M, Munnich A, Scherman D, Kaplan J, et al. (2012) AON-mediated Exon Skipping Restores Ciliation in Fibroblasts Harboring the Common Leber Congenital Amaurosis CEP290 Mutation. *Mol Ther Nucleic Acids*; **1**: e29.
104. Garanto A, Chung DC, Duijkers L, Corral-Serrano JC, Messchaert M, Xiao R, Bennett J, Vandenberghe LH, Collin RW. (2016) In vitro and in vivo rescue of aberrant splicing in CEP290-associated LCA by antisense oligonucleotide delivery. *Hum Mol Genet*; **25**: 2552-2563.
105. Slijkerman RW, Vache C, Dona M, Garcia-Garcia G, Claustres M, Hetterschijt L, Peters TA, Hartel BP, Pennings RJ, Millan JM, et al. (2016) Antisense Oligonucleotide-based Splice Correction for

- USH2A-associated Retinal Degeneration Caused by a Frequent Deep-intronic Mutation. *Mol Ther Nucleic Acids*; **5**: e381.
106. Murray SF, Jazayeri A, Matthes MT, Yasumura D, Yang H, Peralta R, Watt A, Freier S, Hung G, Adamson PS, et al. (2015) Allele-Specific Inhibition of Rhodopsin With an Antisense Oligonucleotide Slows Photoreceptor Cell Degeneration. *Invest Ophthalmol Vis Sci*; **56**: 6362-6375.
107. Hammond SM, Wood MJ. (2011) Genetic therapies for RNA mis-splicing diseases. *Trends Genet*; **27**: 196-205.
108. den Hollander AI, Koenekoop RK, Yzer S, Lopez I, Arends ML, Voeseke KE, Zonneveld MN, Strom TM, Meitinger T, Brunner HG, et al. (2006) Mutations in the CEP290 (NPHP6) gene are a frequent cause of Leber congenital amaurosis. *Am J Hum Genet*; **79**: 556-561.
109. Garanto A, van Beersum SE, Peters TA, Roepman R, Cremers FP, Collin RW. (2013) Unexpected CEP290 mRNA splicing in a humanized knock-in mouse model for Leber congenital amaurosis. *PLoS One*; **8**: e79369.
110. Albert S, Garanto A, Sangermano R, Khan M, Bax NM, Hoyng CB, Zernant J, Lee W, Allikmets R, Collin RWJ, et al. (2018) Identification and Rescue of Splice Defects Caused by Two Neighboring Deep-Intronic ABCA4 Mutations Underlying Stargardt Disease. *Am J Hum Genet*; **102**: 517-527.
111. Bonifert T, Gonzalez Menendez I, Battke F, Theurer Y, Synofzik M, Schols L, Wissinger B. (2016) Antisense Oligonucleotide Mediated Splice Correction of a Deep Intronic Mutation in OPA1. *Mol Ther Nucleic Acids*; **5**: e390.
112. Aartsma-Rus A, van Ommen GJ. (2007) Antisense-mediated exon skipping: a versatile tool with therapeutic and research applications. *RNA*; **13**: 1609-1624.
113. Rutten JW, Dauwse HG, Peters DJ, Goldfarb A, Venselaar H, Haffner C, van Ommen GJ, Aartsma-Rus AM, Lesnik Oberstein SA. (2016) Therapeutic NOTCH3 cysteine correction in CADASIL using exon skipping: in vitro proof of concept. *Brain*; **139**: 1123-1135.
114. Wood MJA, Talbot K, Bowerman M. (2017) Spinal muscular atrophy: antisense oligonucleotide therapy opens the door to an integrated therapeutic landscape. *Hum Mol Genet*; **26**: R151-R159.
115. Tucker BA, Mullins RF, Stone EM. (2014) Stem cells for investigation and treatment of inherited retinal disease. *Hum Mol Genet*; **23**: R9-R16.
116. Mead B, Berry M, Logan A, Scott RA, Leadbeater W, Scheven BA. (2015) Stem cell treatment of degenerative eye disease. *Stem Cell Res*; **14**: 243-257.
117. Duebel J, Marazova K, Sahel JA. (2015) Optogenetics. *Curr Opin Ophthalmol*; **26**: 226-232.

# Chapter 2



# ***EYS* mutation update: *In silico* assessment of 271 reported and 26 novel variants in patients with retinitis pigmentosa**

Muriël Messchaert<sup>1,2</sup>, Lonneke Haer-Wigman<sup>1</sup>, Muhammad I. Khan<sup>1,2</sup>,  
Frans P. M. Cremers<sup>1,2</sup>, Rob W. J. Collin<sup>1,2</sup>

- <sup>1</sup> Department of Human Genetics, Radboud University Medical Center, Nijmegen, The Netherlands.
- <sup>2</sup> Donders Institute for Brain, Cognition and Behaviour, Radboud University Medical Center, Nijmegen, The Netherlands.

**Abstract**

Mutations in Eyes shut homolog (EYS) are one of the most common causes of autosomal recessive (ar) retinitis pigmentosa (RP), a progressive blinding disorder. The exact function of the EYS protein and the pathogenic mechanisms underlying EYS-associated RP are still poorly understood, which hampers the interpretation of the causality of many EYS variants discovered to date. We collected all reported EYS variants present in 377 arRP index cases published before June 2017, and uploaded them in the Leiden Open Variation Database ([www.LOVD.nl/EYS](http://www.LOVD.nl/EYS)). We also describe 36 additional index cases, carrying 26 novel variants. Of the 297 unique EYS variants identified, almost half (n=130) are predicted to result in premature truncation of the EYS protein. Classification of all variants using the American College of Medical Genetics and Genomics guidelines revealed that the predicted pathogenicity of these variants cover the complete spectrum ranging from likely benign to pathogenic, although especially missense variants largely fall in the category of uncertain significance. Besides the identification of likely benign alleles previously reported as being probably pathogenic, our comprehensive analysis underscores the need of functional assays to assess the causality of EYS variants, in order to improve molecular diagnostics and counseling of patients with EYS-associated RP.

**Key words:**

EYS, in silico assessment, LOVD, retinitis pigmentosa (RP)

## 2.1 Introduction

*Eyes shut homolog* (*EYS*; MIM# 612424) is one of the most frequently mutated genes in patients with retinitis pigmentosa (RP; MIM# 26800), a group of inherited retinal dystrophies. Retinitis pigmentosa is the most common form of retinal degeneration, with a prevalence of approximately 1 in 4,000 individuals, and is characterized by progressive degeneration of rod photoreceptor cells causing constriction of the visual field and eventually, often, total blindness.<sup>1</sup> Different modes of inheritance including autosomal recessive (ar), autosomal dominant, and X-linked, have been observed in the disease.<sup>1</sup> To date, 58 causal genes for arRP are known (RetNet, <http://www.sph.uth.tmc.edu/RetNet/>), most of them only being responsible for 1-2% of all the cases. However, a few genes are mutated in a larger number of patients, including *EYS*, accounting for approximately 5-10% of all arRP cases.<sup>2-4</sup>

*EYS* encodes the 3,144 amino acids long protein eyes shut homolog (*EYS*) and is predominantly expressed in the retina.<sup>5,6</sup> Loss of *EYS* protein function is thought to be the molecular mechanism underlying *EYS*-associated RP. The *EYS* protein consists of 28 epidermal growth factor-like (EGF) domains and five laminin A G-like (LamG) domains, which are highly conserved (Supp. Figure S1). EGF domains are defined by six cysteine residues which are able to form disulphide bonds, and form two beta-sheets connected to each other by a loop. The exact role of EGF-domains in proteins is not yet clear, but it has been described to be important in intracellular signaling and cell adhesion.<sup>7</sup> The LamG domain is found in many different proteins and is often located at the C-terminus of the protein, as is seen for *EYS*. A wide variety of roles is described for proteins harboring LamG domains, like cell adhesion, migration and signalling.<sup>8</sup>

*EYS* is an ortholog of the *Drosophila* spacemaker (*spam*) protein, which plays a major role in maintenance of the photoreceptor morphology.<sup>9</sup> Recently, two independent groups reported retinal degeneration in different *Eys* knockout zebrafish.<sup>10,11</sup> Yu, et al. revealed that *Eys* is located near the connecting cilium and is required for maintaining the ciliary pocket.<sup>10</sup> The study by Lu et al. showed mislocalization of the outer segment proteins red opsin, UV opsin and rhodopsin in the absence of *Eys*.<sup>11</sup> Due to its retina-specific expression, and supported by the fact that the *Eys* locus is lacking in several rodent species (mouse, rat, guinea pig)<sup>5</sup>, still very little is known about the exact function of *EYS* and the pathogenic mechanism underlying *EYS*-associated RP, which hampers the interpretation of the causality of many *EYS* variants discovered to date.

In this study, we performed a systematic analysis of all 271 reported *EYS* variants reported in patients with RP. Therefore, we collected all *EYS* variants published up to June 2017 that were associated with arRP or allied diseases. We also report 26 novel *EYS* variants not reported previously. All variants were uploaded into the Leiden Open source Variant Database (LOVD) for *EYS*, and were classified according to their pathogenicity based on the American College of Medical Genetics and Genomics (ACMG) guidelines.<sup>12</sup> In addition, we discuss future prospects on how to experimentally assess the true causality of *EYS*



variants. With that, we aim to facilitate a better interpretation of the pathogenicity of *EYS* variants in relation to arRP.

## 2.2 Materials and methods

### 2.2.1 Literature search

We collected all publications from before June 2017 in which *EYS* variants (NM\_001142800.1) were reported in patients with arRP. Variant combinations, age of onset, and disease phenotype were collected. Obvious duplicates were removed.

### 2.2.2 Subjects

This study was approved by the institutional review boards of the Radboud University Medical Center and adhered to the tenets of the Declaration of Helsinki. Sanger sequencing of *EYS*, Multiplex Ligation-dependent Probe Amplification (MLPA, MRC-Holland) of *EYS*, microarray chip based on APEX technology (Asper Biotech, Tartu, Estonia) and/or whole exome sequencing was requested at the genome diagnostic laboratory of the Radboudumc to determine the genetic cause in patients with visual impairment. We extracted all homozygous and (possible) compound heterozygous variants in the *EYS* gene that were reported to the patients, as well as individuals with one (potentially) pathogenic allele. In addition, in 11 index patients, *EYS* variants were identified through a targeted sequencing approach which was based on molecular inversion probes (Khan, MI et al., manuscript in preparation).

### 2.2.3 Variant analysis

For numbering of the cDNA, the A of the ATG translation initiation codon in the *EYS* reference sequence (NM\_001142800.1) was numbered as +1 and the initiation codon as codon 1. Frequencies of the variants present in controls were extracted from the Exome Aggregation Consortium (ExAC) database Version 0.3.1, which gives access to exome data of more than 60,000 individuals from all over the world (<http://exac.broadinstitute.org>).

The majority of the reported *EYS* variants in patients were identified in either non-Finnish Caucasian individuals or East-Asian (Chinese and Japanese) individuals. Statistical analysis was performed to assess whether *EYS* variants were enriched in the *EYS* patient group vs. the ExAC database. To increase the power and specificity, this analysis was performed separately for non-Finnish Caucasians and East-Asians. We used the Fisher's exact test as implemented in R (<http://www.R-project.org>) to compare *EYS* variants found in the Caucasian index patients in the *EYS*-LOVD dataset to non-Finnish European controls in ExAC, and did the same for the East-Asian population. To select only true statistical significant findings, a correction by the false discovery rate (FDR) of Benjamini-Hochberg, classical one stage method<sup>13</sup> was performed with an error margin of 5% on the total data.

In case a certain genomic position was not listed in ExAC, the allele number of the closest variant was used for statistical analysis.

#### 2.2.4 In silico predictions

We obtained Combined Annotation Dependent Depletion (CADD), Grantham and PhyloP scores for all missense variants reported in *EYS*. CADD scores were obtained from the website <http://cadd.gs.washington.edu/home><sup>14</sup> and Grantham scores were obtained from the paper by Grantham in 1974.<sup>15</sup> PhyloP scores were obtained from the table browser tool provided by the UCSC Genome Browser (<http://genome.ucsc.edu/>). We used the Cons 46-way track and the Vertebrate PhyloP Conservation table for GRCh37/hg19 (clade: Mammal, genome: Human, assembly: Feb. 2009 (GRCh37/hg19), group: Comparative Genomics, track: Cons 46-way, table: Vertebrate Cons (phyloP46wayAll)). To compare the average PhyloP score of *EYS* to that of all genes in the human genome, conservation scoring by PhyloP and genomic positions of coding exons were downloaded from UCSC genome browser (<http://hgdownload.cse.ucsc.edu/downloads.html>). Bedtools and in-house scripts were used to generate gene average PhyloP scores, based on the scores of all base-pairs within the coding regions of each gene. Software available via Alamut Visual version 2.7 (Interactive Biosoftware, Rouen, France) was used to obtain splicing scores. The following software programs were used: SpliceSiteFinder-like, MaxEntScan, NNSPLICE, Genesplicer, and Human Splice Finder.

#### 2.2.5 Variant pathogenicity classification

The predicted pathogenicity of all *EYS* variants was assessed according to the ACMG guidelines,<sup>12</sup> allowing to classify all variants into one of the five following categories: pathogenic, likely pathogenic, benign, likely benign, or uncertain significance. First, we scored the variants based on the evidence of pathogenicity in different categories published in the guidelines. These categories are as follows:

- pathogenic, very strong (PVS), for example, this variant is protein truncating,
- pathogenic, strong (PS), for example, this variant leads to the same amino acid change as a previously described pathogenic variant,
- pathogenic, moderate (PM), for example, this variants is located in a mutational hot spot and/or well-established functional domain,
- pathogenic, supporting (PP), for example, all computational evidence support the variant to be pathogenic.

After scoring the variants for the different categories, the ACMG guidelines combine these scores to come to the final classification in one of the five pathogenicity categories as further described in Supp. Table S1.

### 2.2.6 LOVD submission

All the 271 collected published and 26 novel *EYS* variants, together with patient data such as a description of the phenotype, age of onset and segregation information, when available, were uploaded in the Leiden Open Variation Database (LOVD). In case of multiplex families, affected relatives were also uploaded to the LOVD. Scores given to all variants in the column ID\_pathogenic, were based on the pathogenicity assessment that was performed as described in the previous section.

## 2.3 *EYS* Variants

### 2.3.1 The spectrum of *EYS* mutations

In total, we collected information of 377 RP patients described in 43 papers<sup>2-6,16-53</sup>, in which 630 alleles with *EYS* variants were reported. In addition, we identified 26 novel variants found in 36 index patients that were not published previously (Table 2.1). From the in total 413 index patients, 129 patients had homozygous *EYS* variants, 187 patients had compound heterozygous variants, and 97 patients carried only one variant. The total amount of 698 alleles represent 297 unique *EYS* variants (Table 2.1, Supp. Table S2), with protein-truncating variants as the most common type (130 variants), followed by missense variants (116 variants) (Figure 2.1A, Table 2.2). All the collected published variants and the 26 novel variants together with a description of the phenotype and segregation analysis, when available, were uploaded in the LOVD ([www.LOVD.nl/EYS](http://www.LOVD.nl/EYS)).

To analyze whether variants were significantly enriched in the LOVD dataset, Fisher's exact tests were performed separately for the Caucasian population and the East-Asian population. We did this analysis in two different ways. First, we analyzed which *EYS* variants were enriched in the RP patients carrying *EYS* mutations. In addition, we were also interested in the enrichment of *EYS* variants in the complete RP population. For the latter, we have taken into account that approximately fifty percent of the RP patients have arRP and that of these arRP patients, five percent can be explained by mutations in *EYS*. This was done for variants present in all index cases, relatives with the same mutations were excluded from this analysis. Large deletions and duplications were not tested, because copy number variants are not listed in ExAC.

The first analysis revealed that in the non-Finnish European population, 60 variants were significantly enriched in the *EYS*-LOVD (Fisher's exact test,  $P < 0.05$ , FDR of 5%) compared to controls in ExAC. The majority of these variants were protein-truncating mutations ( $n=29$ ). The other variants were missense ( $n=18$ ), splice site ( $n=5$ ), in-frame indels and synonymous variants ( $n=3$ ), and variants in the 5'-UTR ( $n=5$ ). In the East-Asian individuals, 11 variants were significantly enriched in East-Asian patients in the *EYS*-LOVD (Fisher's exact test,  $P < 0.05$ , FDR of 5%) compared to the East-Asian control population in ExAC. These were comprised of 5 missense variants and 6 protein-truncating variants. Interestingly, two variants, p.(Cys2139Tyr) and p.(Trp2640\*), were significantly enriched in the *EYS*-LOVD

**Table 2.1.**  
EYS variants identified in index patients not published previously.

PID	Allele 1		Allele 2		Classification	
	DNA change	Protein change	DNA change	Protein change	Allele 1	Allele 2
<b>Bi-allelic cases</b>						
1	c.[3906C>A; 9405T>A]	p.[His1302Gln; Tyr3135*]	c.[3906C>A; 9405T>A]	p.[His1302Gln; Tyr3135*]	P	P
2	c.1299+5_1299+8del	p.?	c.6050G>T	p.(Gly2017Val)	LP	LP
3	<b>c.4955C&gt;G</b>	<b>p.(Ser1652*)</b>	c.8984T>A	p.(Ile2995Asn)	P	US
4	c.2024-?_3443+?del	p.?	c.2024-?_3443+?del	p.?	P	P
5	<b>c.2308C&gt;T</b>	<b>p.(Gln770*)</b>	<b>c.2308C&gt;T</b>	<b>p.(Gln770*)</b>	P	P
6	c.9405T>A	p.(Tyr3135*)	c.9405T>A	p.(Tyr3135*)	P	P
7	c.8648_8655del	p.(Thr2883Lysfs*4)	c.9405T>A	p.(Tyr3135*)	P	P
8	c.6799_6800del	p.(Gln2267Glu fs*15)	c.7095T>G	p.(Tyr2365*)	P	P
9	c.6799_6800del	p.(Gln2267Glu fs*15)	c.6714del	p.(Ile2239Serfs*17)	P	P
10	<b>c.1185-6T&gt;G</b>	<b>p.?</b>	c.3695T>C	p.(Ile1232Thr)	US	US
	c.7868G>A	p.(Gly2623Glu)			US	US
11	c.4350_4356del	p.(Ile1451Profs*3)	<b>c.7811G&gt;A</b>	<b>p.(Arg2604His)</b>	P	US
12	<b>c.5666del</b>	<b>p.(Tyr1889Leu fs*6)</b>	<b>c.3562C&gt;T</b>	<b>p.(Gln1188*)</b>	P	P
13	c.6714del	p.(Ile2239Serfs*17)	c.6714del	p.(Ile2239Serfs*17)	P	P
14	<b>c.2041G&gt;T</b>	<b>p.(Asp681Tyr)</b>	<b>c.7115T&gt;A</b>	<b>p.(Phe2372Tyr)</b>	US	US
15	<b>c.522C&gt;A</b>	<b>p.(Cys174*)</b>	<b>c.5283T&gt;A</b>	<b>p.(Tyr1761*)</b>	P	P
16	<b>c.454dup</b>	<b>p.(Met152Asn fs*37)</b>	<b>c.9061G&gt;C</b>	<b>p.(Ala3021Pro)</b>	P	US
17	<b>c.9036del</b>	<b>p.(Leu3013Ser fs*6)</b>	c.9405T>A	p.(Tyr3135*)	P	P
18	c.2380C>T	p.(Arg794*)	c.4350_4356del	p.(Ile1451Profs*3)	P	P
19	<b>c.1185-6T&gt;G</b>	<b>p.?</b>	c.7228+1G>A	p.?	US	P
20	<b>c.1349A&gt;C</b>	<b>p.(Asn450Thr)</b>	<b>c.3165-13T&gt;C</b>	<b>p.?</b>	US	US
21	<b>c.8255_8260del</b>	<b>p.(Leu2752_Asn2754del ins Tyr)</b>	<b>c.8255_8260del</b>	<b>p.(Leu2752_Asn2754del ins Tyr)</b>	US	US
22	c.4120C>T	p.(Arg1374*)	c.2024-?_c.2259+?del	p.?	P	P

23	c.4350_4356del	p.(Ile1451Profs*3)	c.9405T>A	p.(Tyr3135*)	P	P	RP
24	<b>c.6191+1G&gt;A</b>	<b>p.?</b>	<b>c.454dup</b>	<b>p.(Met152Asnfs*37)</b>	P	P	RP
25	c.9019G>T	p.(Asp3007Tyr)	c.3890del	p.(Thr1297Lysfs*17)	US	P	RP
26	c.7228+1G>A	p.?	<b>c.2953_2961del</b>	<b>p.(Thr985_Gly987del)</b>	P	US	RP
27	c.32dup	p.(Met12Aspfs*14)	c.32dup	p.(Met12Aspfs*14)	P	P	RP
28	<b>c.865C&gt;G</b>	<b>p.(Pro289Ala)</b>	<b>c.8893del</b>	<b>p.(Val2944Trpfs*31)</b>	US	P	RP
29	<b>c.2023G&gt;C</b>	<b>p.(Gly675Arg)</b>	c.281C>A	p.(Pro94Gln)	US	US	RP
30	<b>c.6725+1G&gt;A</b>	<b>p.?</b>	c.6416G>A	p.(Cys2139Tyr)	P	LP	RP
31	<b>c.522C&gt;A</b>	<b>p.(Cys174*)</b>	<b>c.5283T&gt;A</b>	<b>p.(Tyr1761*)</b>	P	P	RP

#### Mono-allelic cases

32	<b>c.4748A&gt;G</b>	<b>p.(Tyr1583Cys)</b>	Not identified	-	US	-	RP
33	<b>c.296C&gt;T</b>	<b>p.(Pro99Leu)</b>	Not identified	-	US	-	RP
34	c.6976C>T	p.(Arg2326*)	Not identified	-	P	-	RP
35	<b>c.1376del</b>	<b>p.(Cys459Serfs*56)</b>	Not identified	-	P	-	RP
36	<b>c.5098A&gt;T</b>	<b>p.(Lys1700*)</b>	Not identified	-	P	-	RP

CRD: cone-rod dystrophy, LP: likely pathogenic, MD: macula dystrophy, P: pathogenic, RP: retinitis pigmentosa, US: uncertain significance. Novel mutations are depicted in bold.

in Caucasian as well as in East-Asian patients. After performing the corrections for the percentage of arRP cases and the proportion of RP caused by mutations in *EYS*, only the p.(Ile1451Profs\*3) variant was significantly enriched (Fisher's exact test,  $P < 0.05$ , FDR of 5%) in the Caucasian population.

**Table 2.2.**

Distribution of the *EYS* variants found in arRP patients.

Variant type	Unique variants	Total number of alleles
Missense	116	222
Protein truncating	130	399
Splice site	27	42
In-frame indels	7	8
Synonymous	12	17
5' UTR	5	7
Complex alleles	-	3
Total	297	698

### 2.3.2 Complex alleles

Three unique complex alleles have been reported, p.[Gln1751\*; Tyr3059\*], p.[Cys2139Tyr; Ile1698Thr], and p.[His1302Gln; Tyr3135\*]. The p.[Gln1751\*; Tyr3059\*] variant has been reported heterozygously in two patients. Both p.(Gln1751\*) and p.(Tyr3059\*) are protein-truncating variants and thus predicted to be pathogenic. None of the two variants has ever been reported without the other. The p.(Cys2139Tyr) variant present in the complex allele p.[Cys2139Tyr; Ile1698Thr] however also occurred as a standalone variant in 14 patients. Moreover, this was the most frequently reported missense variant and classified as likely pathogenic. Lastly, of the complex allele p.[His1302Gln; Tyr3135\*], the p.(Tyr3135\*) variant is found in ten patients and is classified as pathogenic since this is a protein-truncating variant and absent from controls. The p.(His1302Gln) variant was not reported as a standalone variant and was classified as being of uncertain significance. For the complex alleles, the pathogenicity of each variant was assessed at the individual level.

### 2.3.3 Frequent *EYS* variants

The most frequently reported variant in arRP patients is p.(Ser1653Lysfs\*2), which was found in 79 index patients. Interestingly, this variant was mainly found in Japanese patients as well as three Korean patients. The majority of patients (63/79) were compound heterozygous for this mutation. Of these, 21 individuals (all Japanese) carried another recurrent mutation p.(Tyr2935\*) on the other allele. This p.(Tyr2935\*) variant was reported in 37 patients and thereby the second most frequent mutation in the Japanese population. In the Caucasian population, the most frequently reported variant is p.(Ile1451Profs\*3), reported in 12 arRP patients, three of which carried the variant in homozygous state. Besides the above mentioned frequent variants, a few other variants were also reported

more often (p.(Trp2640\*), p.(Tyr3135\*), p.(Cys2139Tyr) and p.(Gly2186Glu)). In general however, the vast majority of variants (276/297) were reported in only one or a few index cases, demonstrating the tremendous allelic heterogeneity of *EYS*-associated RP.

## 2.4 Pathogenicity assessment of all *EYS* variants

We classified all the *EYS* variants according to the ACMG guidelines as described in the Methods section. Based on our analysis, we have classified 144 variants as pathogenic, 11 variants as likely pathogenic, 17 variants as likely benign, 6 as benign, and 119 as being of uncertain significance.

### 2.4.1 Protein-truncating variants

Most of the *EYS* variants reported in patients with arRP were protein-truncating variants. In total, 399 protein-truncating alleles were reported, corresponding to 57% of all reported *EYS* alleles (n=698) (Supp. Table S2). Of the 130 unique protein-truncating variants, 51 were nonsense mutation and 79 were causing a frameshift (including large deletions). Most of the truncating variants are rare, since only 10 out of these 130 variants were present in the ExAC database. Protein-truncating variants were classified as pathogenic if the variant leads to a termination of the protein before the amino acid position 3135, since it has been described repeatedly that this p.(Tyr3135\*) variant is disease-causing<sup>2,6,39</sup>. It thus appeared that all protein-truncating variants could be classified as pathogenic.

### 2.4.2 Splice site variants

Mutations that affect the canonical di-nucleotides of the splice acceptor (AG) or splice donor (GT) site were considered pathogenic. For all the non-canonical splice site variants, we assessed splice scores using five different splice prediction tools in Alamut Visual. Variants are considered probably pathogenic in case an increase or decrease of >10% of the splice prediction score was predicted by all five programs. Based on this assessment, only the c.1299+5\_1299+8del mutation was classified as likely pathogenic. All other non-canonical splice variants were classified as of uncertain significance. Five splice site variants were enriched in the Caucasian *EYS*-LOVD, one of which was a canonical splice variant, whereas the other four were non-canonical splice variants, including the c.1299+5\_1299+8del mutation.

### 2.4.3 Missense variants

In total, 116 unique missense variants in *EYS* were reported in arRP patients. Prior to the classification of the missense variants according to the ACMG guidelines, we obtained CADD, Grantham and PhyloP scores for all missense variants and used this for the computational evidence. To be supporting evidence (PP3), the threshold for these *in silico* predictions for a variant to be pathogenic were set at CADD >15, Grantham >80, and PhyloP >2.8. Next to that, we assessed the distribution of the missense variants over

the protein to be able to identify mutational hotspots or frequently mutated domains. To obtain the protein domains and their location, we used the SMART prediction tool from <http://smart.embl-heidelberg.de/>. The EYS protein consists of 28 EGF- and EGF-like domains, mainly clustered at the N-terminus of the protein, and 5 LamG domains located at the C-terminal part of the protein that are separated by one or two EGF domains (Figure 1C). We could not identify clear mutational hotspots, although we could observe that there are slightly more missense variants located at the C-terminus of the protein (Figure 1C). Moderate evidence (PM) for a variant to be pathogenic was counted if the variant affects the number of cysteines in an EGF domain or if the variant is located in a LamG domain. EGF-domains are conserved domains that are found to be present in a variety of proteins and might play a role in intracellular signaling and cell adhesion. An important component of these domains are the six cysteine residues that form disulphide bonds. Therefore, variants that affect the number of cysteines in an EGF domain are likely to disrupt the structure of the domain. The C-terminus of the EYS protein contains five LamG domains that are highly conserved. Proteins containing LamG domains appear to have roles in cell adhesion, migration and signaling. Therefore, we counted moderate evidence for pathogenicity when the variant is affecting an amino acid residue that is located in a LamG domain.

Finally, we combined all this information in the pathogenicity assessment. Of all missense variants, three were classified as benign, seven as likely benign, and nine as likely pathogenic (Table 2.3, Figure 2.1B). The majority of the missense variants ( $n=96$ ) had to be classified as of uncertain significance, mainly due to insufficient criteria for these variants to be able to classify them otherwise. For instance, for the p.(Cys2396Ser), p.(Cys2668Phe), p.(Cys2890Tyr) and p.(Gly2907Glu) variants, some evidence points towards a likely pathogenic variant, however additional moderate (PM1-6) or supporting (PP1-5) evidence was lacking.

There were 18 missense variants significantly enriched in the Caucasian EYS-LOVD. Three of these, p.(Gly2017Val), p.(Cys2139Tyr) and p.(Gly2945Glu), were classified as likely pathogenic. All other variants were classified as being of uncertain significance. The pathogenic evidence for these variants is very limited, so even when taking into account that the variants are enriched is not enough to classify them as likely pathogenic. Interestingly, p.(Cys2139Arg) was not enriched in the Caucasian EYS-LOVD, however it was classified as likely pathogenic due to its absence in controls, its location in an EGF domain and the fact that another variant affecting this amino acid is disease-causing as well. In the East-Asian patients, five missense variants were statistically enriched (Fisher's exact test,  $P<0.05$ , FDR of 5%) compared to the East-Asian control population. Of these variants, p.(Cys2139Tyr) and p.(Gly2186Glu) were classified as likely pathogenic whereas the other three (p.(Glu47Asp), p.(Gly843Glu) and p.(Ile2188Thr) were classified as of uncertain significance. Taken into account that these variants are significantly enriched in the East-Asian EYS-LOVD, p.(Gly843Glu) and p.(Ile2188Thr) shifted towards the likely



pathogenic category. For p.(Glu47Asp), even when adding the enrichment data, the evidence was still not sufficient for classification into the likely pathogenic category. After applying corrections for the percentage of arRP cases and the proportion of arRP caused by mutations in *EYS*, it appeared that none of the missense variants was significantly enriched in either the Caucasian or the Asian RP population.

**Table 2.3.**

Likely pathogenic missense mutations.

DNA variant	Protein variant	Homozygous	Heterozygous	Domain
c.2510G>T	p.(Cys837Phe)	-	1	EGF, cysteine
c.6050G>T	p.(Gly2017Val)	3	2	LamG
c.6415T>C	p.(Cys2139Arg)	-	1	EGF, cysteine
c.6557G>A	p.(Gly2186Glu)	2	9	LamG
c.8236G>C	p.(Asp2746His)	-	1	LamG
c.8236G>T	p.(Asp2746Tyr)	1	-	LamG
c.8288T>G	p.(Leu2763Arg)	-	3	LamG
c.8834G>A	p.(Gly2945Glu)	-	2	EGF, no cysteine
c.8861T>C	p.(Phe2954Ser)	-	1	LamG

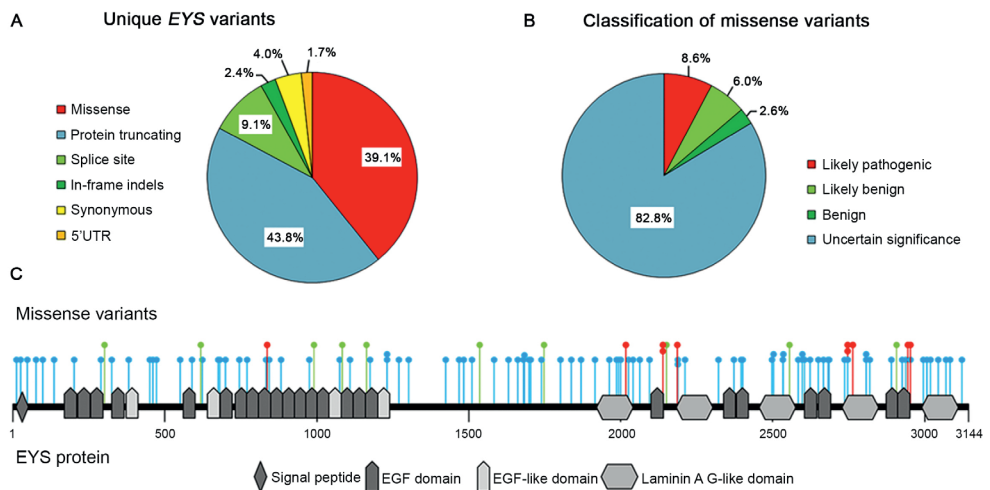


**Figure 2.1.**

(A) Distribution of the unique *EYS* variants found in patients with retinitis pigmentosa. (B) Pie-chart representing the distribution of the missense variants over the different pathogenicity classes (C) Schematic representation of the localization of all 116 missense variants in *EYS*. Likely pathogenic missense variants are depicted in red, benign and likely benign variants in green, and variants of uncertain significance in blue.

#### 2.4.4 New insights into previously reported pathogenic variants

In a number of cases, evaluation of the pathogenicity of a variant resulted in contradictory outcome. For example, the p.(Gly618Ser) variant was reported to be pathogenic by Audo et al.<sup>20</sup> However, Gonzalez-del Pozo et al. reported this variant as unlikely pathogenic, because it did not segregate with the disease in the family.<sup>28</sup> In our pathogenicity assessment this variant was classified as likely benign.

Another example is the p.(Val834Ile) variant that was reported in compound heterozygous state in two patients, one by Littink et al.<sup>4</sup> and the other one by Audo et al.<sup>20</sup> In the paper by Littink et al. this variant was classified as probably pathogenic, mainly because it was excluded in 180 controls. In this patient, it was found in conjunction with a protein-truncating variant. Moreover, recently a third variant was found to be present in this patient. This was a large deletion (c.(-448+1\_-332-1)\_(748+1\_749-1)del) which together with the protein-truncating mutation is most probably the cause of RP in this patient, thus rendering the p.(Val834Ile) variant being most likely benign, similar to the classification by Audo et al. In our *in silico* analysis, this variant was also classified as likely benign, because it is found in the ExAC database (AF=0.001072) and the bio-informatic predictions for this variant met the criteria for supporting evidence (BP4) to be benign.

Furthermore, there were also a few variants that were reported as pathogenic, however, were classified as likely benign upon our pathogenicity assessment. The p.(Leu302Phe) variant was reported in a compound heterozygous state in two patients by Xu et al. and Ge et al.<sup>50,52</sup> In both papers, the variant is not explicitly discussed, although they are listed in tables with “causative” or “pathogenic” variants. Xu et al. detected this variant in 1/314 patients versus 0/192 controls,<sup>52</sup> which could be their main reason to classify this variant as pathogenic. We classified the variant as likely benign, because the allele frequency of 0.0003051 in ExAC is higher than expected in controls (cut-off value = 0.00005) for a pathogenic variant and the *in silico* predictions of CADD, PhyloP and Grantham all point towards this variant being benign. Ge et al. also reported another variant as being pathogenic, p.(Thr1084Pro), which we classified as likely benign for the same reason as p.(Leu302Phe). The p.(Thr1084Pro) variant reported by Ge et al. was found homozygously in a patient which also had the p.(Leu302Phe) variant and the p.(Phe2954Leu) variant.<sup>50</sup>

#### 2.4.5 Genotype-phenotype correlation

Of all reported arRP patients that carried one or more *EYS* variants, we collected information about disease phenotype and age of onset, when available. These data were used to evaluate if there was any genotype-phenotype correlation between the *EYS* variant and the manifestation of the disease. However, unfortunately, for many patients phenotypic details were not available. Moreover, reporting of the disease manifestation is not always consistent and the methods used for diagnosing patients is variable between medical centers. Therefore, we could not draw any conclusions regarding the relationship between *EYS* variants and disease phenotype, nor were there obvious indications that

individuals with protein-truncated variants had a more severe phenotype compared to patients with missense variants. However, for almost all patients with bi-allelic *EYS* mutations, night blindness was reported as the initial symptom. Furthermore, all these patients had hallmark RP symptoms including bone-spicule pigmentation, attenuated retinal arterioles and low visual acuity. Pale optic disc was not reported for all patients, however was a frequently described phenomenon. The age of disease onset was highly variable, ranging from 13 to over 50 years.

## 2.5 Future directions

### 2.5.1 Expanding molecular diagnostics

From the 413 index patients, 97 patients carried only one *EYS* variant. It is possible that a second *EYS* mutation in these patients is not present; however, it is more likely that a second mutation was not detected using the sequencing methods that were used. Most likely, the reason for this would be that the second mutation is not located in the region that is targeted by the mutation detection approach. For instance, with whole exome sequencing that is commonly used to date, variants in intronic regions are missed. To be able to detect these type of variants, techniques such as whole genome sequencing or targeted molecular inverted probe (MIP) sequencing of the complete gene can be used. The use of such approaches will most likely lead to the identification of more variants, but at the same time will make the interpretation of these variants more challenging.

### 2.5.2 Improvement of *in silico* analysis

For the classification of the missense variants we obtained CADD, Grantham and PhyloP scores as computational evidence. The PhyloP is a measure for the conservation of a nucleotide at a certain position. Since *EYS* is not present in certain rodent species (mouse, rat, guinea pig), there is a probability that scores obtained for PhyloP are lower compared to other genes. Therefore, we calculated the average PhyloP score of all coding nucleotides of 19640 protein-coding genes in the human genome. Indeed, the average PhyloP score of *EYS* was 0.887, compared to an average PhyloP score of 1.72 for all other genes. This calculation suggests that the 2.8 cut-off of the PhyloP score for a variant to be probably pathogenic might be too high for some genes in the human genome, including *EYS*. As a result, there could be an underestimation of the missense variants that are classified as likely pathogenic. Thus, caution has to be taken by using these *in silico* scores for the classification of the variants.

### 2.5.3 Experimental assessment of variants of unknown significance

The majority of the missense mutations had to be classified as being of uncertain significance, mainly because the available evidence was not sufficient to robustly meet the criteria of one of the four pathogenicity categories. Also a number of intronic variants

and variants in the 5'-UTR region were classified as of uncertain pathogenicity. Additional experimental evidence would definitely help to classify these missense variants, however, these data are not available at the moment. To our opinion, there are three main reasons that limit a (large-scale) experimental assessment of the pathogenicity of *EYS* variants. First, the *Eys* gene is absent in the genome of several rodent species, including mouse and rat, species that are widely used to study gene and protein function in vision research.<sup>54</sup> Second, the expression of *EYS* is restricted to the retina, thus preventing the use of easily accessible (patient) cells to study *EYS* function. Third, the cDNA size of *EYS* (9.4 kb) is considerable, thereby complicating cellular transfections studies. However, depending on the mutation, there are some possibilities to assess the effect of a certain variant.

For example, to determine whether a variant has an effect on *EYS* pre-mRNA splicing, one ideally would make use of patient-derived cells, by extracting RNA and study *EYS* mRNA composition and levels. Given the retina-specific expression of *EYS*, one would have to make use of induced pluripotent stem cell (iPSC) technology, i.e. reprogram somatic cells to pluripotency, and differentiate the iPSC cells into retinal cells.<sup>55</sup> This is however very labor-intensive and time-consuming. A more manageable approach would be to use minigene splice assay, as described previously.<sup>56</sup> This is an *in vitro* assay in which HEK293T cells are transfected with either a wild type minigene or a minigene carrying a (splice site) variant of interest. These minigenes are plasmids in which a fragment of the gene of interest is cloned between *Rhodopsin* exon 3 and *Rhodopsin* exon 5 under the control of the CMV promoter. Forty-eight hours post-transfection, cells can be harvested to assess potential splice defects via RT-PCR analysis.

For the classification of missense variants, again patient-derived iPSC cells could be used. For this, the phenotype of iPSCs derived from patients can be compared with iPSCs derived from healthy individuals, although a difference in cellular morphology between control and patient-derived cells does not necessarily mean that *EYS* is indeed the causal gene. Therefore, dedicated assays such as western blot analysis or immunolocalization studies would be necessary to reveal whether *EYS* function is compromised. Another possibility is to study the effect of *EYS* variants in an *in vivo* situation, using zebrafish as a model organism. Recently, two independent groups demonstrated that targeted disruption of *Eys* in zebrafish leads to retinal degeneration.<sup>10,11</sup> With genome editing methods such as the CRISPR/Cas9 system available,<sup>11,57</sup> it is possible to introduce specific *Eys* mutations into the zebrafish genome, of which the effect can then be studied by a variety of molecular and/or functional assays. However, the use of iPSCs as well as of zebrafish models are very time-consuming, labor intensive and expensive, thus rendering the *in vitro* or *in vivo* assessment of *EYS* variant still very challenging.

As described in this manuscript, the assessment of the pathogenicity of many *EYS* variants remains very challenging, yet this analysis occurs at the single variant level. Given that *EYS*-associated RP is a strictly autosomal recessively inherited disorder, there are always two pathogenic alleles needed to molecularly confirm this diagnosis. Thus, even in case

there is one clear pathogenic allele, the uncertainty of the second allele complicates molecular diagnostics. In such cases, segregation analysis in available relatives can shed further light on this. However, experimental evidence would be necessary to provide a clear molecular diagnosis.

## 2.6 Concluding remarks

Taken together, we have uploaded all the reported *EYS* variants in the LOVD for *EYS*, which thus far only included a small number of *EYS* variants. This is a first step towards a complete overview of all *EYS* variants in one big database. As the identification of *EYS* was less than ten years ago, we expect more *EYS* variants to be identified in the near future. Furthermore, data of already identified *EYS* variants is probably still missing from the *EYS* LOVD, since not all variants have been published. Adding genetic data of additional patients to this dataset can aid the classification of more pathogenic variants. Next to that, it may support the identification of genotype-phenotype correlations for which the data available so far were not sufficient to draw any conclusions on this.

In conclusion, our comprehensive analysis resulted in the *in silico* classification of all reported *EYS* variants. Furthermore, our study underscores the need of functional assays to assess the causality of *EYS* variants that are now classified as being of uncertain significance, in order to improve molecular diagnostics and counseling of patients with *EYS*-associated RP.

## 2.7 Acknowledgements

We would like to thank Stéphanie Cornelis for helping with the statistical analysis, Dr. Jordi Corominas Galbany and Marc Pauper for bioinformatic support, Dr. Johan T den Dunnen for advising on LOVD updating, and Drs. Camiel J.F. Boon, L. Ingeborgh van den Born, Carel B. Hoyng, Suzanne IJzer, Caroline C.W. Klaver, Hester Y. Kroes, José Schuil, Anneke Vulto-van Silfthout and Wendy van Zelst-Stams for clinical assistance. None of the authors have any financial interest or conflicting interest to disclose.

## 2.8 References

1. Hartong DT, Berson EL, Dryja TP. (2006) Retinitis pigmentosa. *Lancet*; **368**: 1795-1809.
2. Barragan I, Borrego S, Pieras JI, Gonzalez-del Pozo M, Santoyo J, Ayuso C, Baiget M, Millan JM, Mena M, Abd El-Aziz MM, et al. (2010) Mutation spectrum of EYS in Spanish patients with autosomal recessive retinitis pigmentosa. *Hum Mutat*; **31**: E1772-1800.
3. Hosono K, Ishigami C, Takahashi M, Park DH, Hiram Y, Nakanishi H, Ueno S, Yokoi T, Hikoya A, Fujita T, et al. (2012) Two novel mutations in the EYS gene are possible major causes of autosomal recessive retinitis pigmentosa in the Japanese population. *PLoS One*; **7**: e31036.
4. Littink KW, van den Born LI, Koenekoop RK, Collin RW, Zonneveld MN, Blokland EA, Khan H, Theelen T, Hoyng CB, Cremers FP, et al. (2010) Mutations in the EYS gene account for approximately 5% of autosomal recessive retinitis pigmentosa and cause a fairly homogeneous phenotype. *Ophthalmology*; **117**: 2026-2033, 2033 e2021-2027.
5. Abd El-Aziz MM, Barragan I, O'Driscoll CA, Goodstadt L, Prigmore E, Borrego S, Mena M, Pieras JI, El-Ashry MF, Safieh LA, et al. (2008) EYS, encoding an ortholog of *Drosophila* spacemaker, is mutated in autosomal recessive retinitis pigmentosa. *Nat Genet*; **40**: 1285-1287.
6. Collin RW, Littink KW, Klevering BJ, van den Born LI, Koenekoop RK, Zonneveld MN, Blokland EA, Strom TM, Hoyng CB, den Hollander AI, et al. (2008) Identification of a 2 Mb human ortholog of *Drosophila* eyes shut/spacemaker that is mutated in patients with retinitis pigmentosa. *Am J Hum Genet*; **83**: 594-603.
7. Wouters MA, Rigoutsos I, Chu CK, Feng LL, Sparrow DB, Dunwoodie SL. (2005) Evolution of distinct EGF domains with specific functions. *Protein Sci*; **14**: 1091-1103.
8. Tisi D, Talts JF, Timpl R, Hohenester E. (2000) Structure of the C-terminal laminin G-like domain pair of the laminin alpha2 chain harbouring binding sites for alpha-dystroglycan and heparin. *EMBO J*; **19**: 1432-1440.
9. Husain N, Pellikka M, Hong H, Klimentova T, Choe KM, Clandinin TR, Tepass U. (2006) The agrin/perlecan-related protein eyes shut is essential for epithelial lumen formation in the *Drosophila* retina. *Dev Cell*; **11**: 483-493.
10. Yu M, Liu Y, Li J, Natale BN, Cao S, Wang D, Amack JD, Hu H. (2016) Eyes shut homolog is required for maintaining the ciliary pocket and survival of photoreceptors in zebrafish. *Biol Open*; **5**: 1662-1673.
11. Lu Z, Hu X, Liu F, Soares DC, Liu X, Yu S, Gao M, Han S, Qin Y, Li C, et al. (2017) Ablation of EYS in zebrafish causes mislocalisation of outer segment proteins, F-actin disruption and cone-rod dystrophy. *Sci Rep*; **7**: 46098.
12. Richards S, Aziz N, Bale S, Bick D, Das S, Gastier-Foster J, Grody WW, Hegde M, Lyon E, Spector E, et al. (2015) Standards and guidelines for the interpretation of sequence variants: a joint consensus recommendation of the American College of Medical Genetics and Genomics and the Association for Molecular Pathology. *Genet Med*; **17**: 405-424.
13. Benjamini Y, Hochberg Y. (1995) Controlling the False Discovery Rate - a Practical and Powerful Approach to Multiple Testing. *J Roy Stat Soc B Met*; **57**: 289-300.

14. Kircher M, Witten DM, Jain P, O’Roak BJ, Cooper GM, Shendure J. (2014) A general framework for estimating the relative pathogenicity of human genetic variants. *Nat Genet*; **46**: 310-315.
15. Grantham R. (1974) Amino acid difference formula to help explain protein evolution. *Science*; **185**: 862-864.
16. Abd El-Aziz MM, O’Driscoll CA, Kaye RS, Barragan I, El-Ashry MF, Borrego S, Antinolo G, Pang CP, Webster AR, Bhattacharya SS. (2010) Identification of novel mutations in the ortholog of *Drosophila* eyes shut gene (EYS) causing autosomal recessive retinitis pigmentosa. *Invest Ophthalmol Vis Sci*; **51**: 4266-4272.
17. Abu-Safieh L, Alrashed M, Anazi S, Alkuraya H, Khan AO, Al-Owain M, Al-Zahrani J, Al-Abdi L, Hashem M, Al-Tarimi S, et al. (2013) Autozygome-guided exome sequencing in retinal dystrophy patients reveals pathogenetic mutations and novel candidate disease genes. *Genome Res*; **23**: 236-247.
18. Arai Y, Maeda A, Hirami Y, Ishigami C, Kosugi S, Mandai M, Kurimoto Y, Takahashi M. (2015) Retinitis Pigmentosa with EYS Mutations Is the Most Prevalent Inherited Retinal Dystrophy in Japanese Populations. *J Ophthalmol*; **2015**: 819760.
19. Audo I, Bujakowska KM, Leveillard T, Mohand-Said S, Lancelot ME, Germain A, Antonio A, Michiels C, Saraiva JP, Letexier M, et al. (2012) Development and application of a next-generation-sequencing (NGS) approach to detect known and novel gene defects underlying retinal diseases. *Orphanet J Rare Dis*; **7**: 8.
20. Audo I, Sahel JA, Mohand-Said S, Lancelot ME, Antonio A, Moskova-Doumanova V, Nandrot EF, Doumanov J, Barragan I, Antinolo G, et al. (2010) EYS is a major gene for rod-cone dystrophies in France. *Hum Mutat*; **31**: E1406-1435.
21. Bandah-Rozenfeld D, Littink KW, Ben-Yosef T, Strom TM, Chowers I, Collin RW, den Hollander AI, van den Born LI, Zonneveld MN, Merin S, et al. (2010) Novel null mutations in the EYS gene are a frequent cause of autosomal recessive retinitis pigmentosa in the Israeli population. *Invest Ophthalmol Vis Sci*; **51**: 4387-4394.
22. Beryozkin A, Zelinger L, Bandah-Rozenfeld D, Shevach E, Harel A, Storm T, Sagi M, Eli D, Merin S, Banin E, et al. (2014) Identification of mutations causing inherited retinal degenerations in the israeli and palestinian populations using homozygosity mapping. *Invest Ophthalmol Vis Sci*; **55**: 1149-1160.
23. Bonilha VL, Rayborn ME, Bell BA, Marino MJ, Pauer GJ, Beight CD, Chiang J, Traboulsi EI, Hollyfield JG, Hagstrom SA. (2015) Histopathological comparison of eyes from patients with autosomal recessive retinitis pigmentosa caused by novel EYS mutations. *Graefes Arch Clin Exp Ophthalmol*; **253**: 295-305.
24. Chen X, Liu X, Sheng X, Gao X, Zhang X, Li Z, Li H, Liu Y, Rong W, Zhao K, et al. (2015) Targeted next-generation sequencing reveals novel EYS mutations in Chinese families with autosomal recessive retinitis pigmentosa. *Sci Rep*; **5**: 8927.
25. Di Y, Huang L, Sundaresan P, Li S, Kim R, Ballav Saikia B, Qu C, Zhu X, Zhou Y, Jiang Z, et al. (2016) Whole-exome Sequencing Analysis Identifies Mutations in the EYS Gene in Retinitis Pigmentosa in the Indian Population. *Sci Rep*; **6**: 19432.

26. Eisenberger T, Neuhaus C, Khan AO, Decker C, Preising MN, Friedburg C, Bieg A, Gliem M, Charbel Issa P, Holz FG, et al. (2013) Increasing the yield in targeted next-generation sequencing by implicating CNV analysis, non-coding exons and the overall variant load: the example of retinal dystrophies. *PLoS One*; **8**: e78496.
27. Glockle N, Kohl S, Mohr J, Scheurenbrand T, Sprecher A, Weisschuh N, Bernd A, Rudolph G, Schubach M, Poloschek C, et al. (2014) Panel-based next generation sequencing as a reliable and efficient technique to detect mutations in unselected patients with retinal dystrophies. *Eur J Hum Genet*; **22**: 99-104.
28. Gonzalez-del Pozo M, Borrego S, Barragan I, Pieras JI, Santoyo J, Matamala N, Naranjo B, Dopazo J, Antinolo G. (2011) Mutation screening of multiple genes in Spanish patients with autosomal recessive retinitis pigmentosa by targeted resequencing. *PLoS One*; **6**: e27894.
29. Gu S, Tian Y, Chen X, Zhao C. (2016) Targeted next-generation sequencing extends the phenotypic and mutational spectrums for EYS mutations. *Mol Vis*; **22**: 646-657.
30. Habibi I, Chebil A, Falfoul Y, Allaman-Pillet N, Kort F, Schorderet DF, El Matri L. (2016) Identifying mutations in Tunisian families with retinal dystrophy. *Sci Rep*; **6**: 37455.
31. Hashmi JA, Albarry MA, Almatrafi AM, Albalawi AM, Mahmood A, Basit S. (2017) Whole exome sequencing identified a novel single base pair insertion mutation in the EYS gene in a six generation family with retinitis pigmentosa. *Congenit Anom (Kyoto)*.
32. Huang XF, Huang F, Wu KC, Wu J, Chen J, Pang CP, Lu F, Qu J, Jin ZB. (2015) Genotype-phenotype correlation and mutation spectrum in a large cohort of patients with inherited retinal dystrophy revealed by next-generation sequencing. *Genet Med*; **17**: 271-278.
33. Huang Y, Zhang J, Li C, Yang G, Liu M, Wang QK, Tang Z. (2010) Identification of a novel homozygous nonsense mutation in EYS in a Chinese family with autosomal recessive retinitis pigmentosa. *BMC Med Genet*; **11**: 121.
34. Iwanami M, Oshikawa M, Nishida T, Nakadomari S, Kato S. (2012) High prevalence of mutations in the EYS gene in Japanese patients with autosomal recessive retinitis pigmentosa. *Invest Ophthalmol Vis Sci*; **53**: 1033-1040.
35. Jinda W, Taylor TD, Suzuki Y, Thongnoppakhun W, Limwongse C, Lertrit P, Suriyaphol P, Trinavarat A, Atchaneeyasakul LO. (2014) Whole exome sequencing in Thai patients with retinitis pigmentosa reveals novel mutations in six genes. *Invest Ophthalmol Vis Sci*; **55**: 2259-2268.
36. Kastner S, Thiemann IJ, Dekomien G, Petrasch-Parwez E, Schreiber S, Akkad DA, Gerding WM, Hoffjan S, Gunes S, Gunes S, et al. (2015) Exome Sequencing Reveals AGBL5 as Novel Candidate Gene and Additional Variants for Retinitis Pigmentosa in Five Turkish Families. *Invest Ophthalmol Vis Sci*; **56**: 8045-8053.
37. Katagiri S, Akahori M, Hayashi T, Yoshitake K, Gekka T, Ikeo K, Tsuneoka H, Iwata T. (2014) Autosomal recessive cone-rod dystrophy associated with compound heterozygous mutations in the EYS gene. *Doc Ophthalmol*; **128**: 211-217.
38. Khan MI, Collin RW, Arimadyo K, Micheal S, Azam M, Qureshi N, Faradz SM, den Hollander AI, Qamar R, Cremers FP. (2010) Missense mutations at homologous positions in the fourth and fifth



- laminin A G-like domains of eyes shut homolog cause autosomal recessive retinitis pigmentosa. *Mol Vis*; **16**: 2753-2759.
39. Littink KW, Koenekoop RK, van den Born LI, Collin RW, Moruz L, Veltman JA, Roosing S, Zonneveld MN, Omar A, Darvish M, et al. (2010) Homozygosity mapping in patients with cone-rod dystrophy: novel mutations and clinical characterizations. *Invest Ophthalmol Vis Sci*; **51**: 5943-5951.
  40. Neveling K, Collin RW, Gilissen C, van Huet RA, Visser L, Kwint MP, Gijzen SJ, Zonneveld MN, Wiskamp N, de Ligt J, et al. (2012) Next-generation genetic testing for retinitis pigmentosa. *Hum Mutat*; **33**: 963-972.
  41. Nishiguchi KM, Tearle RG, Liu YP, Oh EC, Miyake N, Benaglio P, Harper S, Koskiniemi-Kuendig H, Venturini G, Sharon D, et al. (2013) Whole genome sequencing in patients with retinitis pigmentosa reveals pathogenic DNA structural changes and NEK2 as a new disease gene. *Proc Natl Acad Sci U S A*; **110**: 16139-16144.
  42. Oishi M, Oishi A, Gotoh N, Ogino K, Higasa K, Iida K, Makiyama Y, Morooka S, Matsuda F, Yoshimura N. (2014) Comprehensive molecular diagnosis of a large cohort of Japanese retinitis pigmentosa and Usher syndrome patients by next-generation sequencing. *Invest Ophthalmol Vis Sci*; **55**: 7369-7375.
  43. O'Sullivan J, Mullaney BG, Bhaskar SS, Dickerson JE, Hall G, O'Grady A, Webster A, Ramsden SC, Black GC. (2012) A paradigm shift in the delivery of services for diagnosis of inherited retinal disease. *J Med Genet*; **49**: 322-326.
  44. Perez-Carro R, Corton M, Sanchez-Navarro I, Zurita O, Sanchez-Bolivar N, Sanchez-Alcudia R, Lelieveld SH, Aller E, Lopez-Martinez MA, Lopez-Molina MI, et al. (2016) Panel-based NGS Reveals Novel Pathogenic Mutations in Autosomal Recessive Retinitis Pigmentosa. *Sci Rep*; **6**: 19531.
  45. Pieras JI, Barragan I, Borrego S, Audo I, Gonzalez-Del Pozo M, Bernal S, Baiget M, Zeitz C, Bhattacharya SS, Antinolo G. (2011) Copy-number variations in EYS: a significant event in the appearance of arRP. *Invest Ophthalmol Vis Sci*; **52**: 5625-5631.
  46. Pierrottet CO, Zuntini M, Digiuni M, Bazzanella I, Ferri P, Paderni R, Rossetti LM, Cecchin S, Orzalesi N, Bertelli M. (2014) Syndromic and non-syndromic forms of retinitis pigmentosa: a comprehensive Italian clinical and molecular study reveals new mutations. *Genet Mol Res*; **13**: 8815-8833.
  47. Siemiatkowska AM, Arimadyo K, Moruz LM, Astuti GD, de Castro-Miro M, Zonneveld MN, Strom TM, de Wijs IJ, Hoefsloot LH, Faradz SM, et al. (2011) Molecular genetic analysis of retinitis pigmentosa in Indonesia using genome-wide homozygosity mapping. *Mol Vis*; **17**: 3013-3024.
  48. Suto K, Hosono K, Takahashi M, Hiram Y, Arai Y, Nagase Y, Ueno S, Terasaki H, Minoshima S, Kondo M, et al. (2014) Clinical phenotype in ten unrelated Japanese patients with mutations in the EYS gene. *Ophthalmic Genet*; **35**: 25-34.
  49. Consugar MB, Navarro-Gomez D, Place EM, Bujakowska KM, Sousa ME, Fonseca-Kelly ZD, Taub DG, Janessian M, Wang DY, Au ED, et al. (2015) Panel-based genetic diagnostic testing

- for inherited eye diseases is highly accurate and reproducible, and more sensitive for variant detection, than exome sequencing. *Genet Med*; **17**: 253-261.
50. Ge Z, Bowles K, Goetz K, Scholl HP, Wang F, Wang X, Xu S, Wang K, Wang H, Chen R. (2015) NGS-based Molecular diagnosis of 105 eyeGENE((R)) probands with Retinitis Pigmentosa. *Sci Rep*; **5**: 18287.
  51. Haer-Wigman L, van Zelst-Stams WA, Pfundt R, van den Born LI, Klaver CC, Verheij JB, Hoyng CB, Breuning MH, Boon CJ, Kievit AJ, et al. (2017) Diagnostic exome sequencing in 266 Dutch patients with visual impairment. *Eur J Hum Genet*; **25**: 591-599.
  52. Xu Y, Guan L, Shen T, Zhang J, Xiao X, Jiang H, Li S, Yang J, Jia X, Yin Y, et al. (2014) Mutations of 60 known causative genes in 157 families with retinitis pigmentosa based on exome sequencing. *Hum Genet*; **133**: 1255-1271.
  53. Yoon CK, Kim NK, Joung JG, Shin JY, Park JH, Eum HH, Lee HO, Park WY, Yu HG. (2015) The diagnostic application of targeted re-sequencing in Korean patients with retinitis pigmentosa. *BMC Genomics*; **16**: 515.
  54. Slijkerman RW, Song F, Astuti GD, Huynen MA, van Wijk E, Stieger K, Collin RW. (2015) The pros and cons of vertebrate animal models for functional and therapeutic research on inherited retinal dystrophies. *Prog Retin Eye Res*; **48**: 137-159.
  55. Wiley LA, Burnight ER, Mullins RF, Stone EM, Tucker BA. (2014) Stem cells as tools for studying the genetics of inherited retinal degenerations. *Cold Spring Harb Perspect Med*; **5**: a017160.
  56. Sangermano R, Bax NM, Bauwens M, van den Born LI, De Baere E, Garanto A, Collin RW, Goercharn-Ramlal AS, den Engelsman-van Dijk AH, Rohrschneider K, et al. (2016) Photoreceptor Progenitor mRNA Analysis Reveals Exon Skipping Resulting from the ABCA4 c.5461-10T-->C Mutation in Stargardt Disease. *Ophthalmology*; **123**: 1375-1385.
  57. Sander JD, Joung JK. (2014) CRISPR-Cas systems for editing, regulating and targeting genomes. *Nat Biotechnol*; **32**: 347-355.

## 2.9 Supplemental information

## Supplementary Figure S1.

Multiple sequence alignment of EYS protein in different species.

Human	(1)	--MTDKSIVILSLVVFHSSFFINGKTCRRQLVVEWHHPQSSSVVNVNWTITENICLDYRDCWFICVN-TKIDTSGNQAVPC
Macaque	(1)	--MTDKSIVILSLVVFHSSFFINGKTCRRQLVVEWHHPQSSSVVNVNWTITENICLDYRDCWFICVN-TKIDTSGNQAVPC
Pig	(1)	--MTNKLNTVTLVVFHSLMGLNKTKCRHLVVEWHHPQSSSVVNVNWTITENICLDYRDCWFICVN-TKIDTSGNHVPC
Chicken	(1)	--MTPKSTHIVLVCFLICIKKQIICRRQLVVEWHHPQSSSVVNVNWTITENICLDYRDCWFICVN-TKIDTSGNHVPC
Zebrafish	(1)	MRNPKLAIIVFLSLCYLGFYSQVTRRATSRREWHHPQSSSVVNVNWTITENICLDYRDCWFICVN-TKIDTSGNHVPC
		Signal peptide
Human	(77)	ICFLQIQQLGDFLIVISSEPSLQPEINIMNVSETSFVGCVQNTTTEDCLLGGCLKCMHTVNSRWISVCTHYFHTVMASGF
Macaque	(77)	ICFLQIQQLGDFLIVISSEPSLQPEINIMNVSETSFVGCVQNTTTEDCLLGGCLKCMHTVNSRWISVCTHYFHTVMASGF
Pig	(78)	ICFLQIQQLGDFLIVISSEPSLQPEINIMNVSEASITDQNTTTEDCLLGGCLKCMHTVNSRWISVCTHYFHTVMANGK
Chicken	(77)	ICFLQIQQLGDFLIVISSEPSFQVYGNLIMNVSEETINPKIGFLQDQLEVCQICGHOVDSSWISVCTHYFAEIKHRGF
Zebrafish	(81)	ICFEIQQLGDFLIVISADGILDQHGVLKVSKEEEDKAIILEPRKQQLVASSNITLQVESRWISVCTHYFHTVMASGF
Human	(157)	SPPCLGLRLNIVVNRQFCQESLSSEFCSGHCKLSEANSKTYSCHQPPFSGKYQELDACSERCKKNNGSCHNKRENWD
Macaque	(157)	SPPCLGLRLNIVVNRQFCQESLSSEFCSGHCKLSEANSKTYSCHQPPFSGKYQELDACSERCKKNNGSCHNKRENWD
Pig	(158)	SICQLGLRLNIVVNRQFCQEQSSSEFCSGHCKLSEANSKTYSCHQPPFSGKYQELDACSERCKKNNGSCHNKRETNW
Chicken	(157)	YLNCGLRLNIVVNRQFCQEPNIPICSGHCKLSEANSKTYSCHQPPFSGKYQELDACSERCKKNNGSCHNKRETNW
Zebrafish	(161)	HLCPGLRLNIVVNRQFCQSSPLLRICSGHCKLSEANSKTYSCHQPPFSGKYQELDACSERCKKNNGSCHNKRETNW
		EGF domain
Human	(237)	IQ-NYRCVCPPEFHGKNCSEITIG-QCQPHVCFHGNCSNITSNSTFCEDDEQFSQPFCEVSAKHQVSLLFIKRGCNPNSS
Macaque	(237)	IQ-NYRCVCPPEFHGKNCSEITIG-QCQPHVCFHGNCSNITSNSTFCEDDEQFSQPFCEVSAKHQVSLLFIKRGCNPNSS
Pig	(238)	KQ-NYRCVCPPEFHGKNCSEITIG-KCQPHVCFHGNCSNITSNSTFCEDDEQFSQPFCEVSAKHQVSLLFIKRGCNPNSS
Chicken	(237)	N-NYRCVCPPEFHGKNCSEITIG-QCQPHVCFHGNCSNITSNSTFCEDDEQFSQPFCEVSAKHQVSLLFIKRGCNPNSS
Zebrafish	(241)	ILPEVYCPPEFHGKNCSEITIGNONCSKWKCKGALKVSSTSRCEFTGVCNCRKRRLKCSNFCRNDRGRCEETAN
		EGF domain
Human	(315)	IYTYCPKGSISONGITDVSSEFLVPCQNGTDCIKISNDVMCICSPIFTDLICKSQTSCSEFPLRNNATCKKCEKIP
Macaque	(315)	IYTYCPKGSISONGITDVSSEFLVPCQNGTDCIKISNDVMCICSPIFTDLICKSQTSCSEFPLRNNATCKKCEKIP
Pig	(307)	-----QN-----YITDVSSEFLVPCQNGTDCIITPKDMCCLPIFTDKIKKHQHPHEAFCRHTKATDKYEEIYK
Chicken	(314)	IYICCPAGFLGDDQVDINECSSRRCQNGTDCIITDNDVSCSCLPFTKQCFERILNPELPLPLNATCISEQOYK
Zebrafish	(321)	IYVTCPCGFLGLNCEITTAEADLYCKSSGCQLDEACATDKLNAICICVDPELEQAQVQGLPLPLNGICITVPLNGYK
		EGF domain
Human	(395)	SCISGTEKNCCKATIEHCKLLSINCLNEEWCENITGRFRYVCPGCTNPFVFLRNVLHILHPEYVC-----
Macaque	(395)	SCMSGTEKNCCKVTDIEHCKLLSINCLNEEWCENITGRFRYVCPGCTNPFVFLRNVLHILHPEYVC-----
Pig	(375)	SFMFGTEKNCCKVTDIEHCKLLSINCLNEEWCENITGRFRYVCPGCTNPFVFLRNVLHILHPEYVC-----
Chicken	(394)	RCMFSGTEKNCCKVIDIEHCKLLSINCLNEEGLCLNITIGGTCICAFGMEFCQVAENACLIIPKSSGTCIDMSQLQEG
Zebrafish	(400)	RCRQGFSGTEKNCCKVIDIEHCKLLSINCLNEEGLCLNITIGGTCICAFGMEFCQVAENACLIIPKSSGTCIDMSQLQEG
		EGF-CA domain
Human	(463)	-----VTFHGLQDKGP--AQFYYVWQLGFASSGCEKQGVIDYFFFLAANGTADATYVNDPED
Macaque	(463)	-----VTFHGLQDKGP--AHFYYVWQLGFASSGCEKQGVIDYFFFLAANGTADATYVNDPED
Pig	(443)	-----AISHNIOAEDASPPQFKYVWRGLGSSGCEKQGVIDYFFFLAANGTADATYVNDPED
Chicken	(474)	PLFQCLCPHGTGEFCCKVQINDCNSTENGCTCVNEDDFKCCPMEFEGCEEDIDVCLFENISCAPGAVCNKSHG
Zebrafish	(480)	PHYMCTCLPGTYGTYCEAEVNECDSSPQHQGCTCTDFVGYKCTCPSYGTICDCEIDINCLPLNATCPPPTICVDLEGD
Human	(520)	INSQCFPEHGETEFCANGCSCLSEEDSQEYRYLCFLRWAGMYLENITDDQENECQHEAVKDEINPRCSLSIYIGR
Macaque	(520)	INSQCFPEHGETEFCANGCSCLSEEDSQEYRYLCFLRWAGMYLENITDDQENECQHEAVKDEINPRCSLSIYIGR
Pig	(502)	LGHVCFWLHEGKREVSNGRCLEENNKRYOCLIPFWLCKMYLENITDYENECQHEAVKDEINPRCSLSIYIGR
Chicken	(554)	FNYVCLSPGIGKTEVFCANGSCFYDEGNQRSHCVAGHGTGTCLENINCEINOCAGATCEDEVNYRICHPLGYTGT
Zebrafish	(560)	LFPKHTPCPHYLQPCANGSHCLHN-ITSYSCVAPGWTGATCEVNEINCVQHRCCNRATCVDEGGYSCLCGHGYTGT
		EGF domain
Human	(600)	LCVNVNDYCLNGHSISVHGLCHALSINCNCSGCFQYERNICETITEDCKSASRNG-----
Macaque	(600)	LCVNVNDYCLNGHSISVHGLCHALSINCNCSGCFQYERNICETITEDCKSASRNG-----
Pig	(582)	FYIVSVDCLGSQNTSVHGLCHVHLSGNFICPQICERHICETITEDGEPAPRNG-----
Chicken	(634)	FCEIDIDNGLGNQCSEHGFQDHLFNYSICICLGYGGPFCVEINQESSPRTNNGICMNLIGSFSCHCAEGFKGETCT
Zebrafish	(639)	HCEIDDFCSGHQC---SEHAVGVDQCENYTRCRLGYEGTICETITEDCKSASRNG-----
Human	(656)	-----
Macaque	(656)	-----
Pig	(638)	-----
Chicken	(713)	AHVNECLDRPCWNGGTECEDINGFKNCPLGFEGLNCEINFDECTYGFCKNNSICLDLIA--DYSCVCPGFTDKNCSTD
Zebrafish	(716)	ESMNECWSRPCNNGGSCIDLVDNYICNCPGLFGTHDCSMPATGCTSNFCNTKGTSMCEQQDGFKCVCHGHTGLFCETS
Human	(656)	-----
Macaque	(656)	-----
Pig	(638)	-----
Chicken	(791)	IDECAFKPCQNGGHCHNLIGFYCSCLPGFTGQFCEADVAACLSPQCGASSICKDMSDGVVFCAPFGIGNNCEIEVDEC
Zebrafish	(796)	INHCVGLCHHGSECVDLTKGFMECLPGLRGLCEVNIIDCLDKPCGALSIKCKDGINAYDFCPCAPFGVGNCEIEVDEC



Human	(1581)	HFYETFWMNSAILASWYALMGAQITISGHFSFSSATEITPSVAFTEVPSLFFSPKSKAKRTILSSSIEESITLSSNLDVNLIC
Macaque	(1581)	HFYETFWMNSAILASWYALMGAQITISGHFSFSSATEITPSVAFTEVPSLFFSPKSKAKRTILSSSIEESITLSSNLDVNLIC
Pig	(1565)	QFYETFSMYAILASWYALMGQTTTISGHFSFSSSEIEMPSVAITEPSSLFFSPKSKTKRRILVSSVEEYITQSSNLDANLC
Chicken	(1642)	-----
Zebrafish	(1647)	-----
Human	(1661)	LDKTCLSIIVPSQTSISDLNNSDLTSEKTTDLSVSENLKLLKTRQYGITMGPTLELNQDSLLDEKSKGSHTPFKLHPS
Macaque	(1661)	LHKTKCLSIIVPSQTSISDLNNSDLTSEKTTDLSVSENLKLLKTRQYGITMGPTLELNQDSLLDEKSKGSHTPFKLHPS
Pig	(1645)	LNMCLSIIVPSQTSISDLTNSDLTSEKTKGFLIGSENLKLLKIGHYGITMDPTELELNQKLLIQEHESSQTPSKLHAR
Chicken	(1642)	-----
Zebrafish	(1647)	-----
Human	(1741)	DSLDFELNLQIPDVLTKTYSBITLNDFKNNLPPLTGSVPDFSEVTLNFAFVTVSAIPALPIQTSSSMVITPDWPY-
Macaque	(1741)	DSSLDFELNLRSIPDVLTKTYSBITLNDLKNLPPLTGSVPDFSEVTLNFAFVTVSAIPALPIQTSSSMVITPDWPY-
Pig	(1725)	DCSLDFELNLRSIE-----ETMHSDDLKSNLPPSIDSTDFSEVSSHITFSAVSAQIFPIQTSVPMSVITPDWTYT
Chicken	(1642)	-----
Zebrafish	(1647)	-----
Human	(1820)	-FDYIMSLKKEVETISEWSKWELOQPSVQYQEFPTASRHPPFTRSLLSLSESLVAPQRLMISDFSCVRYGDSVLEFQN
Macaque	(1820)	-FDYIMSLNKKEVETISEWSKWELOQPSVQYQEFPTASWHPPFTRSLLSLSESLVAPQRLMISDFSCVRYGDSVLEFQN
Pig	(1797)	DLLNLTLYKENTETISEWSKWELOQPSGHGQESPAASQRISITRSLLSLSELEIPASFWLKIISDFSCVRYGDSVLEFQN
Chicken	(1642)	-----
Zebrafish	(1647)	-----
Human	(1899)	VALNPNNSISLEFCTSSVYGLLYLKQDSNVDGFIQLIETENGILVYFVCPGGEAKFKSINLTVRVNDSOKYTLIIRQE
Macaque	(1899)	VVLNPNNSISLEFCTSSVYGLLYLKQDSNVDGFIQLIETENGILVYFVCPGGEAKFKSINLTVRVNDSOKYTLIIRQE
Pig	(1877)	VFLNPNNSISLEFCTSSVYGLLYLKQDPDADGFFQLIETENGILVYFVCPGGEAKFKSINLTVRVNDSOKYTLIIRQE
Chicken	(1658)	LHNQVNFTHLEPTEKPCDLYLIEESSETLCELIQLIETRHCHLYVYVCGATKKNLITARVDDQWYKTLIQRON
Zebrafish	(1656)	FEIIVPISVITRECTESMGTLLYS--ASAKRSVFEKLIETENGILVYFVCPGGEAKFKSINLTVRVNDSOKYTLIIRQE
		Laminin-G domain
Human	(1979)	LDFPCAEITLILGRNTQICESINHWLKGKPLPISGVSFVIGGEPDLHGKIQVPEVHNITGCEVETIENNWRSFIPSKAVRNY
Macaque	(1979)	LDFPCAEITLILGRNTQICESINHWLKGKPLPISGVSFVIGGEPDLRGKIQVPEVHNITGCEVETIENNWRSFIPSKAVRNY
Pig	(1957)	LDFPCAEITLILGRNTQIKASKSINHWLKGKPLPISGVSFVIGGEPDLHGKIQVPEVHNITGCEVETIENNWRSFIPSKAVRNY
Chicken	(1738)	YKPCAEITLILVSAKTGIPSNFSSSPYGLIIGSIFVGGEPYSSIKQIPBEVHNITGCEVETIENNWRSFIPSKAVRNY
Zebrafish	(1734)	LDFPCAEITVSEVTRVRSAPCNITSLRLQKIDHVFVIGGEPHRSRSPYKEAPEHNITGCEVETIENKILRSEHMDHAAIAGN
		Laminin-G domain
Human	(2059)	HINNCRSQGFMLSPTASFVDSVDVTOGVDT--WTSVSPSVAAPSVQDDVCHNGGTCRAIFSSGIIISFCDCDLHFTG
Macaque	(2059)	HINNCRSQGLMLSPTASFVDSVDVTOGVDA--WTSVSPSVAAPSVQDDVCHNGGTCRAIFSSGIIISFCDCDLHFTG
Pig	(2037)	HIDSRQDSTPAAANSVAPSRATLQAGS--FCISLAP-HLAPLQGGPVCNNGGTCRSLLLEGAGSFCDCDLHFTG
Chicken	(1818)	NIDSRIPVPHLPTFPPTFSDVLAPEL--WTPSLSS-PELPSVQGGIICHNGGTCRHSIPGALISFCDCDLHFTG
Zebrafish	(1814)	NIDNCRSQWHHEPPTSTHSPHILITETPPGEVWRVLSPTQAPVPOGICLNNGTCRHSIPGASFCDCDLHFTG
		EGF domain
Human	(2137)	RCECDAGLFFRPSNGNSVLELFFLK-----FVLEKEHNRTVITVLAIKTNSLNGTILVSNGNCFKQETHLLEVEGR
Macaque	(2137)	RCECDAGLFFRPSNGNSVLELFFLN-----FVLEKEHNRTVITVLAIKTNSLNGTILVSNGNCFKQETHLLEVEGR
Pig	(2114)	RCECDAGLFFRPSNGNSVLELFFFTQEE-LKFVLEKEHNRTVITVLAIKTNSLNGTILVSNSEKNEQREHLLEVEGR
Chicken	(1895)	RCECDVTLFFRPSNGNSVLELPSLTSVSO-MRTASGOETSNLTIYVLAIKTNSLNGTILVSNSEKNEQREHLLEVEGR
Zebrafish	(1894)	RICECDITTFRPSFDGNSVLELPSLTSLFQSDTFFPSSEDEKRTVLAIKRIRPSSLVCREDLEREFHLLEQNDR
		Laminin-G domain
Human	(2210)	PSVKYCGGNSQNILTVSANYSININAFPTITIRYTFVGSFGVQMEIEMADGKPPVQKQDTEISHASQAVFBSMFLGHI
Macaque	(2210)	PSVKYCGGNSQNILTVSANYSININAFPTITIRYTFVGSFGVQMEIEMADGKPPVQKQDTEISHASQAVFBSMFLGHI
Pig	(2193)	PVVKYCGGSSQNILTVSANYSININAFPTITIRYTFVGSFGVQMEIEMADGKPLRKEDEVETPQDFQGYEERKFLGHI
Chicken	(1974)	PAVRESCGNSQNILTVSNQIISKGIFLPIIISYMPVWSLEGYQMEIEMADRNPPVQHLHLHSYQASQITFGSTFLGN
Zebrafish	(1974)	AVARLCCG-NHILTAVAAQNRIDSLVAITVRYALPSQNNQICETIEMADNGTANQQKYMPDEVSEVFSPTFLGGF
		Laminin-G domain
Human	(2290)	PENVQIHKKAGPVYGFPGCITLDLVNNEKEFFIIDBARHSENIENCHVPMCAHHICRNNGTCSNENLFCBCPRLYSGKL
Macaque	(2290)	PENVQIHKKAGSVYGFPGCITLDLVNNEKEFFIIDBARRSENIENCHVPMCAHHICRNNGTCSNENLFCBCPRLYSGKL
Pig	(2273)	PENVKIKKNAGHYGFGCITLDLVNNEKEFFIIDBARRSENIENCLHCHCAHHICRNNGTCSNENLFCBCPRLYSGKL
Chicken	(2054)	PVHKIEPCRCRIRGKYGGRDFVANNKELFIIDALCENNIENCHVPMCAHHICRNNGTCSNENLFCBCPRLYSGKL
Zebrafish	(2053)	PSVTEIHNHNSVSGYGFPGCITRDLVSGKELVYGEARFSENIENCHVPMCAHHICRNNGTCSNENLFCBCPRLYSGKL
		Laminin-G domain
		EGF domain
Human	(2370)	COFASCENNPCNGATCQVFKSGTDIVCLCPYGRSGLCTDAINTQCFRSGDAFGYTSFLAYSRSIDISFHYEFHQRFO
Macaque	(2370)	COFASCENNPCNGATCQVFKSGTDIVCLCPYGRSGLCTDAINTQCFRSGDAFGYTSFLAYSRSIDISFHYEFHQRFO
Pig	(2353)	COFASCENNPCNGATCQVFKSGTDIVCLCPYGRSGLCTDAINTQCFRSGDAFGYTSFLAYSRSIDISFHYEFHQRFO
Chicken	(2134)	COFALCESENCGATCFRKSQDIVCLCPYGRSGLCLNDVINTQCFRSGDAFGYTSFLAYSRSIDISFHYEFHQRFO
Zebrafish	(2133)	COFTACERNPCNGATCQVQLAAALCLCPYGRSGLCTDAINTQCFRSGDAFGYTSFLAYSRSIDISFHYEFHQRFO
		EGF domain
Human	(2450)	LANNHSLQNNLIFFTQKQKGLNGDDEFLAVGGLLNGSVVWSYNLGSGTASIRSDPFLNLSLGFHTVHLKRFQEGWLVKVD
Macaque	(2450)	LANNHSLQNNLIFFTQKQKGLNGDDEFLAVGGLLNGSVVWSYNLGSGTASIRSDPFLNLSLGFHTVHLKRFQEGWLVKVD
Pig	(2433)	LADDSAVQDNLIFFTQKQKGRANGDDEFLAVGGRGRVWWSYNLGSGTASIRSDPFLNLSLGFHTVHLKRFQEGWLVKVD
Chicken	(2214)	LLNHSLQDNLIFFTQKQKGLNGDDEFLVGLCPGRVWWSYNLGSGTASIRSDPFLNLSLGFHTVHLKRFQEGWLVKVD
Zebrafish	(2213)	FANNASALRNNLIFFTQKQKGLSDDDEFLAVGRNGRIVWWSYNLGSGTASIRSDPFLNLSLGFHTVHLKRFQEGWLVKVD
		Laminin-G domain



**Supplementary Table S1.**

Rules for combining criteria to classify sequence variants.

<b>Pathogenic</b>	(i)	1 Very strong (PVS1) <i>AND</i> (a) $\geq 1$ Strong (PS1–PS4) <i>OR</i> (b) $\geq 2$ Moderate (PM1–PM6) <i>OR</i> (c) 1 Moderate (PM1–PM6) and 1 supporting (PP1–PP5) <i>OR</i> (d) $\geq 2$ Supporting (PP1–PP5)
	(ii)	$\geq 2$ Strong (PS1–PS4) <i>OR</i>
	(iii)	1 Strong (PS1–PS4) <i>AND</i> (a) $\geq 3$ Moderate (PM1–PM6) <i>OR</i> (b) 2 Moderate (PM1–PM6) <i>AND</i> $\geq 2$ Supporting (PP1–PP5) <i>OR</i> (c) 1 Moderate (PM1–PM6) <i>AND</i> $\geq 4$ Supporting (PP1–PP5)
	<hr/>	
<b>Likely pathogenic</b>	(i)	1 Very strong (PVS1) <i>AND</i> 1 moderate (PM1–PM6) <i>OR</i>
	(ii)	1 Strong (PS1–PS4) <i>AND</i> 1–2 moderate (PM1–PM6) <i>OR</i>
	(iii)	1 Strong (PS1–PS4) <i>AND</i> $\geq 2$ supporting (PP1–PP5) <i>OR</i>
	(iv)	$\geq 3$ Moderate (PM1–PM6) <i>OR</i>
	(v)	2 Moderate (PM1–PM6) <i>AND</i> $\geq 2$ supporting (PP1–PP5) <i>OR</i>
	(vi)	1 Moderate (PM1–PM6) <i>AND</i> $\geq 4$ supporting (PP1–PP5)
<hr/>		
<b>Benign</b>	(i)	1 Stand-alone (BA1) <i>OR</i>
	(ii)	$\geq 2$ Strong (BS1–BS4)
<hr/>		
<b>Likely benign</b>	(i)	1 Strong (BS1–BS4) and 1 supporting (BP1–BP7) <i>OR</i>
	(ii)	$\geq 2$ Supporting (BP1–BP7)
<hr/>		
<b>Uncertain significance</b>	(i)	Other criteria shown above are not met <i>OR</i>
	(ii)	The criteria for benign and pathogenic are contradictory

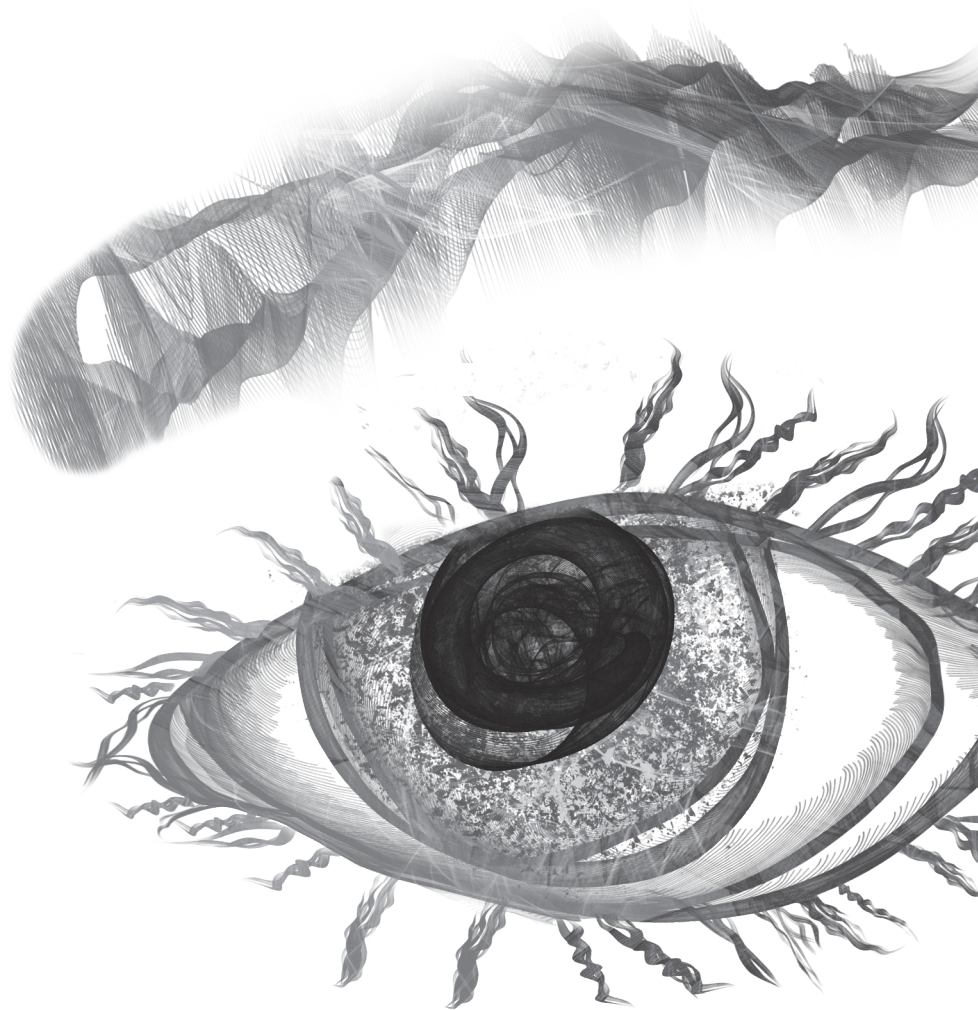
**Supplementary Table S2.**Overview of all *EYS* variants.

Overview of all *EYS* variants, with separate tabs for protein-truncating mutations, missense variants, splice site variants, silent variants and in-frame indels, and variants detected in the 5'-UTR. The following principles are taken into account by scoring the pathogenic evidence as very strong (PVS1): **A** loss of function is a known mechanism of disease, **B** variants are located upstream of the most 3' truncating variant reported as pathogenic, **C** the impact of splice-site variants is confirmed by functional analysis, **D** alternate gene transcripts which are biologically relevant do not play a role, and **E** null-alleles are described disease causing in other patients.<sup>12</sup> This table is available online via: <https://doi.org/10.1002/humu.23371>.





# Chapter 3



# Extending the spectrum of *EYS*-associated retinal disease to macular dystrophy

Laurence H.M. Pierrache<sup>1,2,3,4</sup>, Muriël Messchaert<sup>5,6</sup>,  
Alberta A.H.J. Thiadens<sup>3</sup>, Lonneke Haer-Wigman<sup>5</sup>,  
Yvonne de Jong-Hesse<sup>7</sup>, Wendy A.G. van Zelst-Stams<sup>5</sup>,  
Rob W.J. Collin<sup>5,6</sup>, Caroline C.W. Klaver<sup>3,4,8</sup>,  
L. Ingeborgh van den Born<sup>1,2</sup>

<sup>1</sup> The Rotterdam Eye Hospital, Rotterdam, The Netherlands.

<sup>2</sup> Rotterdam Ophthalmic Institute, Rotterdam, The Netherlands.

<sup>3</sup> Department of Ophthalmology, Erasmus Medical Center, Rotterdam, the Netherlands.

<sup>4</sup> Department of Epidemiology, Erasmus Medical Center, Rotterdam, the Netherlands.

<sup>5</sup> Department of Human Genetics, Radboud University Medical Center, Nijmegen, the Netherlands.

<sup>6</sup> Donders Institute for Brain, Cognition and Behaviour, Radboud University Medical Center, Nijmegen, the Netherlands.

<sup>7</sup> Department of Ophthalmology, Amsterdam Medical Center, VU University Medical Center, Amsterdam, The Netherlands.

<sup>8</sup> Department of Ophthalmology, Radboud University Medical Center, Nijmegen, the Netherlands.

**Abstract**

Inherited retinal diseases (IRDs) are a heterogeneous group of genetic eye diseases. Mutations in *Eyes shut homolog* (*EYS*) are one of the most common causes of autosomal recessive (ar) retinitis pigmentosa (RP), but have also been described in patients with cone-rod dystrophy (CRD). The aim of this study was to assess the phenotypic variability and natural course of IRDs caused by *EYS* mutations. We performed a multiethnic cohort study (N=30) with biallelic *EYS* variants from a clinical IRD database (RP (N=27), CRD (N=1), and macular dystrophy (N=2)). Medical records were reviewed to extract medical history, visual function testing and retinal imaging. An *in vitro* minigene splice assay was performed to determine the effect on *EYS* pre-mRNA splicing of the c.1299+5\_1299+8del variant in macular dystrophy patients. We found 27 different *EYS* variants in RP patients, seven of these were novel. Eleven RP patients met low vision criteria (visual field <20°) at first examination. The rate of visual field loss of the V4 isopter area was 9% per year. Four patients became visually impaired (visual acuity >0.3logMAR), the rate of visual acuity loss was 0.75 EDTRS letters/year. An isolated CRD patient carried a homozygous *EYS* variant (c.9405T>A) that was previously identified in RP patients. Two siblings with macular dystrophy, carried compound heterozygous *EYS* variants: c.1299+5\_1299+8del and c.6050G>T. The former was novel and shown to result in skipping of exon 8, the latter was a known RP variant. In conclusion, we report on *EYS*-associated macular dystrophy, thereby extending the spectrum of *EYS*-associated retinal disease. We observed heterogeneity between RP patients in age of onset and disease progression. Identical *EYS* variants were found in cases with RP, CRD, and macular dystrophy. Screening for *EYS* variants in CRD and macular dystrophy patients might increase the diagnostic yield in previously unsolved cases.

**Key words:**

*EYS*, disease spectrum, retinal dystrophy

### 3.1 Introduction

Inherited retinal diseases (IRDs) are a heterogeneous group of genetic eye diseases characterized by progressive degeneration of photoreceptor and/or retinal pigment epithelium (RPE) cells, leading to severe visual impairment and blindness. Retinitis pigmentosa (RP), a rod-cone dystrophy, is the most common subtype of IRD with an estimated prevalence of 1 in 4000 individuals.<sup>1</sup> Patients report night blindness, and visual field constriction from early adolescence and gradually decreasing visual acuity later in life. Over 250 genes have been described to be mutated in IRD, of which several can be mutated in different clinical subtypes of IRD.<sup>2</sup>

Eyes shut homolog (*EYS*; OMIM: 612424) was first reported in 2008 by two independent groups,<sup>3,4</sup> and both described this gene as the human ortholog of the *Drosophila* 'eyes shut' (*eyes*), also known as Spacemaker (*spam*). Mutations in *EYS* account for ~5-35% of European and Asian autosomal recessive retinitis pigmentosa (arRP) cases,<sup>5-11</sup> but have also been described in three patients with autosomal recessive cone-rod dystrophy (CRD).<sup>4,12,13</sup> *EYS* is located on chromosome 6p12 (*RP25* locus), spans over 2 Mb, and consists of 44 exons that together code for a protein that is predicted to harbor 28 epidermal growth factor-like (EGF) domains and five Laminin A G-like (LamG) domains. There are at least four isoforms, all of which are expressed in the human retina.<sup>14</sup> The *Drosophila* ortholog plays an important role in retinal morphogenesis and architecture.<sup>15</sup> In zebrafish, *Eys* is expressed in the outer segments and connecting cilium/transition zone (CC/TZ) of both rod and cone photoreceptors.<sup>16-18</sup> Functional studies in zebrafish suggest *Eys* helps to maintain the stability of the ciliary axoneme in both rods and cones, and the integrity of the ciliary pocket in cones.<sup>16-18</sup> *Eys* knockout zebrafish showed a cone-rod pattern of retinal degeneration,<sup>16</sup> and the *Eys* protein was assumed to be essential for the structural integrity of photoreceptor cells.<sup>18</sup> However, the exact function of the *EYS* protein and the role of the different isoforms in the human retina still remains unclear.

We have assessed the spectrum of retinal disease and the course of visual function in our multiethnic cohort of 30 patients carrying biallelic *EYS* mutations to improve patient counseling on prognosis, and to provide guidance for the timing of therapeutic intervention if available. Twenty-seven patients were diagnosed with RP, one patient was diagnosed with cone-rod dystrophy, and two patients with macular dystrophy. To find an explanation for the generalized versus more localized retinal dystrophy among our subjects, we performed functional testing of a novel splice site variant, and bioinformatically assessed the nature of other (presumed) pathogenic variants.

### 3.2 Materials and Methods

#### 3.2.1 Study subjects

We gathered all available DNA testing results from IRD patients from two tertiary care hospitals (the Rotterdam Eye Hospital and Erasmus Medical Center) and selected patients

with biallelic *EYS* mutations. In total, we included 30 IRD patients from 25 families. Four patients were previously described by Littink et al.<sup>5</sup> Eighteen patients were isolated cases with a negative family history of inherited retinal dystrophies. Twenty-seven patients were diagnosed with RP, one patient with CRD, and two patients with macular dystrophy based on clinical characteristics, retinal imaging, and visual function testing. The study protocol adhered to the tenets of the Declaration of Helsinki and was approved by the Institutional Review Board and the Ethics Committee of the Erasmus Medical Center (Rotterdam, The Netherlands).

### 3.2.2 Molecular diagnosis

We obtained blood samples and extracted DNA from peripheral blood lymphocytes by standard procedures. The molecular diagnosis of *EYS* variants (NM\_001142800.1) was made using Sanger sequencing (9 patients), autosomal recessive RP APEX genotyping array (3 patients) and targeted analysis of 256 IRD-associated genes after exome sequencing (18 patients). To determine the effect of the c.1299+5\_1299+8del variant on *EYS* pre-mRNA splicing, an *in vitro* minigene splice assay was performed. For this, we generated a wild type minigene and a mutant minigene harboring the c.1299+5\_1299+8del variant, which each contain exon 8 and parts of the flanking introns of *EYS* (Figure 1a). To investigate if the c.1299+5\_1299+8del variant leads to alterations in splicing, HEK293T cells were transfected with the wild type or mutant minigene constructs, followed by RT-PCR analysis. A detailed description of the applied techniques is provided in the Supplemental information.

### 3.2.3 Clinical examination

Retrospective data were collected from our own medical charts and historical data were retrieved from referring ophthalmologists to maximize the follow-up period. Ophthalmologic examination included best-corrected visual acuity (BCVA), Goldmann kinetic visual field testing, full-field electroretinogram (ffERG) according to ISCEV standards (Diagnosys, Lowell, MA, United States), multifocal electroretinogram (mfERG) (Diagnosys, Lowell, MA, United States), dilated fundus examination, color fundus photography (D300, Nikon, Tokyo, Japan and, Topcon, Tokyo, Japan, and Zeiss FF 450 Plus Fundus Camera, Carl Zeiss Meditec, Jena, Germany), spectral domain optical coherence tomography (SD-OCT) (Spectralis, Heidelberg Engineering GmbH, Dossenheim, Germany) and 30° field fundus autofluorescence (FAF) (Spectralis, Heidelberg Engineering GmbH, Dossenheim, Germany). Visual fields were digitized using a method described by Dagnelie.<sup>19</sup> We measured the retinal area of the V4-target, because this target was consistently used in all examinations.

### 3.2.4 Statistical analysis

Visual impairment was defined as either low vision (BCVA worse than 0.50 LogMAR but equal or better than 1.30 LogMAR and/or central visual field (VF) diameter smaller than 20° but equal or larger than 10° in the better eye) or blindness (BCVA worse than 1.30 LogMAR and/or central VF diameter smaller than 10° in the better eye) in accordance with the WHO criteria. To calculate the annual rate of decline in visual function, we used mixed effects linear regression modeling with visual acuity in logMAR and with log-transformed area of the V4 isopter expressed in degrees squared (deg<sup>2</sup>) for visual field, and corrected for repeated measurements by entering a fixed effect.<sup>20</sup> Patients with a single visit were excluded from longitudinal analysis. We used a Student T-test to compare differences in age of onset, age at diagnosis, and age at last examination between patients with and without constricted visual fields at last examination.

## 3.3 Results

### 3.3.1 Cohort characteristics

We have collected clinical data from 30 patients with biallelic *EYS* variants from 25 families with a median follow-up of seven years (range: 0-24 years) (Table 3.1). Twenty-seven patients were diagnosed with RP, two siblings had macular dystrophy, and one isolated patient was diagnosed with cone-rod dystrophy. Our multi-ethnic cohort consisted of 15 patients from European, 13 from Asian, and 2 from African descent. The current mean age was 45 years (range: 19-75 years), and gender distribution was equal, 16 patients (53%) were male.

### 3.3.2 Molecular diagnosis

Of 27 RP patients, fifteen carried compound heterozygous variants (Table 3.2), and twelve patients had homozygous *EYS* variants, of which eight reported a history of consanguinity. We found 27 different variants: eight frame shift, eight nonsense, eight indels, three missense, and one splice site variant (Table 3). Seven of these variants were novel. All missense variants were classified as pathogenic by SIFT and Polyphen2 algorithms, and were located in conserved residues of *EYS* protein. According to the ACMG classification one missense variant, p.(Gly2186Glu), was classified as likely pathogenic, and two variants, p.(Arg2604His) and p.(Ile2995Asn), were classified as being of uncertain significance (Table 3.3).

In patient XXV, diagnosed with CRD, a homozygous *EYS* variant, p.(Tyr3135\*), was detected using whole exome sequencing. Besides this change, no other pathogenic variants were found. The p.(Tyr3135\*) variant was previously identified homozygously in two Dutch siblings: one with CRD and one with RP,<sup>4</sup> and three Spanish siblings with RP.<sup>6</sup> In our cohort, two RP patients were heterozygous carriers of this variant.

For patient XXIV-1, diagnosed with macular dystrophy, *ABCA4* was initially screened with Sanger sequencing, but no variants were found. Subsequently, targeted whole-exome sequencing identified two variants in *EYS*, c.1299+5\_1299+8del and p.(Gly2017Val).<sup>21</sup> Using Sanger sequencing, these *EYS* variants were detected in his brother, patient XXIV-2. Segregation analysis of the offspring of patient XXIV-1 confirmed that both variants were located on different alleles. The first variant (c.1299+5\_1299+8del) was novel, whereas the second variant p.(Gly2017Val) was previously found homozygously in an RP patient.<sup>6</sup> This missense variant was predicted to be pathogenic by *in silico* prediction tools (Table 3.3).

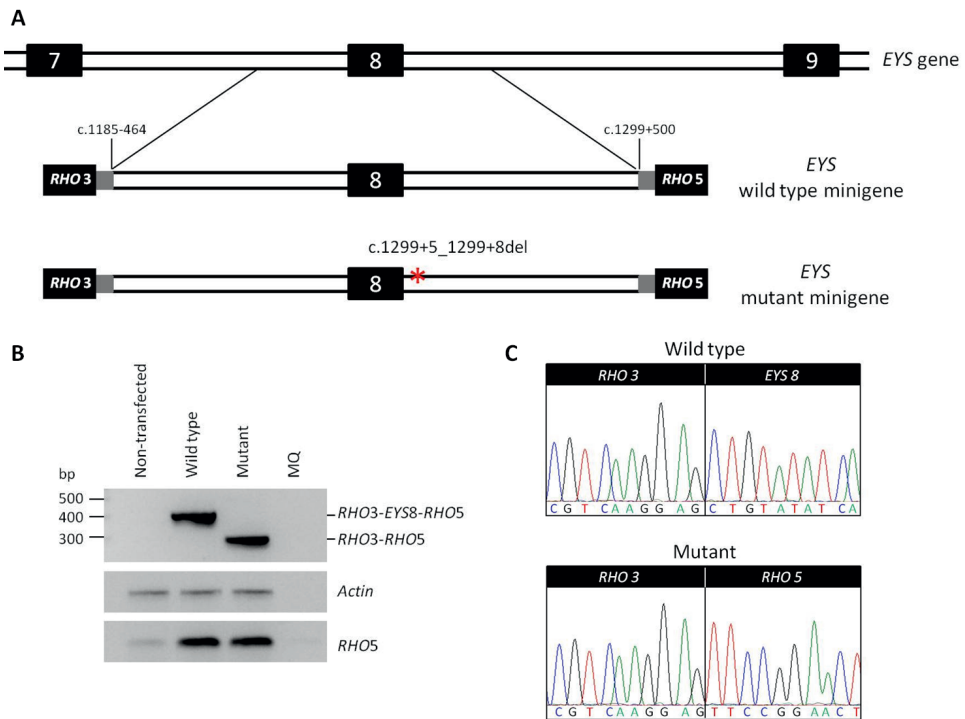


**Figure 3.1. *In vitro* splice assay showing that the c.1299+5\_1299+8del variant results in the skipping of *EYS* exon 8.**

(A) Schematic overview of the genomic region of *EYS* exon 7 to 9 including the mutation observed in patient XXIV-1 and wild type and mutant minigenes that were generated. (B) RT-PCR analysis of Rhodopsin exon 3 (*RHO3*) to Rhodopsin exon 5 (*RHO5*), Actin (loading control) and Rhodopsin exon 5 (transfection control) 48 hours after transfection. The wild type minigene shows a fragment of ~390 bp, which corresponds to normal splicing (*RHO3-EYS8-RHO5*). The mutant minigene shows a fragment of ~280 bp, which corresponds to *RHO3* and *RHO5* spliced together without *EYS* exon 8. The mutant minigene showed complete exon skipping of *EYS* exon 8. (C) Skipping of *EYS* exon 8 (*EYS* 8) in cells transfected with the mutant minigene was validated by Sanger sequencing.

### 3.3.3 Minigene splice assay in HEK293T cells

To investigate potential splice defects associated with the novel c.1299+5\_c.1299+8del variant, wild-type and mutant minigenes harboring this change were generated and transfected into HEK293T cells. RT-PCR analysis showed that transfection of the mutant minigene resulted in skipping of *EYS* exon 8, whereas transfection of the wild type minigene resulted in normal splicing (Figure 3.1B). Skipping of *EYS* exon 8 for the mutant minigene was validated by Sanger sequencing (Figure 3.1C).

### 3.3.4 Phenotype and visual function of patients with *EYS*-associated RP

Most RP patients developed symptoms of night blindness and visual field constriction in the second and third decade of life, the mean age at diagnosis was 30 years (range: 11 – 56 years). Demographic information, and clinical features are available in Table 3.1. All RP patients had one or more characteristic fundus feature, such as peripheral retinal degeneration, bone spicule pigmentations, attenuated retinal vasculature or pale waxy optic disc (Supp. Figure S1).

We gathered 146 visual acuity measurements, with a mean of six measurements per patient (range: 1-22 measurements). Four patients became visually impaired (BCVA worse than 0.3 logMAR) during follow-up at ages 41, 43, 64, and 70 years, and already had constricted visual fields (<20°) at previous examinations. Mixed effects linear regression modeling showed an overall increase in LogMAR visual acuity of 0.015 in the best performing eye per year, which corresponds to a loss of 0.75 ETDRS letters per year ( $P < 0.001$ ).

Fifty-seven Goldmann visual field examinations were available, ranging from one to eight measurements per patient. At first examination, eleven patients were visually impaired (central visual field <20°), and five were blind (central visual field <10°). One patient became visually impaired during follow-up at age 39. Ten patients had a central visual field larger than 20° at last examination. They did not significantly differ from patients that were visually impaired in terms of age of onset ( $p = 0.2262$ ), age at diagnosis ( $p = 0.259$ ), or age at last examination ( $p = 0.136$ ). All ten patients carried two truncating *EYS* variants, of which nine were located in the N-terminal part of the protein, and eleven in the C-terminal part. The rate of visual field loss of the V4 isopter area was 9% per year.

In 23 patients, ffERG was performed: in fifteen patients (mean age: 40 years) no scotopic or photopic responses could be elicited, in five patients (mean age: 43 years) both scotopic and photopic responses were severely reduced, and in three patients (mean age: 29 years) there were no scotopic responses and severely reduced photopic responses. OCT scans of 24 patients, and autofluorescence imaging of 23 patients were available for analysis. In 19 patients the ellipsoid



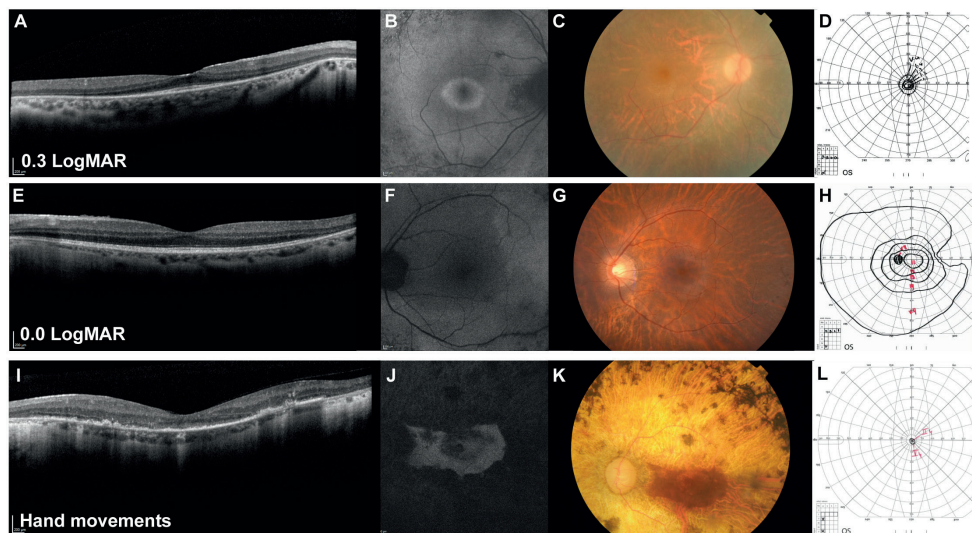


**Figure 3.2. Optical coherence tomography, fundus autofluorescence, fundus photography and visual field of three RP patients with different RP phenotypes.**

Patients II-3 (age 23) shows a typical RP phenotype with (A) shortening of the ellipsoid layer length and (B) a hyperautofluorescent ring surrounding the fovea, (C) the optic disk appears pale and vessels are narrow. Visual field (D) is severely constricted ( $\sim 10^\circ$ ). Patient VII-2 (age 41) has a milder phenotype, (E) the ellipsoid layer length is longer and there is (F) a 'crescent-shaped' hyperautofluorescent pattern visible. (G) the optic disk appears pink and vessels are narrow. There is decreased sensitivity of the peripheral visual field (H), with an absolute scotoma nasally. Patient XX (age 73) has end-stage RP, (I) the ellipsoid zone and other outer segment layers are no longer discernible. There is a (J) small relatively hyperautofluorescent patch in the perifoveal area, surrounded by hypoautofluorescence, the fovea itself appears hypoautofluorescent as well. In fundus (K), the optic disk appears pale, vessels are very narrow, and there is extensive retinal atrophy with bone spicule pigmentations. A small island of RPE remains in the macula with RPE-alterations. The visual field (L) is severely constricted ( $< 10^\circ$ ) and there is foveal sensitivity loss.

layer length was shortened but continuous in the foveal area, 16 of them had an hyperautofluorescent ring (Figure 3.2AB), and three had a crescent shape hyperautofluorescence pattern (I, VI-1, VII-2)(Figure 3.2EF). In a single patient (VII-1), the ellipsoid layer was continuous over the width of the 4mm single line scan, accompanied by a crescent shape pattern on autofluorescence imaging. Four patients (II-2, XV, XVI, XX) had foveal abnormalities in at least one eye (Figure 3.2IJ), and it became impossible to discriminate between the different outer retinal layers, because retinal architecture in the macula, including the fovea, appeared severely distorted. The majority of RP patients had epiretinal membranes, but there were no patients with macular holes or tractional macular edema. Four patients developed cystoid maculopathy during follow-up; one

patient was treated with Acetazolamide tablets, and two with Somatostatin injections. In patients with a distinguishable hyperautofluorescent ring, the length of the ellipsoid zone was shorter than in patients with a 'crescent' autofluorescence pattern as described by Sengillo et al. (Figure 3.2).<sup>22</sup>

### 3.3.5 Phenotype and visual function of a patient with *EYS*-associated cone-rod dystrophy

One isolated patient (XXV) noted both a decrease in visual acuity and night blindness as first symptoms, he previously underwent refractive surgery to correct for high myopia. At first examination visual acuity was 0.3 LogMAR in the best eye. On funduscopy, the optic disks appeared pale, and white flecks in the macula were noted, vessels were thin with mottling of the RPE in the periphery. OCT imaging showed atrophy of the outer retinal layers in the posterior pole, and fundus autofluorescence showed a hyperautofluorescent ring with diffuse atrophy in the macula (Figure 3.3).

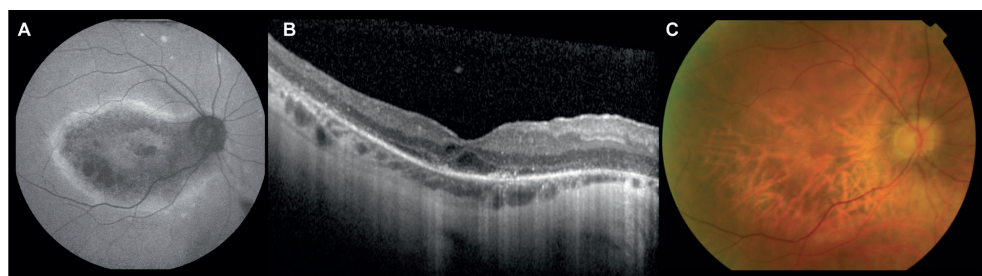


**Figure 3.3. Autofluorescence, SD-OCT and fundus pictures of patient with cone-rod dystrophy.**

(A) Fundus autofluorescence of patient XXV shows a hyperautofluorescent ring within the vascular arcade, surrounding the macular area, which appears patchy, with diffuse hypoautofluorescent lesions. The fovea appears hypoautofluorescent. (B) On OCT, there is a parafoveal cyst, the outer retinal layers are distorted and the ellipsoid zone can no longer be distinguished. (C) Atrophy of the posterior pole with discernable choroidal vasculature, the retinal vessels are attenuated.

### 3.3.6 Phenotype and visual function of patients with *EYS*-associated macular dystrophy

The proband (XXIV-2) was the youngest in a family of five siblings; he suffered from decreased visual acuity from the age of 7. He was first examined at age 12, binocular visual acuity was 1.0 LogMAR with excentric fixation. At age 22, he was diagnosed with juvenile macular dystrophy, visual acuity was 0.8 LogMAR and funduscopy revealed a bull's eye maculopathy. Central visual field testing with Humphrey Field Analyzer 10-2 showed a central scotoma, and color vision testing with Lanthony's desaturated 15-Hue test revealed a tritan defect. fERG showed normal scotopic and photopic responses.

At age 23, pronounced macular atrophy was seen on OCT imaging (Figure 3.4G). His older brother (XXIV-1) noted a decrease in visual acuity and color vision problems from the age of 18. At age 32, visual acuity was 0.3 LogMAR, funduscopy revealed normal foveal reflexes, perimacular RPE alterations and yellow dots, with normal aspect of the peripheral retina. OCT imaging showed atrophy of the ellipsoid zone in the fovea, and fundus autofluorescence revealed a hyperautofluorescent ring (Figure 3.4A-C). At age 36, ffERG rod and cone responses were within normal range, and mfERG showed decreased foveal responses (Supplementary Figure 2). At age 38, visual acuity was 0.7 LogMAR and OCT imaging showed atrophy of all outer retinal layers and thinning of the RPE. Fundus autofluorescence revealed a larger hyperautofluorescent ring surrounding the hypoautofluorescent macula (Figure 3.4D-F).

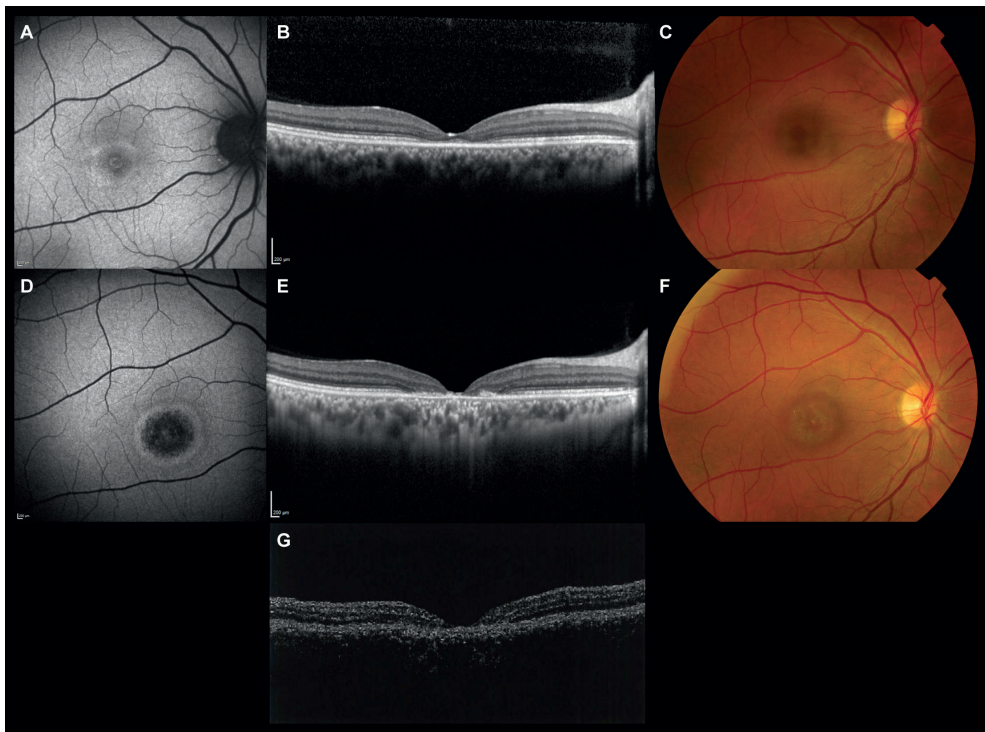


**Figure 3.4. Infrared imaging, OCT imaging and fundus photography in patients with macular dystrophy.**

Disease progression of *EYS*-associated macular dystrophy in patient XXIV-1 using spectral domain optical coherence tomography (SD-OCT) scans, fundus autofluorescence (FAF) and fundus images of the right eye. (A-C) At age 32, SD-OCT scan shows foveal atrophy with local disruption of the ellipsoid zone and thinning of the outer nuclear layer, on FAF a hyperautofluorescent ring is discernable surrounding the fovea. Fundus photograph reveals a normal optic disk, normal caliber of the retinal vessels and subtle RPE alterations in the foveal region, but no abnormalities in the

peripheral retina. (D-F) At age 38 , SD-OCT shows progression of the foveal atrophy with disruption of the inner retinal layers, hyperreflective pigment deposits and thinning of the RPE. FAF shows a Bull's eye maculopathy with a hypopigmented fovea and a hyperreflective ring. Fundus photograph reveals a hypopigmented fovea surrounded by RPE alterations and RPE atrophy, there were no peripheral abnormalities. (G) SD-OCT of patient XXIV-2 at age 23, showing macular atrophy.

**Table 3.1.** Clinical characteristics of patients with EYS-associated inherited retinal dystrophies.

ID	Current age (yrs), Sex	Age at diagnosis (yrs)	Initial Symptoms	Ophthalmic history	Visual acuity at first visit (LogMAR)		Refractive error (SE, D)		Ophthalmoscopy at baseline	ffERG rod-derived	ffERG cone-derived	Phenotype
					RE	LE	RE	LE				
I	61, M	56	Night blindness, decreased visual acuity (high myopia)	amblyopia LE, CE BE	0.10	0.52	-7.75	-12.25	Tilted, waxy optic disks with peripapillary atrophy, bone spicules in the periphery and severe attenuation of the retinal vessels.	NR	NR	(56) RP
II-1	43, M	35	Night blindness, visual field constriction	refractive surgery BE for myopia	0.1	0.0	-5.25	-4.25	Waxy optic disks, normal aspect of the macula, attenuated retinal vessels, intraretinal pigmentations in the periphery.	NR	NR	(35) RP
II-2	42, F	23	Night blindness, decreased visual acuity		0.4	0.3	-4.00	-3.75	Normal aspect of the optic disk, peripheral RPE atrophy and bone spicules, preserved posterior pole and attenuated retinal vessels.	NR	NR	(24) RP
II-3	29, M	16	Night blindness		0.1	0.22	-1.50	-0.50	Pallor of the optic disc, peripheral bone spicules and pigment alterations and attenuated retinal vessels.	NR	NR	(22) RP
III	32, M	19	Night blindness, decreased visual acuity (CME)	Somatostatin treatment for CME	0.0	0.05	-0.25	-0.50	Pale aspect of the optic disk, CME, peripheral atrophy and bone spicules, attenuated retinal vessels.	↓↓	↓↓	(19) RP
IV	55, F	26	Night blindness	CE BE	0.3	0.3	+2.00	NA	Pale aspect of the optic disk, Bull's eye maculopathy RE, extensive peripheral atrophy and intraretinal pigmentations, attenuated retinal vessels.	NP	NP	NA RP
V	36, M	22	Night blindness	CE LE	0.22	0.22	-0.75	-0.50	Waxy optic disks, peripheral bone spicules, mild attenuated retinal vessels.	NP	NP	NA RP

VI-1	18, F	15	14	Night blindness, visual field constriction	0.22	0.1	-0.50	-0.50	Normal aspect of the optic disks, cellophane maculopathy, midperipheral bone spicules and intraretinal pigmentations and attenuated retinal vessels.	↓↓	↓↓	(15)	RP	
VI-2	21, M	21	21	Night blindness, visual field constriction	0.05	0.15	-0.75	-0.50	Normal aspect of the optic disk, absent foveal reflex, peripheral RPE alterations, narrow vessels	NR	NR	(21)	RP	
VII-1	39, F	35	35	Night blindness, visual field constriction	0.1	0.0	-1.75	-1.25	Waxy optic disks, midperipheral bone spicules, attenuated retinal vessels.	NR	NR	(35)	RP	
VII-2	42, M	40	40	Night blindness, visual field constriction	-0.1	-0.1	-0.50	-2.00	Normal aspect of the optic disks, peripheral bone spicules and attenuated retinal vessels.	NP	NP	NA	RP	
VIII	52, M	40	26	Night blindness	0.05	0.1	-5.25	-4.25	Pale aspect of the optic disk, pigment alterations in the macular region, RPE atrophy and bone spicules in the periphery and severely attenuated retinal vessels.	NR	NR	(40)	RP	
IX	61, F	46	53	Night blindness, adaptation	0.6	0.8	-13.00	-14.00	Pale aspect of the optic disk with peripapillary atrophy, atrophy of the RPE in the macula, midperipheral bone spicules and severely attenuated retinal vessels.	NR	↓↓	(46)	RP	
X	71, M	38	40	Visual field constriction	0.1	0.1	+0.00	+1.00	Optic nerve head drusen, atrophic macular region with foveal island, relatively preserved RPE midperipheral, atrophic RPE far periphery with bone spicules and paving stone degenerations and severely attenuated retinal vessels.	NR	↓↓	(56)	RP	
XI	40, F	32	34	Night blindness, decreased visual acuity	CE BE	0.4	0.3	-1.00	-1.00	Pale aspect of the optic disk, CME, bone spicules in the midperiphery and attenuated retinal vessels.	NR	NR	(34)	RP

XII	34, F	14	26	Night blindness	refractive laser surgery BE	0.0	0.0	-1.00	-1.25	Pale aspect of the optic disk, small island with intact RPE in the macula, perimacular creasing of the ILM, extensive lobular atrophy of the RPE in the posterior pole and far periphery, severely attenuated retinal vessels, intraretinal bone spicules on the nasal side.	NR	NR	(26)	RP
XIII	53, F	53	52	Night blindness, visual field constriction		0.1	0.05	+0.25	+0.5	Normal aspect of the optic disk, maculae coarsely pigmented, tapetal reflex temporally, RPE atrophy in the far periphery with bone spicule pigmentations, mildly attenuated vessels.	↓	↓	(53)	RP
XIV	56, M	50	50	Night blindness, color vision disturbances		0.05	0.0	-7.25	-7.00	Waxy optic disks with peripapillary atrophy, perimacular pigment alterations, peripheral bone spicules and attenuated retinal vessels.	NR	NR	(53)	RP
XV	66, M		62			0.0	0.4	NA	NA	Pale optic disks, RPE alterations macula, midperipheral and peripheral bone spicules, attenuated retinal vessels.	NR	NR	(61)	RP
XVI	46, F	26	26	Night blindness, decreased visual acuity	Diamox treatment for CME	0.4	0.1	-5.50	-5.50	Moderate pallor of the optic disk, CME, RPE atrophy and bone spicules in the periphery, attenuated vessels.	↓↓	↓↓	(27)	RP
XVII	53, F	11	52	Night blindness, visual field constriction	Cuba therapy BE, CE BE	0.5	0.7	NA	NA	Pale optic disks with peripapillary atrophy, normal aspect of the macula, midperipheral and peripheral bone spicules, attenuated retinal vessels.	NR	NR	(53)	RP
XVIII	43, F	21	30	Night blindness		0.05	0.05	NA	NA	Mild pallor optic disk, vessels near normal caliber, preserved RPE in the posterior pole with mild epiretinal membrane formation, RPE changes in the macula with three intraretinal crystals. Midperipheral and peripheral atrophy of the RPE RE.	↓↓	↓↓	(30)	RP
XIX	32, F	27	27	Night blindness	Somatostatine treatment IM for CME	0.0	0.0	0.50	0.25	Normal optic disks, attenuated retinal vessels, creasing and fibrosis of the ILM and bone spicules in the far periphery.	NR	↓↓	(27)	RP

XX	75, M	26	66	Night blindness, visual field constriction	DM II, CE BE	0.6	0.5	NA	NA	Pale excavated optic disks, severely attenuated vessels and peripheral atrophy of the RPE with bone spicules.	NR	NR	(71)	RP
XXI	31, F	28	30	Night blindness	refractive surgery BE for myopia	0.15	0.3	NA	NA	Tilted disks with peripapillary atrophy, attenuated vessels, no bone spicules	NR	NR	(30)	RP
XXII	33, M	33	33	Night blindness, visual field constriction		0.2	0.1	-4.00	-3.00	Pink aspect of the optic disks, attenuated vessels, preserved RPE in the posterior pole with mild wrinkling of the ILM LE > RE. Midperipheral mottling of the RPE with intraretinal bone spicule pigmentations.	NP	NP	NA	RP
XXIII	37, F	36	36	Night blindness	CE LE, post-operative steroid-induced glaucoma LE	0.0	0.3	-1.50	-2.00	Moderate pallor of the optic disk, attenuated blood vessels with sheathing, normal aspect of the RPE in the posterior pole, wrinkling of the ILM, and pigment alterations and bone spicule pigmentations in the periphery.	NR	NR	(36)	RP
XXIV-1	38, M	32	28	Decreased visual acuity, color vision disturbances		0.8	0.8	+0.25	+0.25	Normal aspect of the optic disk, positive foveal reflexes, Bull's eye maculopathy with pigment alterations and white dots, normal retinal vessels.	NL	NL	(32)	MD
XXIV-2	34, M	18	22	Decreased visual acuity		1.0	0.8	-1.00	-0.50	Normal aspect of the optic disk, normal caliber of the retinal vessels, RPE alterations in the fovea with subfoveal atrophy OD, normal appearance of the peripheral retina.	NL	NL	(22)	MD
XXV	55, M	55	55	Decreased visual acuity, night blindness	Artisan cataract extraction, night blindness implant BE	0.5	0.3	-8.00	-9.00	Pale aspect of the optic disk, white flecks in the macula, peripheral mottling of the RPE, narrow vessels.	NR	NR	(55)	CRD

BE: both eyes, CE: cataract extraction, CME: cystoid macular edema, CRD: cone-rod dystrophy, DMII: diabetes mellitus type 2, F: female, fFERG: full-field electroretinogram, LE: left eye, M: male, MD: macular dystrophy, IM: intramuscular, NA: not applicable, NL: normal, NP: not performed, NR: no response, RE: right eye, RP: retinitis pigmentosa, RPE: retinal pigment epithelium, SE: spherical equivalent.



**Table 3.2.**  
Genotype of patients with EYS-associated inherited retinal dystrophies.

ID	Nucleotide change 1	Protein effect 1	Nucleotide change 2	Protein effect 2	Phenotype	Ethnicity
I	c.2308C>T	p.(Gln770*)	c.2308C>T	p.(Gln770*)	RP	Iraqi - Asian <sup>1</sup>
II-1	c.(331+1_332-1)_(1056+1-1057_1)del	p.?	c.(331+1_332-1)_(1056+1-1057_1)del	p.?	RP	Turkish - Asian <sup>1</sup>
II-2	c.(331+1_332-1)_(1056+1-1057_1)del	p.?	c.(331+1_332-1)_(1056+1-1057_1)del	p.?	RP	Turkish - Asian <sup>1</sup>
II-3	c.(331+1_332-1)_(1056+1-1057_1)del	p.?	c.(331+1_332-1)_(1056+1-1057_1)del	p.?	RP	Turkish - Asian <sup>1</sup>
III	c.4350_4356del	p.(Ile1451Profs*3)	c.4350_4356del	p.(Ile1451Profs*3)	RP	Dutch - European <sup>1</sup>
IV	c.6714del	p.(Ile2239Serfs*17)	c.6714del	p.(Ile2239Serfs*17)	RP	Dutch - European
V	c.4350_4356del	p.(Ile1451Profs*3)	<b>c.5319_5342del</b>	p.(Asn1773_Val1781delinsLys)	RP	Dutch - European
VI-1	c.6799_6800del	p.(Gln2267Glufs*15)	c.7095T>G	p.(Tyr2365*)	RP	Dutch - European
VI-2	c.6799_6800del	p.(Gln2267Glufs*15)	c.7095T>G	p.(Tyr2365*)	RP	Dutch - European
VII-1	<b>c.5928-3_5928-1del</b>	p.?	<b>c.5928-3_5928-1del</b>	p.?	RP	Pakistan - Asian <sup>1</sup>
VII-2	<b>c.5928-3_5928-1del</b>	p.?	<b>c.5928-3_5928-1del</b>	p.?	RP	Pakistan - Asian <sup>1</sup>
VIII	c.5167_5168del	p.(Leu1723Glyfs*6)	<b>c.(6424-1_6425+1)_(6751+1_6752-1)del</b>	p.?	RP	Dutch - European
IX	c.4350_4356del	p.(Ile1451Profs*3)	c.7811G>A	p.(Arg2604His)	RP	Dutch - European
X	c.1673G>A	p.(Trp558*)	c.2811C>A	p.(Cys937*)	RP	Dutch - European
XI	c.4955C>G	p.(Ser1652*)	c.8984T>A	p.(Ile2995Asn)	RP	Dutch - European
XII	c.7919G>A	p.(Trp2640*)	c.7919G>A	p.(Trp2640*)	RP	Turkish - Asian
XIII	c.9036del	p.(Leu3013Serfs*6)	c.9405T>A	p.(Tyr3135*)	RP	Dutch - European
XIV	c.4350_4356del	p.(Ile1451Profs*3)	c.6714del	p.(Ile2239Serfs*17)	RP	Dutch - European
XV	c.32dup	p.(Met12Aspfs*14)	c.32dup	p.(Met12Aspfs*14)	RP	Iraqi - Asian
XVI	c.1161del	p.(Lys387Asnfs*34)	<b>c.(2137+1_2137-1)_(2259+1_2260-1)dup</b>	p.?	RP	Turkish - Asian
XVII	c.4350_4356del	p.(Ile1451Profs*3)	<b>c.6079-2A&gt;G</b>	p.?	RP	Dutch - European
XVIII	c.4712C>G	p.(Ser1571*)	c.6557G>A	p.(Gly2186Glu)	RP	South Korea-USA
XIX	c.6714del	p.(Ile2239Serfs*17)	c.1185-3C>T	p.?(splice)	RP	Turkish - Asian

XX	c.1376del	p.(Cys459Serfs*56)	<b>c.(331+1_332-1)_(862+1_863-1)dup</b>	p.?	RP	Dutch - European
XXI	c.4045C>T	p.(Arg1349*)	c.4045C>T	p.(Arg1349*)	RP	Turkish - Asian <sup>†</sup>
XXII	c.8255_8260del	p.(Leu2752_Asn2754delinsTyr)	c.8255_8260del	p.(Leu2752_Asn2754delinsTyr)	RP	Turkish - Asian <sup>†</sup>
XXIII	c.4350_4356del	p.(Ile1451fs)	c.9405T>A	p.(Tyr3135*)	RP	Dutch - European
XXIV-1	c.1299+5_1299+8del	p.?	c.6050G>T	p.(Gly2017Val)	MD	Moroccan - African
XXIV-2	c.1299+5_1299+8del	p.?	c.6050G>T	p.(Gly2017Val)	MD	Moroccan - African
XXV	c.9405T>A	p.(Tyr3135*)	c.9405T>A	p.(Tyr3135*)	CRD	Dutch - European

<sup>†</sup>=consanguinity, CRD= cone-rod dystrophy, RP= retinitis pigmentosa; MD= macular dystrophy. Novel variants are displayed in bold font.

**Table 3.3.** Missense EYS variants identified in this study and their *in silico* functional analyses.

Exon	cDNA change	Protein change	PhyloP	Grantham	PolyPhen-2 score	PolyPhen-2 prediction	SIFT score	SIFT prediction	AC (gnomAD)	AF (gnomAD)	Classification
29	c.6050G>T	p.(Gly2017Val)	1.60	109	1.0	Deleterious	0	Deleterious	5	0.00002904	Likely pathogenic
32	c.6557G>A	p.(Gly2186Glu)	2.44	98	0.933	Probably damaging	0	Deleterious	5	0.00003471	Likely pathogenic
40	c.7811G>A	p.(Arg2604His)	1.73	29	0.877	Probably damaging	0	Deleterious	6	0.00003285	Uncertain significance
43	c.8984T>A	p.(Ile2995Asn)	6.32	149	0.996	Deleterious	0	Deleterious	1	0.000006598	Uncertain significance

AC: Allele count; AF: Allele frequency. Classification was assessed according to the ACMG guidelines.

### 3.4 Discussion

In this study, we have assessed the spectrum of retinal disease and the course of visual function in 30 patients carrying biallelic *EYS* variants. Twenty-seven patients had RP, one patient had CRD, and two patients had macular dystrophy, based on clinical characteristics, functional testing, and retinal imaging. *EYS* mutations are one of the most common causes of arRP in Asia and Europe. Novel findings included the presence of homozygous *EYS* mutations in CRD patients, and compound heterozygous *EYS* mutations in patients with macular dystrophy.

The age of onset in RP patients ranged from 7 to 51 years, all had one or more typical fundus features corresponding with retinitis pigmentosa (Supp. Figure S1). Four patients became visually impaired (BCVA worse than 0.3 LogMAR) during follow-up at ages 41, 43, 64, and 70 years. Mixed effects linear regression modeling showed an overall increase in LogMAR visual acuity of 0.015 in the best performing eye per year, which corresponds to a loss of 0.75 ETDRS letters per year ( $P < 0.001$ ). Based on visual field constriction, 11 out of 27 RP patients were visually impaired (41%) and five were blind (19%) according to WHO-criteria at first examination in our centers. The rate of peripheral visual field loss for the V4 target was 9% per year in our cohort, which is markedly slower than 23% per year reported by McGuigan et al.<sup>23</sup> Ten RP patients had a central visual field larger than 20° at last follow-up (mean age: 39 years). They did not differ from RP patients with visual field constriction in age of onset, or age at last examination. All ten of these patients carried compound heterozygous or homozygous truncating variants.

Differences in disease manifestation and progression are often attributed to a difference in underlying causal variants (e.g. missense versus truncating variants). Three out of 27 RP patients carried one heterozygous missense *EYS* variant, and one truncating *EYS* variant. There were no patients with homozygous missense *EYS* variants, therefore we could not study whether missense variants were associated with milder retinal disease in our cohort. Siblings with the same *EYS* genotype can differ substantially in age of onset, disease presentation, and rate of disease progression. Our study was not suited to determine genotype-phenotype correlations in detail as many variants were observed only once.

Two-third of RP patients in our cohort had typical hyperautofluorescent rings, and one third had a crescent shape hyperautofluorescent pattern, as described by Sengillo et al.<sup>22</sup> The crescent pattern was associated with larger visual fields and therefore milder disease progression. Three out of four patients had two mutations near the C-terminal domain, which could have a less detrimental impact on protein structure or function. Additional studies would be most helpful to study the effect of these mutations on the different isoforms.

Three cases of *EYS*-associated CRD have been published so far; the first case was a Dutch patient that carried the same homozygous variant as our CRD patient, p.(Tyr3135\*<sup>4</sup>). The second case was a Japanese patient, carrying compound heterozygous *EYS* variants, p.(Tyr2935\*) and p.(Ser1653fs). Segregation analysis confirmed that these variants were

located on different alleles. Each separate variant homozygous, as well as the identical compound heterozygous combination of these variants, were previously identified as causal in RP patients.<sup>9,24-26</sup> The third case, was a French patient with compound heterozygous variants, p.(Trp558\*), and p.(Asn745Ser). The pathogenicity of the missense variant was questionable, as it proved to be not conserved, and the pathogenicity is uncertain according to the ACMG classification.<sup>18</sup> The homozygous nonsense variant, p.(Tyr3135\*), that our CRD patient, as well as the first mentioned CRD case carried, was also detected in RP patients,<sup>4,5</sup> including in two RP patients of this cohort. The variant is located in the last *EYS* exon and leads to a premature stop codon. Functional assays might reveal whether the variant leads to nonsense mediated decay, or the formation of a C-terminally truncated *EYS* protein. It is unclear why identical genotypes can result in both RP and CRD phenotypes. The *EYS* variants found in CRD patients did not cluster in a specific domain. Of the 4 known *EYS* isoforms, only the two long isoforms (isoform 1 and 4) are predicted to be affected by the mutations, as all CRD-associated variants are all located after the 594<sup>th</sup> amino acid. Unfortunately, this does not help explain the difference in phenotype because some of the underlying genotypes were also found in RP patients. The presence of genetic and epigenetic modifiers, or environmental factors, could also play a role in the observed differences in phenotype in these patients.

Macular dystrophy is an IRD in which the central retina is primarily affected and peripheral photoreceptor function is spared. Patients XXIV-1 and XXIV-2 presented with an isolated macular dystrophy, with a normal ffERG. Targeted whole exome sequencing identified compound heterozygous *EYS* variants: c.1299+5\_1299+8del and c.6050G>T. To assure the functional effect of the splice site variant we generated a mutant minigene. RT-PCR analysis showed that transfection of the mutant minigene resulted in skipping of *EYS* exon 8, suggesting that similar mis-splicing events can occur in the retina. The second variant was previously found homozygous in an RP patient.<sup>6</sup> *EYS* is expressed in the outer segments of both rods and cones, and is thought to be crucial for the stability of the ciliary axonema and photoreceptor homeostasis in humans. In several mammal lineages, such as rodents, *EYS* is not expressed, which limits the availability of animal models that better mimic human anatomy and physiology. *EYS* zebrafish knockout studies showed cone-rod dystrophy pattern of retinal degeneration,<sup>16</sup> RP or macular dystrophy phenotypes have not been described in animals that are mutant for *Eys*.

Since molecular testing can uncover pathogenic variants in genes that have not been associated with the phenotype of interest, it remains crucial to perform segregation analysis and to keep looking for variants in other genes. Reassessing the phenotype might be worthwhile; especially in patients with end-stage disease in whom discriminating between different subtypes of IRD might prove difficult, as both central and peripheral retinal architecture are frequently severely distorted. To better understand the pathophysiology of *EYS*-associated IRDs it is essential to perform functional studies that

focus on the effect of mutations on the different *EYS* isoforms and their effect within the retina.

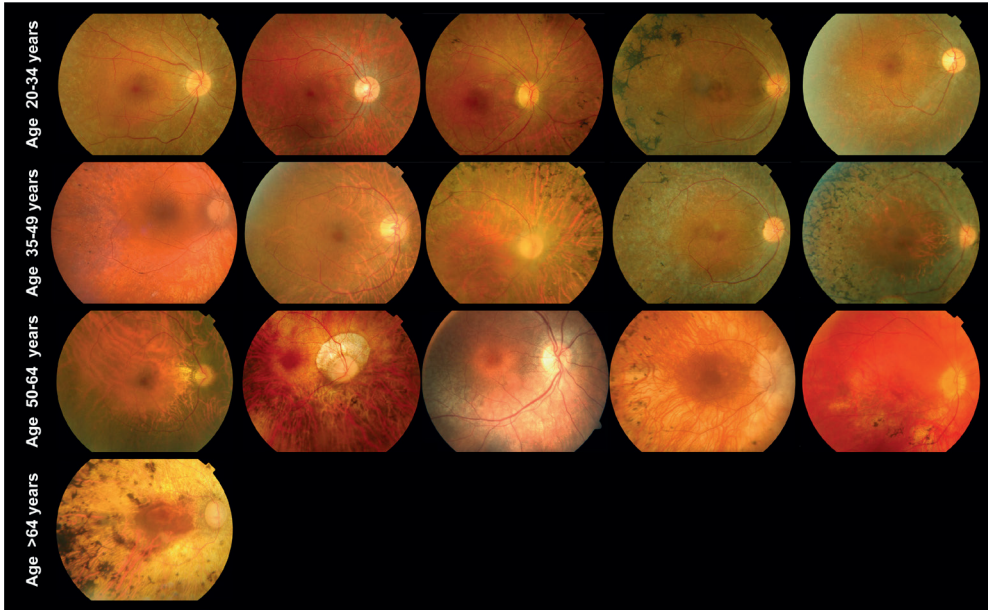
### 3.5 References

1. Hartong DT, Berson EL, Dryja TP. (2006) Retinitis pigmentosa. *Lancet*; **368**: 1795-1809.
2. Verbakel SK, van Huet RAC, Boon CJF, den Hollander AI, Collin RWJ, Klaver CCW, Hoyng CB, Roepman R, Klevering BJ. (2018) Non-syndromic retinitis pigmentosa. *Prog Retin Eye Res*.
3. Abd El-Aziz MM, Barragan I, O'Driscoll CA, Goodstadt L, Prigmore E, Borrego S, Mena M, Pieras JI, El-Ashry MF, Safieh LA, et al. (2008) EYS, encoding an ortholog of *Drosophila* spacemaker, is mutated in autosomal recessive retinitis pigmentosa. *Nat Genet*; **40**: 1285-1287.
4. Collin RW, Littink KW, Klevering BJ, van den Born LI, Koenekoop RK, Zonneveld MN, Blokland EA, Strom TM, Hoyng CB, den Hollander AI, et al. (2008) Identification of a 2 Mb human ortholog of *Drosophila* eyes shut/spacemaker that is mutated in patients with retinitis pigmentosa. *Am J Hum Genet*; **83**: 594-603.
5. Littink KW, van den Born LI, Koenekoop RK, Collin RW, Zonneveld MN, Blokland EA, Khan H, Theelen T, Hoyng CB, Cremers FP, et al. (2010) Mutations in the EYS gene account for approximately 5% of autosomal recessive retinitis pigmentosa and cause a fairly homogeneous phenotype. *Ophthalmology*; **117**: 2026-2033.
6. Barragan I, Borrego S, Pieras JI, Gonzalez-del Pozo M, Santoyo J, Ayuso C, Baiget M, Millan JM, Mena M, Abd El-Aziz MM, et al. (2010) Mutation spectrum of EYS in Spanish patients with autosomal recessive retinitis pigmentosa. *Hum Mutat*; **31**: E1772-1800.
7. Arai Y, Maeda A, Hirami Y, Ishigami C, Kosugi S, Mandai M, Kurimoto Y, Takahashi M. (2015) Retinitis Pigmentosa with EYS Mutations Is the Most Prevalent Inherited Retinal Dystrophy in Japanese Populations. *J Ophthalmol*; **2015**: 819760.
8. Bandah-Rozenfeld D, Littink KW, Ben-Yosef T, Strom TM, Chowers I, Collin RW, den Hollander AI, van den Born LI, Zonneveld MN, Merin S, et al. (2010) Novel null mutations in the EYS gene are a frequent cause of autosomal recessive retinitis pigmentosa in the Israeli population. *Invest Ophthalmol Vis Sci*; **51**: 4387-4394.
9. Iwanami M, Oshikawa M, Nishida T, Nakadomari S, Kato S. (2012) High prevalence of mutations in the EYS gene in Japanese patients with autosomal recessive retinitis pigmentosa. *Invest Ophthalmol Vis Sci*; **53**: 1033-1040.
10. Abd El-Aziz MM, O'Driscoll CA, Kaye RS, Barragan I, El-Ashry MF, Borrego S, Antinolo G, Pang CP, Webster AR, Bhattacharya SS. (2010) Identification of novel mutations in the ortholog of *Drosophila* eyes shut gene (EYS) causing autosomal recessive retinitis pigmentosa. *Invest Ophthalmol Vis Sci*; **51**: 4266-4272.
11. Audo I, Sahel JA, Mohand-Said S, Lancelot ME, Antonio A, Moskova-Doumanova V, Nandrot EF, Doumanov J, Barragan I, Antinolo G, et al. (2010) EYS is a major gene for rod-cone dystrophies in France. *Hum Mutat*; **31**: E1406-1435.
12. Katagiri S, Akahori M, Hayashi T, Yoshitake K, Gekka T, Ikeo K, Tsuneoka H, Iwata T. (2014) Autosomal recessive cone-rod dystrophy associated with compound heterozygous mutations in the EYS gene. *Doc Ophthalmol*; **128**: 211-217.
13. Boulanger-Scemama E, El Shamieh S, Demontant V, Condroyer C, Antonio A, Michiels C, Boyard F, Saraiva JP, Letexier M, Souied E, et al. (2015) Next-generation sequencing applied to

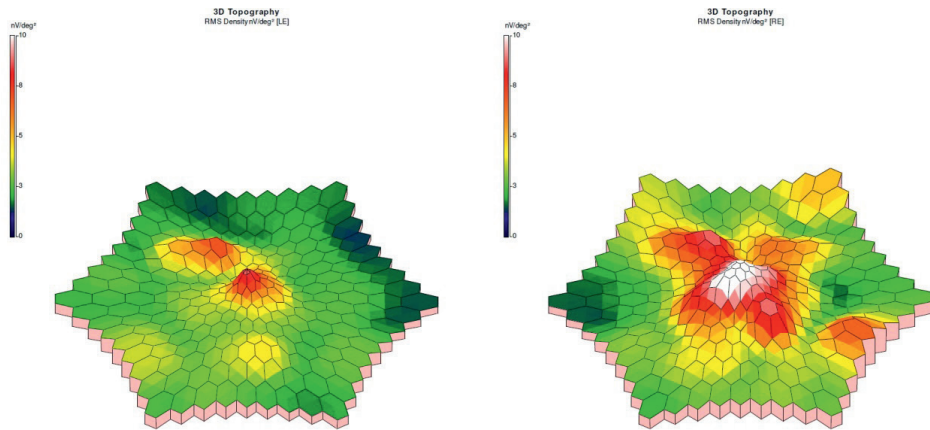
- a large French cone and cone-rod dystrophy cohort: mutation spectrum and new genotype-phenotype correlation. *Orphanet J Rare Dis*; **10**: 85.
14. Alfano G, Kruczek PM, Shah AZ, Kramarz B, Jeffery G, Zelhof AC, Bhattacharya SS. (2016) EYS Is a Protein Associated with the Ciliary Axoneme in Rods and Cones. *PLoS One*; **11**: e0166397.
  15. Zelhof AC, Hardy RW, Becker A, Zuker CS. (2006) Transforming the architecture of compound eyes. *Nature*; **443**: 696-699.
  16. Lu Z, Hu X, Liu F, Soares DC, Liu X, Yu S, Gao M, Han S, Qin Y, Li C, et al. (2017) Ablation of EYS in zebrafish causes mislocalisation of outer segment proteins, F-actin disruption and cone-rod dystrophy. *Sci Rep*; **7**: 46098.
  17. Yu M, Liu Y, Li J, Natale BN, Cao S, Wang D, Amack JD, Hu H. (2016) Eyes shut homolog is required for maintaining the ciliary pocket and survival of photoreceptors in zebrafish. *Biol Open*; **5**: 1662-1673.
  18. Messchaert M, Dona M, Broekman S, Peters TA, J.C. C-S, R.W.N S, van Wijk E, Collin RWJ. (2018) Eyes shut homolog is important for the maintenance of photoreceptor morphology and visual function in zebrafish. *PLOS one, in press*.
  19. Dagnelie G. (1990) Conversion of planimetric visual field data into solid angles and retinal areas. *Clin Vision Sciences*: 95-100.
  20. Iannaccone A, Kritchevsky SB, Ciccarelli ML, Tedesco SA, Macaluso C, Kimberling WJ, Somes GW. (2004) Kinetics of visual field loss in Usher syndrome Type II. *Invest Ophthalmol Vis Sci*; **45**: 784-792.
  21. Haer-Wigman L, van Zelst-Stams WA, Pfundt R, van den Born LI, Klaver CC, Verheij JB, Hoyng CB, Breuning MH, Boon CJ, Kievit AJ, et al. (2017) Diagnostic exome sequencing in 266 Dutch patients with visual impairment. *Eur J Hum Genet*; **25**: 591-599.
  22. Sengillo JD, Lee W, Nagasaki T, Schuerch K, Yannuzzi LA, Freund KB, Sparrow J, Allikmets R, Tsang SH. (2018) A Distinct Phenotype of Eyes Shut Homolog (EYS)-Retinitis Pigmentosa is Associated with Variants Near the C-Terminus. *Am J Ophthalmol*.
  23. McGuigan DB, Heon E, Cideciyan AV, Ratnapriya R, Lu M, Sumaroka A, Roman AJ, Batmanabane V, Garafalo AV, Stone EM, et al. (2017) EYS Mutations Causing Autosomal Recessive Retinitis Pigmentosa: Changes of Retinal Structure and Function with Disease Progression. *Genes (Basel)*; **8**.
  24. Oishi M, Oishi A, Gotoh N, Ogino K, Higasa K, Iida K, Makiyama Y, Morooka S, Matsuda F, Yoshimura N. (2014) Comprehensive molecular diagnosis of a large cohort of Japanese retinitis pigmentosa and Usher syndrome patients by next-generation sequencing. *Invest Ophthalmol Vis Sci*; **55**: 7369-7375.
  25. Suto K, Hosono K, Takahashi M, Hiram Y, Arai Y, Nagase Y, Ueno S, Terasaki H, Minoshima S, Kondo M, et al. (2014) Clinical phenotype in ten unrelated Japanese patients with mutations in the EYS gene. *Ophthalmic Genet*; **35**: 25-34.
  26. Hosono K, Ishigami C, Takahashi M, Park DH, Hiram Y, Nakanishi H, Ueno S, Yokoi T, Hikoya A, Fujita T, et al. (2012) Two novel mutations in the EYS gene are possible major causes of autosomal recessive retinitis pigmentosa in the Japanese population. *PLoS One*; **7**: e31036.



### 3.6 Supplemental information



**Supplementary Figure S1. Fundus photographs of patients in different stages of RP disease.**



**Supplementary Figure S2. Multifocal electroretinogram of patient XXIV-1 with macular dystrophy showing decreased foveal responses.**

**Supplementary Table S1.**

Primers used for cloning and RT-PCR.

Primer name	Primer sequence (5' > 3')
Wild type minigene forward in intron 7	5'- <u>G</u> GGGACAAGTTTGTACA <u>AAAAAGCAGGCTTCAGTCCTATAAGTAGCCCAAC</u> -3'
Wild type minigene reverse in intron 8	5'- <u>G</u> GGGACCACTTTGTACA <u>AAGAAAGCTGGGTGGTCTCTCTCAGTAAATATCTG</u> -3'
Mutagenesis primer forward	5'-GAAGATTCAAAGTAATTAATACATGGCAAC-3'
Mutagenesis primer reverse	5'-GTTGCCATGTATTAATTAATTACTTTGAATCTTC-3'
Rhodopsin exon 3 forward	5'-CGGAGGTCAACAACGAGTCT-3'
Rhodopsin exon 5 forward	5'-ATCTGCTGCGCAAGAAC-3'
Rhodopsin exon 5 reverse	5'-AGGTGTAGGGGATGGGAGAC-3'
Actin forward	5'-ACTGGGACGACATGGAGAAG-3'
Actin reverse	5'-TCTCAGCTGTGGTGGTGAAG-3'

Sequences used for Gateway cloning are underlined.

**Supplementary methods***Generation of minigenes*

PCR primers were designed in intron 7 (forward) and intron 8 (reverse) of the *EYS* gene using Primer3 software<sup>1</sup>. Fifty nanograms of genomic DNA from a control individual was incubated together with 0.5 μM of the forward and reverse primer, 100 μM dNTPs (Roche), 0.25 U Phusion high fidelity polymerase, 1x Phusion PCR buffer and 1x Q-solution (Qiagen, Venlo, the Netherlands) in a total volume of 25 μl. The following program was run in a 2720 Thermal Cycler (Applied Biosystems): samples were denatured at 98°C for 3 minutes followed by 35 cycles of amplification consisting of 30 seconds at 98°C, 30 seconds at 58°C and 1.5 minutes at 72°C, and a final extension for 5 minutes at 72°C. PCR products were separated on a 1% agarose gel and DNA products were excised, and purified on Nucleospin Gel and PCR Clean-up columns (Macherey Nagel). 150 ng of the purified insert was cloned into the pDONR201 entry vector using the Gateway BP Clonase Enzyme mix (Thermo Fisher Scientific). Entry clones were validated by Sanger sequencing.

For generation of the mutant minigene, the c.1299+5\_1299+8del mutation was introduced via site-directed mutagenesis, using the entry clone containing the wild-type construct as a template. Following Sanger sequencing of the mutated construct, both the wild-type and mutant entry clone were transferred into the destination vector pCI-NEO-RHO exon3,5/DEST using the Gateway LR Clonase enzyme mix (Thermo Fisher Scientific). The pCI-NEO-RHO exon3,5/DEST vector is a homemade destination vector that allows cloning of the fragment of interest between Rhodopsin exon 3 and 5 under the control of

the CMV promoter<sup>2</sup>. Primer sequences used to generate wild type and mutant minigenes are listed in Supp. Table S1.

#### *Cell culture and transfection*

HEK293T cells were grown in DMEM supplemented with 10% fetal calf serum, 1% penicillin-streptomycin and 1% sodium pyruvate at 37°C and 5% CO<sub>2</sub>. Confluent HEK293T cells were diluted 1 to 5 and ~400.000 cells per well were seeded in a 12-wells plate and grown for 24 hours at 37°C in a total volume of 1 ml. For transfection, 750 ng of the minigene vector was incubated together with 2.25 µl Fugene<sup>®</sup> HD Transfection Reagent (Promega, Madison, WI, USA) in a total volume of 100 µl Optimem for 20 minutes at room temperature and subsequently, the transfection mix was added to the cells. After incubation for 48 hours at 37°C, cells were harvested for RNA isolation.

#### *RNA isolation and cDNA synthesis*

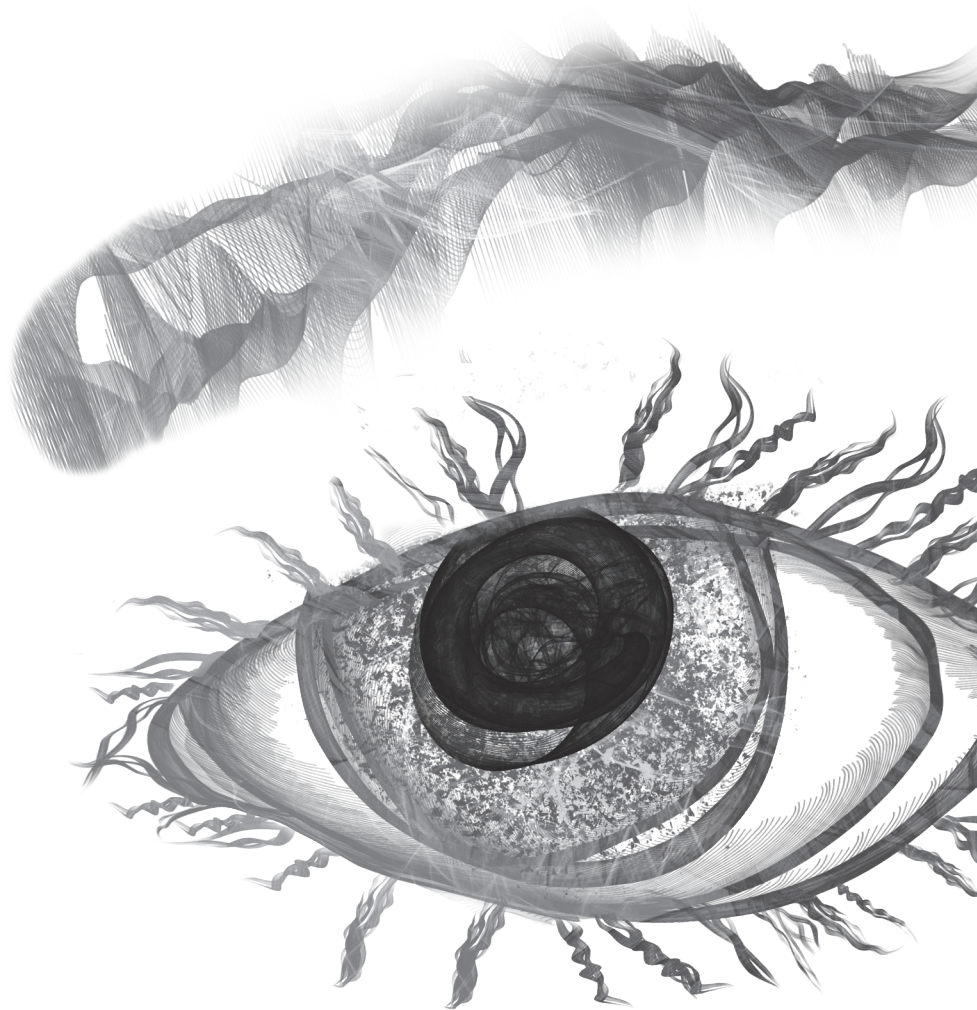
Total RNA from HEK293T cells was extracted using NucleoSpin RNA columns (Macherey-Nagel, Düren, Germany) according to the manufacturer's protocols. For cDNA synthesis, the iScript<sup>™</sup> cDNA synthesis kit (Bio-Rad, Hercules, CA, USA) was used. One microgram of total RNA was incubated with 1 µl iScript Reverse Transcriptase and 1x reaction mix in a total volume of 20 µl nuclease free water. For the RT-reaction, the mixture was incubated for 5 min at 25°C, 20 min at 46°C and the reaction was stopped by heating at 95°C for 1 min.

#### *RT-PCR analysis*

Two µl of cDNA was incubated together with 0.5 µM of the forward and reverse primer, 100 µM dNTPs (Roche), 0.25 U Taq polymerase (Roche), 1x PCR buffer + Mg<sup>+</sup> (Roche) in a total volume of 25 µl milliQ. PCR conditions were 3 minutes at 94°C followed by 35 cycles of amplification consisting of 30 seconds at 94°C, 30 seconds at 58°C and 2 minutes at 72°C, and a final extension for 5 minutes at 72°C. Primer sequences are listed in Supplementary Table 1. PCR products were purified on Nucleospin Gel and PCR Clean-up columns (Macherey Nagel). After purification, PCR samples were sent for Sanger sequencing with the same primers that were used for the RT-PCR reaction.



# Chapter 4



# Eyes shut homolog is important for the maintenance of photoreceptor morphology and visual function in zebrafish

Muriël Messchaert<sup>1,2</sup>, Margo Dona<sup>3,4</sup>, Sanne Broekman<sup>3</sup>, Theo A. Peters<sup>2,3</sup>, Julio C. Corral-Serrano<sup>1,4</sup>, Ralph W.N. Slijkerman<sup>3,4</sup>, Erwin van Wijk<sup>2,3</sup>, Rob W.J. Collin<sup>1,2</sup>

<sup>1</sup> Department of Human Genetics, Radboud University Medical Center, Nijmegen, The Netherlands

<sup>2</sup> Donders Institute for Brain, Cognition and Behaviour, Radboud University Medical Center, Nijmegen, The Netherlands

<sup>3</sup> Department of Otorhinolaryngology, Radboud University Medical Center, Nijmegen, The Netherlands

<sup>4</sup> Radboud Institute for Molecular Life Sciences, Radboud University Medical Center, Nijmegen, The Netherlands

**Abstract**

Mutations in *eyes shut homolog (EYS)*, a gene predominantly expressed in the photoreceptor cells of the retina, are among the most frequent causes of autosomal recessive (ar) retinitis pigmentosa (RP), a progressive retinal disorder. Due to the absence of *EYS* in several rodent species and its retina-specific expression, still little is known about the exact function of *EYS* and the pathogenic mechanism underlying *EYS*-associated RP. We characterized *eyes* in zebrafish, by RT-PCR analysis on zebrafish eye-derived RNA, which led to the identification of a 8,715 nucleotide coding sequence that is divided over 46 exons. The transcript is predicted to encode a 2,905-aa protein that contains 39 EGF-like domains and five laminin A G-like domains, which overall shows 33% identity with human *EYS*. To study the function of *EYS*, we generated a stable *eyes<sup>rmc101/rmc101</sup>* mutant zebrafish model using CRISPR/Cas9 technology. The introduced lesion is predicted to result in premature termination of protein synthesis and lead to loss of *Eys* function. Immunohistochemistry on retinal sections revealed that *Eys* localizes at the region of the connecting cilium and that both rhodopsin and cone transducin are mislocalized in the absence of *Eys*. Electroretinogram recordings showed diminished b-wave amplitudes in *eyes<sup>rmc101/rmc101</sup>* zebrafish (5 dpf) compared to age- and strain-matched wild-type larvae. In addition, decreased locomotor activity in response to light stimuli was observed in *eyes* mutant larvae. Altogether, our study shows that absence of *Eys* leads to a disorganized retinal architecture and causes visual dysfunction in zebrafish.

**Key words:**

*Eyes shut homolog*, CRISPR/Cas9, photoreceptors, retinal dysfunction, zebrafish

## 4.1 Introduction

Retinitis pigmentosa (RP) is a clinically diverse and genetically heterogeneous disorder with a prevalence of approximately 1 in 4,000 individuals. Retinitis pigmentosa is characterized by night blindness and visual field constriction, and often leads to total blindness.<sup>1</sup> For RP, different modes of inheritance including autosomal recessive, autosomal dominant, and X-linked, have been observed. To date, 58 genes are described in which mutations can cause arRP (RetNet, <http://www.sph.uth.tmc.edu/RetNet/>), most of them only being responsible for 1-2% of all arRP cases. Mutations in the *eyes shut homolog* (*EYS*) gene are among the most frequent causes of arRP, accounting for approximately 5-10% of all cases.<sup>2-4</sup> *EYS* is located on chromosome 6p12 and is predominantly expressed in the retina. Human *EYS* encodes for the 3,144 amino acid protein eyes shut homolog (EYS) that consists of five laminin A G-like (LamG) domains and 28 epidermal growth factor (EGF) or EGF-like domains.<sup>5,6</sup>

Eyes shut homolog is an ortholog of the *Drosophila* spacemaker (*spam*) protein, which plays a major role in the development of photoreceptors and the maintenance of the photoreceptor morphology.<sup>7</sup> Since the composition of the *Drosophila* eye is substantially different compared to that of the human eye, it remains questionable whether *Drosophila* can serve as a good model to study *EYS*-associated RP. Extensive bio-informatic analysis showed that *Eys* is absent from several rodent genomes (e.g. mice),<sup>6</sup> which also excludes these animals for being used as a model system to study *Eys* function. In the zebrafish genome, several gene predictions encoding EGF-like domains and LamG domains are predicted on chromosome 13, including Chr13.1401, Chr13.1402, Chr13.1403, ENSDART00000108504 and ENSDART00000122834. This indicates that *eyes* probably is present in zebrafish, although its complete sequence was not characterized. Furthermore, the zebrafish retina is morphologically similar to that of the human retina, in the sense that all the major cell layers found in humans are also present in zebrafish,<sup>8</sup> thereby providing a promising model to study the function of *EYS*.

Recently, two independent groups reported degeneration of the photoreceptor cell layer in different *eyes* knock-out zebrafish models.<sup>9,10</sup> Yu *et al.* generated an *eyes* mutant zebrafish line using CRISPR/Cas9 technology in which degradation of the outer nuclear layer was observed. In addition, they revealed that *eyes* localizes near the photoreceptor connecting cilium and that it might play a role in maintaining the ciliary pocket.<sup>10</sup> In a study of Lu *et al.*, TALEN technology was used to generate an *eyes* knock-out zebrafish, which showed visual impairment by recording electroretinography (ERG). Furthermore, they demonstrated F-actin disruption and mislocalization of the retinal proteins red opsin, UV opsin and rhodopsin in the absence of *Eys*.<sup>9</sup> Both studies imply a role of *Eys* in maintaining retinal morphology and visual function, although the exact mechanism underlying *EYS*-associated RP still remains to be elucidated.

In this study, we generated a stable *eyes*<sup>-/-</sup> mutant zebrafish line, designated *eyes*<sup>rmc101/rmc101</sup>, using CRISPR/Cas9 technology to study the function of *Eys* in the zebrafish retina. Similar



to previous studies,<sup>9,10</sup> we observed progressive degeneration of the photoreceptor outer segments, mislocalization of rhodopsin and decreased ERG responses in absence of *Eys*. In addition, we show diminished locomotor activity of *eyes<sup>tmc101/rmc101</sup>* zebrafish larvae in response to light stimuli, which has not been shown before.

## 4.2 Materials and methods

### 4.2.1 Animal experiments

The zebrafish experiments were approved by the Centrale Commissie Dierproeven (CCD, RU-DEC 2016–0091) and were performed in accordance with the Dutch law (Wet op de Dierproeven 1996) and European regulations (Directive 86/609/EEC).

### 4.2.2 Fish husbandry

We used the in-house bred Tupfel Longfin strain. Adult zebrafish were maintained in 4.5-liter polyethylene tanks (Tecniplast) in an Aqua Schwarz holding system (Göttingen) supplied continuously with circulating filtered tap water (electrical conductivity of 300  $\mu\text{S cm}^{-1}$ , 27.5 °C, pH 7.5–8) under cycles providing 14 hrs of light and 10 hrs of dark (14:10 LD; lights on 9 AM; lights off 11 PM). The fish were fed with Gemma Micro 300 (Skretting) twice a day and living *Artemia* once a day.

### 4.2.3 RNA isolation

Total RNA from adult zebrafish eyes was obtained by snap-freezing isolated eyes in liquid nitrogen and subsequently homogenizing the eyes in Trizol (Thermo Fischer Scientific) using a pestle and moving through a syringe five times. After incubation on ice for 15 minutes, 250  $\mu\text{l}$  chloroform was added, incubated for 3 minutes and centrifuged at 4°C at 12,000 $\times g$  for 15 minutes. The supernatant was mixed with 1  $\mu\text{l}$  glycogen (5  $\mu\text{g}/\mu\text{l}$ ) and 250  $\mu\text{l}$  isopropanol and stored at -80°C o/n. The RNA was further purified and DNase treated using RNeasy spin columns (Qiagen) according to manufacturer's protocol.

### 4.2.4 RT-PCR analysis of *eyes*

For cDNA synthesis, one  $\mu\text{g}$  of total RNA was reverse transcribed using the iScript™ cDNA synthesis kit (Bio-Rad) according to the manufacturer's instructions. For the characterization of zebrafish *eyes*, RT-PCR was performed. One microliter cDNA was incubated together with 0.5  $\mu\text{M}$  of the forward and reverse primer, 100  $\mu\text{M}$  dNTPs (Roche), 0.25 U Taq polymerase (Roche), 10 $\times$  PCR buffer + 15 mM  $\text{MgCl}_2$  (Roche) and 1 $\times$  Q solution (Qiagen) in a total volume of 25  $\mu\text{l}$ . The following program was run in a 2720 Thermal Cycler (Applied Biosystems): the samples were denatured at 94°C for 3 minutes followed by 35 cycles of amplification consisting of 94°C for 20 seconds, 58°C for 30 seconds and 72°C for 50 seconds, and a final primer extension at 72°C for 5 minutes. Primers targeting all exons of *eyes* were designed, based on gene predictions Chr13.1401, Chr13.1402, Chr13.1403, ENSDART00000108504

and ENSDART00000122834 using the UCSC Genome Browser on Zv9/danRer7 assembly. Primer sequences are listed in S1 Table. A number of these primer combinations were used for nested PCRs resulting in the amplification of PCR products representing parts of the *eyes* transcript expressed in zebrafish eyes. To verify that the amplified products indeed correspond to *eyes*, PCR products were purified on Nucleospin Gel and PCR Clean-up columns (Macherey Nagel) and either directly sequenced or cloned in the pCR4-TOPO vector with the use of the TOPO TA Cloning Kit (Invitrogen) for sequencing with T7 and T3 sequencing primers.

To study the presence of *eyes* transcript in wild-type and *eyes<sup>rnc101/rnc101</sup>* larvae, total RNA from 20 pooled larvae was extracted as described above. RT-PCR was performed using a primer pair covering the region in exon 20 of *eyes* where the deletion was located (Supp. Table S1).

#### 4.2.5 Multiple sequence alignment

A multiple sequence alignment of EYS proteins from different species was generated using AlignX in the Vector NTI software package (Vector NTI Advance 11). Accession numbers of the protein sequences used for sequence comparison are as follows: human, NM\_001142800.1 (RefSeq); macaque, XM\_011737495.1 (RefSeq); chicken, XM\_015284845.1 (RefSeq); *Drosophila*, NM\_001032399.3 (RefSeq).

#### 4.2.6 Target site selection and gRNA synthesis

Target sites for genome editing were selected by using the online web tool CHOPCHOP (<https://chopchop.rc.fas.harvard.edu/>).<sup>11</sup> Guide RNAs (gRNAs) were synthesized as described previously.<sup>12</sup> Templates for gRNA transcription were generated by annealing gene-specific oligonucleotides containing the T7 (5'-TAATACGACTCACTATA-3') promoter sequence, the 20-base target sequence without the PAM, and a complementary region to a constant oligonucleotide encoding the reverse complement of the tracrRNA tail. T4 DNA polymerase (New England Biolabs) was used to fill the ssDNA overhang and the template was then purified using the GenElute PCR clean-up kit (Sigma). Transcription of the gRNAs was performed using the T7 MEGashortscript Kit (Ambion). Oligos used for gRNA synthesis are listed in Supp. Table S2.

#### 4.2.7 Microinjections

Zebrafish embryos were collected after natural spawning and injected at the single cell stage with one nanoliter of injection mix (4.5  $\mu$ l gRNA (1  $\mu$ g/ $\mu$ l), 2.5  $\mu$ l Cas9 protein (2  $\mu$ g/ $\mu$ l, PNA Bio), 2  $\mu$ l 1M KCl and 1  $\mu$ l 0.5% phenol red dye). To screen for genomic lesions, genomic DNA was extracted from a pool of 15 embryos at 2.5 days post fertilization (dpf).

#### 4.2.8 Genotyping

Genomic DNA was extracted from larvae at 2.5 dpf or caudal fin tissue from adult zebrafish. Tissue was incubated in 25  $\mu$ l (larvae) or 75  $\mu$ l (fin tissue) lysis buffer (40 mM NaOH 0.2

mM EDTA) at 95°C for 20 minutes. The lysed samples were diluted 10 times of which 1  $\mu$ l was incubated together with 0.5  $\mu$ M of the forward and reverse primer, 100  $\mu$ M dNTPs (Roche), 0.25 U Taq polymerase (Roche) and 10x PCR buffer + 15 mM MgCl<sub>2</sub> (Roche) in a total volume of 25  $\mu$ l. Samples were denatured at 94°C for 3 minutes followed by 35 cycles of amplification consisting of 20 seconds at 94°C, 30 seconds at 58°C and 50 seconds at 72°C, and a final primer extension of 5 minutes at 72°C. To screen for genomic lesions, PCR products were sequenced directly. Primer sequences are listed in Supp. Table S1.

#### 4.2.9 Immunohistochemistry

Dissected adult zebrafish eyes (2 mpf and/or 5 mpf) and larvae (5 dpf) from *eyes<sup>rmc101/rmc101</sup>* mutants and their age- and strain-matched wild-type controls were cryoprotected with 10% sucrose in PBS for 10 minutes prior to embedding in OCT compound. Embedded samples were snap frozen in liquid nitrogen-cooled isopentane and cryosectioned following standard protocols. Cryosections (7  $\mu$ m) were fixed with 4% paraformaldehyde (PFA) at room temperature for 10 minutes, permeabilized with 0.01% PBS-Tween20 and hereafter blocked in 10% normal goat serum and 2% BSA in PBS at room temperature for 1 hour. Subsequently, they were incubated with primary antibodies directed against EYS/RP25 (rabbit, 1:300, Novus Biological NBP1-90038), Centrin (mouse, 1:250, Millipore 04-1624) or GFAP (rabbit, 1:750, Dako) at 4°C overnight. After washing with PBS, cryosections were incubated with secondary antibodies (rabbit IgG, Alexa Fluor 488, goat, 1:800, Molecular Probes A11008; mouse IgG, Alexa Fluor 568, goat, 1:800, Life Technologies A11031) at room temperature for one hour.

For rhodopsin and cone transducin staining, zebrafish eyes were fixed with 4% PFA at 4°C overnight, followed by incubation in a MeOH gradient. After embedding, freezing and cryosectioning, slides were permeabilized with 0.1% PBS-Tween20 and incubated in antigen retrieval solution (10 mM sodium citrate pH 8.5) at 121°C for 1 minute. After washing, cryosections were blocked in block solution (10% Non Fat Dry Milk in 0.1% PBS-Tween20) at RT for 1 hour, followed by incubation with the primary antibodies Rhodopsin (clone 4D2, mouse, 1:2,000, Novus Biological NBP1-48334) and GNAT2 (rabbit, 1:500, MBL PM075) in block solution at 4°C overnight. After washing with 0.1% PBS-Tween20, slides were incubated with the secondary antibodies (rabbit IgG, Alexa Fluor 488, goat, 1:800, Molecular Probes A11008; mouse IgG, Alexa Fluor 488, goat, 1:800, Invitrogen A11029) together with Phalloidin Alexa Fluor 568 (1:100, Molecular Probes, A-12380).

For staining with boron-dipyrromethene (BODIPY), zebrafish larvae or eyes were fixed in 4% PFA for 2 hours, cryoprotected in 10% sucrose in PBS for 30 minutes, embedded in OCT, snap frozen in melting isopentane and cryosectioned. BODIPY was applied to the cryosections at room temperature for 20 minutes.

In all cases, nuclei were counterstained with DAPI (1:8,000). Imaging was performed on a ZEISS LSM 880 microscope with Airyscan. Zen software was used for processing the images. To analyze the thickness of ONL and INL in 5 dpf, 2 mpf and 5 mpf zebrafish, up

to 10 different measurements were taken for each section. Two different sections were analyzed for one wild-type fish and one *eys* mutant fish per time-point.

#### 4.2.10 Optokinetic response (OKR) measurements

Optokinetic response measurements were performed as described previously.<sup>13</sup> In brief, zebrafish larvae were mounted in 3% methylcellulose in a small Petri-dish, which was placed on a platform surrounded by a rotating drum of 8 cm in diameter. A pattern of alternating black and white vertical stripes was displayed on the drum interior (each stripe subtended an angle of 36°). Larvae (5 dpf) were placed in an upright position and visualized through a stereomicroscope positioned over the drum and illuminated with fiberoptic lights. Eye movements were recorded while larvae were optically stimulated by the rotating stripes. Larvae were subjected to a protocol of 30 seconds 5 rpm counterclockwise rotation, 10 seconds rest, 30 seconds 5 rpm clockwise rotation, 10 seconds rest, 30 seconds 8 rpm counterclockwise rotation, 10 seconds rest, 30 seconds 8 rpm clockwise rotation. The amount of eye movements were counted from the recorded movies afterwards and plotted using Graphpad Prism (version 5.03).

#### 4.2.11 Electroretinography (ERG)

Electroretinography measurements were performed on isolated larval eyes (5 dpf) as previously described.<sup>14</sup> Larvae were dark-adapted for a minimum of 30 minutes prior to the measurements, and subsequently handled under dim red illumination. The isolated eye was positioned to face the light source. Under visual control via a standard microscope (Stemi SV8, Zeiss) equipped with red illumination (KL1500 electronic, Zeiss), the recording electrode with an opening of approximately 15 μm at the tip was placed against the center of the cornea with a micromanipulator. This electrode was filled with E3 medium (5 mM NaCl, 0.17 mM KCl, 0.33 mM CaCl<sub>2</sub>, and 0.33 mM MgSO<sub>4</sub>). A custom-made stimulator was invoked to provide light pulses of 100 ms duration, with a 100% light intensity of 6000 lux. It uses a ZEISS XBO 75W light source and a fast shutter (custom made) driven by the self-developed NI Labview program. Electronic signals were amplified 1,000 times by a pre-amplifier (P55 A.C. Preamplifier, Astro-Med. Inc, Grass Technology) with a band pass between 0.1 and 100 Hz, digitized by DAQ Board NI BNC-2090 (National Instruments) and displayed via the self-developed NI Labview program. All experiments were performed at room temperature.

#### 4.2.12 Visual motor response

Locomotor activity in response to light-dark conditions, also known as visual motor response (VMR), was analyzed using the Danio Vision system (Noldus B.V.). Collected embryos were raised in E3 medium (5mM NaCl, 0.17mM KCL, 0.33mM CaCl<sub>2</sub>, 0.33mM MgSO<sub>4</sub>, supplemented with 0.1% methylene blue) in a 28°C incubator, subsequently under 14 hrs of light and 10 hrs of dark. Medium was changed every day and during the

process curved and dead larvae were discarded. Behavioral tests were carried out at 5 dpf. Larvae were transferred to a 48-wells plate filled with 200  $\mu$ l E3 medium without methylene blue. In each run, 24 mutant larvae and 24 age- and strain-matched control wild-type zebrafish larvae were tested. During the experiment, the temperature was kept constant at 28°C using a heating/cooling system (Noldus B.V.). The protocol consisted of 20 min acclimation (with lid of the system open; room light: 500-650 lux), closing of the lid followed by alternating periods of 10 minutes dark, 10 minutes bright light (about 3000 lux) and 10 minutes dark (in total 12 cycles). Variables of interest were: *distance moved* (mm) and *maximum velocity* ( $V_{max}$ , mm/s), and *difference in distance moved* and *difference in  $V_{max}$*  (maximum distance moved/ $V_{max}$  of first 30 seconds light condition minus average distance moved/ $V_{max}$  last 30 seconds of dark condition) for the change from dark to light.

#### 4.2.13 Statistical analysis

Statistical analysis was performed using Graphpad Prism software. For data obtained using Danio Vision, RStudio version 1.0.153 (<https://www.r-project.org>) was used to generate graphs and perform statistical analysis. The difference between wild-type and mutant zebrafish was analyzed using two-tailed, unpaired Student's *t*-test, and *p*-values were corrected for multiple testing using the Benjamini-Hochberg method. Statistical significance was set at  $p < 0.05$ . The means and standard errors of the mean are shown. Exact *p*-values are shown in Supp. Table S3.

### 4.3 Results

#### 4.3.1 Characterization of zebrafish *ey*s cDNA

The complete zebrafish *ey*s sequence was not completely identified, however, in the UCSC genome browser, several gene predictions for zebrafish *ey*s were present. On zebrafish chromosome 13, genes encoding EGF-like domains and LamG domains were predicted, including Chr13.1401, Chr13.1402, Chr13.1403, ENSDART00000108504 and ENSDART00000122834 (Supp. Figure S1). Based on these gene predictions, we hypothesized that *ey*s is present in zebrafish. We performed RT-PCR using primers targeting *ey*s on RNA derived from adult zebrafish eyes as a template. This resulted in the identification of a 8,715 nucleotide long transcript encompassing 46 exons. Most of these exons were previously predicted by several gene prediction programs, although also a number of new exons were identified (Supp. Figure S1A). The resulting *ey*s transcript translates into a protein of 2,905 amino acids that is predicted to harbor 39 EGF-like domains and five LamG domains. This domain organization is similar to what is observed for the human and *Drosophila* EYS proteins (Supp. Figure S1B). Interestingly, the zebrafish Eys protein appears to lack a so called low-complexity region, as seen for the human and

*Drosophila* protein, in which no domains are predicted. In human, this region is completely encoded by exon 26, which is lacking in zebrafish *eyes*.

We performed a multiple sequence alignment of the predicted Eys protein with the sequence of Eys from several other species (Supp. Figure S2). From this, we could deduce that the amino acids coding for the N-terminal EGF- and EGF-like domains as well as the C-terminal LamG domains are conserved over macaque, chicken, *Drosophila*, human and zebrafish. Overall, the predicted zebrafish Eys protein shows a 33% sequence identity compared to human EYS.

### 4.3.2 Generation of an *eyes*<sup>-/-</sup> zebrafish line by CRISPR/Cas9 technology

To better study the zebrafish Eys protein in the retina, we generated a stable zebrafish *eyes* knock-out line using CRISPR/Cas9 technology. By screening zebrafish larvae for genetic lesions, several different types of mutations were identified. For subsequent experiments, zebrafish carrying a five base pair deletion (c.3488\_3492del) in exon 20 were selected for the creation of a stable zebrafish line and named *eyes*<sup>rmc101/rmc101</sup> (Figure 4.1A). The deletion is predicted to lead to a frameshift and premature termination of protein translation (p.Gly1163Valfs\*14) (Figure 4.1C). To determine whether *eyes* mRNA is present in homozygous mutant zebrafish or whether this mRNA undergoes nonsense mediated decay, RNA was isolated from a pool of larvae (n=15). Subsequently, the presence of *eyes* transcripts was determined by RT-PCR analysis. PCR products were observed for both wild-type and mutant zebrafish larvae (Figure 4.1B), indicating that mutant *eyes* transcripts are not rapidly degraded. Sanger sequencing confirmed that *eyes* knock-out fish express the *eyes* mRNA with the five base pair deletion.

### 4.3.3 Eys is absent from the retina of *eyes*<sup>rmc101/rmc101</sup> zebrafish and localizes with the ciliary protein Centrin

To determine the localization of the Eys protein in the zebrafish retina, immunohistochemistry with an antibody against Eys was performed on retinal cryosections of zebrafish at 5 days post fertilization (dpf) and 5 months post fertilization (mpf). Co-staining of wild-type and mutant retinas using the Eys antibody together with an antibody against centrin, a marker for the connecting cilium, was performed to determine whether Eys localizes near the connecting cilium. Eys expression was observed adjacent to the immunoreactive signal of centrin (Figure 4.2A). This suggests that Eys localizes near the photoreceptor connecting cilium. Since two puncta of Eys were always observed close to the immunofluorescence signal of centrin, it might be that Eys is located in the ciliary basal body and the daughter centriole. The Eys signal was completely absent in the retinas of *eyes* knock-out zebrafish, indicating that the Eys protein is not properly expressed in the mutants and that the immunofluorescence signal observed in the wild-type retinas is specific (Figure 4.2A).

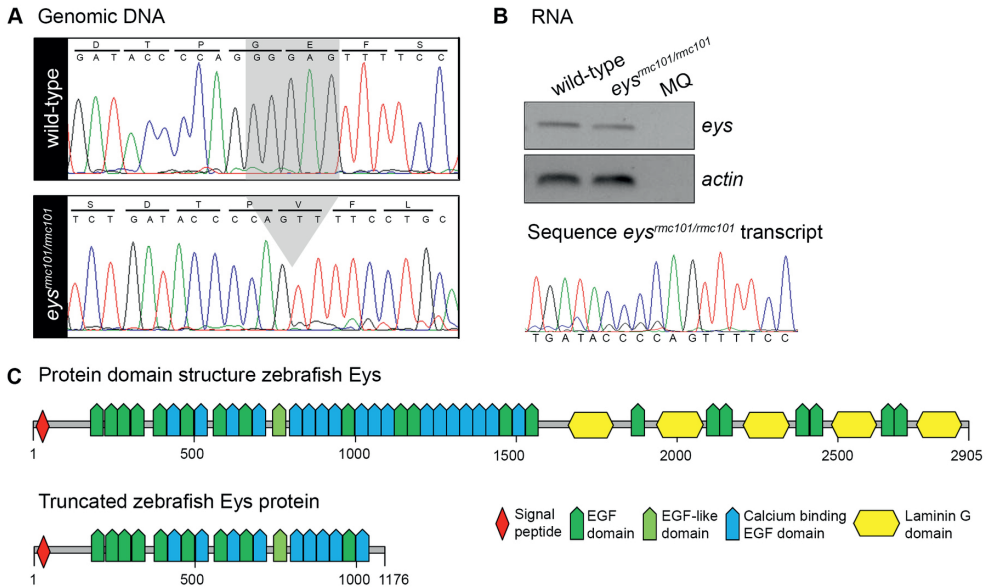


**Figure 4.1. Characterization of a stable  $eys^{rmc101/rmc101}$  zebrafish line.**

(A) Sanger sequencing identified a five base pair deletion in exon 20 in  $eys^{rmc101/rmc101}$  zebrafish. (B) Representative gel image of RT-PCR analysis using RNA from a pool of larvae ( $n=15$ ), which shows that *eys* transcripts are present in both wild-type and  $eys^{rmc101/rmc101}$  zebrafish (upper panel). Sanger sequencing confirmed the presence of the five base pair deletion in the  $eys^{rmc101/rmc101}$  transcript (lower panel). (C) Protein domain structures of wild-type Eys and the truncated Eys protein that is predicted in  $eys^{rmc101/rmc101}$  zebrafish.

#### 4.3.4 Disorganization of photoreceptor outer segments and mislocalization of outer segments proteins in $eys^{rmc101/rmc101}$ zebrafish

Next, we evaluated the effect of Eys deficiency on overall photoreceptor outer segment morphology by staining with BODIPY. This is a fluorescent dye that stains lipids and allows to visualize the outer segments of the photoreceptor cells. In the mutant retinas, the outer segments appear to be less in numbers, shorter, thicker and also more disorganized compared to outer segments in the wild-type retinas (Figure 4.2B). In addition, a reduction in inner and/or outer nuclear thickness was observed in  $eys^{rmc101/rmc101}$  fish of 2 mpf and 5 mpf (Supp. Figure S3). As Müller glia activation is a feature of retinal degeneration in zebrafish, we investigated the presence of activated Müller glia cells by immunohistochemistry. Müller glia cells were detected using an antibody against a specific cytoskeletal protein, glial fibrillary acidic protein (GFAP). Glial fibrillary acidic protein is described to be upregulated in glial cells in response to injury.<sup>15</sup> However, we did not observe any differences in GFAP staining between wild-type and  $eys^{rmc101/rmc101}$  zebrafish, at 5 dpf nor at

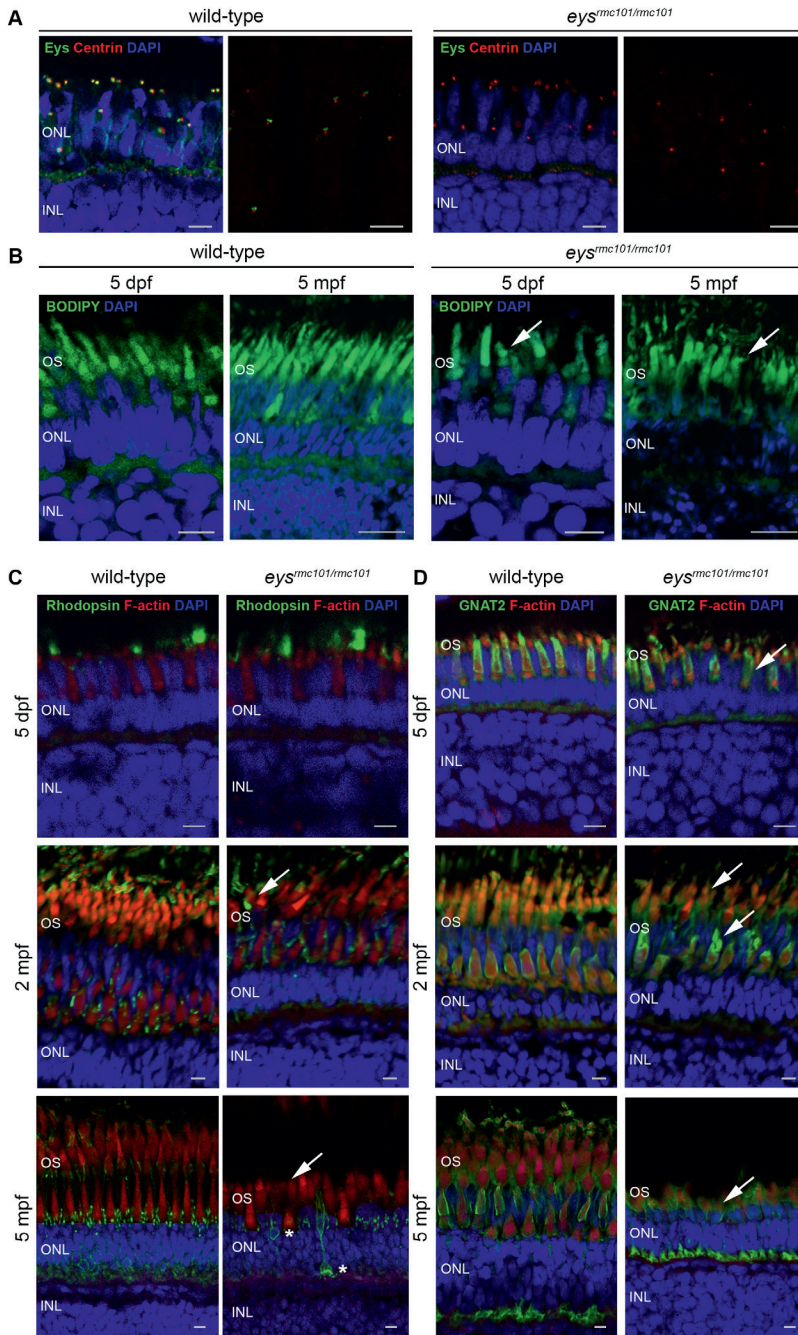


**Figure 4.2. Immunohistochemistry on retinal sections of wild-type and *eys<sup>mc101/mc101</sup>* zebrafish.**

(A) Retinal sections of wild-type and *eys<sup>mc101/mc101</sup>* zebrafish at 5 dpf and 5 mpf stained with antibodies



against Eys (green) and centrin (red). (B) BODIPY (green) staining showing disorganization of photoreceptor outer segments in *eys<sup>rmc101/rmc101</sup>* zebrafish (5 dpf and 5 mpf) compared to age- and strain-matched wild-type zebrafish (arrows). (C) Retinal sections of wild-type and *eys<sup>rmc101/rmc101</sup>* zebrafish at 5 dpf (upper panel), 2 mpf (middle panel) and 5 mpf (lower panel) stained with antibodies against rhodopsin (green) and F-actin (red). Asterisks indicate mislocalization of rhodopsin to the inner segments and synapses of photoreceptor cells. (D) Retinal sections of wild-type and *eys<sup>rmc101/rmc101</sup>* zebrafish at 5 dpf, 2 mpf and 5 mpf stained with antibodies against GNAT2 (green) and F-actin (red). Arrows indicate dysmorphic outer segments in mutant zebrafish. In all images, nuclei are counterstained with DAPI (blue). INL: inner nuclear layer; ONL: outer nuclear layer; OS: outer segments. Scale: 5  $\mu$ m.

2 mpf (Supp. Figure S4). In addition, we stained the fish retinas (5 dpf, 2 mpf and 5 mpf) with an antibody against F-actin. In contrast to what was observed in the wild-type retinas, F-actin expression was disrupted in retinas of *eys<sup>rmc101/rmc101</sup>* zebrafish (Figure 4.2C,D), which further illustrates outer segment disorganization and is in agreement with findings by Lu et al. 2017.<sup>9</sup> Finally, we examined the localization of the photoreceptor proteins rhodopsin and cone transducin (GNAT2) in retinas of wild-type and *eys<sup>rmc101/rmc101</sup>* larvae and adult zebrafish (5 dpf, 2 mpf and 5 mpf). In the wild-type retinas, rhodopsin localization was observed in the outer segments as well as lining the outer segment membranes (Figure 4.2C). Cone transducin was mainly observed lining the outer segments (Figure 4.2D). In retinas of *eys<sup>rmc101/rmc101</sup>* adult zebrafish and larvae, dysmorphic outer segments were observed together with aberrant localization of rhodopsin and cone transducin (Figure 4.2C,D). In the retinas of *eys* mutant fish at 5 mpf, rhodopsin was partially mislocalized to the inner segments and synapses of photoreceptor cells (Figure 4.2C). This suggests that the change in outer segment morphology due to absence of Eys also affects the proper localization of other photoreceptor-specific proteins.

### 4.3.5 Visual function is impaired in *eys<sup>rmc101/rmc101</sup>* zebrafish

To assess whether depletion of Eys results in visual dysfunction, we performed behavioral and functional assays. All assays were performed with larvae at 5 dpf. First, ERG recordings were performed to measure the visual function of wild-type and *eys<sup>rmc101/rmc101</sup>* zebrafish larvae at 5 dpf. Mutant larvae showed significantly diminished b-wave amplitudes ( $640.4 \mu\text{V} \pm 37.31$  (mean  $\pm$  SEM,  $n=30$ )) compared to the b-wave amplitude of wild-type zebrafish larvae ( $451.0 \mu\text{V} \pm 34.37$  (mean  $\pm$  SEM,  $n=30$ )) (Figure 4.3A,C). No difference was observed in a-wave amplitude between wild-type ( $-102.9 \mu\text{V} \pm 8.047$  (mean  $\pm$  SEM,  $n=20$ )) and *eys<sup>rmc101/rmc101</sup>* larvae ( $-89.06 \mu\text{V} \pm 8.040$  (mean  $\pm$  SEM,  $n=20$ )) (Figure 4.3B,D). The diminished b-wave amplitude in the mutant larvae indicates that the *eys<sup>rmc101/rmc101</sup>* larvae are visual impaired already in an early stage of life. Subsequently, optokinetic responses were measured using an in-house experimental set-up. The number of saccades was used as a measure for the optokinetic response. No significant difference in the number of eye

movements between wild-type and *eyes<sup>mc101/mc101</sup>* larvae was observed ( $p=0.9710$ ,  $n=19$ ) (Figure 4.3E).

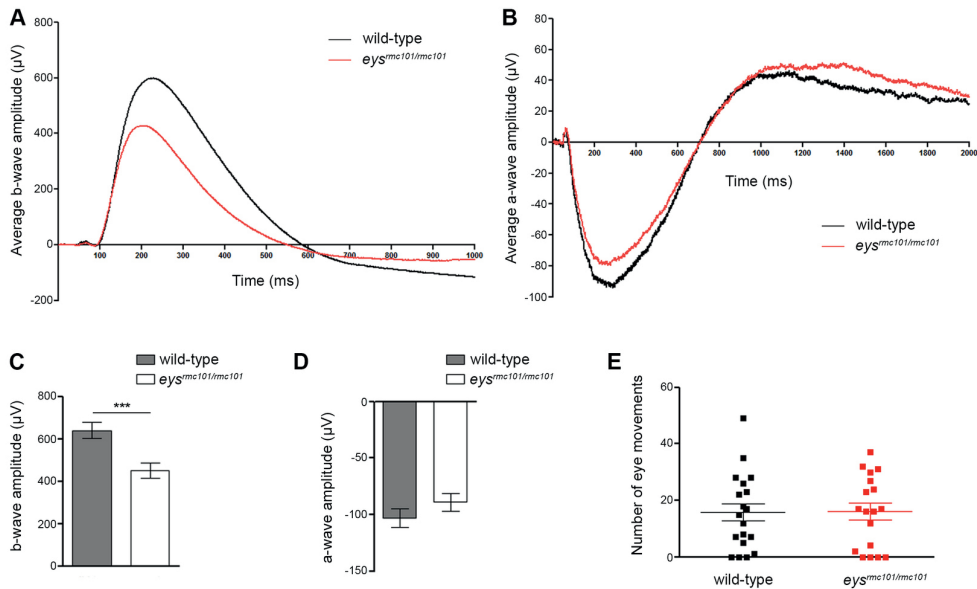


**Figure 4.3. Visual function of wild-type and *eyes<sup>mc101/mc101</sup>* zebrafish larvae.**

(A) ERG measurements of the b-wave of wild-type (black line) and *eyes<sup>mc101/mc101</sup>* (red line) zebrafish larvae at 5 dpf. (B) ERG measurements of the a-wave of wild-type (black line) and *eyes<sup>mc101/mc101</sup>* (red line) zebrafish larvae at 5 dpf. (C) Quantification of the ERG b-wave amplitude of wild-type and *eyes<sup>mc101/mc101</sup>* zebrafish larvae at 5 dpf ( $n=30$ ;  $p=0.0004$ ). (D) Quantification of the ERG a-wave amplitude of wild-type and *eyes<sup>mc101/mc101</sup>* zebrafish larvae at 5 dpf ( $n=20$ ;  $p=0.2324$ ). (E) Optokinetic response measurements of wild-type and *eyes<sup>mc101/mc101</sup>* larvae at 5 dpf ( $n=19$ ).

#### 4.3.6 Impaired locomotor activity of *eyes<sup>mc101/mc101</sup>* zebrafish in response to light

Locomotor activity of wild-type and *eyes<sup>mc101/mc101</sup>* larvae ( $n=120$ ) in response to a light stimulus, the visual motor response (VMR), was examined using the Danio Vision system. Larvae were exposed to alternating periods of 10 minutes dark and 10 minutes bright light for 12 cycles in total and parameters of interest were the distance moved and the maximum velocity (Vmax). We specifically analyzed these parameters during the transition from dark-to-light (last 30 seconds of dark period and first 30 seconds of light period), since this is described to contain the visual startle response.<sup>16,17</sup> Both wild-type and mutant larvae start to move at the moment the light is switched on. However, the response to light was less pronounced in the *eyes* knock-out larvae compared to the wild-

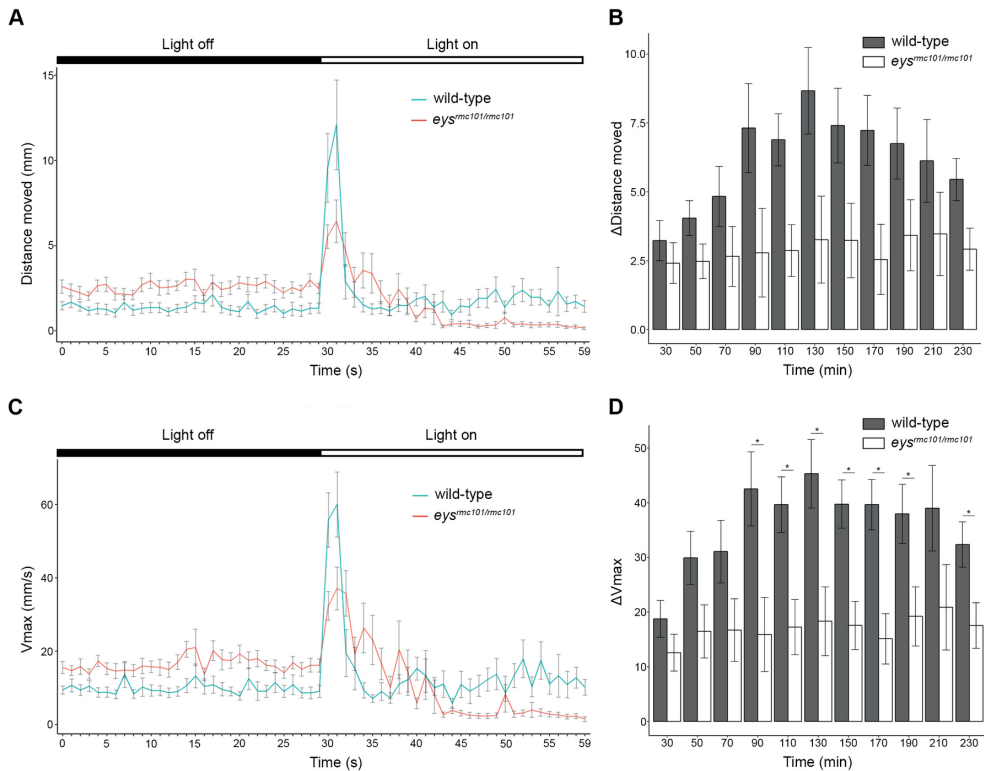


**Figure 4.4. Visual motor response of zebrafish larvae.**

(A) Distance moved (mm) of wild-type (blue line) and *eys<sup>mc101/mc101</sup>* (red line) larvae in response to a light stimulus (dark-to-light transition at  $t=50$  minutes). (B) Comparison of difference in distance moved between wild-type and *eys<sup>mc101/mc101</sup>* larvae at the dark to light transition zones. (C) Maximum velocity ( $V_{max}$ ; mm/s) of wild-type (blue line) and *eys<sup>mc101/mc101</sup>* (red line) larvae in response to a light stimulus (dark-to-light transition at  $t=50$  minutes). (D) Comparison of difference in  $V_{max}$  between wild-type and *eys<sup>mc101/mc101</sup>* larvae at the dark to light transition zones. All experiments were done with larvae at 5 dpf ( $n=120$ ). Statistical significance ( $p < 0.05$ ) is indicated with an asterisk.

type larvae (Figure 4.4A,C). Furthermore, we analyzed the change in distance moved and the change in  $V_{max}$  during the transition from dark-to-light, since the baseline activity of wild-type and *eys<sup>mc101/mc101</sup>* fish were not equal. Overall, our data showed that the difference in  $V_{max}$  was decreased in *eys<sup>mc101/mc101</sup>* larvae compared to wild-type larvae and that this decreased response was significantly lower at seven out of twelve dark-to-light transition zones (Figure 4.4D). Similarly, we observed a major decrease of the difference in distance moved in *eys<sup>mc101/mc101</sup>* fish compared to wild-type fish for all dark-to-light transition zones (Figure 4.4B), though not significantly different. These data show that

there is a diminished response to light by *eys* mutant larvae compared to age- and strain-matched wild-type larvae.

#### 4.4 Discussion

Mutations in *EYS* are among the most frequent causes of arRP, yet the exact retinal function of *EYS* and the pathogenic mechanism underlying *EYS*-associated RP are still poorly understood. In this study, we characterized *eys* in zebrafish and showed that absence of *Eys* leads to disorganization of the photoreceptor cell layer and functional impairment of the zebrafish retina. Furthermore, we showed decreased locomotor activity in response to light stimuli in *eys<sup>rmc101/rmc101</sup>* knock-out zebrafish larvae compared to wild-type larvae.

The zebrafish *Eys* protein lacks the low-complexity region as observed in human *EYS* protein, in which no protein domains are predicted. In human, this region is completely encoded by exon 26 of *EYS*. When analyzing the cDNA sequence of zebrafish *eys*, no corresponding exon of human *EYS* exon 26 could be found. In our multiple sequence alignment, one can also observe that this low complexity region is also missing from chicken *EYS*. This might suggest that the low complexity region, as observed in human *EYS*, is not of great importance for *EYS* to be a functional protein, at least not in all vertebrate species. In addition, a blast search with the amino acid sequence of this region only gave hits of human *EYS* protein and a number of *EYS* orthologs, such as gorilla, macaque, pig and dog.

A role of *Eys* in the morphogenesis of photoreceptors is described in *Drosophila*.<sup>7</sup> In the human retina, *EYS* might play a role in photoreceptor survival, however, certain rodent species including mouse, rat and guinea pig completely lack the *Eys* gene.<sup>6</sup> This raises the interesting questions on how photoreceptors in these species can survive.

In humans, retinitis pigmentosa is characterized by the progressive degeneration of rod photoreceptor cells, and in a later stage also cone photoreceptor cells. In our study, we also observed degeneration of photoreceptor outer segments in our zebrafish *eys<sup>rmc101/rmc101</sup>* knock-out model. It is remarkable that the *eys<sup>rmc101/rmc101</sup>* zebrafish show this clear morphological phenotype, since it is known that retinal regeneration can occur in zebrafish.<sup>18</sup> The Müller glia cells in zebrafish have the capacity to reprogram into retinal stem cells in response to injury, in contrast to mammals, where Müller glia cells rarely divide.<sup>19</sup> We investigated the presence of Müller glia activation in *eys<sup>rmc101/rmc101</sup>* zebrafish by immunohistochemistry using an antibody against GFAP. This specific cytoskeletal protein is shown to be upregulated in response to different types of retinal injury, such as mechanical damage and photoreceptor degeneration.<sup>15,20,21</sup> In our study, we did not observe any Müller glia activation by immunohistochemistry on retinal sections of wild-type and *eys* mutant fish (5 dpf and 2 mpf). It is possible that Müller glia activation occurs in later stages when degeneration is more severe. Another explanation could be that at the protein level, Müller glia activation in this stage of degeneration is not detectable yet. Studying gene expression levels in Müller glia cells might be a good alternative, since it

is shown that these levels change rapidly after photoreceptor loss.<sup>22</sup> However, our data suggests that the regeneration capacity in the zebrafish is not sufficient to overcome outer segment degeneration caused by absence of Eys.

Rhodopsin, which is located in the outer segments of rod photoreceptors, is a light-sensitive receptor protein and plays a major role in visual phototransduction cascade. In the absence of Eys, rhodopsin was mislocalized to the photoreceptor inner segments and synapses. An explanation for the mislocalization of rhodopsin might be that the absence of Eys directly affects the transport of rhodopsin to the photoreceptor outer segments. Another reason could be that rhodopsin is not able to reach the outer segments of the photoreceptor as a consequence of the morphological changes within *eys<sup>rmc101/rmc101</sup>* zebrafish. A previous study by Lu et al. also showed mislocalization of rhodopsin in *eys<sup>-/-</sup>* zebrafish retinas, as well as mislocalization of two other outer segment proteins, guanine nucleotide-binding protein G(I)/G(S)/G(T) subunit beta-3 (GNB3) and peripherin-2 (PRPH2).<sup>9</sup> Besides the peripheral mislocalization of rhodopsin, we also observed mislocalization of cone transducin (GNAT2). Next to that, GNAT2 immunofluorescence was decreased in *eys<sup>rmc101/rmc101</sup>* retinas compared to wild-type retinas, indicating mislocalization of GNAT2 or degeneration of cone photoreceptors which is in agreement with previous studies of both Yu et al. and Lu et al. that show degeneration of cone photoreceptor cells in their *eys<sup>-/-</sup>* zebrafish lines.<sup>9,10</sup>

In line with the paper of Yu et al.,<sup>10</sup> we showed that Eys localizes in the region of the photoreceptor connecting cilium. Two immunofluorescent dots of Eys were observed together near the centrin signal, suggesting that Eys might localize in the ciliary basal body and the daughter centriole. These data also implicate a possible role of Eys in facilitating ciliary transport of proteins towards the base of the cilium. To be able to further investigate the function of EYS it will be important to know the exact localization of eys in the ciliary zone, for instance by performing electromicroscopy studies.

To determine the effect of *eys* knock-out on the visual function of the zebrafish larvae (5dpf), we performed OKR, ERG and VMR experiments. No differences in OKR were observed between wild-type and mutant zebrafish larvae; however, ERG and VMR experiments showed that *eys<sup>rmc101/rmc101</sup>* zebrafish were visually impaired. A reason why we did not see any difference in OKR between wild-type and mutant zebrafish might be that this assay was not sensitive enough. In *eys<sup>rmc101/rmc101</sup>* larvae, the VMR was significantly decreased compared to wild-type larvae. When analyzing the data of the VMR experiments, we specifically focused on the transition between light and dark, which is shown to be the eye-specific startle response.<sup>16,17</sup> The light-off response is not only driven by photoreceptors in the retina, but also deep brain photoreceptors play an important role in this process.<sup>23,24</sup> Electroretinography data showed a significantly diminished b-wave amplitude in *eys* mutant fish compared to age- and strain-matched wild-type fish, however, no difference was observed for the a-wave amplitude between mutant and wild-type fish. The a-wave is a result of photoreceptor activity, whereas the b-wave mainly reflects depolarization of

ON bipolar cells.<sup>25</sup> The diminished b-wave amplitude in *eys<sup>rmc101/rmc101</sup>* zebrafish could either be the result of a defect of the ON bipolar cells itself, or the signal transduction towards the ON bipolar cells. Since in zebrafish of 5 dpf, rod photoreceptors are not fully functional yet,<sup>26,27</sup> the normal a-wave response indicates that the cone photoreceptors of larvae at least partially remain their function in the absence of Eys.

Since *EYS* is not present in several rodent species, we used zebrafish to study the function of Eys *in vivo*. Furthermore, the morphology of the zebrafish retina is similar to that of the human retina, in the sense that all the major cell layers found in humans are also present in zebrafish. Another approach to further study the function of *EYS* and the pathogenic mechanism underlying *EYS*-related RP, would be to make use of patient-derived cells. Due to the retina-specific expression of *EYS*, one would have to use induced pluripotent stem cells (iPSCs), which can be differentiated into retinal cells.<sup>28,29</sup> Cells derived from patients with *EYS* mutations can be compared to cells derived from controls, by looking at gene expression levels, *EYS* localization, and morphological differences.

In conclusion, we generated an *eys<sup>rmc101/rmc101</sup>* zebrafish line, which showed disorganization of the photoreceptor outer segments and impaired visual function. Furthermore, absence of Eys leads to a significantly decreased VMR, which was not shown previously. In addition, this *eys<sup>rmc101/rmc101</sup>* zebrafish line is a powerful model to further study the pathophysiological mechanism underlying *EYS*-associated RP.

#### 4.5 Acknowledgements

We would like to gratefully thank Tom Spanings and Antoon van der Horst for technical assistance and Dyah Karjosukarso for helping with the statistical analysis.

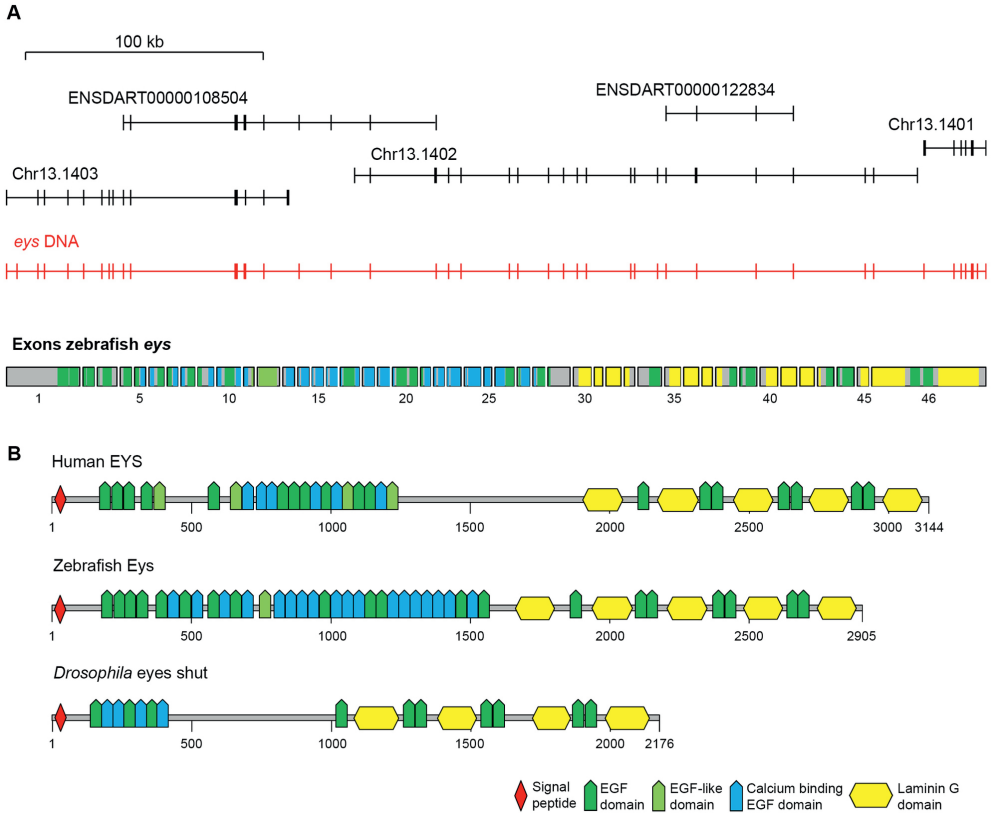
## 4.6 References

1. Hartong DT, Berson EL, Dryja TP. (2006) Retinitis pigmentosa. *Lancet*; **368**: 1795-1809.
2. Littink KW, van den Born LI, Koenekoop RK, Collin RW, Zonneveld MN, Blokland EA, Khan H, Theelen T, Hoyng CB, Cremers FP, et al. (2010) Mutations in the EYS gene account for approximately 5% of autosomal recessive retinitis pigmentosa and cause a fairly homogeneous phenotype. *Ophthalmology*; **117**: 2026-2033, 2033 e2021-2027.
3. Barragan I, Borrego S, Pieras JI, Gonzalez-del Pozo M, Santoyo J, Ayuso C, Baiget M, Millan JM, Mena M, Abd El-Aziz MM, et al. (2010) Mutation spectrum of EYS in Spanish patients with autosomal recessive retinitis pigmentosa. *Hum Mutat*; **31**: E1772-1800.
4. Hosono K, Ishigami C, Takahashi M, Park DH, Hirami Y, Nakanishi H, Ueno S, Yokoi T, Hikoya A, Fujita T, et al. (2012) Two novel mutations in the EYS gene are possible major causes of autosomal recessive retinitis pigmentosa in the Japanese population. *PLoS One*; **7**: e31036.
5. Collin RW, Littink KW, Klevering BJ, van den Born LI, Koenekoop RK, Zonneveld MN, Blokland EA, Strom TM, Hoyng CB, den Hollander AI, et al. (2008) Identification of a 2 Mb human ortholog of *Drosophila* eyes shut/spacemaker that is mutated in patients with retinitis pigmentosa. *Am J Hum Genet*; **83**: 594-603.
6. Abd El-Aziz MM, Barragan I, O'Driscoll CA, Goodstadt L, Prigmore E, Borrego S, Mena M, Pieras JI, El-Ashry MF, Safieh LA, et al. (2008) EYS, encoding an ortholog of *Drosophila* spacemaker, is mutated in autosomal recessive retinitis pigmentosa. *Nat Genet*; **40**: 1285-1287.
7. Husain N, Pellikka M, Hong H, Klimentova T, Choe KM, Clandinin TR, Tepass U. (2006) The agrin/perlecan-related protein eyes shut is essential for epithelial lumen formation in the *Drosophila* retina. *Dev Cell*; **11**: 483-493.
8. Slijkerman RW, Song F, Astuti GD, Huynen MA, van Wijk E, Stieger K, Collin RW. (2015) The pros and cons of vertebrate animal models for functional and therapeutic research on inherited retinal dystrophies. *Prog Retin Eye Res*; **48**: 137-159.
9. Lu Z, Hu X, Liu F, Soares DC, Liu X, Yu S, Gao M, Han S, Qin Y, Li C, et al. (2017) Ablation of EYS in zebrafish causes mislocalisation of outer segment proteins, F-actin disruption and cone-rod dystrophy. *Sci Rep*; **7**: 46098.
10. Yu M, Liu Y, Li J, Natale BN, Cao S, Wang D, Amack JD, Hu H. (2016) Eyes shut homolog is required for maintaining the ciliary pocket and survival of photoreceptors in zebrafish. *Biol Open*; **5**: 1662-1673.
11. Montague TG, Cruz JM, Gagnon JA, Church GM, Valen E. (2014) CHOPCHOP: a CRISPR/Cas9 and TALEN web tool for genome editing. *Nucleic acids research*; **42**: W401-407.
12. Gagnon JA, Valen E, Thyme SB, Huang P, Akhmetova L, Pauli A, Montague TG, Zimmerman S, Richter C, Schier AF. (2014) Efficient mutagenesis by Cas9 protein-mediated oligonucleotide insertion and large-scale assessment of single-guide RNAs. *PLoS One*; **9**: e98186.
13. Huber-Reggi SP, Mueller KP, Neuhauss SC. (2013) Analysis of optokinetic response in zebrafish by computer-based eye tracking. *Methods Mol Biol*; **935**: 139-160.
14. Sirisi S, Figueira M, Lopez-Hernandez T, Minieri L, Perez-Rius C, Gaitan-Penas H, Zang J, Martinez A, Capdevila-Nortes X, De La Villa P, et al. (2014) Megalencephalic leukoencephalopathy with

- subcortical cysts protein 1 regulates glial surface localization of GLIALCAM from fish to humans. *Hum Mol Genet*; **23**: 5069-5086.
15. Chen H, Weber AJ. (2002) Expression of glial fibrillary acidic protein and glutamine synthetase by Muller cells after optic nerve damage and intravitreal application of brain-derived neurotrophic factor. *Glia*; **38**: 115-125.
  16. Burgess HA, Granato M. (2007) Modulation of locomotor activity in larval zebrafish during light adaptation. *J Exp Biol*; **210**: 2526-2539.
  17. Easter SS, Jr., Nicola GN. (1996) The development of vision in the zebrafish (*Danio rerio*). *Dev Biol*; **180**: 646-663.
  18. Wan J, Goldman D. (2016) Retina regeneration in zebrafish. *Curr Opin Genet Dev*; **40**: 41-47.
  19. Goldman D. (2014) Muller glial cell reprogramming and retina regeneration. *Nat Rev Neurosci*; **15**: 431-442.
  20. Nagashima M, Barthel LK, Raymond PA. (2013) A self-renewing division of zebrafish Muller glial cells generates neuronal progenitors that require N-cadherin to regenerate retinal neurons. *Development*; **140**: 4510-4521.
  21. de Raad S, Szczesny PJ, Munz K, Reme CE. (1996) Light damage in the rat retina: glial fibrillary acidic protein accumulates in Muller cells in correlation with photoreceptor damage. *Ophthalmic Res*; **28**: 99-107.
  22. Sifuentes CJ, Kim JW, Swaroop A, Raymond PA. (2016) Rapid, Dynamic Activation of Muller Glial Stem Cell Responses in Zebrafish. *Invest Ophthalmol Vis Sci*; **57**: 5148-5160.
  23. Fernandes AM, Fero K, Arrenberg AB, Bergeron SA, Driever W, Burgess HA. (2012) Deep brain photoreceptors control light-seeking behavior in zebrafish larvae. *Curr Biol*; **22**: 2042-2047.
  24. Ganzen L, Venkatraman P, Pang CP, Leung YF, Zhang M. (2017) Utilizing Zebrafish Visual Behaviors in Drug Screening for Retinal Degeneration. *Int J Mol Sci*; **18**.
  25. Fleisch VC, Jametti T, Neuhauss SC. (2008) Electroretinogram (ERG) Measurements in Larval Zebrafish. *CSH Protoc*; **2008**: pdb prot4973.
  26. Morris AC, Fadool JM. (2005) Studying rod photoreceptor development in zebrafish. *Physiol Behav*; **86**: 306-313.
  27. Branchek T, Bremiller R. (1984) The development of photoreceptors in the zebrafish, *Brachydanio rerio*. I. Structure. *J Comp Neurol*; **224**: 107-115.
  28. Zhong X, Gutierrez C, Xue T, Hampton C, Vergara MN, Cao LH, Peters A, Park TS, Zambidis ET, Meyer JS, et al. (2014) Generation of three-dimensional retinal tissue with functional photoreceptors from human iPSCs. *Nat Commun*; **5**: 4047.
  29. Tucker BA, Mullins RF, Streb LM, Anfinson K, Eyestone ME, Kaalberg E, Riker MJ, Drack AV, Braun TA, Stone EM. (2013) Patient-specific iPSC-derived photoreceptor precursor cells as a means to investigate retinitis pigmentosa. *Elife*; **2**: e00824.



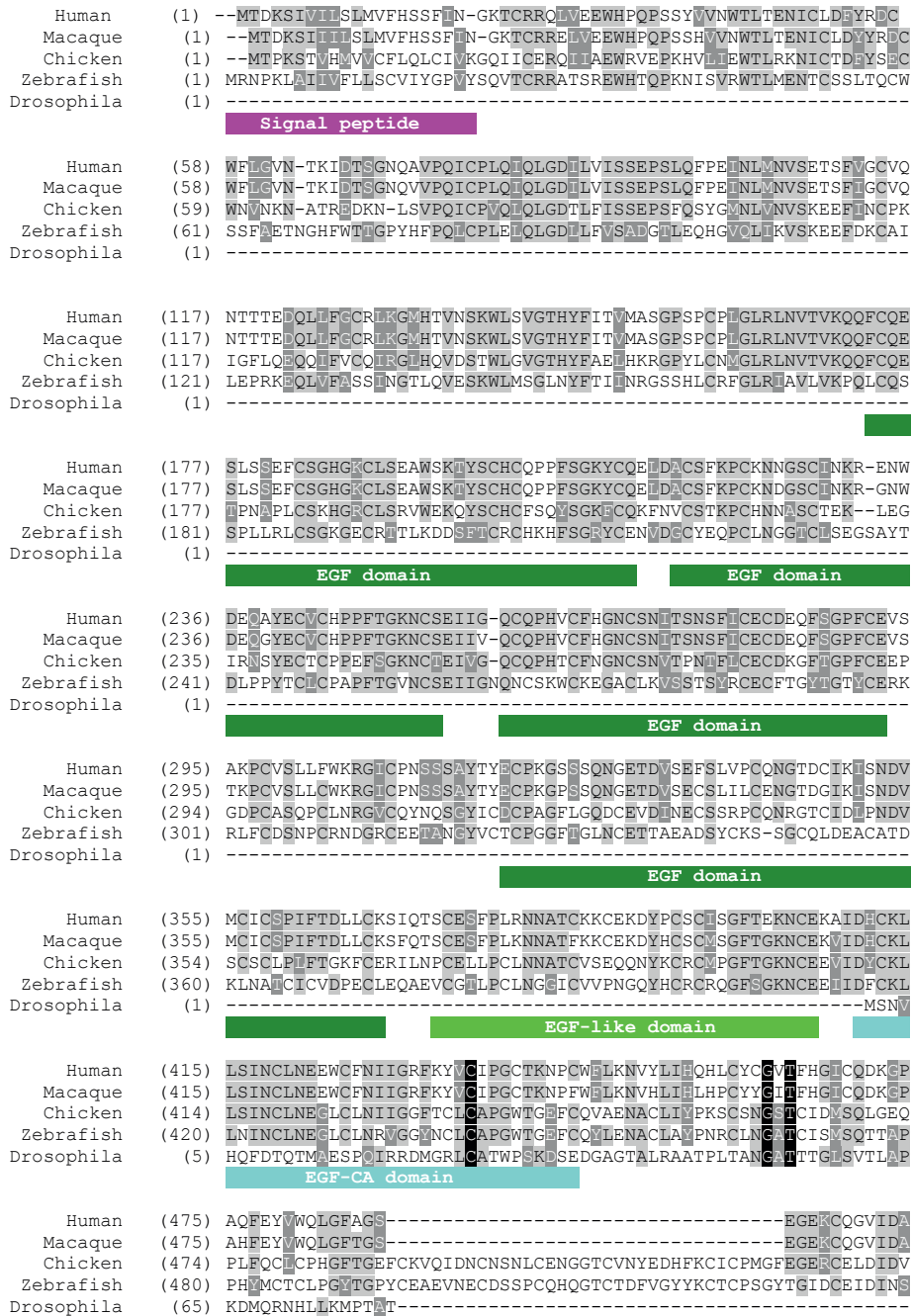
### 4.7 Supplemental information



**Supplementary Figure S1. Gene predictions, exons and protein domain structure.**

(A) Upper panel: gene predictions present for zebrafish *eys* in the UCSC Genome Browser on chromosome 13. Lower panel: Exon structure of zebrafish *eys*. (B) Protein domain structure of human EYS and zebrafish Eys proteins. Note the conservation of Laminin G domains at the C-terminal part of the protein.

**Supplementary Figure S2. Multiple sequence alignment of EYS protein in different species.**



Human (500) YF<sup>1</sup>FLAANCTE<sup>2</sup>DATYVNDPED<sup>3</sup>NNS<sup>4</sup>CW<sup>5</sup>FPHEG<sup>6</sup>TKE<sup>7</sup>ICANGC<sup>8</sup>SCL<sup>9</sup>SE<sup>10</sup>EDSQEY<sup>11</sup>RY<sup>12</sup>LCFL<sup>13</sup>RWA  
 Macaque (500) YF<sup>1</sup>FLTANCTE<sup>2</sup>DALTYVNNPED<sup>3</sup>NNS<sup>4</sup>CS<sup>5</sup>FPCEG<sup>6</sup>TKE<sup>7</sup>ICANGC<sup>8</sup>SCL<sup>9</sup>SE<sup>10</sup>EDNQEY<sup>11</sup>RY<sup>12</sup>LCFL<sup>13</sup>RWT  
 Chicken (534) CL<sup>1</sup>FYNISCA<sup>2</sup>PGAV<sup>3</sup>CYN<sup>4</sup>KSHGF<sup>5</sup>NY<sup>6</sup>CL<sup>7</sup>SFCI<sup>8</sup>GKTE<sup>9</sup>ICANGG<sup>10</sup>SFCY<sup>11</sup>EG<sup>12</sup>NQRSH<sup>13</sup>CV<sup>14</sup>CHGWT  
 Zebrafish (540) C<sup>1</sup>L<sup>2</sup>LPNAT<sup>3</sup>CP<sup>4</sup>PE<sup>5</sup>T<sup>6</sup>CV<sup>7</sup>DL<sup>8</sup>PG<sup>9</sup>D<sup>10</sup>LFK<sup>11</sup>CH<sup>12</sup>T<sup>13</sup>PC<sup>14</sup>PHYL<sup>15</sup>Q<sup>16</sup>CANG<sup>17</sup>GH<sup>18</sup>CV<sup>19</sup>LHN<sup>20</sup>-ITS<sup>21</sup>Y<sup>22</sup>SC<sup>23</sup>V<sup>24</sup>CA<sup>25</sup>PGWT  
 Drosophila (80) -----IEKPTITAT<sup>1</sup>LASS<sup>2</sup>-----SSTS<sup>3</sup>-----LSTTRKSVTAT<sup>4</sup>REL<sup>5</sup>RLN<sup>6</sup>

Human (560) G<sup>1</sup>NMY<sup>2</sup>LENIT<sup>3</sup>DDQENE<sup>4</sup>COHEA<sup>5</sup>VCK<sup>6</sup>DE<sup>7</sup>IN<sup>8</sup>PRC<sup>9</sup>SCL<sup>10</sup>SY<sup>11</sup>GR<sup>12</sup>LCV<sup>13</sup>NVDY<sup>14</sup>LG<sup>15</sup>NHSI<sup>16</sup>SVHG<sup>17</sup>I  
 Macaque (560) S<sup>1</sup>NMY<sup>2</sup>LENIT<sup>3</sup>DDQENK<sup>4</sup>SOHEA<sup>5</sup>ICE<sup>6</sup>DE<sup>7</sup>IN<sup>8</sup>PRC<sup>9</sup>SCL<sup>10</sup>SY<sup>11</sup>GR<sup>12</sup>LCV<sup>13</sup>NVDY<sup>14</sup>LG<sup>15</sup>QST<sup>16</sup>SVHG<sup>17</sup>I  
 Chicken (594) G<sup>1</sup>Q<sup>2</sup>T<sup>3</sup>LENIN<sup>4</sup>DCE<sup>5</sup>IN<sup>6</sup>Q<sup>7</sup>QHGAT<sup>8</sup>CE<sup>9</sup>DEVN<sup>10</sup>KY<sup>11</sup>RCI<sup>12</sup>CP<sup>13</sup>LG<sup>14</sup>Y<sup>15</sup>TG<sup>16</sup>TC<sup>17</sup>ED<sup>18</sup>DN<sup>19</sup>CIGN<sup>20</sup>-QC<sup>21</sup>SEY<sup>22</sup>GF  
 Zebrafish (599) GATC<sup>1</sup>LVNIN<sup>2</sup>CVQ<sup>3</sup>HRC<sup>4</sup>NRAT<sup>5</sup>CV<sup>6</sup>DEV<sup>7</sup>GGYS<sup>8</sup>CL<sup>9</sup>CGHY<sup>10</sup>TGVH<sup>11</sup>CE<sup>12</sup>DF<sup>13</sup>CSGH<sup>14</sup>QC---SE<sup>15</sup>HAV<sup>16</sup>  
 Drosophila (114) P<sup>1</sup>N<sup>2</sup>L<sup>3</sup>L<sup>4</sup>P<sup>5</sup>T<sup>6</sup>RILARG<sup>7</sup>LLLPAL<sup>8</sup>LAIL<sup>9</sup>VG--SSQAG<sup>10</sup>FAC<sup>11</sup>SN<sup>12</sup>PC<sup>13</sup>V<sup>14</sup>FC<sup>15</sup>VIDGLN---SS<sup>16</sup>ISC<sup>17</sup>

EGF domain

Human (620) C<sup>1</sup>L<sup>2</sup>ALSHNC<sup>3</sup>NSG<sup>4</sup>QR<sup>5</sup>YERN<sup>6</sup>ICE<sup>7</sup>LE<sup>8</sup>TE<sup>9</sup>DCK<sup>10</sup>SA<sup>11</sup>SCR<sup>12</sup>NG-----  
 Macaque (620) C<sup>1</sup>L<sup>2</sup>ALSHNC<sup>3</sup>NSD<sup>4</sup>OK<sup>5</sup>YEGN<sup>6</sup>ICE<sup>7</sup>LE<sup>8</sup>TE<sup>9</sup>DCK<sup>10</sup>SV<sup>11</sup>SCR<sup>12</sup>NG-----  
 Chicken (653) Q<sup>1</sup>DHL<sup>2</sup>HNYS<sup>3</sup>CIC<sup>4</sup>LG<sup>5</sup>YGG<sup>6</sup>PF<sup>7</sup>CE<sup>8</sup>VE<sup>9</sup>INE<sup>10</sup>CSS<sup>11</sup>PC<sup>12</sup>R<sup>13</sup>NGG<sup>14</sup>ICMNL<sup>15</sup>IG<sup>16</sup>S<sup>17</sup>FS<sup>18</sup>CHCA<sup>19</sup>E<sup>20</sup>G<sup>21</sup>FK<sup>22</sup>GET<sup>23</sup>CT  
 Zebrafish (656) C<sup>1</sup>V<sup>2</sup>DQ<sup>3</sup>QHNY<sup>4</sup>TCRC<sup>5</sup>LG<sup>6</sup>YEGT<sup>7</sup>ICE<sup>8</sup>LE<sup>9</sup>TE<sup>10</sup>DCK<sup>11</sup>SA<sup>12</sup>PC<sup>13</sup>R<sup>14</sup>NNAT<sup>15</sup>CIDL<sup>16</sup>VAG<sup>17</sup>YQ<sup>18</sup>CLCA<sup>19</sup>PG<sup>20</sup>FK<sup>21</sup>GRT<sup>22</sup>CS  
 Drosophila (169) YCIDG-----VT<sup>1</sup>GI<sup>2</sup>QC<sup>3</sup>TN<sup>4</sup>WD<sup>5</sup>EC<sup>6</sup>WS<sup>7</sup>SP<sup>8</sup>C<sup>9</sup>NG-----

Human (656) -----  
 Macaque (656) -----  
 Chicken (713) AHVNECLDRPCWNGGTCEEDINGFKCNCPLGFEGLNCEINFDECTYGFCKNNSTCLDLIA  
 Zebrafish (716) ESMNECWSRPCNNGGSCIDLVNDYICNCPLGFTGHDCSMPATGCTSNPCNTKGTSMCEEQ  
 Drosophila (195) -----

Human (656) -----  
 Macaque (656) -----  
 Chicken (773) --DYSCVCP<sup>1</sup>PGFT<sup>2</sup>DKNC<sup>3</sup>STD<sup>4</sup>ID<sup>5</sup>ECAF<sup>6</sup>KPC<sup>7</sup>QNG<sup>8</sup>GH<sup>9</sup>CHNL<sup>10</sup>LIGE<sup>11</sup>FY<sup>12</sup>CS<sup>13</sup>CL<sup>14</sup>PG<sup>15</sup>FT<sup>16</sup>GQ<sup>17</sup>FC<sup>18</sup>EADVA  
 Zebrafish (776) Q<sup>1</sup>DG<sup>2</sup>FK<sup>3</sup>CV<sup>4</sup>CH<sup>5</sup>GY<sup>6</sup>TGL<sup>7</sup>FC<sup>8</sup>ETS<sup>9</sup>INH<sup>10</sup>CV<sup>11</sup>EGL<sup>12</sup>CH<sup>13</sup>HG<sup>14</sup>SP<sup>15</sup>CV<sup>16</sup>DL<sup>17</sup>T<sup>18</sup>K<sup>19</sup>GM<sup>20</sup>CE<sup>21</sup>CL<sup>22</sup>PL<sup>23</sup>GR<sup>24</sup>RL<sup>25</sup>CE<sup>26</sup>VNI<sup>27</sup>D  
 Drosophila (195) -----

Human (656) -----  
 Macaque (656) -----  
 Chicken (831) ACLSQPCGASSICKDMSDGYVCFAPGFIGNNCEIEVDECLSDPCHSGATCIDHLNGFSC  
 Zebrafish (836) DCLDKPCGALSICKDGINAYDCFAPGFVGNNCEIEVNECLSQPCQNGASCDELNSFSC  
 Drosophila (195) -----

Human (656) -----T<sup>1</sup>STHL<sup>2</sup>RGY<sup>3</sup>FF<sup>4</sup>FK<sup>5</sup>CV<sup>6</sup>PF<sup>7</sup>RG<sup>8</sup>TC<sup>9</sup>CE<sup>10</sup>DID<sup>11</sup>ECAS<sup>12</sup>LP  
 Macaque (656) -----T<sup>1</sup>STHL<sup>2</sup>RGY<sup>3</sup>FF<sup>4</sup>FK<sup>5</sup>CV<sup>6</sup>PF<sup>7</sup>RG<sup>8</sup>TR<sup>9</sup>CE<sup>10</sup>DID<sup>11</sup>ECAL<sup>12</sup>LP  
 Chicken (891) ICQGGFQGTTCETNINECHSSPCLHN<sup>1</sup>TCAD<sup>2</sup>FVGG<sup>3</sup>YEC<sup>4</sup>IC<sup>5</sup>PG<sup>6</sup>FT<sup>7</sup>GR<sup>8</sup>TC<sup>9</sup>ET<sup>10</sup>DID<sup>11</sup>ECASS<sup>12</sup>P  
 Zebrafish (896) LCLAGTTGSLCEINIDECQSSPCMN<sup>1</sup>CT<sup>2</sup>DLSDG<sup>3</sup>FK<sup>4</sup>IC<sup>5</sup>PS<sup>6</sup>GF<sup>7</sup>GP<sup>8</sup>CS<sup>9</sup>VDINE<sup>10</sup>CVS<sup>11</sup>NP  
 Drosophila (195) -----G<sup>1</sup>TC<sup>2</sup>MD<sup>3</sup>GV<sup>4</sup>AY<sup>5</sup>NCT<sup>6</sup>CP<sup>7</sup>E<sup>8</sup>GF<sup>9</sup>SG<sup>10</sup>NC<sup>11</sup>EN<sup>12</sup>VD<sup>13</sup>EC<sup>14</sup>MS<sup>15</sup>NP

Human (690) CK<sup>1</sup>NG<sup>2</sup>GAT<sup>3</sup>CID<sup>4</sup>QPGNY<sup>5</sup>FCQC<sup>6</sup>V<sup>7</sup>PP<sup>8</sup>FK-----  
 Macaque (690) CK<sup>1</sup>SGAT<sup>2</sup>CID<sup>3</sup>QPGNY<sup>4</sup>FCQC<sup>5</sup>G<sup>6</sup>PP<sup>7</sup>FK-----  
 Chicken (951) CK<sup>1</sup>NGAT<sup>2</sup>CID<sup>3</sup>QPGNY<sup>4</sup>FCQC<sup>5</sup>V<sup>6</sup>AP<sup>7</sup>FK<sup>8</sup>GLNCE<sup>9</sup>FR<sup>10</sup>CEAS<sup>11</sup>NP<sup>12</sup>CEN<sup>13</sup>AV<sup>14</sup>CT<sup>15</sup>EM<sup>16</sup>NL<sup>17</sup>DA<sup>18</sup>F<sup>19</sup>PL<sup>20</sup>GF<sup>21</sup>Q<sup>22</sup>Q  
 Zebrafish (956) CK<sup>1</sup>NGSS<sup>2</sup>CID<sup>3</sup>QPGNY<sup>4</sup>Y<sup>5</sup>CR<sup>6</sup>CA<sup>7</sup>AP<sup>8</sup>FK<sup>9</sup>GLNCELL<sup>10</sup>PCEAV<sup>11</sup>NP<sup>12</sup>CN<sup>13</sup>GA<sup>14</sup>EC<sup>15</sup>VEE<sup>16</sup>AD<sup>17</sup>LV<sup>18</sup>F<sup>19</sup>PL<sup>20</sup>GF<sup>21</sup>Q<sup>22</sup>CR  
 Drosophila (229) C<sup>1</sup>QNG<sup>2</sup>EL<sup>3</sup>CR<sup>4</sup>R-----

EGF-CA domain

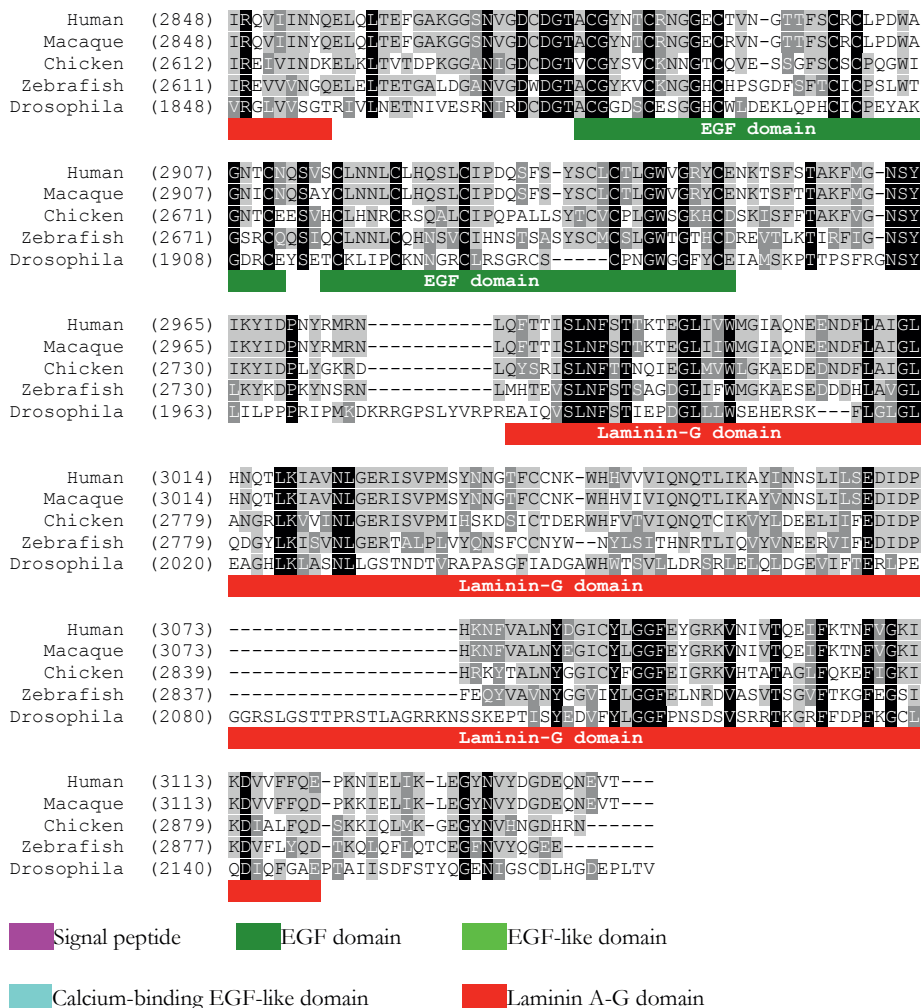
Human (713) -----V<sup>1</sup>VD<sup>2</sup>GF<sup>3</sup>SC<sup>4</sup>LC<sup>5</sup>NE<sup>6</sup>GY<sup>7</sup>VG<sup>8</sup>TR<sup>9</sup>CE<sup>10</sup>Q<sup>11</sup>DID<sup>12</sup>DC<sup>13</sup>IL<sup>14</sup>NACE  
 Macaque (713) -----V<sup>1</sup>VD<sup>2</sup>GF<sup>3</sup>SC<sup>4</sup>LC<sup>5</sup>NE<sup>6</sup>GY<sup>7</sup>VG<sup>8</sup>TR<sup>9</sup>CE<sup>10</sup>Q<sup>11</sup>DN<sup>12</sup>DC<sup>13</sup>IL<sup>14</sup>NA<sup>15</sup>FE  
 Chicken (1011) CVKGFAGP<sup>1</sup>RCE<sup>2</sup>IN<sup>3</sup>VNE<sup>4</sup>CSS<sup>5</sup>NP<sup>6</sup>CL<sup>7</sup>HGY<sup>8</sup>CY<sup>9</sup>DL<sup>10</sup>VN<sup>11</sup>GFY<sup>12</sup>CL<sup>13</sup>NP<sup>14</sup>GY<sup>15</sup>AG<sup>16</sup>TR<sup>17</sup>CE<sup>18</sup>Q<sup>19</sup>DID<sup>20</sup>DC<sup>21</sup>IN<sup>22</sup>NACE  
 Zebrafish (1016) CRKGF<sup>1</sup>TG<sup>2</sup>PR<sup>3</sup>CE<sup>4</sup>VNI<sup>5</sup>DE<sup>6</sup>CSS<sup>7</sup>NP<sup>8</sup>CL<sup>9</sup>NG<sup>10</sup>FCY<sup>11</sup>DA<sup>12</sup>VD<sup>13</sup>GFY<sup>14</sup>CL<sup>15</sup>NE<sup>16</sup>GY<sup>17</sup>AG<sup>18</sup>TR<sup>19</sup>CE<sup>20</sup>QH<sup>21</sup>IND<sup>22</sup>CAS<sup>23</sup>NM<sup>24</sup>CE  
 Drosophila (239) -----T<sup>1</sup>NG<sup>2</sup>IT<sup>3</sup>CT<sup>4</sup>CP<sup>5</sup>GH<sup>6</sup>LS<sup>7</sup>SH<sup>8</sup>CE<sup>9</sup>LD<sup>10</sup>AV<sup>11</sup>CE<sup>12</sup>TGTGA

Human	(744)	----HNSTCKDLHLSYQ <b>CVCLSDWEGNFC</b> EO <b>ESNECKMNPCKNNSTCTDL</b> YKSY <b>RRCBCT</b> S
Macaque	(744)	----HNSTYKDLHLSYQ <b>CVCLSGWPGNFC</b> EO <b>ESNECKMNPCKNNSTCTDL</b> YKSY <b>RRCBCT</b> S
Chicken	(1071)	----HNSTCVDLHLRYQ <b>CVCLPGWEGTFC</b> EY <b>ESNECDSEPCRNNGTCTDL</b> FN <b>SYRCLCTA</b>
Zebrafish	(1076)	----NNSTCVDLHLSYN <b>CLCLPGWEGNFC</b> Q <b>REINECLSNPCKNNACTDL</b> LN <b>AYRVCVCPQ</b>
Drosophila	(269)	RCQHGGECIEG <b>FGLE</b> ET <b>EDCPAGW</b> HC <b>RIQ</b> OE <b>EINEGASSPCQNGGV</b> VD <b>LDL</b> AY <b>ACACPM</b>
		<b>EGF-CA domain</b> <b>EGF-CA domain</b>
Human	(800)	<b>GWTCQNCSE</b> EINE <b>CDSDPC</b> M <b>NGGLCHE</b> STIP <b>GQFVCLCP</b> FL <b>YTGQF</b> CH <b>QRYNLC</b> DL <b>LHNP</b>
Macaque	(800)	<b>GWTCQNCSE</b> EINE <b>CDSDPC</b> M <b>NGGLCHE</b> STIP <b>GQFVCLCP</b> FL <b>YTGQF</b> CH <b>QRYNLP</b> CD <b>LNNP</b>
Chicken	(1127)	<b>GWTCQNCSE</b> EINE <b>CDSEPC</b> L <b>NGATC</b> Y <b>ESVKQGFVCLCP</b> FL <b>YTGQF</b> CH <b>QRYNLP</b> CD <b>LNNP</b>
Zebrafish	(1132)	<b>GWTCGLDCE</b> DE <b>VKES</b> SS <b>PC</b> L <b>NGAHC</b> V <b>ESDT</b> P <b>GFE</b> ST <b>CP</b> FF <b>ITG</b> PL <b>CEQ</b> PY <b>DF</b> PE <b>LDRNP</b>
Drosophila	(329)	<b>GWTCINCE</b> EE <b>ELI</b> C <b>ADN</b> PC <b>Q</b> NN <b>ALCL</b> ME <b>EG</b> --V <b>PTCY</b> CV <b>PDY</b> H <b>GEK</b> CE <b>FQY</b> DE <b>CC</b> LG---
		<b>EGF domain</b>
Human	(860)	CR <b>NNSTCLALVD</b> AN <b>QHCIO</b> REE <b>FEGK</b> N <b>CEID</b> V <b>KD</b> CF <b>IF</b> SC <b>QDY</b> GD <b>ED</b> M <b>VN</b> N <b>FR</b> CI <b>CR</b> PG
Macaque	(860)	CR <b>NNSTCLALVD</b> GN <b>QHCIO</b> REE <b>FEGK</b> H <b>CEID</b> V <b>KD</b> CF <b>IF</b> SC <b>QDY</b> GD <b>ED</b> M <b>VN</b> N <b>FR</b> CI <b>CR</b> PG
Chicken	(1187)	C <b>INNSTCLAQ</b> AD <b>GNPM</b> CI <b>CKT</b> GV <b>EGY</b> TC <b>EV</b> NS <b>DE</b> CS <b>H</b> PC <b>Q</b> NG <b>IC</b> VD <b>GL</b> NS <b>YR</b> CF <b>Q</b> HG
Zebrafish	(1192)	CL <b>HNSTCR</b> AQ <b>SDGTAL</b> CV <b>PV</b> GF <b>EG</b> TR <b>CEID</b> SD <b>DC</b> SR <b>PC</b> NR <b>IC</b> VD <b>GL</b> NS <b>YR</b> CF <b>Q</b> EP <b>G</b>
Drosophila	(384)	-----P <b>RC</b> M <b>NG</b> ---G <b>VC</b> LD <b>GVD</b> TF <b>SC</b> CP <b>PL</b>
		<b>EGF domain</b> <b>EGF-domain</b>
Human	(920)	F <b>S</b> GL <b>CE</b> EE <b>INE</b> CS <b>SE</b> PC <b>K</b> NN <b>GT</b> CV <b>DL</b> NR <b>FF</b> C <b>N</b> CE <b>PEY</b> IG <b>PF</b> CE <b>LD</b> V <b>N</b> K <b>CK</b> SP <b>CL</b> D <b>EE</b>
Macaque	(920)	F <b>S</b> GL <b>CE</b> EE <b>INE</b> CS <b>SE</b> PC <b>K</b> NN <b>GT</b> CV <b>DL</b> NR <b>FF</b> C <b>N</b> CE <b>PEY</b> IG <b>PF</b> CE <b>LD</b> V <b>N</b> K <b>CK</b> SP <b>CL</b> D <b>EE</b>
Chicken	(1247)	F <b>T</b> GL <b>CE</b> EE <b>INE</b> CL <b>SR</b> PC <b>K</b> NN <b>GT</b> CV <b>DL</b> NR <b>FF</b> C <b>N</b> CE <b>PEY</b> IG <b>PF</b> CE <b>LD</b> V <b>N</b> K <b>CK</b> SP <b>CL</b> D <b>EE</b>
Zebrafish	(1252)	F <b>S</b> GL <b>H</b> CE <b>E</b> INE <b>CS</b> SN <b>PC</b> Q <b>AV</b> Q <b>DL</b> V <b>NG</b> F <b>QC</b> SC <b>V</b> PG <b>Y</b> FG <b>PH</b> CL <b>LD</b> V <b>N</b> EC <b>D</b> SS <b>PC</b> L <b>H</b> ES
Drosophila	(407)	L <b>T</b> GL <b>CE</b> CL <b>V</b> GE <b>ES</b> LD <b>C</b> NY <b>T</b> A <b>P</b> AT <b>Q</b> SP <b>PR</b> RT <b>TT</b> ST <b>M</b> AP <b>P</b> TV <b>R</b> PT <b>TP</b> PE <b>TT</b> V <b>SP</b> S <b>R</b> ---
		<b>EGF-CA domain</b>
Human	(980)	NC <b>V</b> Y <b>R</b> T <b>G</b> Y <b>N</b> CL <b>C</b> AP <b>G</b> Y <b>T</b> GIN <b>C</b> E <b>IN</b> L <b>D</b> E <b>C</b> L <b>S</b> E <b>P</b> CL <b>H</b> D <b>G</b> VC <b>ID</b> GIN <b>H</b> Y <b>T</b> CD <b>C</b> K <b>S</b> FF <b>G</b> TH <b>C</b>
Macaque	(980)	NC <b>V</b> Y <b>R</b> T <b>R</b> Y <b>N</b> CL <b>C</b> AP <b>G</b> Y <b>T</b> GIN <b>C</b> E <b>IN</b> L <b>D</b> E <b>C</b> L <b>S</b> E <b>P</b> CL <b>H</b> D <b>G</b> VC <b>ID</b> GIN <b>H</b> Y <b>T</b> CD <b>C</b> K <b>S</b> FF <b>G</b> TH <b>C</b>
Chicken	(1307)	SC <b>IN</b> RL <b>GGY</b> CF <b>C</b> PG <b>F</b> T <b>G</b> DR <b>CE</b> T <b>NT</b> DE <b>CT</b> ST <b>PC</b> LN <b>NG</b> CS <b>ID</b> IN <b>SY</b> K <b>HC</b> RS <b>G</b> FI <b>GT</b> NC
Zebrafish	(1312)	VC <b>IN</b> RL <b>GGY</b> CF <b>C</b> AG <b>F</b> SG <b>K</b> WC <b>E</b> IN <b>V</b> DE <b>CK</b> SN <b>PC</b> R <b>NG</b> CS <b>ID</b> IN <b>Y</b> QC <b>V</b> CS <b>R</b> FM <b>G</b> D <b>H</b> C
Drosophila	(464)	---A <b>S</b> E <b>VE</b> II <b>V</b> TT <b>S</b> A <b>P</b> EV <b>V</b> TS <b>V</b> LS <b>P</b> SS <b>S</b> SS <b>S</b> EE <b>G</b> VS <b>VE</b> IK <b>TP</b> TV <b>AP</b> PE <b>S</b> GS <b>H</b> S <b>IS</b> V
		<b>EGF domain</b> <b>EGF-CA domain</b>
Human	(1040)	<b>ET</b> N <b>AN</b> D <b>CL</b> - <b>SN</b> P <b>CL</b> H <b>GR</b> CT <b>EL</b> IN <b>EY</b> PC <b>SC</b> D <b>AD</b> GT <b>S</b> I <b>Q</b> CK <b>TK</b> IND <b>CT</b> S <b>IP</b> CM <b>NE</b> GF <b>---</b> C
Macaque	(1040)	<b>ET</b> N <b>AN</b> D <b>CL</b> - <b>SN</b> P <b>CL</b> H <b>GR</b> CT <b>EP</b> IN <b>EY</b> PC <b>SC</b> D <b>AD</b> GT <b>S</b> I <b>Q</b> CK <b>TK</b> IND <b>CT</b> S <b>MP</b> CM <b>NE</b> GF <b>---</b> C
Chicken	(1367)	<b>ET</b> N <b>V</b> N <b>EC</b> W <b>-PE</b> P <b>CL</b> H <b>GR</b> CI <b>DL</b> D <b>G</b> Y <b>QC</b> SC <b>D</b> AG <b>WT</b> S <b>SR</b> CE <b>IN</b> IN <b>CE</b> SV <b>PC</b> LN <b>GG</b> S <b>---</b> C
Zebrafish	(1372)	<b>ER</b> NT <b>DE</b> CS <b>-SC</b> PC <b>V</b> H <b>GS</b> CL <b>DE</b> IDA <b>SC</b> Q <b>CE</b> V <b>G</b> WT <b>G</b> HR <b>CO</b> IN <b>IN</b> CE <b>HP</b> CL <b>NG</b> GS <b>---</b> C
Drosophila	(521)	<b>E</b> QT <b>AV</b> PA <b>Q</b> PP <b>E</b> SE <b>Q</b> EP <b>ES</b> K <b>PH</b> PE <b>SES</b> ASE <b>TE</b> EE <b>E</b> IP <b>GT</b> T <b>AR</b> PT <b>S</b> RS <b>SS</b> SS <b>ES</b>
		<b>EGF-like domain</b>
Human	(1095)	<b>Q</b> KS <b>A</b> H <b>G</b> FT <b>C</b> I <b>C</b> PR <b>G</b> Y <b>T</b> GA <b>Y</b> CE <b>K</b> S <b>ID</b> NC <b>A</b> E <b>P</b> EL <b>NS</b> V <b>CL</b> NG <b>G</b> I <b>C</b> VD <b>G</b> F <b>G</b> H <b>T</b> FD <b>R</b> CL <b>RP</b> GF <b>S</b>
Macaque	(1095)	<b>Q</b> KS <b>A</b> H <b>G</b> FT <b>C</b> I <b>C</b> PR <b>G</b> Y <b>T</b> GA <b>Y</b> CE <b>K</b> S <b>ID</b> NC <b>A</b> E <b>P</b> EL <b>NS</b> V <b>CL</b> NG <b>G</b> I <b>C</b> VD <b>G</b> F <b>G</b> H <b>T</b> FD <b>R</b> CL <b>RP</b> GF <b>S</b>
Chicken	(1422)	<b>Q</b> D <b>V</b> NE <b>F</b> AC <b>IC</b> LT <b>G</b> Y <b>T</b> G <b>K</b> CE <b>F</b> D <b>ID</b> IC <b>NE</b> PT <b>SS</b> V <b>CH</b> NG <b>CS</b> ID <b>IN</b> SY <b>K</b> HC <b>RS</b> G <b>FI</b> GT <b>NC</b>
Zebrafish	(1427)	<b>V</b> D <b>L</b> DK <b>AC</b> IC <b>AD</b> GT <b>G</b> K <b>NC</b> I <b>D</b> Q <b>N</b> CL <b>Q</b> T <b>S</b> FN <b>S</b> I <b>CF</b> NG <b>GT</b> CV <b>D</b> GF <b>G</b> V <b>N</b> FT <b>CS</b> CR <b>PG</b> FM
Drosophila	(581)	<b>P</b> S <b>I</b> FT <b>TT</b> LP <b>P</b> PG <b>K</b> P <b>Q</b> TS <b>AS</b> SE <b>SS</b> GV <b>V</b> T <b>SE</b> E <b>Y</b> TV <b>PH</b> F <b>EV</b> SG <b>S</b> K <b>SE</b> SG <b>-SE</b> V <b>TT</b> VR <b>PTA</b>
		<b>EGF domain</b> <b>EGF domain</b>
Human	(1155)	<b>G</b> Q <b>F</b> CE <b>I</b> N <b>INE</b> CS <b>SP</b> CL <b>H</b> GA <b>D</b> CE <b>D</b> H <b>ING</b> Y <b>V</b> CK <b>Q</b> CP <b>G</b> WS <b>G</b> H <b>H</b> CE <b>N</b> -E <b>LEC</b> IP <b>NS</b> CV <b>H</b> E <b>IC</b> M
Macaque	(1155)	<b>G</b> Q <b>F</b> CE <b>I</b> N <b>INE</b> CS <b>SP</b> CL <b>H</b> GA <b>D</b> CE <b>D</b> H <b>ING</b> Y <b>V</b> CK <b>Q</b> CP <b>G</b> WS <b>G</b> H <b>H</b> CE <b>K</b> -E <b>LEC</b> IP <b>NS</b> CV <b>H</b> Q <b>IC</b> M
Chicken	(1482)	<b>G</b> Q <b>F</b> CE <b>I</b> N <b>INE</b> CS <b>SP</b> CL <b>H</b> GS <b>T</b> CE <b>D</b> H <b>ING</b> Y <b>T</b> CC <b>Q</b> KG <b>W</b> EG <b>T</b> H <b>CE</b> LD <b>DEC</b> SN <b>PC</b> L <b>H</b> GT <b>CV</b>
Zebrafish	(1487)	<b>G</b> DF <b>CE</b> VE <b>INE</b> CC <b>SE</b> PC <b>F</b> NG <b>A</b> IC <b>Q</b> DL <b>ING</b> Y <b>Q</b> CH <b>CR</b> PG <b>WT</b> GH <b>CE</b> DD <b>NE</b> CC <b>L</b> OP <b>C</b> N <b>Q</b> GV <b>CT</b>
Drosophila	(640)	<b>P</b> PS <b>I</b> TI <b>S</b> VD <b>IT</b> SS <b>SS</b> SS <b>SS</b> SE <b>SV</b> EV <b>TT</b> PA <b>P</b> V <b>F</b> V <b>Q</b> RV <b>TT</b> ETS <b>IS</b> VD <b>Y</b> VT <b>PT</b> PL <b>P</b> ET <b>TP</b>
		<b>EGF-CA domain</b>
Human	(1214)	<b>E</b> NE <b>E</b> --G <b>S</b> T <b>CL</b> CT <b>EG</b> F <b>T</b> CS <b>I</b> GL <b>LC</b> GD <b>ERR</b> T <b>CL</b> TP <b>I</b> F <b>Q</b> RT <b>D</b> PI <b>ST</b> Q <b>TY</b> TP <b>P</b> SE <b>IL</b> VS
Macaque	(1214)	<b>E</b> NE <b>E</b> --G <b>S</b> T <b>CL</b> CT <b>EG</b> F <b>T</b> CS <b>I</b> GL <b>LC</b> GD <b>ERR</b> T <b>CL</b> TP <b>S</b> F <b>Q</b> RT <b>D</b> PI <b>ST</b> Q <b>HT</b> TP <b>P</b> SE <b>IL</b> VS
Chicken	(1542)	<b>Q</b> S <b>D</b> PS <b>F</b> Y <b>SC</b> FC <b>K</b> EG <b>F</b> GR <b>S</b> CE <b>L</b> N <b>Y</b> ND <b>CI</b> Q <b>S</b> CS <b>S</b> GF <b>L</b> CV <b>D</b> DP <b>IN</b> IT <b>CT</b> PT <b>IS</b> Q <b>S</b> ----
Zebrafish	(1547)	<b>Q</b> NE <b>E</b> GH <b>G</b> Y <b>T</b> CF <b>CR</b> EG <b>F</b> GEN <b>C</b> E <b>Y</b> NY <b>DD</b> CI <b>Q</b> SC <b>PE</b> TF <b>S</b> CK <b>D</b> GIN <b>N</b> V <b>CV</b> P <b>V</b> K <b>T</b> D <b>S</b> SL <b>P</b>
Drosophila	(700)	<b>R</b> V <b>V</b> EV <b>PR</b> PT <b>F</b> A <b>P</b> E <b>P</b> LD <b>V</b> VE <b>T</b> AS <b>T</b> H <b>L</b> W <b>TE</b> PT <b>T</b> A <b>AP</b> FT <b>E</b> Y <b>PA</b> EV <b>L</b> TT <b>H</b> R <b>T</b> S <b>AG</b> ---
		<b>EGF-like domain</b>
Human	(1272)	S <b>F</b> PS <b>I</b> K <b>A</b> TR <b>PA</b> IM <b>D</b> TY <b>VD</b> G <b>PK</b> Q <b>T</b> G <b>I</b> V <b>K</b> H <b>D</b> IL <b>P</b> TT <b>G</b> L <b>A</b> TL <b>R</b> IS <b>T</b> PL <b>E</b> SY <b>LL</b> Q <b>E</b> L <b>I</b> V <b>T</b> R
Macaque	(1272)	S <b>F</b> PS <b>I</b> K <b>A</b> TR <b>PT</b> IM <b>D</b> TY <b>VD</b> G <b>PK</b> Q <b>T</b> G <b>I</b> V <b>K</b> H <b>D</b> IL <b>P</b> TT <b>G</b> L <b>A</b> TL <b>R</b> IS <b>T</b> PL <b>K</b> Y <b>L</b> E <b>E</b> L <b>I</b> V <b>T</b> R
Chicken	(1597)	----- <b>K</b> K <b>T</b> E <b>VA</b> E <b>L</b> F <b>P</b> T <b>S</b> E <b>LD</b> N----- <b>D</b> L <b>P</b> S <b>A</b> L <b>A</b> V <b>S</b> M
Zebrafish	(1606)	----- <b>P</b> I <b>S</b> V <b>V</b> SW <b>R</b> ST <b>D</b> ST
Drosophila	(757)	----- <b>R</b> F <b>T</b> V <b>Q</b> P <b>A</b> G <b>V</b> TT

Human	(1332)	ELSAKHSLLSSADVSSSRFLNFGIRDPAQIVQDKTSVSHMPIRTSAAATLGFFFPDRRART
Macaque	(1332)	ELSAKHSLLSSTDVSSSPFLNFGIHDPQIVQDKTSVSHMRIRTSAAATLGFFFPDRRART
Chicken	(1623)	ELWSKHALP-----
Zebrafish	(1620)	ELQPTFAPVEN-----
Drosophila	(770)	TSPTEDSSVELP-----
Human	(1392)	PFIMSSLMDFIFPTQSLLFENCQTVALSATPTTSVIRSI PGADIELNRQSLLSRGFLLI
Macaque	(1392)	SFIRSSLMDFIFPTQSLLFENYQTVASSATPTTSVIRSI PGADIELNRHSLLSRGFLLT
Chicken	(1632)	-----
Zebrafish	(1631)	-----
Drosophila	(782)	-----
Human	(1452)	AASISATPVVSRGAQEDIEEYSADSLISRREHWRLSPMSPIFPAKVIISKQVTILNSS
Macaque	(1452)	AASISATPVVSRGAQEDIKEYSAVSLISRREHWRLSISSMSPIFPAKKIISKQVTILNSS
Chicken	(1632)	-----
Zebrafish	(1631)	-----
Drosophila	(782)	-----
Human	(1512)	ALHRFSTKAFNPSEYQAITEASSNQRLTNIKSQAADSLRELSQTCATCSMTEIKSREFFS
Macaque	(1512)	ALHRFGTKAFIPSEYQAITEASSNQRLTNIKSQAADSLRELSQTCATCSMTEIKSHHFFS
Chicken	(1632)	-----D---FHTEEVA
Zebrafish	(1631)	-----IQHTEQPA
Drosophila	(782)	-----TPHTPQIV
Human	(1572)	DQVLHSHKQSHFYETFFWNMSAILASWYALMGAQTITSGHSFSSATEITPSVAFTEVPSLFP
Macaque	(1572)	DQVLHSHKQSHFYETFFWNMSAILASWYALMGAQTITSGHSFSSATEITPSVAFTEVPSLFP
Chicken	(1640)	--QDFS-----
Zebrafish	(1639)	DASFGG-----
Drosophila	(790)	VTMLDSN-----
Human	(1632)	SKKSARKRTILSSSLEESITLSSNLDVNLCLDKTCLSI VPSQTISSDLMNSDLT SKMTTDE
Macaque	(1632)	SKKSARKRTILSSSLEESITLSSNLDVNLCLHKTCLSI VPSQTISSDLMNSDLTSELTTDE
Chicken	(1644)	-----
Zebrafish	(1645)	-----
Drosophila	(797)	-----
Human	(1692)	LSVSENILKLLKIRQYGITMGPTTEVLNQESLLDMEKSKGSHTL FKLHPSDSSLDFELNLQ
Macaque	(1692)	LSVSENILKLLKIRQYGITMGPTTEVLNQESLLDMEKSKGSHTL FKLHPSDSSLDFELNLQ
Chicken	(1644)	-----
Zebrafish	(1645)	-----
Drosophila	(797)	-----
Human	(1752)	IYPDVTLKYTSEITHANDFKNNLPPLTGSVPDFSEVTTNVAFYTVSATPALSIQTSSSMS
Macaque	(1752)	SYPDVTLKYTSEITLANDLKNLPLTGSVPDFSEVTTNVAFYTVSATPALPIQTSSSMS
Chicken	(1644)	-----
Zebrafish	(1645)	-----
Drosophila	(797)	-----
Human	(1812)	VIRPDWPYFTDYMTSLKKEVKTSSEWSKWELQPSVQYQEFPTASRHLPFTRSLTLSSLES
Macaque	(1812)	VITPDWPYFIDYMTSLNKEVKTYSEWSKWELQPSVQYQEFPTASRHLPFTRSLTLSSLES
Chicken	(1644)	-----
Zebrafish	(1645)	-----
Drosophila	(797)	-----

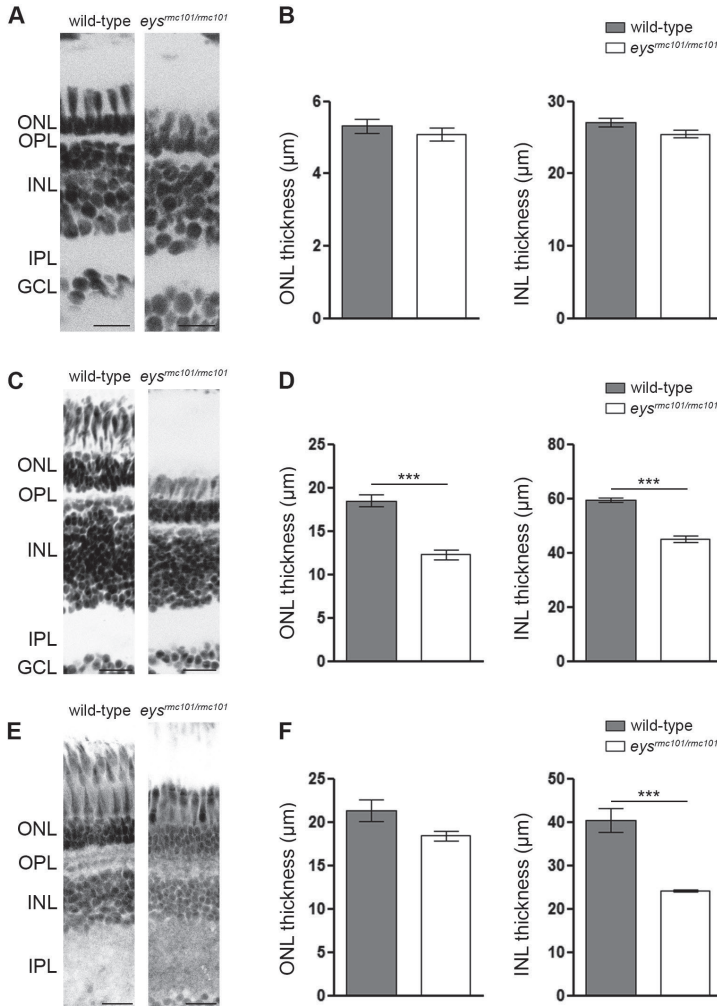
Human	(1872)	ILAPQRLMISDFSCVRYYGDSYLEFQNVLNPQNNISLEFQTFSSYGLLLYKQDSNLD
Macaque	(1872)	IVAPQQLMISDFSCVRYYGDSYLEFQNVLNPQNNISLEFQTFSSYGLLLYKQDSNLD
Chicken	(1644)	-YA-----RYYGDSYLEFQVHLNVQNFHLEFKTKPDGLLLYEESETG
Zebrafish	(1645)	-----YSGNSLEFQGGFEAVPISVTVRFQTESMYGTLLES--ASAKRS
Drosophila	(797)	-----EVIPSTIITTGSPPTHHHHHHHPHHEAEGTTLQPLEEEDHHHHHDEFTT
<b>Laminin-G domain</b>		
Human	(1932)	GFFIQLSIENGLTKYHFYCPGEAKFKSINTTVRVDNGQKYTLIRQELDPCKNAETILGR
Macaque	(1932)	GFFIQLSIENGLTKYHFYCPGEAKFKSINTAIRVDGQKYTLIRQELDPCKNAETILGR
Chicken	(1691)	QFLIQLSIRHGLTQYQFVCGKATQVKNITTTARVDDGQYKQIRQNPCKCAEMLILEV
Zebrafish	(1687)	VFEIKLMSINGTQYDFLCKQKQVQRINTAQWVADGFEVTVFRQCLEPCVAEYTVSGV
Drosophila	(848)	POPVEITTGHPQTEDLGVQEPAVVTEPFAPATTVVVVPATAPLGTAAAPPATP
<b>Laminin-G domain</b>		
Human	(1992)	NTQICEINIVLQKPLPKSGSVFIGGFDLHGKIQMPVVKNFTGCIIEVIEINNWRSFIP
Macaque	(1992)	NTQTCESINIVLQKPLPKSGSVFIGGFDLRQKIQMPVVKNFTGCIIEVIEINNWRSFIP
Chicken	(1751)	SAKTGIPSNFSSPYGLTGSFVGGLYPSSAIKQPPVYKFTGCIQVIEINNVPFNF
Zebrafish	(1747)	RTVRSAPGNVTSLRLQRTDHFVIGGLPRHRSPYKEAPFFHNYTGCIEIEINKLRRFHM
Drosophila	(908)	APVPPATTPPPPPSLATEPTPPTLPPVTLPPVTEPPTIPPTPPSTQSACTLPPPT
<b>Laminin-G domain</b>		
Human	(2052)	SKAVKNYHINNCRSQGFMLSPTASFVDASDVTOGVD---TWTSVSPSVAAPSVCCQEDVC
Macaque	(2052)	SKAVRNYHINNCRSQGLMLSPTASFVDASDVTOGVD---AWTSVSPSVAAPSVCCQEDVC
Chicken	(1811)	SNAVGRRNIDSCRTPVPTHLPFPPTVSDVLALPE---LWTPSLSSPELPSVCCQEGIC
Zebrafish	(1807)	DHAFARNVNDNCRSQWHHEPPTSTHSPILLITVETPP-GEVVRVLSPTQPAPVCCQGGIC
Drosophila	(968)	SAINVYVTPDGPPTASQTKPSVTESSVEVGTNTVSTGGRGSGGVPEEKAQDVCIKLCC
<b>Laminin-G domain</b>		
Human	(2109)	HNGGTCHEAIFLSSGIVSFCDCPLHFTGRFCEKDAGLFFPSENGNSYLELPLKFLVLEKE
Macaque	(2109)	HNGGTCRPIFLSSGIVSFCDCPLHFTGRFCEKDAGLFFPSENGNSYLELPLKFLVLEKE
Chicken	(1867)	HNGGTCHEPISLPGALSFCDCQLHFTGRFCEKDTLFLIPSENGNSYLELPSLTSVSQMR
Zebrafish	(1866)	LNGGTCRPIFLSSGIVSFCDCPLHFTGRFCEKDTLFLIPSPREDGNSYLELPSLTSVFSQSR
Drosophila	(1028)	HNGGTCVTTSEGS----RWCVRFDRCPLCELPILRNALPSSGNSYLVSHRIYKDLGGHE
<b>EGF domain</b>		
Human	(2169)	HN-----RTVTIYLTKTNSLNGTILYSNGN-NCGQKFLHLEVEGRPSVKYCGGNSQ
Macaque	(2169)	HN-----RTVTIYLTKTNSLNGTILYSNGN-NFGQKFLHLEVEGRPSVKYCGGNSQ
Chicken	(1927)	TASGQETS-NTLTYLTVKRTAPSGTILYS-SEK-NFGQKFLHLEVEGRPTVRESVCGNSQ
Zebrafish	(1926)	TYFPSSRSEDKRIYLPKMKRTPHCSLYLCREQ-DLGERFLHLEVQNRARAVLCCG-NA
Drosophila	(1083)	SLDAVLP----MHICLRVTRATNGLTMLAAAGTKGKGGHYMALFTQKGLMQFQSSCGLQT
<b>Laminin-G domain</b>		
Human	(2221)	NIITVSN-----YSINTNAFTPIITRYTTPVGSFGVCMIEMTADGKPPVQKQDTEISH
Macaque	(2221)	NIITVSN-----YSINTNAFTPIITRYTTPVGSFGVCMIEMTADGKPPVQKQDTEISH
Chicken	(1985)	NIITVSN-----QTEKSGIFPIIISYMPVSSLEGYCMIEMTADRNPPVQHRHLHSYQ
Zebrafish	(1984)	HIIITAVAA-----QNRIDLVAITVRYALPSQNGQCFIEIADNGTANQQQKYMDEP
Drosophila	(1139)	MILSELETPVNTGELITIRAEIDFSRNYTHCNASLLVNDTAMSGDQPTWIKLLPPIHT
<b>Laminin-G domain</b>		
Human	(2276)	ASQAYFESMFLGHIPANVQHKKAG---PVYGFRCCLLDLQVNNKEFFIIDEARHCKNI
Macaque	(2276)	ASQVYFESMFLGHIPENVQHKKAG---SVYGFRCCLLDLQVNNKEFFIIDEARHCKNI
Chicken	(2040)	ASQTEFGSTELGNVPHKVEPECAG---QIRGYKGERDFQVNNKEFFIIDALGGRNI
Zebrafish	(2039)	VSEVVEGPTFLGGFPSVLEHNSG---NVSGFRCCLRLDQVNSKELVVGEARVGNQNI
Drosophila	(1199)	PEALNLTWHLGGAFQAPIGLIIELPQAQSGSGFTGCCHTLRLRNGQAREIFGALDGFGT
<b>Laminin-G domain</b>		
Human	(2332)	ENCHVPWCAHHLCRNNGTCLSDNEN-----LFCECPRIYSKGLCQFASCENNPC
Macaque	(2332)	ENCHVPWCAHHLCRNNGTCLSDSEN-----LFCECPRIYSKGLCQFASCENNPC
Chicken	(2096)	ENGNVPICDVHPCRNGGTCTSDAEN-----WFCECPRIYSKGLCQFASCENNPC
Zebrafish	(2095)	QNCDAVCCQHPCRNGGTCTSDAES-----WFCACPSIYSKGLCQFASCENNPC
Drosophila	(1259)	TECGSLACLSSPCRNGTACIKIETNDLDENGEKAEKWKCKOFTGMVGTCEISVCEDNPC
<b>EGF domain</b>		

Human	(2381)	GNGATCVPKSGTIDIVCLCPYGRSGPLCTDAINITQPRFSGTDAFCYTSFLAYSRISDISF
Macaque	(2381)	GNGATCVPKSGTIDIVCLCPYGRSGPLCTDAINITQPRFSGTDAFCYTSFLAYSRISDISF
Chicken	(2145)	GNGATCFPKSRQDVVCLCPYGRSGLLCNDVYVNIQSPFSGTDVFCYTSFLAYSTIPDITE
Zebrafish	(2144)	ARGATCVFQQLLEAACLCPYGRQGLLCEDAINITRPFKSLGDEFYGSYVAYPSIPSTGH
Drosophila	(1319)	OYGGTCVQFPGSYGLCLCELGKHGHYCEHNIEVALPSFSG-SVNGLSSEVAYVPIPIEY
		<b>EGF domain</b>
Human	(2441)	HYEFHLKQFLANNHSALQNNLIFFTGQKQGHGLNGDDFLAVGLNGSVVYSYNLGSGLASTI
Macaque	(2441)	HYEFHLKQFLANNHSALQNNLIFFTGQKQGHGLNGDDFLAVGLNGSVVYSYNLGSGLASTI
Chicken	(2205)	YYEFHLKQFLNHNHSALQDNLIFFTGQKQGLNGDDFLVYGLCDGRVVYSYNLGSGLASTI
Zebrafish	(2204)	FYEFHLKLTFFANNASALRNNLILFSGQKQGLSGDFFFAIGWRNCRIVYKYNLGSGLASTI
Drosophila	(1378)	SLLELSFKILPQTMS---QISLVAFFGOSYHDEKSDHLAVSFTQGYLMLLWNLCAGPRRI
		<b>Laminin-G domain</b>
Human	(2501)	RSEPF----LNLISLGVHTVHLCKRFQEGWLRVDDHKNKSIIPGRLVGLNVFSQFYVGGY
Macaque	(2501)	RSDPF----LNLISLGVHTVHLCKRFQEGWLRVDDHKNKSIIPGRLVGLNVFSQFYVGGY
Chicken	(2265)	ISKPE----LDLNLNHVTHLGRYLQKQWLKVDQKNKTTSFGRLVGLNVFSQFYVGGY
Zebrafish	(2264)	ISDR----LNPRLNHTVHFGRYLKTCWLKVNQKRRRTGTSFGPLMLNLTFSQLYVGGY
Drosophila	(1435)	FTQKPIDFRLDAPRVPEIKVGRIGRQWLSVDGKFNITGRSPGSGSRVDVLPILYVGGH
		<b>Laminin-G domain</b>
Human	(2556)	SEYTPDLLPNGADFKNGFOGCIFFTQVRTEKDGHFRLGNPEGHPNAGRSVGGCHASPCS
Macaque	(2556)	SEYTPDLLPNGADFKNGFOGCIFFTQVRTEKDGHFRLGNPEGHPNAGRSVGGCHASPCS
Chicken	(2320)	HEYTPDLLPKGSRFKNGFOGCIFFDQVRINMNEQEPSPGTPEGHPNAGRSVGGCKASPCS
Zebrafish	(2319)	EYTPPELLPPGSRFQNSFOGCIFFDLFRTRODGKFEHLGGPDIRPLSGRNVGGQGVNPCS
Drosophila	(1495)	EIANFTLPHDLPLHSGFOGCIYDVLKAGQVTP---LQETRGVRGRVGGQGTRECH
		<b>Laminin-G domain</b>
Human	(2616)	LMKQGNQGTCEESGLSVYCNCTTGKKGSEFCTETVSTCDPEHDPPHCSRGATCSLPHGY
Macaque	(2616)	LMKQGNQGTCEESGLSVYCNCTTRKCAFCTETVSTCDPEHDPPHCSRGATCSLPHGY
Chicken	(2380)	LTKQRNGGKQVESGLSVYCNCLAGMKCAFCTEMVIVCDPEHDPPHCKQGGTCVPLPNGY
Zebrafish	(2379)	LVFCHNGGTCVDSGLSVYCCVFGKGCALCSKQVSCDAEHIPPPFCARGSTCVPLSDGY
Drosophila	(1551)	RHAQHDGACQHGATFTCIQCEGNYGPICAOFTNCDSEFN---KGYEDATCVPLVNGY
		<b>EGF domain</b> <span style="margin-left: 150px;"><b>EGF domain</b></span>
Human	(2676)	TCFCPLGTTGLYCEQALISIDPSFRSNE-----
Macaque	(2676)	TCFCPLGTTGLYCEQALISIDPSFRSSE-----
Chicken	(2440)	MCHCPLGTSGLYCEQDISIDPSFRSNK-----
Zebrafish	(2439)	TCCPLGTSAGLHCQQAIIISDFFSNGQ-----
Drosophila	(1608)	ECCDFVGRTEKNCEEVIRSLSDVSLTGRRSYLAVRWPYLYDGGDKLGAKRSQMSYRNFT
		<b>EGF domain</b>
Human	(2704)	-----LSSWMSFASFHYRKKTHIQIQFOPLA
Macaque	(2704)	-----LSSWMSFASFHYRKKTHIQIQFOPLA
Chicken	(2468)	-----SSWMSFAPFYRHKTHIKIQFOPLS
Zebrafish	(2467)	-----SSWMSFPPINIRHRTHYIQIQFOPLS
Drosophila	(1668)	KKLMPPKPIITPSSHFVMKLLNEVEKQRSFSPVPLMGSKSFEEHHRVQFFFIETQLRPLS
		<b>EGF domain</b>
Human	(2729)	ADGILFYAAQHLKAQSGDFLCLISLVNSSVQLRYNLG-DRTIILETTLQKVTINGSTWHIIK
Macaque	(2729)	ADGILFYAAQHLKAQSGDFLCLISLVNGSVQLRYNLG-DRTIILETTLQKVTINGSTWHIIK
Chicken	(2493)	PDCILFYTAQRLGTQSGDFLCLISLVNGFVQLRYNLG-DRTIVLQAQKVDHAGQTHWIIK
Zebrafish	(2492)	PEGILFYTAQHLSTHSGDFLSTLSL SAGFVQLRYNLG-NQITIVLQSPKEIDVTGVRWHTVK
Drosophila	(1728)	ERGLLLYFCTLNNDKKGIFVLSLQGGVVEERISGSPNHVTVVRSVRMLAIGEWKIK
		<b>Laminin-G domain</b>
Human	(2788)	AGRVGAEGYLDLDCINVTEKASTKMSSLDTNTDFYICGVSSLNLVNPMAIENEFPVGHCGC
Macaque	(2788)	AGRVGAEGYLDLDCINVTEKASTKMSSLDTNTDFYICGVSSLNLVNPMAIENEFPVGHCGC
Chicken	(2552)	VGRVNGEYVLDLDCINTHTASAGMNVLDHTDFYICGVSSLNLVNSMATENEEFTGESCC
Zebrafish	(2551)	AGRCNSGELIYDCESVTRNSSEGSITLVDGANIFICGVSSLNTVSDIAIEKELVCGTGG
Drosophila	(1788)	MAQRGRWLTLWVEGSASALAPSAEVLVEPDLILYIGGKDKVSKPHNALSGFPIERGC
		<b>Laminin-G domain</b>



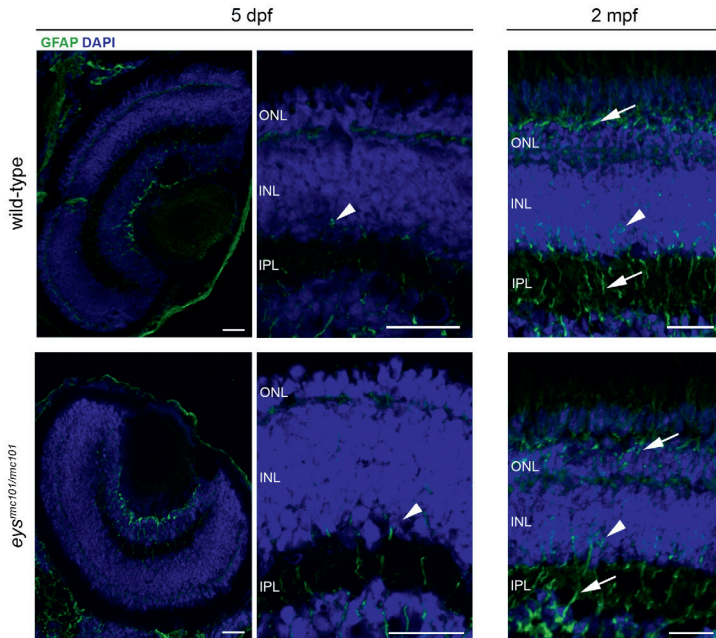
Residues identical in all sequences are white on a black background, whereas similar amino acids are white on a gray background. Residues that are present in at least three of the five proteins are indicated in black on a light gray background. Accession numbers of the protein sequences used for sequence comparison are as follows: human, NM\_001142800.1 (RefSeq); macaque, XM\_011737495.1 (RefSeq); chicken, XM\_015284845.1 (RefSeq); *Drosophila*, NM\_001032399.3 (RefSeq).





### Supplementary Figure S3. Measurement of the thickness of outer and inner nuclear layers in *eys<sup>rmc101/rmc101</sup>* and wild-type zebrafish.

(A, C, E) Representative images of wild-type and *eys<sup>rmc101/rmc101</sup>* zebrafish retinas at (A) 5 dpf, (C) 2 mpf, and (E) 5 mpf. Nuclear layers were stained with DAPI and inverted to grey images. ONL: outer nuclear layer; OPL: outer plexiform layer; INL: inner nuclear layer; IPL: inner plexiform layer; GCL: ganglion cell layer. Scale bars (A): 10  $\mu\text{m}$ . Scale bars (C, E): 20  $\mu\text{m}$ . (B, D, F) Measurements of ONL and INL thickness in wild-type and *eys<sup>rmc101/rmc101</sup>* zebrafish at (A) 5 dpf, (C) 2 mpf, and (E) 5 mpf. Asterisks indicate statistical significance (\*\*\*) =  $p < 0.0001$ ) using Mann-Whitney U test.



**Supplementary Figure S4. Immunohistochemistry on retinal sections of wild-type and *eys<sup>mc101/mc101</sup>* zebrafish in order to investigate Müller glia activation.**

Retinal sections of wild-type and *eys<sup>mc101/mc101</sup>* zebrafish at 5 dpf and 2 mpf stained with antibodies against GFAP (green), as a marker for Müller glia cells. Müller glia cell bodies are located in the inner nuclear layer (arrow heads) and project processes (arrows) in either direction to outer limiting membrane and inner limiting membrane. Nuclei are counterstained with DAPI (blue). INL: inner nuclear layer; IPL: inner plexiform layer; ONL: outer nuclear layer. Scale bar: 20  $\mu$ m.

**Supplementary Table S1.**

Primers used for PCR analysis.

<b>Purpose</b>	<b>Product</b>	<b>Sequence (5' &gt; 3')</b>	<b>Comment</b>
<b>Sequence analysis</b>	<i>eys</i> exon 1-6 forward	TGAGGGAAGTGCCTACACAG	
	<i>eys</i> exon 1-6 forward	GTCTTTGTCCTGCTCCATTC	Nested
	<i>eys</i> exon 1-6 reverse	GCAAGTAGCTCCGTTCAAGC	
	<i>eys</i> exon 1-6 reverse	GATAGGCTAAGCATGCGTTC	Nested
	<i>eys</i> exon 6-10 forward	CTGACCCCCGCATTATATG	
	<i>eys</i> exon 6-10 forward	GCACCTGTCTCCCTGGATAC	Nested
	<i>eys</i> exon 6-10 reverse	CCTCATATCCAGCATGCAG	
	<i>eys</i> exon 6-10 reverse	TAGTTGTGCTGTTGGTCCAC	Nested
	<i>eys</i> exon 10-17 forward	TGATTTGGTGGCAGGATAC	
	<i>eys</i> exon 10-17 forward	ATACCAATGCCTGTGTGCAC	Nested
	<i>eys</i> exon 10-17 reverse	ACACACTCTGCCCGTTATC	
	<i>eys</i> exon 10-17 reverse	GTTATCGCACGGATTAACAGC	Nested
	<i>eys</i> exon 18-20 forward	TAACCTGGTTACGCTGGAG	
	<i>eys</i> exon 18-20 forward	TCAATGACTGCGTAGCAAC	Nested
	<i>eys</i> exon 18-20 reverse	AAACTCCCCTGGGGTATCAG	
	<i>eys</i> exon 18-20 reverse	TCCATCCTTGAGGACACACA	Nested
	<i>eys</i> exon 20-22 forward	GATACCCAGGGGAGTTTTC	
	<i>eys</i> exon 20-22 forward	ACAGCCCTATGACCCTTG TG	Nested
	<i>eys</i> exon 20-22 reverse	GATGCGCATTATTGATGTC	
	<i>eys</i> exon 20-22 reverse	ACAGTGCAGGCCTGAAAATC	Nested
	<i>eys</i> exon 21-25 forward	GTGAAATTGATAGCGATGACTG	
	<i>eys</i> exon 21-25 forward	TGGATGGGGTCAACAGCTAC	Nested
	<i>eys</i> exon 21-25 reverse	CAACTCCCATGAACACAGGG	
	<i>eys</i> exon 21-25 reverse	TGTTTCTCTCGAGTGATCG	Nested
	<i>eys</i> exon 24-28 forward	TCGACGGCCTTAATGTTAC	
	<i>eys</i> exon 24-28 forward	TCACTGCGAGAGAAACTG	Nested
	<i>eys</i> exon 24-28 reverse	CAGGCTCATTCTGGATGCAC	
	<i>eys</i> exon 24-28 reverse	ATTCCCTGGTTGCATGGTTG	Nested
	<i>eys</i> exon 28-32 forward	GGGAATGTGCATCCAGAATG	
	<i>eys</i> exon 28-32 forward	TGGCTACACCTGCTTCTGTC	Nested
	<i>eys</i> exon 28-32 reverse	TCCTGACACCACTAACGGTG	
	<i>eys</i> exon 28-32 reverse	TCAGCCACACCGGAAAAG	Nested
	<i>eys</i> exon 32-36 forward	CCATGTGTTTATTGGAGGTC	
	<i>eys</i> exon 32-36 forward	CTCGTCATCGTTCACCTTAC	Nested
	<i>eys</i> exon 32-36 reverse	CTTGCACTCTGGAGAAACAC	
	<i>eys</i> exon 32-36 reverse	AGAAAACGCTCTCCAAATC	Nested
	<i>eys</i> exon 36-39 forward	TGGCTGCTCAGAATATTAGATC	
	<i>eys</i> exon 36-39 forward	GATAGTTTGGTGGCAATTACAGTG	Nested
	<i>eys</i> exon 36-39 reverse	GGCACAGCTTACGGAGTAG	
	<i>eys</i> exon 36-39 reverse	CATGCACAGAACCAGCTCTC	Nested
	<i>eys</i> exon 39-40 forward	TGTTCTGTGCATGCCTTC	
	<i>eys</i> exon 39-40 forward	CGCTCTACTCCGGTAAGCTG	Nested
	<i>eys</i> exon 39-40 reverse	AGGCATTATTGGCAAAGGTG	

	<i>eyes</i> exon 39-40 reverse	GGGCCGAGTGATGTTGATAG	Nested
	<i>eyes</i> exon 40-44 forward	TCACCTGAAGCTCACCTTTG	
	<i>eyes</i> exon 40-44 forward	TTCTCTTTTCCGGGCAAAAG	Nested
	<i>eyes</i> exon 40-44 reverse	CAGAACGACACTTTCTCTGAGC	
	<i>eyes</i> exon 40-44 reverse	GCACCTTCCATCCAAACAC	Nested
	<i>eyes</i> exon 44-46 forward	GTGTTGGATGAAAGGTGC	
	<i>eyes</i> exon 44-46 forward	GCTCAGAGAAAGTGTCGTTCTG	Nested
	<i>eyes</i> exon 44-46 reverse	TTGAATGGACTGTTGGCATC	
	<i>eyes</i> exon 44-46 reverse	CCCAGATTATAGCGGAGCTG	Nested
	<i>eyes</i> exon 46 forward	TAAGGTTTGCAAGAACGGTG	
	<i>eyes</i> exon 46 forward	TGATCATCTAGCGGTTGGAC	Nested
	<i>eyes</i> exon 46 reverse	ACTTCTCCTTGATAGACATTGAAAC	
	<i>eyes</i> exon 46 reverse	TGGATGAGAGTCCGATTGTG	Nested
<b>RT-PCR analysis</b>	<i>eyes</i> exon 19-21 forward	CTGCACAGACCTCCTCAATG	
	<i>eyes</i> exon 19-21 reverse	CACAGCGAGTTCCTCAAAC	
	<i>actin</i> forward	CAACAGGGAAAGATGACACAGAT	
	<i>actin</i> reverse	CAGCTGGATGGCAACGT	
<b>Genomic lesions</b>	<i>eyes</i> exon 20 forward	TGGTAAAGAATGCCCAACT	In intron 19
	<i>eyes</i> exon 20 reverse	GCAAACAAGCCACAGAACA	In intron 20

### Supplementary Table S2.

Oligo sequences used for gRNA synthesis.

Oligo name	Sequence
Constant oligo	AAAAGCACCGACTCGGTGCCACTTTTTCAAGTTGATAACGGACTAGCCTT
	ATTTAACTTGCTATTCTAGCTCTAAAAC
Gene specific oligo <i>eyes</i> exon 20	<b>TAATACGACTCACTATAGGTGCAGGAAAAC</b> <u>TC</u> <b>CCCTG</b> GTTTTAGAGCTA
	<u>GAAATAGCAAG</u>

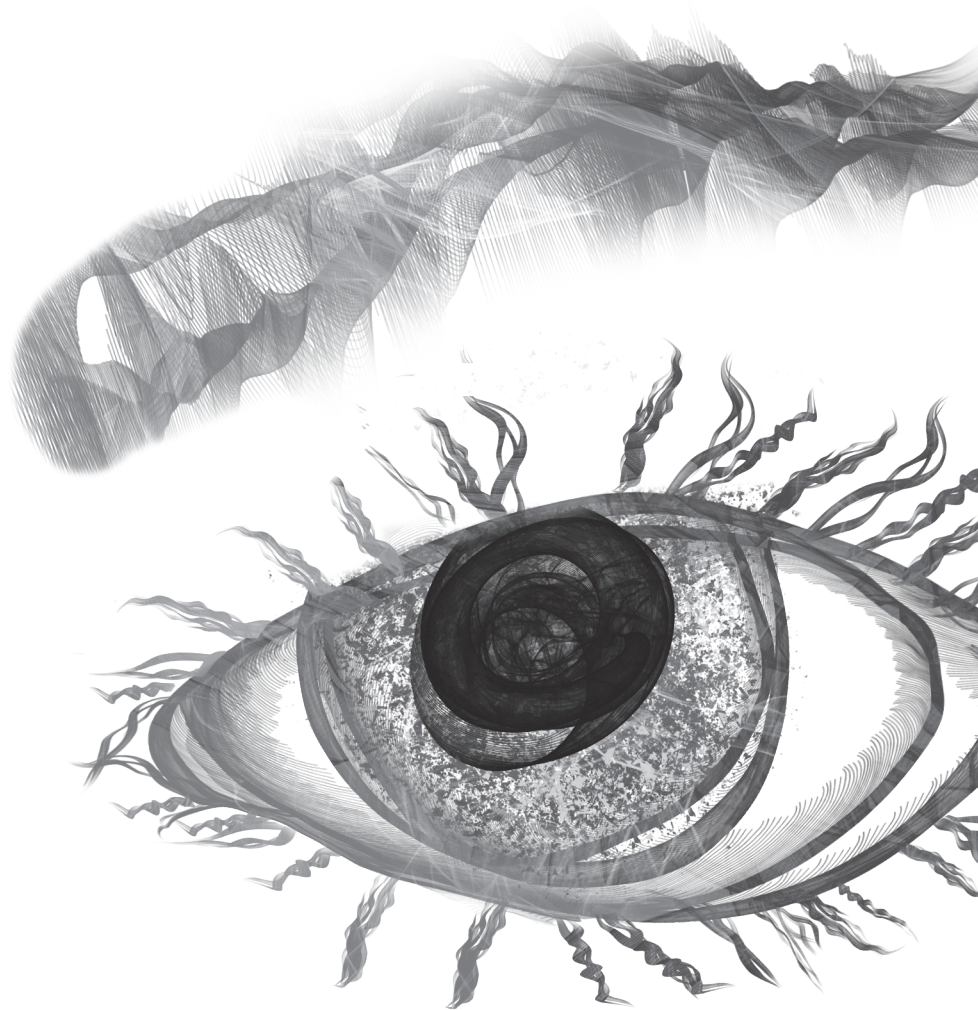
T7 promoter in bold. Gene specific region is red and underlined. Overlapping region is underlined.



<b>150</b>	47.229	27.970	51.420	32.322	39.784	16.925	19.967	18.786	5.851	26.431	0.0045	0.0246
<b>170</b>	43.461	29.880	50.023	27.615	47.284	19.580	15.348	15.604	9.500	15.662	0.0040	0.0246
<b>190</b>	51.698	21.308	39.062	31.346	46.442	21.947	15.285	16.501	14.173	28.282	0.0216	0.0339
<b>210</b>	35.533	20.274	67.925	36.008	35.274	24.047	22.713	17.494	14.651	25.472	0.0802	0.0883
<b>230</b>	35.456	20.734	41.845	39.286	24.518	17.214	13.480	12.548	15.774	28.689	0.0215	0.0339

P-values of (A)  $\Delta$  distance moved (mm) and (B)  $\Delta V_{max}$  (mm/s). R programming language was used to generate plots, calculate mean values and SEM values, and perform statistical tests. The difference between wild-type and mutant was analyzed using two-tailed, unpaired Student's t-test, and p-values were corrected for multiple testing using the Benjamini-Hochberg method.

# Chapter 5



# Development of *EYS* microgenes as a potential therapy for *EYS*-associated retinal dystrophy

Muriël Messchaert<sup>1,2</sup>, Anita Hoogendoorn<sup>1,2</sup>, Marieke Roefs<sup>1</sup>, Lonneke Duijkers<sup>1,2</sup>, Martijn A. Huijnen<sup>3</sup>, Alejandro Garanto<sup>1,2</sup>, Rob W. J. Collin<sup>1,2</sup>

<sup>1</sup> Department of Human Genetics, Radboud University Medical Center, Nijmegen, The Netherlands.

<sup>2</sup> Donders Institute for Brain, Cognition and Behaviour, Radboud University Medical Center, Nijmegen, The Netherlands.

<sup>3</sup> Centre for Molecular and Biomolecular Informatics, Radboud University Medical Center, Nijmegen, The Netherlands.



**Abstract**

Autosomal recessive (ar) retinitis pigmentosa (RP), a subtype of inherited retinal dystrophy, is often caused by mutations in *Eyes shut homolog* (*EYS*), a gene predominantly expressed in the photoreceptor cells of the retina. Currently, there is no treatment for this disorder. Due to its large size, developing a gene augmentation therapy for *EYS* using conventional adeno-associated viral (AAV) vectors is challenging. In this study, we aimed to develop *EYS* microgenes encoding functional proteins, as a potential therapy for *EYS*-associated retinal dystrophy. Based on the protein domain conservation of *EYS*, we generated three *EYS* microgenes, of different sizes, by PCR and Gateway cloning. To investigate their expression, HEK293T cells were transfected with plasmids encoding the *EYS* microgenes and their cell lysates were used for western blot analysis in order to determine protein expression. Two out of three microgenes appeared to be stable and expressed in HEK293T cells. Next, we investigated the localization of the microgenes in hTERT-RPE1 cells. However, immunofluorescence data were inconclusive. This study is a first step towards the development of a genetic therapy for *EYS*-associated retinal dystrophy, using microgenes. Additional experiments are required to determine whether the microgenes are targeted to the right location in the cell and whether the microgenes encode functional proteins.

**Key words:**

*Eyes shut homolog*, gene therapy, microgenes, retinitis pigmentosa

## 5.1 Introduction

Mutations in *Eyes shut homolog* (*EYS*) are amongst the most frequent causes of autosomal recessive retinitis pigmentosa (arRP), together accounting for 5-10% of the arRP cases.<sup>1-3</sup> Retinitis pigmentosa is a subtype of inherited retinal dystrophy, with a prevalence of approximately 1 in 4,000 individuals, and is characterized by progressive degeneration of rod photoreceptors causing constriction of the visual field and eventually, often, total blindness.<sup>4</sup> Different modes of inheritance including autosomal recessive, autosomal dominant, and X-linked, have been observed in the disease.

*EYS* encodes the 3,144 amino acids long protein eyes shut homolog (*EYS*) and is predominantly expressed in the photoreceptor cells of the retina. It contains 28 epidermal growth factor (EGF)-like domains and 5 laminin A G-like (LamG) domains. It has been described that EGF domains are important for intracellular signaling and cell adhesion, whereas proteins harboring LamG domains can have a wide variety of functions, such as cell adhesion, migration and signaling.<sup>5,6</sup> *EYS* is an ortholog of the *Drosophila* spacemaker (*spam*) protein, which is shown to play a major role in maintenance of the photoreceptor morphology.<sup>7</sup> In zebrafish, it was demonstrated that *EYS* localizes near the connecting cilium and *eys* knock-out zebrafish show disruption of the retinal architecture and visual impairment.<sup>8-10</sup>

Currently, there is no therapy for RP that has been proven to prevent the development or progression of the disease, or can restore visual function. Drugs currently used in the treatment of RP are focused on slowing down the progression of disease or targeting secondary complications.<sup>11</sup> The retina is an accessible and immune privileged structure, which makes it a suitable target for gene augmentation therapy, i.e. the replacement of a mutated gene that causes disease with a healthy copy of that gene or its cDNA. Adeno-associated virus (AAV) vector-mediated delivery of the transgene into the subretinal space is considered an effective and safe method to treat some subtypes of inherited retinal diseases (IRDs).<sup>11-14</sup> Recently, AAV-mediated *RPE65* gene therapy for LCA (LUXTURNA™) was approved by the US Food and Drug Administration (FDA), which opens the door to explore the potential of gene therapy for other IRDs. However, a drawback of AAV-mediated delivery of transgenes is the limited cargo capacity of AAV vectors, which is 4.7 kb.<sup>15</sup> With a length of 9.4 kb, the *EYS* cDNA exceeds this cargo capacity. This requires the need of a different gene augmentation strategy. One solution can be the use of shorter therapeutic constructs, here called microgenes. Microgenes are smaller versions of a cDNA, containing only the most important regions, that would still encode a functional protein. The use of microgenes as a therapeutic strategy was shown to be promising in Duchenne muscular dystrophy (DMD), a disease caused by mutations in the large *DMD* gene that encodes the dystrophin protein. Several studies showed that AAV-mediated *micro-dystrophin* expression in different mutant mouse models and canine models with DMD could effectively mitigate muscle disease.<sup>16-19</sup> An example of the use of microgene therapy for retinal disease is the study by Zhang et al. They reported the delivery of a

*miniCEP290* gene into a mouse model of LCA. Mice injected with *miniCEP290* significantly improved photoreceptor survival, morphology and function compared to control-injected mice.<sup>20</sup>

In this study, we generated three *EYS* microgenes, that are predicted to encode functional proteins, and assessed protein stability and localization. This study is a first step towards the development of a genetic therapy for *EYS*-associated retinal dystrophy.

## 5.2 Materials and Methods

### 5.2.1 Cloning of full length *EYS* cDNA

For cloning of *EYS* cDNA, PCR primers for the amplification of individual fragments were designed using Primer3 software (<http://bioinfo.ut.ee/primer3-040>). Twenty nanogram of human retina marathon-ready cDNA (Clontech) was incubated with 0.5  $\mu$ M of the forward and reverse primer, 100  $\mu$ M dNTPs (Roche), 0.25 U Phusion high-fidelity polymerase (New England Biolabs), 10x Phusion PCR buffer (New England Biolabs) and 1x Q-solution (Qiagen) in a total volume of 25  $\mu$ l milliQ. Overhang PCR was used to fuse the separate fragments to form full length *EYS* cDNA. The purified sample was cloned into the pDONR201 vector (Invitrogen) using the Gateway BP Clonase enzyme mix (Thermo Fisher Scientific) to generate entry clones. Entry clones were validated by Sanger sequencing and cloned into the destination vector pcDNA520 using the Gateway LR Clonase enzyme mix (Thermo Fisher Scientific). Primer sequences used are listed in Supp. Table S1.

### 5.2.2 Microgene design

To be able to design the microgenes, *EYS* sequence conservation per amino acid position was calculated with the AL2CO program<sup>21</sup> using default values from <http://prodata.swmed.edu/al2co/al2co.php>. Levels of conservation were averaged for each predicted domain, the low complexity region, or the regions between those. Levels of conservation per amino acid position were calculated using the entropy per position, and were subsequently normalized to zero, mean and unit variance (+1 to -1.5). Based on this calculation, conserved regions were selected to be part of one or more of the microgenes.

### 5.2.3 Cloning of microgenes

PCR primers for amplification of individual fragments were designed using Primer3 software (<http://bioinfo.ut.ee/primer3-0.4.0>). Some primers contained 5' overhangs complementary to the 3' end of the adjacent part of the microgene in order to connect the different parts using overhang PCR. Twenty nanogram of the plasmid containing full length human *EYS* cDNA was incubated with 0.5  $\mu$ M of the forward and reverse primer, 100  $\mu$ M dNTPs (Roche), 0.25 U Phusion high fidelity polymerase (New England Biolabs), 1x Phusion PCR buffer (New England Biolabs) and 1x Q-solution (Qiagen) in a total volume of 25  $\mu$ l milliQ. The following program was run in a 2720 Thermal Cycler (Applied

Biosystems): the samples were denatured at 98°C for 3 minutes followed by 35 cycles of amplification consisting of 30 seconds at 98°C, 30 seconds at 58°C and 1.5 minutes at 72°C, and a final extension for 5 minutes at 72°C. PCR products were run on a 1% agarose gel and bands were excised. DNA was purified on Nucleospin Gel and PCR Clean-up columns (Macherey Nagel). One hundred fifty nanogram of the purified insert was cloned into the pDONR201 vector (Invitrogen) using the Gateway BP Clonase Enzyme mix (Thermo Fisher Scientific) to generate entry clones. Entry clones were validated by Sanger sequencing and cloned into the destination vector pcDNA520 using the Gateway LR Clonase enzyme mix (Thermo Fisher Scientific). Primer sequences used to generate the *EYS* microgenes are listed in Supp. Table S2.

#### 5.2.4 Transfection of HEK293T cells or hTERT-RPE1 cells

HEK293T cells or hTERT-RPE1 cells were grown in DMEM (HEK293T) or DMEM/F12 (1:1, hTERT-RPE1) supplemented with 10% fetal calf serum, 1% penicillin-streptomycin and 1% sodium pyruvate at 37°C and 5% CO<sub>2</sub>. Confluent cells were diluted 1 to 6, seeded in a 12-wells plate and grown for 24 hours at 37°C in a total volume of 1 ml. For transfection, 2 µg of the full length *EYS*, *EYS* microgene or *CEP290* expression vector (positive control) was incubated together with 6 µl Fugene<sup>®</sup> HD Transfection Reagent (Promega) in a total volume of 100 µl Optimem for 20 minutes at room temperature and subsequently the transfection mix was added to the cells. After incubation for 96 hours at 37°C, cells were harvested for western blot analysis (HEK293T) or immunocytochemistry (hTERT-RPE1).

#### 5.2.5 Western blot analysis

Medium was removed and cells were collected and washed with PBS. HEK293T cells were resuspended in 100 µl RIPA buffer containing protease inhibitors (Roche). After sonication of the cells for 30 seconds, cells were centrifuged at 11,000 rpm for 5 minutes at 4°C and subsequently supernatant containing protein lysates was collected. Protein concentrations were determined via BCA according to the manufacturer's instructions (Pierce). For detection of *EYS*, samples were subjected to SDS-PAGE (3-5% acrylamide) and transferred to PVDF (polyvinylidene difluoride) membrane (Roche, 03010040001) using standard techniques. Membranes were blocked in 5% non-fat dry milk (blocking buffer, Biorad) in PBS for 6 hours at 4°C and subsequently incubated with primary antibody (rabbit anti-*EYS*, Novus Biological, NBP1-90038, 1:1,000 in blocking buffer or mouse anti-HA, Sigma, H3663, 1:1,000 in blocking buffer) for three days at 4°C. Membranes were washed three times with PBST (0.2% Tween-20 in PBS), incubated with HRP-conjugated secondary antibody (HRP-conjugated goat anti-rabbit, Genscript, A00098, 1:10,000 in blocking buffer or HRP-conjugated goat anti-mouse, Jackson ImmunoResearch Laboratories, 115-035-062, 1:10,000 in blocking buffer) for 1 hour at room temperature, washed and developed using SuperSignal<sup>™</sup> West Femto Maximum Sensitivity Substrate (Thermo Scientific) and scanned on a ChemiDoc Touch Imaging System (Biorad). For the detection of tubulin,

samples were subjected to SDS-PAGE (4-12% Bis-Tris, NuPAGE) and transferred to a PVDF membrane (GE Healthcare Life Sciences) overnight at 4°C. The membrane was blocked in blocking buffer for 1 hour at room temperature and subsequently incubated with primary antibody (mouse anti-alpha tubulin, Abcam, ab7291, 1:2,000 in blocking buffer) overnight at 4°C. The membrane was washed three times with PBST. After incubation with the secondary antibody (goat anti-mouse IRDye800, LI-COR Biosciences, 926-32210, 1:10,000 in blocking buffer) the membrane was washed and scanned on an Odyssey imaging system (LI-COR Biosciences).

### 5.2.6 Immunocytochemistry

hTERT-RPE1 cells were grown on coverslips in 12-well plates and transfected with expression clones containing full length *EYS* or one of the microgenes as described above. After transfection, cells were serum-starved for another 48 hours. Cells were rinsed with 1x PBS, fixed in 2% paraformaldehyde for 20 minutes, permeabilized in PBS supplemented with 1% Triton-X for 3 minutes, and subsequently blocked in 2% bovine serum albumin in 1x PBS (blocking solution) for 30 minutes, all at room temperature. For immunostaining, cells were incubated with primary antibody diluted 1:100 in blocking solution for 60 minutes at room temperature. Cells were washed 3 times for 5 minutes in 1x PBS, incubated for 45 minutes with the corresponding secondary antibody diluted 1:500 in blocking solution. Cells were washed 3 times 5 min in 1x PBS and rinsed in water. Finally, coverslips were mounted in Vectashield with DAPI and imaged on a Zeiss Axio Imager Z1 Fluorescence microscope (Zeiss).

Antibodies used were rabbit anti-EYS (Novus Biological, NBP1-90038), mouse anti-acetylated tubulin (Sigma, T6793), donkey anti-rabbit Alexa Fluor 488 (Life Technologies, A21206), and donkey anti-mouse Alexa Fluor 568 (Molecular Probes, A10037).

## 5.3 Results

### 5.3.1 Cloning of full length *EYS* cDNA

First, we cloned the full length *EYS* cDNA by PCR using human retina marathon-ready cDNA as a template. Since *EYS* is a large gene, it was not possible to obtain the complete cDNA by one single PCR. Therefore, the cDNA was divided in ten smaller fragments which were more easily amplified by PCR (Figure 5.1). There was an overlapping region of at least twenty nucleotides between adjacent fragments. After all the ten fragments were obtained, additional annealing PCRs were performed to combine the fragments resulting into five fragments and ultimately into the complete *EYS* cDNA. Finally, the *EYS* cDNA was cloned into an expression vector in frame with an C-terminal HA-tag using Gateway cloning. The presence of the correct insert was validated by Sanger sequencing (data not shown). This construct formed the basis for the cloning of the *EYS* microgenes, and served as a positive control in expression and localization experiments.

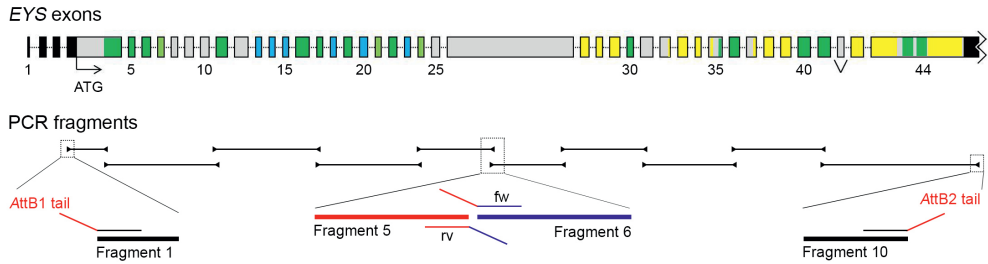


**Figure 5.1. Cloning strategy for full length *EYS* cDNA.**

Upper panel: exonic structure of *EYS*. Lower panel: schematic representation of the 10 initial PCR fragments for the cloning of the full length *EYS* cDNA. The forward primer of the first fragment and the reverse primer of the last fragment contained an *AttB1* or *AttB2* tail for Gateway cloning, respectively. Primers of intermediate fragments contained tails overlapping with their adjacent fragments.

### 5.3.2 Generation of three *EYS* microgenes

In order to be able to select the regions for the design of the *EYS* microgenes, *EYS* sequence conservation per domain was calculated with the AL2CO program.<sup>21</sup> Part of the EGF domains in the N-terminal part of the protein as well as the LamG domains in the C-terminal part of the protein appeared to be most conserved, whereas the intermediate region of *EYS*, where no domains are predicted, showed low conservation scores (Figure 5.2A). The most conserved regions were selected for the generation of three different *EYS* microgenes named microgene A, microgene B and microgene C (Figure 5.2B). The sizes of microgene A, B and C are 3.6 kb, 4.5 kb and 5.8 kb, respectively. Microgene A will fit in a single AAV vector, whereas for delivery of microgenes B and C, a dual AAV approach could be employed for packaging, as described previously.<sup>22</sup> To generate the microgenes, separate regions of the microgenes were amplified by PCR on human *EYS* cDNA, followed by an additional PCR to anneal these regions to form a complete microgene. Finally, gateway cloning was used to clone the three microgenes in a vector in frame with a C-terminal HA-tag.

### 5.3.3 Expression of *EYS* microgenes in HEK293T cells after transfection

To test the stability of the microgenes *in vitro*, HEK293T cells were transfected with HA-tagged versions of either full length *EYS* cDNA, or microgene A, B or C for 96 hours. We also transfected cells with CEP290-HA as a positive control, known to be properly expressed in HEK293T cells after transfection. Microgene protein expression in HEK293T cell lysates was determined by Western blot analysis using anti-HA and anti-*EYS* antibodies. Immunoblotting using the anti-*EYS* antibody revealed that the full length *EYS* (351 kDa), microgene A (137 kDa) and microgene B (171 kDa) proteins were expressed approximately at their predicted molecular weights, while no protein expression was observed for

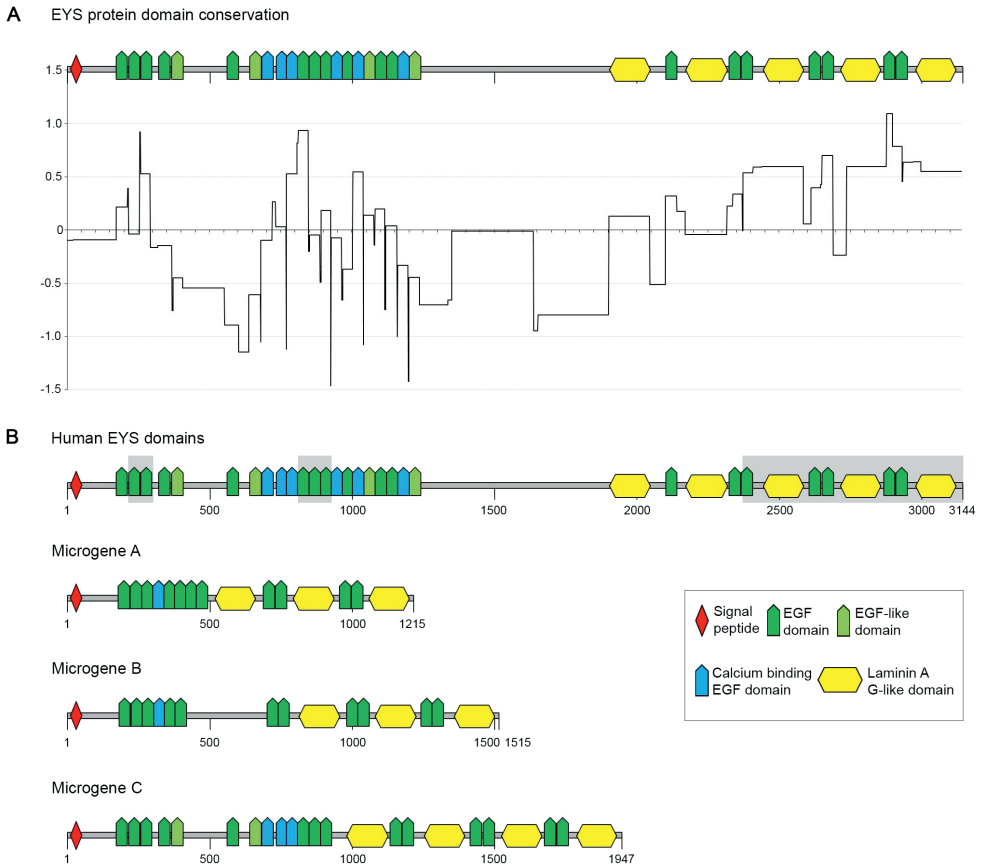


**Figure 5.2. Sequence conservation of EYS and protein structure of EYS microgenes.**

(A) Schematic overview of EYS sequence conservation per domain, which was calculated with the AL2CO program. (B) Protein domain structure of EYS and the EYS microgenes A, B and C, based on the results of the SMART database (<http://smart.embl-heidelberg.de/>). Conserved regions of EYS that were selected to be part of the microgenes are displayed on a grey background. EGF: epidermal growth factor.

microgene C (219 kDa)(Figure 5.3A). Furthermore, no expression was detected in non-transfected cells or cells transfected with CEP290, indicating that positive bands observed for EYS and the microgenes are specific. In contrast to what was observed after immunoblotting using anti-EYS antibody, none of the microgenes or full length EYS was detected on the blots treated with the anti-HA antibody, whereas CEP290 (302 kDa) was clearly visible, confirming that the procedure worked (Figure 5.3B). All constructs were re-sequenced to exclude mutations that could affect the expression of the proteins or the epitope, but no variants were found. These results indicate that microgenes A and

B are stable proteins. Microgene C could not be detected, suggesting that there is no protein formed or that the produced protein is not stable. The fact that the microgenes and full length *EYS* were not observed in the HA-blot, suggests that the HA-tag is lost by for instance proteolytic processing.

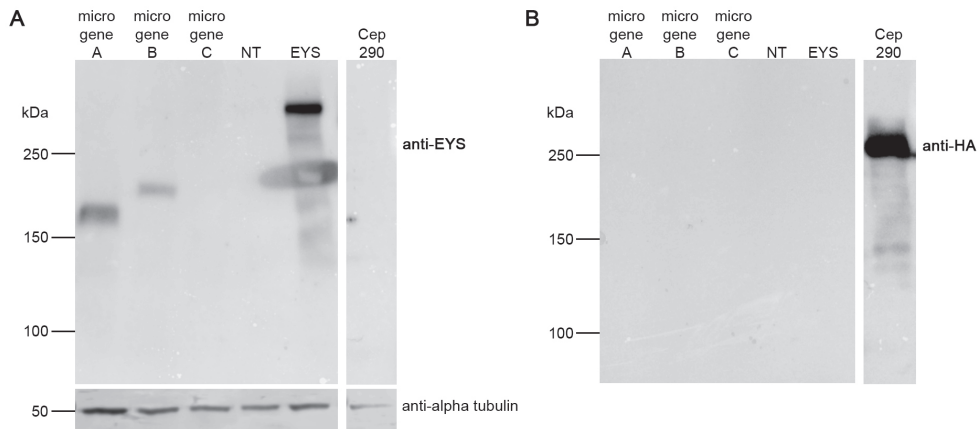


**Figure 5.3. Western blot analysis of HEK293T cells transfected with *EYS* microgenes.**

Western blot analysis was performed after transfection of HEK293T cells with expression vectors of full length *EYS* (351 kDa), microgene A (137 kDa), B (171 kDa), C (219 kDa), or CEP290 (302 kDa), which all contained a C-terminal HA-tag. (A) Upper panel: western blot using anti-*EYS* antibody. Lower panel: western blot using anti-alpha tubulin (50 kDa). (B) Western blot using anti-HA antibody. NT: non-transfected.

#### 5.3.4 Localization of *EYS* and *EYS* microgenes in hTERT RPE1 cells

Next, we examined whether the microgenes were properly localized. Therefore, hTERT-RPE1 cells were transfected with plasmids containing either the full length *EYS* cDNA or microgene A, B, or C, followed by serum starvation to induce ciliogenesis. Previously, in the zebrafish retina, it was namely shown that, *EYS* localizes near the connecting cilium of photoreceptor cells (Chapter 4).<sup>10</sup> The localization of *EYS* was determined by immunocytochemistry using the same *EYS* antibody as used for immunoblotting. In order to investigate whether *EYS* and the microgenes localize near the cilium, cells were co-stained with an antibody against acetylated tubulin, a ciliary marker. Non-transfected, as well as cells transfected with either full length *EYS* or one of the microgenes all showed formation of cilia (Figure 5.4). We barely detected any immunofluorescence signal for *EYS*. Some green spots were observed, however, similar staining was also seen in non-transfected cells, suggesting that this signal is background staining and not specific for *EYS* or the microgenes. So far, the immunofluorescence data were inconclusive and future experiments are needed to analyze the localization of the *EYS* microgenes.



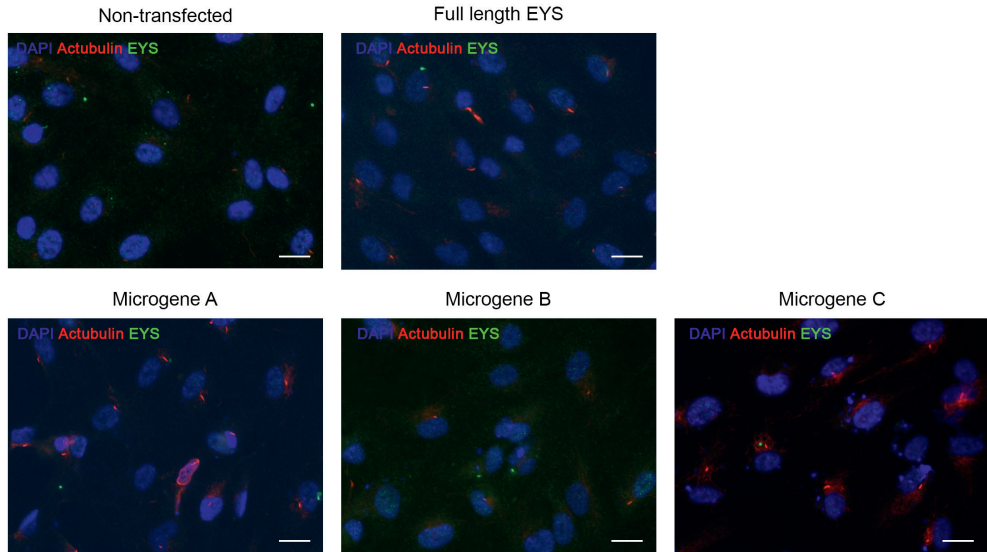


**Figure 5.4. Immunocytochemistry of hTERT-RPE1 cells transfected with the EYS microgenes.**

hTERT-RPE1 cells were transfected with full length EYS or microgene A, B or C. Cells were stained with anti-acetylated tubulin (Actubulin, red) and anti-EYS (green). Nuclei were counterstained with DAPI (blue). Scale: 20  $\mu$ m.

## 5.4 Discussion

In this study, we aimed to develop *EYS* microgenes that would encode functional proteins, as a potential therapy for *EYS*-associated retinitis pigmentosa. We generated three *EYS* microgenes, of different sizes, based on the protein domain conservation of EYS. Two out of three microgenes appeared to be stable and expressed in HEK293T cells. The localization of the microgenes was studied in hTERT-RPE1 cells, but did not yield any reliable results. Thus the potential of microgene therapy for *EYS*-associated inherited retinal dystrophy as of yet remains elusive.

Recently, Zhang et al. reported on the generation of a *miniCEP290* fragment. Injection of *miniCEP290* into the retina of mouse model of LCA showed delay in photoreceptor degeneration.<sup>20</sup> This is the first example of the use of a minigene approach for retinal disease. The use of microgenes as a therapeutic tool has a large history in the development of a genetic therapy for DMD. The full length dystrophin gene is 2.6 Mb in length, with a coding sequence of 11.5 kb that encodes a 427 kDa protein.<sup>23</sup> The development of a microgene therapy for DMD started with the discovery of a highly functional  $\Delta 17-48$  mini-dystrophin by England et al.<sup>24</sup> Although this 6.2 kb construct was still too large for packaging, this initiated an acceleration in the development of mini-dystrophin. In 1997, Yuasa et al published a 3.7 kb  $\Delta$ DysM3 gene that unfortunately appeared not functional.<sup>25</sup>

However, the mini-dystrophin construct evolved quickly and in total over 30 different mini-dystrophin constructs are reported to date. Therapeutic potential of mini-dystrophin was improved with modifications, such as codon optimization and inclusion of important domains.<sup>26,27</sup> Many preclinical studies in animal models showed positive results, such as reduced pathology, increase of muscle force and enhancement of cardiac function.<sup>23</sup> Positive results of pre-clinical *in vivo* studies resulted in the initiation of clinical trials in DMD patients (ClinicalTrials.gov, NCT03368742, NCT03375164, NCT03362502).<sup>23</sup> All together, this shows that the development of microgenes for therapeutic purposes is a challenging process that easily can take many years.

In this study, three *EYS* microgenes were designed, based on the protein domain conservation of the full length *EYS*. Conserved regions of *EYS* were selected to be part of one or more of the microgenes. Of course, we are not sure whether the selected regions will lead to a functional protein. Also, we directly connected the regions to each other. More insights in the function of *EYS* and the function of the specific protein domains may help to improve the microgene design. As has been shown for microgene development for DMD, codon optimization and inclusion of specific functional domains may also help to increase functionality of the protein.<sup>26,27</sup>

Western blot analysis of protein lysates of HEK293T cells transfected with the *EYS* microgenes revealed that microgene A and microgene B are expressed, whereas no protein expression was observed for microgene C. These results indicate that microgene A and B are able to produce stable proteins, while for microgene C, either no protein is formed or the protein is not stable and prone to degradation. Expression of the proteins was observed using an anti-*EYS* antibody, however, no staining was observed when using the anti-HA antibody. One explanation of this could be that the HA signal is not strong enough to be detected by western blot. Another reason could be that the protein is somehow proteolytically processed at the C-terminal end and thereby the HA-tag is lost. At the moment we started this study, we did not have a suitable antibody against *EYS*. Therefore we decided to clone the *EYS* constructs within an expression vector containing an HA-tag. Since a signal peptide is predicted to be present at the N-terminal part of the protein, we decided to place the HA-tag at the C-terminal end to prevent the tag from being lost.

The next step of validation of the microgenes is to investigate whether the *EYS* microgene proteins show proper localization. In this study, we transfected hTERT-RPE1 cells with either full length *EYS* or one of the microgenes. In order to study their localization, immunocytochemistry was performed using anti-*EYS* and anti-acetylated tubulin antibodies. Unfortunately, we were not able to draw any conclusions about the localization of the microgenes, since immunofluorescence signal of *EYS* was barely detected. The green spots that were observed were also seen in non-transfected cells. This could mean that endogenously expressed *EYS* protein was detected, however, since *EYS* expression levels in hTERT-RPE1 cells are very low, this is not very likely. We therefore

assumed that this is background signal and not specific EYS staining. The poor EYS signal that was observed could be due to the fact that the EYS antibody did not work properly. However, the same antibody was successfully used before, for the staining of zebrafish retinal cryosections using a similar procedure (**Chapter 4**). Another explanation could be that the transfection efficiency was not high enough to be able to detect full length EYS or the microgenes. In previous studies, it was observed that EYS localizes near the connecting cilium of photoreceptor cells at least in the zebrafish retina (**Chapter 4**).<sup>10,28</sup> Although in our hands, hTERT-RPE1 have always shown low transfection efficiencies, we selected these cells for localization experiments, because they are able to form cilia and have a large cytoplasmic compartment. Other cells that also contain cilia and possibly can be transfected more easily could be COS-1 cells.<sup>29</sup> There is also a possibility that EYS localizes outside the cilium in hTERT-RPE1 cells. Or, since a signal peptide is predicted to be present at the N-terminus, it might be possible that EYS is excreted.

Once the microgenes are proven to be stable and show proper localization, we need to determine whether the microgene proteins are also functional and will be able to rescue a disease phenotype. To be able to test protein function in a cellular model, one can make use of patient-derived induced pluripotent stem cells (iPSCs). These iPSCs can then be differentiated into photoreceptor cells.<sup>30</sup> After treatment of the cells with the microgenes, the presence of microgene transcripts as well as protein expression should be evaluated. Furthermore, treated patient-derived cells should be compared to untreated patient-derived cells and cells derived from a healthy individual with respect to successful differentiation, morphology and expression of retinal genes. The use of iPSCs represents an important alternative to *in vivo* animal studies. However, there are also some limitations of the use of iPSCs. Interactions with other cells and organ specific influences, as well as the consequences on the surrounding cells cannot be very well studied.

Since *Eys* is not expressed in several rodent species, such as mouse and rat, they are excluded from being suitable animal models.<sup>31</sup> However, the zebrafish does express *eys*<sup>8-10</sup> and its retina is similar to that of the human retina,<sup>32</sup> which makes the zebrafish a good model organism to study the effect of *EYS* microgenes in an *in vivo* situation. Rescue experiments can be performed using a zebrafish *eys* knock-out model which shows a clear retinal phenotype, as described in **Chapter 4**. There are several methods for testing the effect of the microgenes. One option is the injection of mRNA of the human *EYS* microgenes into the *eys* knockout zebrafish embryos, when they are still in their single-cell stage. When the zebrafish larvae are 5 days post-fertilization, expression of the microgenes can be studied by immunoblotting and immunohistochemistry, and functional assays, such as measuring ERG and visual motor response, could be performed. Mutant zebrafish injected with microgenes will be compared to uninjected mutant fish and wild-type fish. Using mRNA injections, the time to perform these experiments is limited due to poor stability of the mRNA. Furthermore, it is difficult to control how many copies of the microgene are present and it is not known whether the RNA will be incorporated in the zebrafish

genome and where in the genome that will be. Initial attempts of injections of microgene A mRNA into *ey*s knockout zebrafish embryos were not successful.

Another strategy to test *EYS* microgenes in zebrafish is to make use of the phiC31 integrase system as described previously by Mosimann et al.<sup>33</sup> There, the *ey*s knock-out zebrafish line needs to be outcrossed with a transgenic line containing genomic *attP* landing sites. In addition, the microgene constructs that will be injected in the zebrafish embryos need to contain *attB* sites and a retina specific promoter. In this way, the phi31C integrase catalyzes a unidirectional recombination reaction between *attP* and *attB* sites and is an efficient strategy for site-directed transgenesis.<sup>33,34</sup> The advantages of this method are that the location of gene incorporation is known and that long-term effects can be studied.

The main reason for generating *EYS* microgenes is that the full length *EYS* does not fit in an AAV vector for delivery. Microgene A has a size of 3.6 kb and can, together with a promoter sequence, still be packaged into a single AAV. However, microgene B and microgene C are by its own already 4.5 kb and 5.8 kb, respectively, so for its delivery two AAV vectors would be required. This two vector approach has been proven to be effective in restoring the retinal phenotype in mouse models of retinal diseases. Trapani et al. reported the use of a so-called dual AAV vector approach in which the gene will be divided in two parts, which will be simultaneously delivered in separate AAV vectors.<sup>22</sup> Since AAVs have the ability to concatemerize, dual AAV vectors can reconstitute large genes by either splicing, homologous recombination or a combination of the two.

It still remains possible that none of the *EYS* microgenes generated in this study appears to be able to rescue *EYS* function. In that case, the most promising option left will be the delivery of full length *EYS*. For this, a dual AAV approach will not be sufficient, and a triple AAV approach will be required. In addition to the use of AAVs, nanoparticle-based delivery strategies for large genes, including *ABCA4*, are also being investigated.<sup>35</sup>

In conclusion, the use of microgenes as a therapeutic approach is promising for the delivery of large genes as has been also demonstrated for *DMD* and *CEP290*.<sup>20,36</sup> Here, we showed the generation and initial characterization of *EYS* microgenes, which is the first step towards the development of a genetic therapy for *EYS*-associated retinal disease.

## 5.5 References

1. Barragan I, Borrego S, Pieras JI, Gonzalez-del Pozo M, Santoyo J, Ayuso C, Baiget M, Millan JM, Mena M, Abd El-Aziz MM, et al. (2010) Mutation spectrum of EYS in Spanish patients with autosomal recessive retinitis pigmentosa. *Hum Mutat*; **31**: E1772-1800.
2. Hosono K, Ishigami C, Takahashi M, Park DH, Hiram Y, Nakanishi H, Ueno S, Yokoi T, Hikoya A, Fujita T, et al. (2012) Two novel mutations in the EYS gene are possible major causes of autosomal recessive retinitis pigmentosa in the Japanese population. *PLoS One*; **7**: e31036.
3. Littink KW, van den Born LI, Koenekoop RK, Collin RW, Zonneveld MN, Blokland EA, Khan H, Theelen T, Hoyng CB, Cremers FP, et al. (2010) Mutations in the EYS gene account for approximately 5% of autosomal recessive retinitis pigmentosa and cause a fairly homogeneous phenotype. *Ophthalmology*; **117**: 2026-2033, 2033 e2021-2027.
4. Hartong DT, Berson EL, Dryja TP. (2006) Retinitis pigmentosa. *Lancet*; **368**: 1795-1809.
5. Wouters MA, Rigoutsos I, Chu CK, Feng LL, Sparrow DB, Dunwoodie SL. (2005) Evolution of distinct EGF domains with specific functions. *Protein Sci*; **14**: 1091-1103.
6. Tisi D, Talts JF, Timpl R, Hohenester E. (2000) Structure of the C-terminal laminin G-like domain pair of the laminin alpha2 chain harbouring binding sites for alpha-dystroglycan and heparin. *EMBO J*; **19**: 1432-1440.
7. Husain N, Pellikka M, Hong H, Klimentova T, Choe KM, Clandinin TR, Tepass U. (2006) The agrin/perlecan-related protein eyes shut is essential for epithelial lumen formation in the Drosophila retina. *Dev Cell*; **11**: 483-493.
8. Lu Z, Hu X, Liu F, Soares DC, Liu X, Yu S, Gao M, Han S, Qin Y, Li C, et al. (2017) Ablation of EYS in zebrafish causes mislocalisation of outer segment proteins, F-actin disruption and cone-rod dystrophy. *Sci Rep*; **7**: 46098.
9. Messchaert M, Dona M, Broekman S, Peters TA, Corral-Serrano JC, Slijkerman RWN, van Wijk E, Collin RWJ. (2018) Eyes shut homolog is important for the maintenance of photoreceptor morphology and visual function in zebrafish. *PLoS One*; **13**: e0200789.
10. Yu M, Liu Y, Li J, Natale BN, Cao S, Wang D, Amack JD, Hu H. (2016) Eyes shut homolog is required for maintaining the ciliary pocket and survival of photoreceptors in zebrafish. *Biol Open*; **5**: 1662-1673.
11. Dias MF, Joo K, Kemp JA, Fialho SL, da Silva Cunha A, Jr., Woo SJ, Kwon YJ. (2018) Molecular genetics and emerging therapies for retinitis pigmentosa: Basic research and clinical perspectives. *Prog Retin Eye Res*; **63**: 107-131.
12. Deng WT, Dyka FM, Dinculescu A, Li J, Zhu P, Chiodo VA, Boye SL, Conlon TJ, Erger K, Cossette T, et al. (2015) Stability and Safety of an AAV Vector for Treating RPGR-ORF15 X-Linked Retinitis Pigmentosa. *Hum Gene Ther*; **26**: 593-602.
13. Beltran WA, Cideciyan AV, Lewin AS, Iwabe S, Khanna H, Sumaroka A, Chiodo VA, Fajardo DS, Roman AJ, Deng WT, et al. (2012) Gene therapy rescues photoreceptor blindness in dogs and paves the way for treating human X-linked retinitis pigmentosa. *Proc Natl Acad Sci U S A*; **109**: 2132-2137.

14. Petersen-Jones SM, Occelli LM, Winkler PA, Lee W, Sparrow JR, Tsukikawa M, Boye SL, Chiodo V, Capasso JE, Becirovic E, et al. (2018) Patients and animal models of CNGbeta1-deficient retinitis pigmentosa support gene augmentation approach. *J Clin Invest*; **128**: 190-206.
15. Vandenberghe LH, Wilson JM, Gao G. (2009) Tailoring the AAV vector capsid for gene therapy. *Gene Ther*; **16**: 311-319.
16. Liu M, Yue Y, Harper SQ, Grange RW, Chamberlain JS, Duan D. (2005) Adeno-associated virus-mediated microdystrophin expression protects young mdx muscle from contraction-induced injury. *Mol Ther*; **11**: 245-256.
17. Yue Y, Li Z, Harper SQ, Davisson RL, Chamberlain JS, Duan D. (2003) Microdystrophin gene therapy of cardiomyopathy restores dystrophin-glycoprotein complex and improves sarcolemma integrity in the mdx mouse heart. *Circulation*; **108**: 1626-1632.
18. Duan D. (2006) Challenges and opportunities in dystrophin-deficient cardiomyopathy gene therapy. *Hum Mol Genet*; **15 Spec No 2**: R253-261.
19. Yue Y, Pan X, Hakim CH, Kodippili K, Zhang K, Shin JH, Yang HT, McDonald T, Duan D. (2015) Safe and bodywide muscle transduction in young adult Duchenne muscular dystrophy dogs with adeno-associated virus. *Hum Mol Genet*; **24**: 5880-5890.
20. Zhang W, Li L, Su Q, Gao G, Khanna H. (2018) Gene Therapy Using a miniCEP290 Fragment Delays Photoreceptor Degeneration in a Mouse Model of Leber Congenital Amaurosis. *Hum Gene Ther*; **29**: 42-50.
21. Pei J, Grishin NV. (2001) AL2CO: calculation of positional conservation in a protein sequence alignment. *Bioinformatics*; **17**: 700-712.
22. Trapani I, Colella P, Sommella A, Iodice C, Cesi G, de Simone S, Marrocco E, Rossi S, Giunti M, Palfi A, et al. (2014) Effective delivery of large genes to the retina by dual AAV vectors. *EMBO Mol Med*; **6**: 194-211.
23. Duan D. (2018) Systemic AAV Micro-dystrophin Gene Therapy for Duchenne Muscular Dystrophy. *Mol Ther*.
24. England SB, Nicholson LV, Johnson MA, Forrest SM, Love DR, Zubrzycka-Gaarn EE, Bulman DE, Harris JB, Davies KE. (1990) Very mild muscular dystrophy associated with the deletion of 46% of dystrophin. *Nature*; **343**: 180-182.
25. Yuasa K, Ishii A, Miyagoe Y, Takeda S. (1997) [Introduction of rod-deleted dystrophin cDNA, delta DysM3, into mdx skeletal muscle using adenovirus vector]. *Nihon Rinsho*; **55**: 3148-3153.
26. Foster H, Sharp PS, Athanasopoulos T, Trollet C, Graham IR, Foster K, Wells DJ, Dickson G. (2008) Codon and mRNA sequence optimization of microdystrophin transgenes improves expression and physiological outcome in dystrophic mdx mice following AAV2/8 gene transfer. *Mol Ther*; **16**: 1825-1832.
27. Lai Y, Thomas GD, Yue Y, Yang HT, Li D, Long C, Judge L, Bostick B, Chamberlain JS, Terjung RL, et al. (2009) Dystrophins carrying spectrin-like repeats 16 and 17 anchor nNOS to the sarcolemma and enhance exercise performance in a mouse model of muscular dystrophy. *J Clin Invest*; **119**: 624-635.

28. Alfano G, Kruczek PM, Shah AZ, Kramarz B, Jeffery G, Zelhof AC, Bhattacharya SS. (2016) EYS Is a Protein Associated with the Ciliary Axoneme in Rods and Cones. *PLoS One*; **11**: e0166397.
29. den Hollander AI, Koenekoop RK, Mohamed MD, Arts HH, Boldt K, Towns KV, Sedmak T, Beer M, Nagel-Wolfrum K, McKibbin M, et al. (2007) Mutations in LCA5, encoding the ciliary protein lebercilin, cause Leber congenital amaurosis. *Nat Genet*; **39**: 889-895.
30. Wiley LA, Burnight ER, Songstad AE, Drack AV, Mullins RF, Stone EM, Tucker BA. (2015) Patient-specific induced pluripotent stem cells (iPSCs) for the study and treatment of retinal degenerative diseases. *Prog Retin Eye Res*; **44**: 15-35.
31. Abd El-Aziz MM, Barragan I, O'Driscoll CA, Goodstadt L, Prigmore E, Borrego S, Mena M, Pieras JI, El-Ashry MF, Safieh LA, et al. (2008) EYS, encoding an ortholog of *Drosophila* spacemaker, is mutated in autosomal recessive retinitis pigmentosa. *Nat Genet*; **40**: 1285-1287.
32. Slijkerman RW, Song F, Astuti GD, Huynen MA, van Wijk E, Stieger K, Collin RW. (2015) The pros and cons of vertebrate animal models for functional and therapeutic research on inherited retinal dystrophies. *Prog Retin Eye Res*; **48**: 137-159.
33. Mosimann C, Puller AC, Lawson KL, Tschopp P, Amsterdam A, Zon LI. (2013) Site-directed zebrafish transgenesis into single landing sites with the phiC31 integrase system. *Dev Dyn*; **242**: 949-963.
34. Hu G, Goll MG, Fisher S. (2011) PhiC31 integrase mediates efficient cassette exchange in the zebrafish germline. *Dev Dyn*; **240**: 2101-2107.
35. Han Z, Conley SM, Makkia RS, Cooper MJ, Naash MI. (2012) DNA nanoparticle-mediated ABCA4 delivery rescues Stargardt dystrophy in mice. *J Clin Invest*; **122**: 3221-3226.
36. Harper SQ, Hauser MA, DelloRusso C, Duan D, Crawford RW, Phelps SF, Harper HA, Robinson AS, Engelhardt JF, Brooks SV, et al. (2002) Modular flexibility of dystrophin: implications for gene therapy of Duchenne muscular dystrophy. *Nat Med*; **8**: 253-261.

## 5.6 Supplemental information

### Supplementary Table S1.

Primers used for cloning of full length *EYS* cDNA.

Fragment	Forward primer (5' > 3')	Reverse primer (5' > 3')
1	<u>GGGGACAAGTTTGTACAAAAAGCAGGCT</u> CCGAAAATGACTGACAAATCAATCG	AGATTCTGGCAGAACTGC
2	GTGGTCCATCACCTTGTC	CCGATATTCTGACTGTCTTCTTCACTC
3	ATTTGTGCAAATGGATGCAG	GCAGGAAAGGAAGAGGCAGTCTTTCAC
4	GACTGCCTCTTCCTTTCCTG	CACATGAGTTGGGAATGCAC
5	GTGCATTCCCACTCATGTG	AGCAGGAAAAATGGGAGACA
6	TGTCTCCCATTTTCTGCT	TGCAACATTGGTGGTGACTT
7	AAGTACCACCAATGTTGCA	CAGAGGGGCTGACAGAAGTC
8	GACTTCTGTCAGCCCTCTG	TCCACATGGGTGTTTTCA
9	TGAAAACAACCCATGTGGAA	GCAGGTTGCTCCTCTGCTAC
10	ACCCTCCACCACTGTAGC	<u>GGGGACCACTTTGTACAAGAAAGCTGGGTCTG</u> TAACCTCATTTGTTCACTCC

AttB sites for Gateway cloning are underlined.



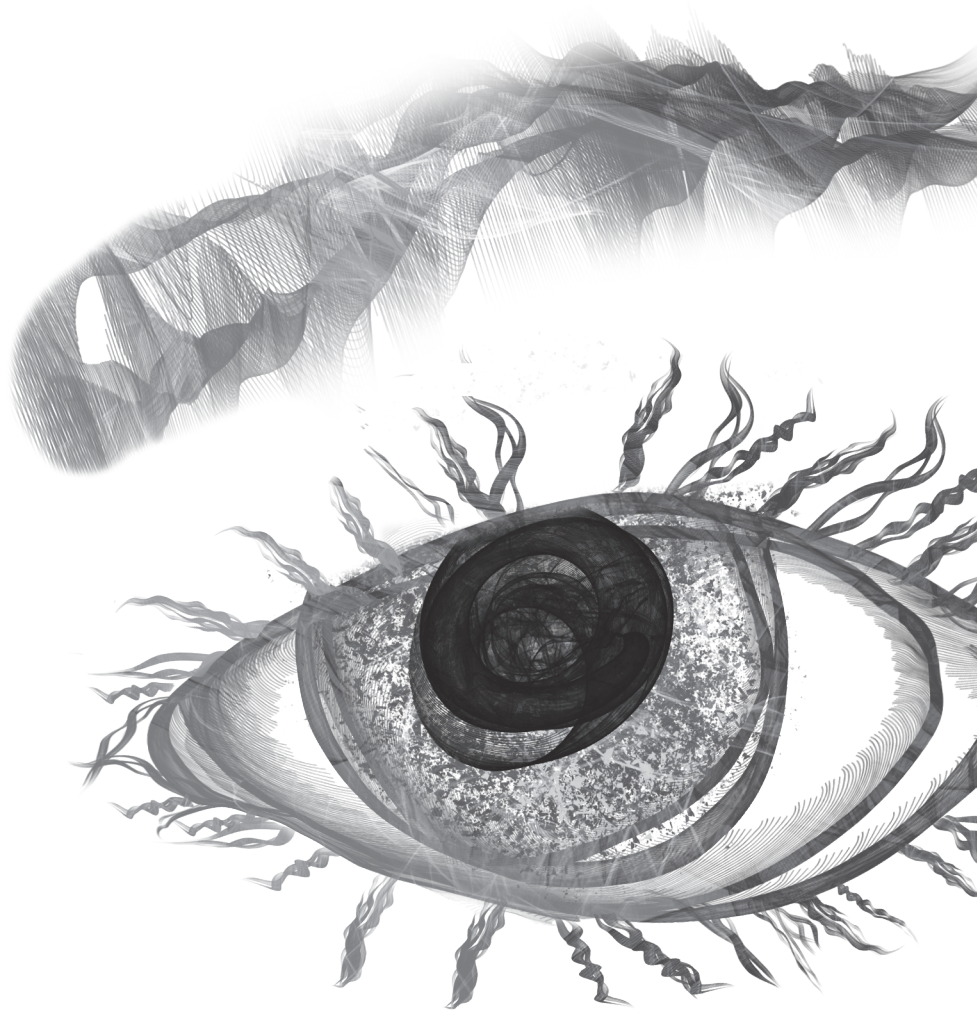
**Supplementary Table S2.**Primers used for the generation of *EYS* microgenes.

Micro gene	Part	Forward/ reverse primer	Primer sequence (5' > 3')
<b>A</b>	1	Forward primer	<u>GGGGACAAGTTTGTACAAAAAAGCAGGCT</u> CCGAAAATGACTGACAA ATCAATCG
		Reverse primer	cattttacactcattggattcCACCTCACAGAATGGACCT
<b>A</b>	2	Forward primer	aggtccattctgtgaggtgGAATCCAATGAGTGTA AAAATG
		Reverse primer	gatgatgagcacaccaaggACCTTCAAATCTTCTCTAC
<b>A</b>	3	Forward primer	tgtagagaagaattgaaggtCCTTGGTGTGCTCATCATC
		Reverse primer	<u>GGGGACCACTTTGTACAAGAAAGCTGGGT</u> CTGTAACTCATT TTTGTTTCACTCC
<b>B</b>	1	Forward primer	<u>GGGGACAAGTTTGTACAAAAAAGCAGGCT</u> CCGAAAATGACTGACAAA TCAATCG
		Reverse primer	cattttacactcattggattcCACCTCACAGAATGGACCT
<b>B</b>	2	Forward primer	aggtccattctgtgaggtgGAATCCAATGAGTGTA AAAATG
		Reverse primer	gggtcacgaatacaaaattGAAGAGGCAGTCTTTCACAT
<b>B</b>	3	Forward primer	atgtgaagactgcctcttAATTTGGTATTGCGACCC
		Reverse primer	gatgatgagcacaccaaggTGTCTTTTTGCACTCTTTT TA
<b>B</b>	4	Forward primer	taaaaagagtgcaaaaagaacaCCTTGGTGTGCTCATCATC
		Reverse primer	<u>GGGGACCACTTTGTACAAGAAAGCTGGGT</u> CTGTAACTCATT TTTGTTTCACTCC
<b>C</b>	1	Forward primer	<u>GGGGACAAGTTTGTACAAAAAAGCAGGCT</u> CCGAAAATGACTGACAA ATCAATCG
		Reverse primer	AAGGAAGAGGCAGTCTTTGACGTCAATTC
<b>C</b>	2	Forward primer	ttgacgtcaaagactgcctcttccctCCCTCTGTTG CAGCACCTC
		Reverse primer	<u>GGGGACCACTTTGTACAAGAAAGCTGGGT</u> CTGTAACTCATT TTTGTTTCACTCC

Overhangs (lower case letters) were required for the connection of the different parts of the microgenes. The primers at the start and end of the microgenes contain *AttB* sites (underlined), necessary for Gateway cloning.



# Chapter 6



# Human-derived photoreceptor-like cells as a model to identify and correct the mechanism underlying *EYS*-associated retinal dystrophy

Muriël Messchaert<sup>1,2</sup>, Anita Hoogendoorn<sup>1,2</sup>, Lonneke Duijkers<sup>1,2</sup>,  
Núria Torres<sup>1</sup>, Tamara Hoppenbrouwers<sup>1</sup>, Silvia Albert<sup>1</sup>,  
Laurence H. M. Pierrache<sup>3,4,5,6</sup>, L. Ingeborgh van den Born<sup>3,4</sup>,  
Frans P.M. Cremers<sup>1,2</sup>, Alejandro Garanto<sup>1,2</sup>, Rob W.J. Collin<sup>1,2</sup>

<sup>1</sup> Department of Human Genetics, Radboud University Medical Center, Nijmegen, The Netherlands.

<sup>2</sup> Donders Institute for Brain, Cognition and Behaviour, Radboud University Medical Center, Nijmegen, The Netherlands.

<sup>3</sup> The Rotterdam Eye Hospital, Rotterdam, The Netherlands.

<sup>4</sup> Rotterdam Ophthalmic Institute, Rotterdam, The Netherlands.

<sup>5</sup> Department of Ophthalmology, Erasmus Medical Center, Rotterdam, the Netherlands.

<sup>6</sup> Department of Epidemiology, Erasmus Medical Center, Rotterdam, the Netherlands.

**Abstract**

Mutations in *Eyes shut homolog (EYS)* are one of the most frequent causes of autosomal recessive (ar) retinitis pigmentosa (RP). Exon 26 of *EYS* is a large exon in which many frameshift and nonsense mutations are described in patients with this subtype of retinal dystrophy. The aim of this study was to develop a therapeutic approach for retinal dystrophy patients with mutations in *EYS* exon 26, using antisense oligonucleotide (AON)-mediated exon skipping, predicted to leave the reading frame intact. Western blot analysis revealed that  $\Delta 26EYS$  protein is stable and equally expressed compared to full length *EYS*. Transcriptional analysis of AON-treated hTERT-RPE1 cells showed that exon 26 could be successfully skipped by using a combination of two AONs (AON6 and AON7), whereas treatment with only one of these AONs did not affect splicing. Furthermore, we differentiated human-derived induced pluripotent stem cells (iPSCs) into three-dimensional (3D) retinal organoids to generate a cellular disease model. We did not observe clear differences between cells derived from a patient or from a healthy control. Differentiated cells expressed some retinal markers; however, expression levels were quite low. In addition, AON efficacy was tested in this cellular model. In contrast to what was observed in hTERT-RPE1 cells, control cells treated with AON6 alone showed skipping of part of exon 25 and the majority of exon 26. In conclusion, we showed that  $\Delta 26EYS$  is a stable protein, and that AONs have the potential to skip *EYS* exon 26 in hTERT-RPE1 cells. However, optimization is required to reproduce this in patient-derived 3D retinal organoids.

**Key words:**

Eyes shut homolog, *EYS*, antisense oligonucleotides, exon skipping, iPSCs, organoids

## 6.1 Introduction

Retinitis pigmentosa (RP) is a group of inherited retinal dystrophies with a prevalence of approximately 1 in 4,000 individuals worldwide.<sup>1,2</sup> Clinical features of the disease are night blindness and visual field constriction, and in later stages of the disease total blindness can occur.<sup>1,2</sup> There are 62 genes described to date in which mutations can lead to autosomal recessive (ar) RP (RetNet <http://www.sph.uth.tmc.edu/Retnet>). Most genes are only responsible for a small proportion of the arRP cases. A few genes, however, are known to be more frequently mutated in arRP patients, including *eyes shut homolog* (*EYS*). Mutations in *EYS* are responsible for approximately 5-10% of all arRP cases,<sup>3</sup> which makes *EYS* one of the most frequently mutated genes in patients with RP.

*EYS* encodes the protein eyes shut homolog and is predominantly expressed in the retina. The *EYS* protein consists of 28 epidermal growth factor (EGF) like domains, mainly at the N-terminal part of the protein, and 5 laminin A G-like (LamG) domains at the C-terminal end of the protein.<sup>4,5</sup> This domain structure is conserved over species. Besides these functional domains, human *EYS* also harbors a so-called low complexity region in which no functional domains are predicted to be present. This region is completely encoded by exon 26. The low complexity region in *EYS* is not present in all species, for instance zebrafish and chicken *Eys* lack this region (**Chapter 4**).<sup>6</sup> The exact function of *EYS* and its role in the pathogenesis of RP is not clear yet. In *Drosophila*, *Eys* is shown to be important for the maintenance of the morphology of photoreceptors.<sup>7</sup> In zebrafish, *Eys* is described to play a major role in the maintenance of retinal architecture and *eys* deficient zebrafish show visual impairment.<sup>6,8,9</sup>

Currently, there is no treatment for *EYS*-associated retinal dystrophy. Great progress has been made to the development of therapeutic approaches for IRDs, such as gene therapy. However, conventional gene therapy has some drawbacks. For instance, delivery most often occurs via adeno-associated viruses (AAVs). The cargo capacity for AAVs is 4.7 kb, which makes it unsuitable to carry the complete *EYS* cDNA (9.4 kb). Recently, the use of antisense oligonucleotides (AONs) for the treatment of IRDs has shown promising results. One of the first examples describing the successful use of AONs for IRD is the prevention of pseudo-exon inclusion caused by the recurrent *CEP290* c.2991+1655A>G mutation.<sup>10-15</sup> Recently, a study by Albert et al. showed the successful rescue of splice defects in photoreceptor precursor cells caused by two neighboring deep-intronic mutations in *ABCA4* using AONs.<sup>16</sup> Splice-correction using AONs was also shown to be successful in proof-of-concept studies for the *USH2A* c.7595-2144A>G mutation<sup>17</sup> and the *OPA1* c.610+364G>A mutation.<sup>18</sup> Besides the correction of the splicing defects caused by intronic mutations, AONs can also be used to modulate splicing and therefore skip regular exons.<sup>19</sup> AON-mediated exon skipping as a therapeutic approach is most developed for Duchenne muscular dystrophy (DMD).<sup>20</sup> Early phase clinical trials are ongoing in DMD patients with promising results.<sup>21,22</sup> The purpose of this strategy was to exclude exons from the pre-mRNA in order to restore the reading frame leading to a shorter, but mature

transcript.<sup>23</sup> As a consequence, the translated protein will still contain most of its essential domains, thereby retaining some function and reducing severity of disease.

A technology that gained tremendous attraction over the last decade is the use of induced pluripotent stem cells (iPSCs)<sup>24</sup> for the directed differentiation towards almost all cell types, including retinal cells.<sup>25</sup> Nakano et al. were the first to show that pluripotent cells have the capacity to self-organize into organoids.<sup>26</sup> Several groups adapted this approach and, with slight changes in the differentiation protocol, were also able to differentiate iPSCs in to three-dimensional (3D) retinal organoids.<sup>13,27,28</sup> When using cells from patients, this technique is a powerful tool to model disease, since these cells will contain the genetic mutation and have the exact genomic and molecular context as present within the corresponding patient.

In this study, we designed AONs for the skipping of *EYS* exon 26. Efficacy of AONs was first examined in hTERT-RPE1 cells. Next, fibroblast from a RP patient carrying c.4350\_4356del, which is located in exon 26 of *EYS*, in a homozygous state, were reprogrammed to generate iPSCs to further differentiated them to 3D retinal organoids. Finally, AON efficacy was also tested in this patient-derived cellular model system.

## 6.2 Materials and methods

### 6.2.1 Ethics statement

Our research was conducted according to the tenets of the Declaration of Helsinki. The procedures for obtaining human skin biopsies to establish primary fibroblasts cell lines were approved by the Ethical Committee of the Radboud University Medical Centre (Commissie Mensgebonden Onderzoek Arnhem-Nijmegen, 2015-1543). Written informed consent was gathered from all participating individuals. All procedures were carried out in the Netherlands.

### 6.2.2 Cloning of $\Delta 26EYS$

The entry clone containing the *EYS* cDNA, that was generated in **Chapter 5**, was used as the basis to obtain the  $\Delta 26EYS$  construct. Site-directed mutagenesis was performed using a forward primer that contained 24 nucleotides complementary to the end of exon 25 and 15 nucleotides complementary to the beginning of exon 27 (5'- GACACTTACCCAGTTGATCAAGATTTCAGTTGTGTTTC-3'), and a reverse primer that contained 22 nucleotides complementary to the beginning of exon 27 and 15 nucleotides complementary to the end of exon 25 (5'- CATAATAACGAACACAACACTGAAATCTTGATCAACTGGGT-3'). For the site-directed mutagenesis reaction, 50 ng of *EYS* cDNA entry clone was incubated together with 0.5  $\mu$ M of the forward and reverse primer, 100  $\mu$ M dNTPs (Roche), 0.25 U Phusion high-fidelity polymerase (New England Biolabs), 10x phusion PCR buffer (New England Biolabs) and 1x Q-solution (Qiagen) in a total volume of 50  $\mu$ l. Samples were denatured for 2 minutes at 94°C, followed by 10 cycles of 30 seconds

at 94°C, 30 seconds at 50°C and 15 minutes at 72°C, an additional 10 cycles of 30 seconds at 94°C, 30 seconds at 55°C and 15 minutes at 72°C, and a final primer extension of 15 minutes at 72°C. Entry clones were validated by Sanger sequencing and cloned into the destination vector pcDNA520 with an HA-tag at the C-terminus using the Gateway LR Clonase enzyme mix (Thermo Fisher Scientific).

### 6.2.3 Transfection of HEK293T cells or hTERT-RPE1 cells

HEK293T cells or hTERT-RPE1 cells were cultured in DMEM (HEK293T) or DMEM/F12 (1:1, hTERT-RPE1) supplemented with 10% fetal calf serum, 1% penicillin-streptomycin and 1% sodium pyruvate at 5% CO<sub>2</sub> at 37°C. Confluent cells were diluted 1 to 6, seeded in a 12-wells plate and grown for 24 hours at 37°C in a total volume of 1 ml. For transfection, 2 µg of the expression vector containing full length *EYS* or  $\Delta 26EYS$  were incubated together with 6 µl Fugene HD Transfection Reagent (Promega) in a total volume of 100 µl Optimem for 20 minutes at room temperature and subsequently the transfection mix was added to the cells. After incubation for 96 hours at 37°C, cells were harvested for western blot analysis (HEK293T) or immunocytochemistry (hTERT-RPE1).

### 6.2.4 Western blot analysis

Medium was removed and cells were collected and washed with phosphate buffered saline (PBS1x). HEK293T cells were resuspended in 100 µl RIPA buffer containing protease inhibitors (Roche). After sonication of the cells for 30 seconds, cells were centrifuged at 11,000 rpm for 5 minutes at 4°C and subsequently supernatant containing soluble proteins were collected. Total protein concentrations were determined via BCA according to the manufacturer's instructions (Pierce). For detection of *EYS*, samples were subjected to SDS-PAGE (3-5% acrylamide) and subsequently transferred to a PVDF (polyvinylidene difluoride) membrane (Roche, 03010040001) o/n at 4°C. Membranes were blocked in 5% non-fat dry milk (blocking buffer, Biorad) in PBS for 6 hour at room temperature and subsequently incubated with primary antibody (rabbit anti-*EYS*, Novus Biological, NBP1-90038, 1:1,000 in blocking buffer) for three days at 4°C. Membranes were washed three times with PBST (0.2% Tween-20 in PBS), incubated with HRP-conjugated secondary antibody (HRP-conjugated goat anti-rabbit, Genscript, A00098, 1:10,000 in blocking buffer) for 1 hour at room temperature, washed and developed using SuperSignal™ West Femto Maximum Sensitivity Substrate (Thermo Scientific) and scanned on a ChemiDoc Touch Imaging System (Biorad). For the detection of tubulin, samples were subjected to SDS-PAGE (4-12% Bis-Tris, NuPAGE) and transferred to a PVDF membrane (GE Healthcare Life Sciences) overnight at 4°C. The membrane was blocked in blocking buffer for 1 hour at room temperature and subsequently incubated with primary antibody (mouse anti-alpha tubulin, Abcam, ab7291, 1:2,000 in blocking buffer) overnight at 4°C. The membrane was washed three times with PBST. After incubation with the secondary antibody (goat



anti-mouse IRDye800, LI-COR Biosciences, 926-32210, 1:10,000 in blocking buffer) the membrane was washed and scanned on an Odyssey imaging system (LI-COR Biosciences).

### 6.2.5 Immunocytochemistry

hTERT-RPE1 cells were grown on coverslips in 12-well plates and transfected with expression clones containing full length *EYS* or  $\Delta 26EYS$  as described above. After transfection, cells were serum starved for another 48 hours. Cells were rinsed with 1x PBS, fixed in 2% paraformaldehyde for 20 minutes, permeabilized in 1x PBS supplemented with 1% Triton-X for 3 minutes, and subsequently blocked in 2% bovine serum albumin in 1x PBS (blocking solution) for 30 minutes, all at room temperature. For immunostaining, cells were incubated with primary antibody diluted 1:100 in blocking solution for 60 minutes at room temperature. Cells were washed 3 times for 5 minutes in 1x PBS, incubated for 45 minutes with the corresponding secondary antibody diluted 1:500 in blocking solution. Cells were washed 3 times 5 min in 1x PBS and rinsed in water. Finally, coverslips were mounted in Vectashield with DAPI (Vector Laboratories) and imaged on a Zeiss Axio Imager Z1 Fluorescence microscope (Zeiss).

Antibodies used were rabbit anti-EYS (Novus Biological, NBP1-90038), mouse anti-acetylated tubulin (Sigma, T6793), donkey anti-rabbit Alexa Fluor 488 (Life Technologies, A21206), and donkey anti-mouse Alexa Fluor 568 (Molecular Probes, A10037).

### 6.2.6 Patient derived fibroblast reprogramming

Skin biopsy samples from an RP patient with a homozygous *EYS* mutation (c.4350\_4356del) and from a control individual were collected, washed in PBS (Sigma Aldrich), dissected and incubated for 1-3 hours in a solution of 1000 U/ml Collagenase type II (Worthington Biochemical Corporation) and penicillin/streptomycin (Sigma Aldrich) in DMEM (Sigma Aldrich) at 37°C. The digestion was stopped by adding 20% fetal calf serum (Sigma Aldrich) and the cell suspension was incubated in DMEM with 20% fetal calf serum for 7 days at 37°C and 5% CO<sub>2</sub>. After approximately 1 month, a pure culture of fibroblasts was reprogrammed as follows. Fibroblasts were transduced with 4 lentiviral vectors containing the stemness-related genes *OCT3/4*, *NANOG*, *KLF4*, and *c-MYC*. Transduced cells were incubated at 37°C for 24 hours, lentiviruses were removed and cells were washed three times with PBS. The following day, cells were transferred onto murine embryonic fibroblast (MEF)-coated plates and cultured for one month at 37°C and 5% CO<sub>2</sub> in a stem cell medium containing DMEM/Ham's F-12 (Sigma Aldrich), 20% knock-out serum replacement (KOSR, Thermo Fisher Scientific), MEM Non-essential amino acids (NEAA, Sigma Aldrich), L-glutamine (Sigma Aldrich),  $\beta$ -mercaptoethanol (Sigma Aldrich),  $\beta$ -FGF (Sigma Aldrich). One month after transduction, iPSC colonies were picked and expanded on vitronectin-coated plates (Thermo Fisher Scientific) in Essential E8 medium (Thermo Fisher Scientific).

### 6.2.7 Mutation validation

Total DNA was isolated from iPSCs using QIAamp DNA mini kit (Qiagen). PCR analysis was performed for mutation detection. Fifty nanogram of DNA was incubated together with 0.5  $\mu\text{M}$  of the forward (5'-ATCTGCTACCCCAACGACTT-3') and reverse primer (5'-GAGACATCGAGGGGCTGAG-3'), 100  $\mu\text{M}$  dNTPs (Roche), 0.25 U Taq Polymerase (Roche) and PCR buffer + 25 mM MgCl<sub>2</sub> (Roche) in a total volume of 25  $\mu\text{l}$ . Samples were denatured at 94°C for 3 minutes, followed by 35 cycles of amplification consisting of 30 seconds at 94°C, 30 seconds at 58°C and 30 seconds at 72°C, and a final primer extension of 5 minutes at 72°C. Samples were analyzed by Sanger sequencing.

### 6.2.8 Differentiation of iPSCs into 3D retinal organoids

Directed differentiation of iPSCs into retinal organoids was based on the protocols by Nakano et al.<sup>26</sup> and Parfitt et al.<sup>13</sup> Briefly, iPSCs were dissociated to single cells using TrypLE Express (Invitrogen) and plated at a density of 10,000 cells per well in low-cell-adhesion 96-well plates with V-shaped bottom in 100  $\mu\text{l}$  EB media (GMEM (Gibco) supplemented with 20% KORS, 0.1 mM nonessential amino acids, 1 mM GlutaMax, 1 mM sodium pyruvate, and 100  $\mu\text{M}$   $\beta$ -mercaptoethanol) supplemented with 20  $\mu\text{M}$  Y-27632 ROCKi (Millipore) and 3  $\mu\text{M}$  IWR1e (Cayman Chemical). After 48 hours, cells were topped up with 100  $\mu\text{l}$  EB media supplemented with 20  $\mu\text{M}$  Y-27632 ROCKi, 3  $\mu\text{M}$  IWR1e, and 2% Matrigel (EB2 media). EB2 media was changed every 2 days until day 12, from which the embryonic bodies (EBs) were further cultured in EB media with 10% FCS, 1% Matrigel, 20  $\mu\text{M}$  Y-27632 ROCKi, and 100 nM smoothened agonist (SAG; Enzo Life Sciences). After 3 days, media was replaced for EB media with 10% FCS, 1% Matrigel, 20  $\mu\text{M}$  Y-27632 ROCKi, and 100 nM SAG, and 3  $\mu\text{M}$  CHIR99021 (MACS). Media was refreshed every 2 days until day 20 when EBs were transferred to non-adherent 24-well plates for further culture in neural retinal differentiation (NR) media (DMEM/F12 (Sigma) supplemented with 10% FCS, 1x N2 supplement (Thermo Fisher), and 0.5  $\mu\text{M}$  retinoic acid (RA, Sigma)). EBs were maintained for up to 90 days, changing NR media every 3-4 days.

### 6.2.9 Quantitative real-time PCR to assess differentiation

Total RNA was isolated using Nucleospin RNA Clean-up Kit (Macherey-Nagel) following the manufacturer's protocol. Reverse transcription was performed using 500 ng of total RNA and the iScript cDNA Synthesis Kit (Bio-rad) according to the manufacturer's instructions. Quantitative real-time PCR (qPCR) was performed using GoTaq Real Time qPCR Master Kit (Promega) and an Applied Biosystem 7900HT fast real-time PCR system (Thermo Fisher Scientific). Samples were assayed in triplicate and normalized against the expression of the housekeeping gene *GUSB*. Relative quantification was based on the  $2^{-\Delta\Delta\text{Ct}}$  method. Primer sequences are listed in Supp. Table S1.

### 6.2.10 AON design

The sequence of *EYS* exon 26 and the 50 bp upstream and downstream of the exon were analyzed as described elsewhere.<sup>29</sup> Briefly, the presence of exonic splice enhancer motifs was assessed using the ESE finder 3.0 program ([http://krainer01.cshl.edu/cgi-bin/tools/ESE3/ese\\_finder.cgi?process=home](http://krainer01.cshl.edu/cgi-bin/tools/ESE3/ese_finder.cgi?process=home)) and RNA structure and free energy predictions were performed using freely available database tools. Modified AONs were designed with a  $T_m$  of  $\geq 48^\circ\text{C}$ , 40-60% of GC content and a length of 18-23 nt. Subsequently, they were purchased from Eurogentec, with a 2'-O-methyl group at the sugar chain and a phosphorothioate backbone. Lyophilized AONs were dissolved in 1x PBS. AON characteristics are listed in Table 6.1.

### 6.2.11 AON treatment

hTERT-RPE1 cells were transfected with 0.5  $\mu\text{M}$  of naked AON using FuGene HD (Promega) for 48 hours, after which cells were harvested for transcriptional analysis. For treatment of differentiated iPSCs, cells were transfected with 2.0  $\mu\text{M}$  of naked AON at day 84. After 96 hours, medium was removed and cells were again transfected with 2.0  $\mu\text{M}$  naked AON for another 96 hours after which cells were harvested for RT-PCR analysis.

### 6.2.12 RT-PCR analysis

Total RNA was isolated using Nucleospin RNA Clean-up Kit (Macherey-Nagel) following the manufacturer's protocol. Reverse transcription was performed using 1  $\mu\text{g}$  (hTERT-RPE1) or 350 ng (iPSC-derived organoids) of total RNA and the SuperScript™ VIL0™ Master Mix (Invitrogen) according to manufacturer's instructions. Four microliter cDNA was incubated together with 0.5  $\mu\text{M}$  of the forward and reverse primer, 100  $\mu\text{M}$  dNTPs (Roche), 0.25 U Taq polymerase (Roche), 10x PCR buffer + 15 mM  $\text{MgCl}_2$  (Roche) and 1x Q-solution (Qiagen) in a total volume of 25  $\mu\text{l}$ . The following program was run in a 2720 Thermal Cycler (Applied Biosystems): the samples were denatured at  $94^\circ\text{C}$  for 3 minutes followed by 35 cycles of amplification consisting of  $94^\circ\text{C}$  for 20 seconds,  $58^\circ\text{C}$  for 30 seconds and  $72^\circ\text{C}$  for 2 minutes, and a final primer extension at  $72^\circ\text{C}$  for 5 minutes. Nested PCR was performed using 2  $\mu\text{l}$  of PCR product and the same conditions as mentioned for the first PCR. PCR products were purified on Nucleospin Gel and PCR Clean-up columns (Macherey Nagel) and subsequently Sanger sequencing was performed. Primer sequences are listed in Supp. Table S2.

## 6.3 Results

### 6.3.1 *EYS* exon 26 as a target for exon skipping

An interesting target exon for AON-mediated exon skipping as a therapeutic approach for *EYS*-related retinal dystrophy is exon 26 of *EYS*. Exon 26 is the largest exon of *EYS* and is thereby also one of the most frequently mutated exons in patients with retinal dystrophy.

The majority of the mutations described in exon 26 are frameshift or nonsense mutations, resulting in premature termination of translation and thereby, assuming the mRNA is not degraded, a non-functional protein is formed (**Chapter 2**).<sup>30</sup> Interestingly, exon 26 does not encode any functional domains and skipping of this exon does not disrupt the reading frame of *EYS* (Figure 6.1). Skipping of exon 26 will result in a shorter *EYS* protein, however, all its functional domains are predicted to be still present (Figure 6.2A). Therefore, exon 26 of *EYS* might be a good candidate for AON-mediated exon skipping.

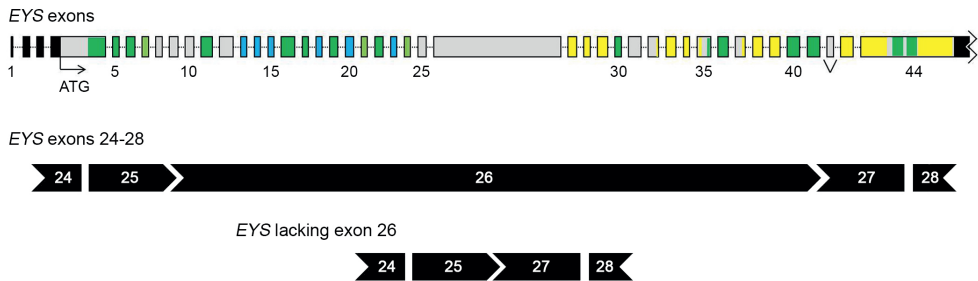


**Figure 6.1. Schematic overview of *EYS* exon 26 skipping.**

Upper panel: exonic structure of *EYS*. Colored exons encode for EGF domains (dark green), EGF-like domains (light green), calcium binding EGF domains (blue) or laminin A G-like domains (yellow). Lower panel: schematic representation of exons 24 till 28 of *EYS* with and without exon 26. Arrow heads indicate the position of the exon related to the reading frame.

### 6.3.2 *EYS* lacking exon 26 encodes a stable protein

We first examined whether *EYS* lacking exon 26 ( $\Delta 26EYS$ ) results in a stable protein. Therefore, we generated two vectors, one containing the full length *EYS* cDNA (see **Chapter 5**) and one vector containing  $\Delta 26EYS$ . HEK293T cells were transfected with either *EYS* or  $\Delta 26EYS$  for 96 hours and protein expression was analyzed. Western blot analysis revealed that both *EYS* and  $\Delta 26EYS$  were expressed in HEK293T cells, and the intensity of the bands was similar (Figure 6.2B). These results indicate that  $\Delta 26EYS$  encodes for a shorter, but stable *EYS* protein.

To determine the localization of  $\Delta 26EYS$  protein, hTERT-RPE1 cells were transfected with either full length or  $\Delta 26EYS$  containing plasmids, and subsequently immunocytochemistry with an antibody against Eys was performed. Previous studies showed that *EYS* localizes near the connecting cilium of photoreceptor cells (**Chapter 4**).<sup>9</sup> Co-staining of transfected cells with the Eys antibody together with an antibody against acetylated tubulin, a ciliary marker, was performed to determine whether the *EYS* proteins localize near the cilium. Cilia were present in non-transfected cells, as well in cells transfected with the full length *EYS* or the  $\Delta 26EYS$  plasmids. We did not observe any specific staining with the *EYS* antibody

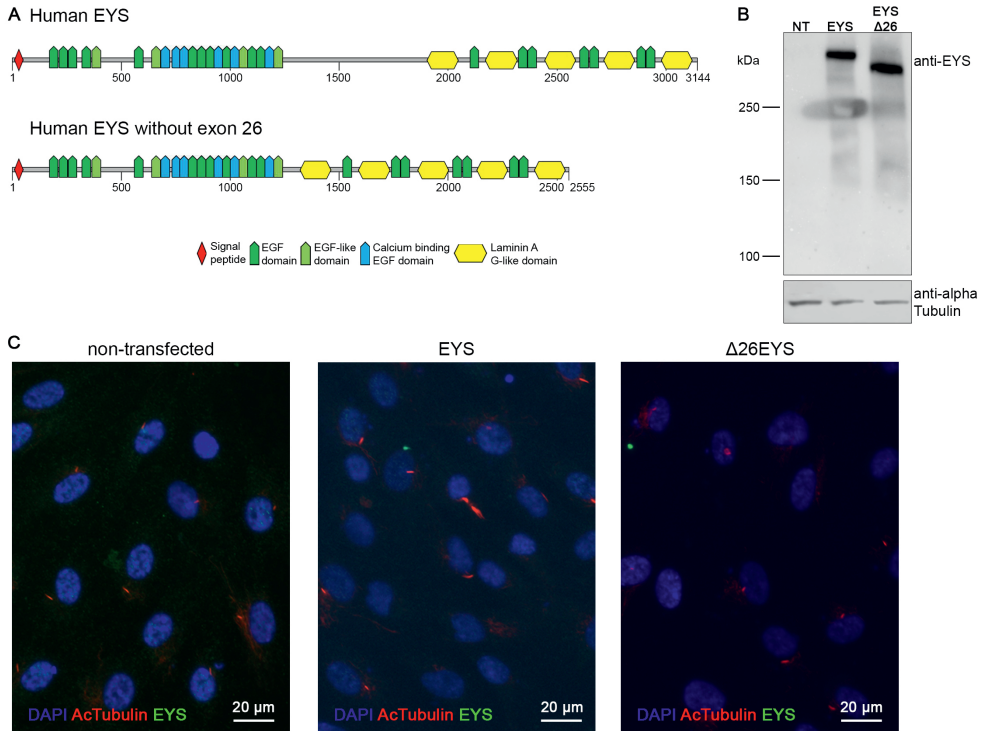


**Figure 6.2. Protein expression of full length EYS and Δ26EYS.**

(A) Protein domain structure of full length EYS and EYS without the protein segment encoded by exon 26, according to results of the SMART database (<http://smart.embl-heidelberg.de/>). EGF: epidermal growth factor. (B) Western blot analysis of HEK293T cells transfected with full length *EYS* or *EYS* lacking exon 26 ( $\Delta 26EYS$ ). NT: non-transfected cells. Upper panel: membrane stained against EYS. Lower panel: membrane stained against alpha-tubulin. (C) Immunofluorescence images of hTERT-RPE1 cells transfected with full length *EYS* or  $\Delta 26EYS$ . DAPI: blue; AcTubulin: acetylated tubulin, red; EYS: green.

in transfected cells. Some green signal could be detected, however, since this was also observed in non-transfected cells, we assumed that this was background staining.

### 6.3.3 AON efficacy in hTERT-RPE1 cells

Next, we evaluated whether we are able to remove exon 26 from the pre-mRNA, using AON-mediated exon skipping. Initially, we designed five different AONs (AON1 till AON5, Table 6.1) based on parameters used in previous studies, that showed a positive correlation between the capability of the AON to induce exon skipping and the presence of predicted SC35 splice factor binding motifs in the target region.<sup>31</sup> The efficacy of the AONs was first assessed in hTERT-RPE1 cells targeting endogenous *EYS*. Cells were treated

**Table 6.1.**

Antisense oligonucleotide characteristics.

RNA oligonucleotide	Length (nt)	GC content	T <sub>m</sub> (°C)
AON1	22	41%	51.1
AON2	20	45%	49.7
AON3	20	45%	49.7
AON4	20	50%	51.8
AON5	18	50%	48
AON6	20	50%	60
AON7	20	50%	60
SON	20	50%	60

AON: antisense oligonucleotide; SON: sense oligonucleotide, complementary to AON6; nt: nucleotide; T<sub>m</sub>: melting temperature.

with a final concentration of 0.5 μM of a single AON or a combination of AONs for 48 hours and subsequently harvested for *EYS* transcript analysis by RT-PCR. Nested PCR was necessary to be able to detect *EYS* transcripts. We did not observe any clear signs of exon skipping after treatment with one of the five AONs (Figure 6.3). An additional, very faint band around 177 bp, which corresponds to the skipping of exon 26, was observed in cells treated with a combination of AON1, 2 and 3 (Figure 6.3A). However, we were not able to confirm exon skipping in this product by Sanger sequencing. These data showed that the five AONs designed so far were not able to successfully skip exon 26 of *EYS*.

Next, two new AONs were designed, named AON6 and AON7 (Table 6.1). The efficacy of these two AONs was assessed in the same way as for AON1 till AON5. Wild-type *EYS* transcript was observed in non-treated cells and cells with either AON6 or AON7. Interestingly, a lower band, corresponding to the size of the transcript in case exon 26 is skipped, was observed for cells treated with a combination of AON6 and AON7 (Figure 6.4A). Sanger sequencing of this PCR product indeed confirmed the exact skipping of exon 26 in cells treated with both AONs (Figure 6.4B). However, we were not able to reproduce these results in a second experiment. For further experiments, we decided to continue only with AON6 and AON7.

### 6.3.4 Differentiation of patient-derived iPSC into 3D retinal organoids

The promising results of AON treatment in hTERT-RPE1 cells prompted us to investigate whether we can also skip *EYS* exon 26 in patient-derived cells. To answer this question, we set-up a patient-derived cellular model for *EYS*-associated IRD. For this, fibroblasts were derived from a dermal skin biopsy of a healthy individual and from an RP patient. This patient carried the c.4350\_4356del mutation in *EYS* homozygously. This mutation in exon 26 is predicted to lead to a frameshift and thereby premature termination of protein translation. Patient and control fibroblasts were reprogrammed to iPSCs by transducing

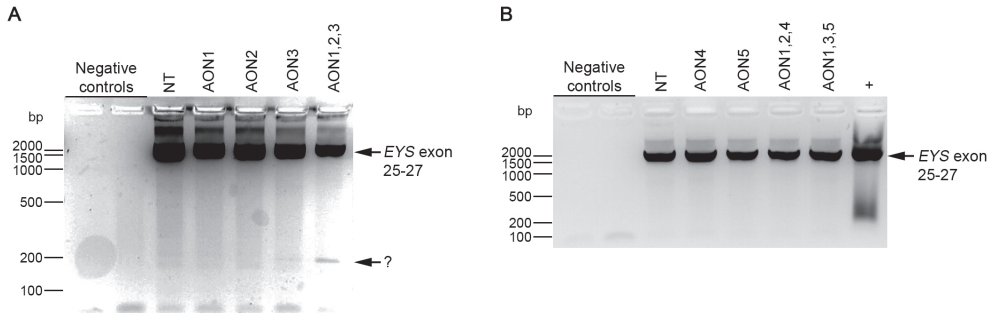


### Figure 6.3 Efficacy of AON1 till AON5 in hTERT-RPE1 cells.

(A) RT-PCR analysis of *EYS* transcripts in hTERT-RPE1 cells treated with 0.5  $\mu\text{M}$  of AON1, AON2, AON3 or a combination of the three. (B) RT-PCR analysis of *EYS* transcripts in hTERT-RPE1 cells treated with 0.5  $\mu\text{M}$  of AON4, AON5, a combination of AON1, 2 and 4, or a combination of AON1, 3 and 5. +: positive control; NT: non-treated.

with 4 lentiviral vectors containing the stemness-related genes *OCT3/4*, *NANOG*, *KLF4*, and *c-MYC*. Colonies of iPSCs were isolated, expanded and selected to generate clonal lines. The cells formed colonies that were positive for iPSC markers (Supp. Figure S1).

In order to study the effect of *EYS* mutations on photoreceptor development, patient and control iPSCs were differentiated into 3D retinal organoids using the differentiation protocol as previously described by Nakano et al (Figure 6.5).<sup>26</sup> First, the presence of the mutation in patient-derived cells was validated by PCR analysis on cDNA isolated from iPSCs (day 0), followed by Sanger sequencing (Figure 6.6A). Progress of their differentiation was monitored using bright field microscopy and qRT-PCR. In general, there were no obvious differences between patient and control cells seen during bright field microscopy (Figure 6.6B). In patient cells, slightly larger organoids were observed. These were balloon-like transparent structures, which appeared to be filled with fluid (Figure 6.6C). Pigmented cells were observed from ~day 35 onwards in both patient and control cells (Figure 6.6D), suggesting the formation of RPE cells.

The expression of pluripotency marker genes was decreased in cells at day 30, 60 and 90 of differentiation compared to iPSCs (day 0), in both patient and control cells (Supp. Figure S1). This indicates that cells are not pluripotent anymore and at least are differentiating towards another cell type. We also analyzed the gene expression of several retinal genes in order to investigate whether the differentiated cells were moving towards a retinal cell fate. In control cells, expression of *EYS*, *CRX*, *PAX6*, *PDE6H* and *RPE65* was detected in differentiated cells (Figure 6.6E). Expression of *EYS*, *PAX6*, *PDE6H* and *RPE65* was also observed in patient-derived cells. In both control and patient cells, *SIX6* expression could be detected at day 0 (iPSC). However, in general, the expression levels of retinal genes were low in both patient and control cells.

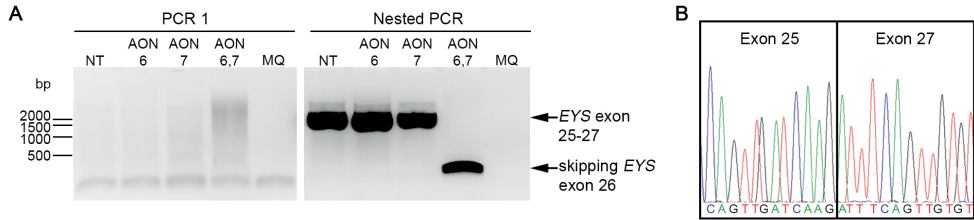


**Figure 6.4. AON-mediated skipping of *EYS* exon 26 in hTERT-RPE1 cells.**

(A) RT-PCR analysis of *EYS* transcripts. hTERT-RPE1 cells with treated with AON6, AON7 or a combination of the two AONs (AON6 and AON7). Bands visible for non-treated (NT), AON6 treated, or AON7 treated cells correspond to normal *EYS* transcript. The band visible for cells treated with AON6 and AON7 corresponds to *EYS* transcript lacking exon 26. MQ: negative control of the PCR. (B) Sanger sequencing of the PCR product of hTERT-RPE1 cells treated with AON6 and AON7 confirmed skipping of exon 26.

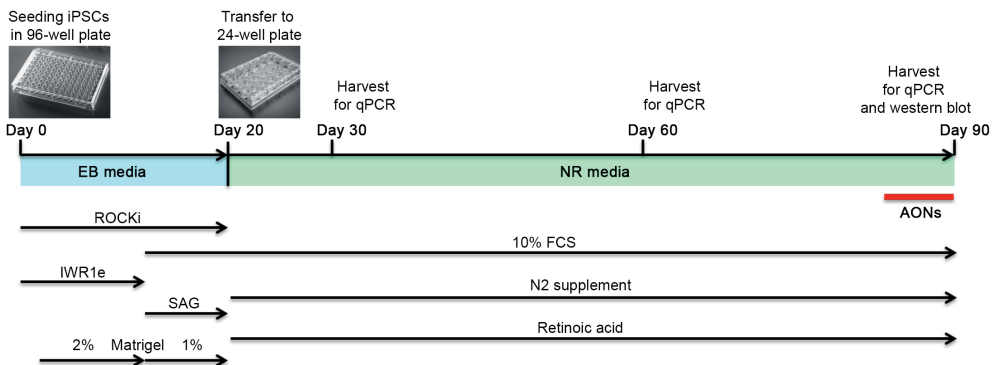


**Figure 6.5. Schematic overview of the differentiation protocol.**

AONs: antisense oligonucleotides; FCS: fetal calf serum; ROCKi: inhibitor of Rho-associated protein kinases; SAG: smoothened agonist.

### 6.3.5 AON efficacy in patient-derived 3D retinal organoids

To investigate the efficacy of AON6 and AON7 in differentiated patient-derived iPSCs, cells were treated with AONs for one week (starting at day 84), after which *EYS* transcripts were analyzed by RT-PCR analysis on day 90. Bands corresponding to the size of the wild-type *EYS* transcript were observed for all samples, except for control cells treated with AON6 alone. In this sample, a band corresponding to a size of ~177 base pair was observed (Figure 6.7A). Sanger sequencing of this band revealed skipping of a 1792-bp fragment. However, the skipped fragment did not represent a deletion of the entire exon 26, but the end of exon 25 and the majority of exon 26 instead (Figure 6.7B). Skipping of this fragment is predicted to disrupt the reading frame and lead to a truncated protein. Remarkably, we



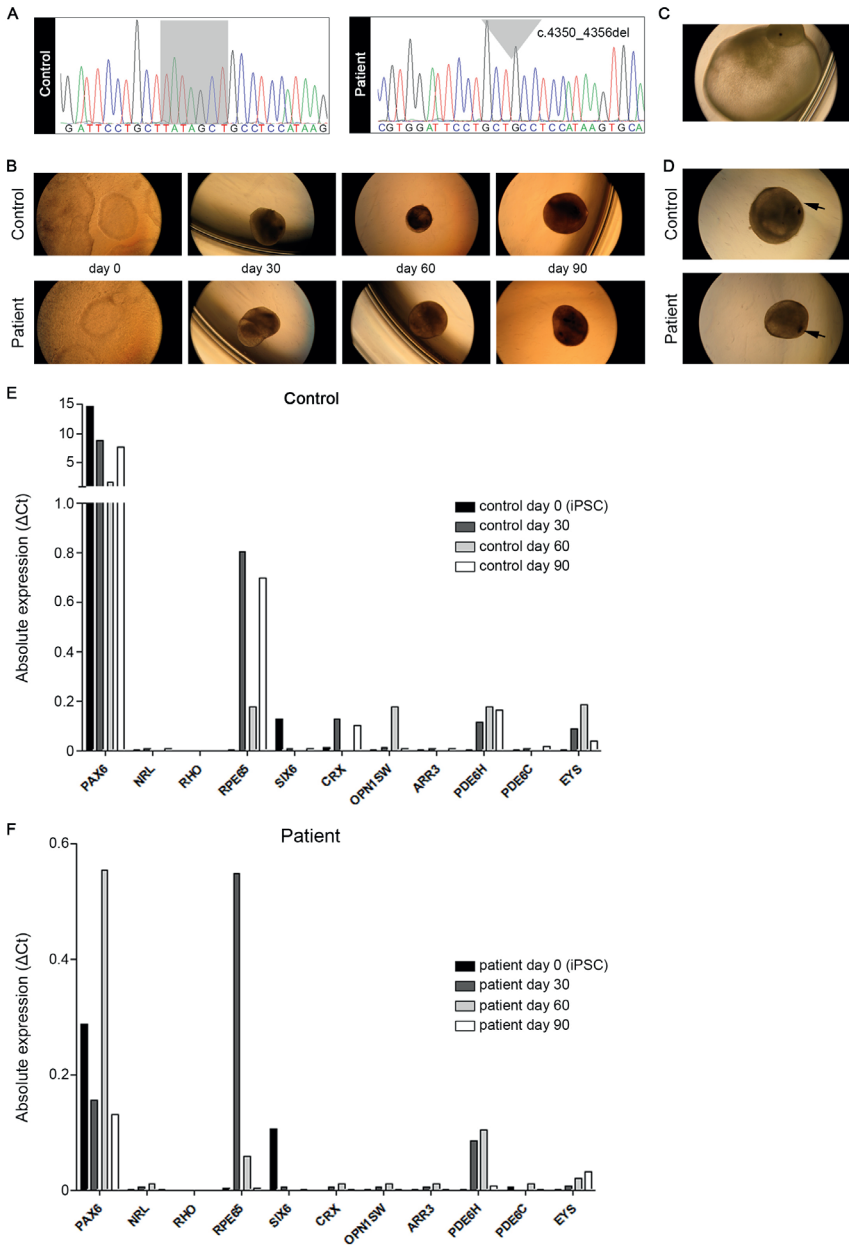


**Figure 6.6. Characterization of patient-derived 3D retinal organoids.**

(A) Sanger sequencing of genomic DNA confirmed the presence of the c.4350\_4356del mutation in patient-derived iPSCs. (B) Bright field microscopy images of iPSCs (day 0) and differentiated cells at day 30, day 60 and day 90. (C) Large balloon-like organoids were observed in patient-derived cells. (D) Pigmented cells (arrow) were seen in control and patient organoids. (E) Absolute gene expression of retinal markers in control and (F) patient cells. Values were normalized to *GUSB*.

did not observe this in patient cells treated with AON6. In addition, in contrast to what was observed in hTERT-RPE1 cells, treatment of control or patient cells with a combination of AON6 and AON7 did not result in the skipping of exon 26.

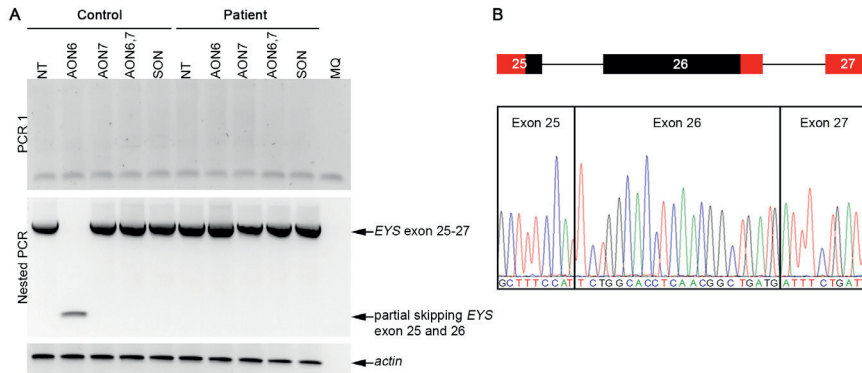


**Figure 6.7. Efficacy of AONs in differentiated iPSCs.**

(A) RT-PCR analysis of *EYS* and *actin* transcripts in differentiated iPSCs from patient and control treated with AONs. SON: sense oligonucleotide (negative control); MQ: negative control of the PCR. (B) Sanger sequencing results of the band of control iPSCs treated with AON6. Parts of the exons that are covered by the sequence are depicted in the schematic overview in red.

## 6.4 Discussion

In this chapter, we aimed to study whether AON-mediated skipping of *EYS* exon 26 could be a potential therapeutic approach for the treatment of retinal dystrophy caused by mutations in exon 26 of this gene. We showed that  $\Delta 26EYS$  is stable and equally expressed compared to full length *EYS* in HEK293T cells. We differentiated iPSCs into 3D retinal organoids in order to generate a cellular disease model. Some retinal markers were expressed in differentiated cells; however, overall expression levels were low. We did not observe clear differences between cells derived from a healthy control or from a patient. Furthermore, we showed that a combination of two AONs has the potential to skip exon 26 in hTERT-RPE1 cells; however, we were not able to reproduce these results in patient-derived 3D retinal organoids.

Antisense oligonucleotide-mediated exon skipping has shown to be successful in the treatment of DMD. The disease is caused by mutations in the *DMD* gene that affect the production of dystrophin protein. AONs have been designed for the skipping of each *DMD* exon or multiple exons.<sup>23</sup> So far, skipping of one single exon of *DMD* seems to be the most promising strategy. Several AONs for single exon skipping of exon 53 (212 bp), exon 51 (233 bp), exon 45 (176 bp), or exon 44 (148 bp) are investigated in clinical trials.<sup>32</sup> These early phase clinical studies for the use of AON-mediated exon skipping as a therapy for DMD showed promising results.<sup>21,22</sup> Aartsma-Rus et al. showed the successful joint

exon skipping of *DMD* exons 43+44, exons 45+51 and exons 45+51 in patient-derived myotubes.<sup>33</sup> *In vitro* proof of concept studies for AON-mediated exon skipping were also reported for NOTCH3. Mutations in NOTCH3 are known to cause cerebral autosomal dominant arteriopathy with subcortical infarcts and leukoencephalopathy (CADASIL). Rutten et al. reported the successful skipping of exon 2-3 (222 bp), exon 4-5 (462 bp) or exon 6 (234 bp) in CADASIL patient-derived vascular smooth muscle cells.<sup>34</sup> Compared to exon 26 of *EYS* (1767 bp), these fragments are all relatively small.

Before applying this strategy for the treatment of *EYS*-associated retinal dystrophy, we first evaluated whether the skipping of *EYS* exon 26 will lead to a stable protein. HEK293T cells were transfected with either full length *EYS* or  $\Delta 26EYS$ . Western blot analysis of the cell lysates revealed that  $\Delta 26EYS$  protein is stable and almost equally expressed compared to full length *EYS*. We also aimed to determine whether the  $\Delta 26EYS$  protein was localized correctly inside the cell. However, the immunocytochemistry data were inconclusive. The *EYS* signal that was observed in transfected cells was also detected in non-transfected cells, suggesting that this was background signal. Another explanation could be that this was endogenously expressed *EYS*, however, this is not very likely since expression levels are very low. The low immunofluorescence signal for *EYS* might be due to the fact that the antibody was not working properly for this purpose. The same antibody was also used for staining of zebrafish retinal sections using a similar procedure, with positive results (**Chapter 4**). Probably, the transfection efficiency was not high enough to be able to detect either full length *EYS* or  $\Delta 26EYS$ . We chose hTERT-RPE1 cells for localization experiments, because these cells have a large cytoplasmic compartment and do form cilia after serum starvation. It might be helpful to repeat this experiment using other cell types that also form cilia, but are easier to transfect compared to hTERT-RPE1 cells, such as COS-1 cells.<sup>35</sup> The next step will be to determine whether the  $\Delta 26EYS$  protein is also functional. Since *Eys* is not present in several rodent species, like mouse and rat, they are not suitable as an animal model.<sup>4,5</sup> Zebrafish might be a good alternative, since *eys* is expressed in this species and its retina is quite similar to that of the human retina. However, zebrafish does not have an equivalent of exon 26 of human *EYS*. As a consequence, functionality of the human  $\Delta 26EYS$  protein in zebrafish is not directly translatable towards humans.

Therefore, we aimed to model retinal dystrophy in a patient-specific genomic context by differentiating iPSCs into photoreceptors. In this study, direct differentiation of iPSCs was based on the differentiation protocol by Nakano et al.<sup>26</sup> We followed the cells during the differentiation process by bright field microscopy and took samples at serial time-points for qRT-PCR analysis. Both patient and control cells formed organoids and size and shape were similar during the 90 days of differentiation. In the patient cell line we observed slightly larger organoids with a balloon-like structure presumably filled with fluid. At the start of differentiation, iPSCs derived from patient and control looked similar, although the patient line started at passage 9 and the control line at passage 28. It has been shown that extended passaging of iPSCs increases the differentiation efficiency into neural cell

types.<sup>36</sup> This has to be taken into account when performing similar experiments in the future.

During differentiation, some morphological changes were observed, indicating differentiation. We could observe quite some pigmented cells, suggesting that some cells differentiated towards RPE cells. In addition, expression of *RPE65* was also observed at different time points of differentiation. Therefore, we assumed that the differentiation went into the proper direction. However, other cell types, like melanocytes, could also show pigments. In our cultures we did not observe any evaginating transparent neuroretinal vesicles. Nakano et al. observed these evaginations after around two weeks of differentiation.<sup>26</sup> In general, we believe that the differentiation of both cell lines was not very efficient. Several recent studies indicated already that the percentage of successful cultures resulting in neuroretinal vesicles is quite low.<sup>28,37</sup> It is also known that there can be quite some variation not only between different cell lines, but also between different organoids derived from the same iPSC line. This is also what we observed and therefore complicated the analysis of the organoids. We did not select organoids based on size or morphology upon analysis, but organoids were randomly picked.

No clear expression of neuroretinal markers, such as *CRX*, *NRL* and *OPN1SW*, was observed after 90 days of differentiation. Some markers were expressed, however, in general, the expression of these genes was quite low. This could suggest that differentiation is not going fully towards neural retinal cell types. Another explanation could be that longer differentiation is required to be able to detect these markers. However, there are studies that report the expression of photoreceptor markers already around 12 weeks post-differentiation.<sup>28,38</sup>

The successful differentiation towards photoreceptors depends on many factors. First of all the choice of cell type can influence the differentiation. We used iPSCs derived from human fibroblast, as what was described in a paper by Parfitt et al.<sup>13</sup> Other groups use human embryonic stem cells (hESCs) for the differentiation into photoreceptors.<sup>26</sup> Looking at the transcriptional profile of iPSCs and ESCs, it appears that both cell types are almost identical, with a small number of genes that is differentially expressed between iPSCs and ESCs.<sup>39</sup> However, due to epigenetic memory, some ESC genes are not highly induced in iPSCs. Furthermore, gene expression patterns from the somatic cell source are not always completely silenced in iPSCs.<sup>39-41</sup> Another factor that influences the efficiency of the differentiation, is the culture medium used for differentiation. From day 20 onwards we used neuroretinal (NR) media, which contains retinoic acid (RA). It is described that RA promotes terminal differentiation of photoreceptors.<sup>42</sup> However, it has also been shown that continuous RA supplementation suppresses cone maturation.<sup>43</sup> Therefore, it might be helpful to optimize the protocol by using different concentration and durations of RA supplementation to the medium. Third, the duration of differentiation is an important factor. Some papers reported the successful differentiation of photoreceptor cells after ~100 days. Others reported that 120-150 days were needed to obtain retinal cells. In our

study, we used a 90-days differentiation protocol that probably might be relatively short, especially when interested in protein expression and morphological differences between cell lines. Furthermore, to be able to monitor whether cells are going towards the right direction, an experienced person has to judge which organoids should continue in the differentiation process and which can be discarded.

Our study showed that a combination of two AONs was able to completely skip exon 26, at least in hTERT-RPE1 cells. However, these results could not be reproduced in further experiments with hTERT-RPE1 cells, nor in patient-derived iPSCs differentiated into 3D retinal organoids. In both cell types, we are working on the limit of detection, as for both cell types, nested PCR was necessary to be able to detect the *EYS* transcript. In addition, qPCR data of the differentiated iPSCs showed that *EYS* is expressed at day 90 in both control and patient cells, however, expression levels were very low. Furthermore, the discrepancy between the results observed in hTERT-RPE1 cells and iPSCs might be due to efficiency of AONs to enter the organoids. A study by Dulla et al. showed successful use of AONs in a 3D retinal organoid model of LCA.<sup>15</sup> Wild-type transcript levels of *CEP290* were increased in a dose-dependent manner, with reaching 90% of the total transcript using an AON concentration of 10  $\mu\text{M}$ . The levels of cryptic-exon including transcripts were reduced and the maximum reduction was already reached using an AON concentration of 3  $\mu\text{M}$ .<sup>15</sup>

In iPSCs derived from a control, treatment with AON6 alone resulted in partly skipping of exon 25 and skipping of the majority of exon 26. Although we aimed to skip exon 26, this could still be a good result if the skipped part would not disrupt the reading frame. However, in total, 1792 base pairs are skipped, which means that this results in a frameshift and premature termination of protein translation. Remarkably, in patient cells, treatment with AON6 did not affect splicing.

A more robust experimental set-up should be used to indeed confirm that these AONs are able to skip exon 26 before continuing. A way to do this is to make use of a so-called minigene. Therefore, an *EYS* construct with flanking introns and exons needs to be cloned. This construct can then be transfected in HEK293T cells, which do not endogenously express *EYS*. Subsequently, cells are transfected with the AON and the effect on splicing can be evaluated by RT-PCR analysis. This experiment can be used to test proof-of-concept. A drawback of using the minigene approach is that no functional protein will be formed. Once AON-mediated skipping of *EYS* exon 26 is proven to be efficacious, the next challenge is how to deliver the AONs to the photoreceptor cells. This will eventually also be important for the delivery of AONs in humans. Systemic delivery of AONs has been shown successful in a DMD mouse model.<sup>44</sup> However, for treatment of retinal cells high doses are required, since it has to pass the blood-retina barrier. An alternative will be the direct delivery of the AON into the human eye via injections, either as naked AON or packaged into an AAV. Naked AONs are small and therefore able to reach and penetrate the photoreceptors more easily upon intravitreal injections, compared to AAVs that are injected subretinally. A drawback of naked AONs is their limited stability, which requires repeated injections.

In contrast, the use of AAVs could give long-time therapeutic benefit. Recently, ProQR published positive interim results of a first-in-human clinical trial (NCT03140969) of AONs (QR-110) in LCA patients. The majority of subjects demonstrated rapid and sustained improvement of vision, measured by visual acuity and mobility course. No serious adverse events were reported. (<https://ir.proqr.com/news-releases/news-release-details/proqr-announces-positive-interim-results-phase-12-clinical-trial>).

In conclusion, we showed that  $\Delta 26EYS$  encodes a stable protein. However, proper localization of the  $\Delta 26EYS$  protein still has to be investigated. Furthermore, we showed that a combination of two AONs targeting exon 26 are able to skip the complete exon in hTERT-RPE1 cells. However, quite some optimization is required to reproduce AON-mediated skipping of *EYS* exon 26 in patient-derived 3D retinal organoids.

## 6.5 Acknowledgements

The authors would like to acknowledge Anke van Dijk and Tessa van der Heijden from the Stem Cell Technology Center of the Radboudumc, and Saskia D. van der Velde-Visser for technical assistance.

## 6.5 References

1. Hartong DT, Berson EL, Dryja TP. (2006) Retinitis pigmentosa. *Lancet*; **368**: 1795-1809.
2. Verbakel SK, van Huet RAC, Boon CJF, den Hollander AI, Collin RWJ, Klaver CCW, Hoyng CB, Roepman R, Klevering BJ. (2018) Non-syndromic retinitis pigmentosa. *Prog Retin Eye Res*.
3. Littink KW, van den Born LI, Koenekoop RK, Collin RW, Zonneveld MN, Blokland EA, Khan H, Theelen T, Hoyng CB, Cremers FP, et al. (2010) Mutations in the EYS gene account for approximately 5% of autosomal recessive retinitis pigmentosa and cause a fairly homogeneous phenotype. *Ophthalmology*; **117**: 2026-2033.
4. Abd El-Aziz MM, Barragan I, O'Driscoll CA, Goodstadt L, Prigmore E, Borrego S, Mena M, Pieras JI, El-Ashry MF, Safieh LA, et al. (2008) EYS, encoding an ortholog of *Drosophila* spacemaker, is mutated in autosomal recessive retinitis pigmentosa. *Nat Genet*; **40**: 1285-1287.
5. Collin RW, Littink KW, Klevering BJ, van den Born LI, Koenekoop RK, Zonneveld MN, Blokland EA, Strom TM, Hoyng CB, den Hollander AI, et al. (2008) Identification of a 2 Mb human ortholog of *Drosophila* eyes shut/spacemaker that is mutated in patients with retinitis pigmentosa. *Am J Hum Genet*; **83**: 594-603.
6. Messchaert M, Dona M, Broekman S, Peters TA, Corral-Serrano JC, Slijkerman RWN, van Wijk E, Collin RWJ. (2018) Eyes shut homolog is important for the maintenance of photoreceptor morphology and visual function in zebrafish. *PLoS One*; **13**: e0200789.
7. Husain N, Pellikka M, Hong H, Klimentova T, Choe KM, Clandinin TR, Tepass U. (2006) The agrin/perlecan-related protein eyes shut is essential for epithelial lumen formation in the *Drosophila* retina. *Dev Cell*; **11**: 483-493.
8. Lu Z, Hu X, Liu F, Soares DC, Liu X, Yu S, Gao M, Han S, Qin Y, Li C, et al. (2017) Ablation of EYS in zebrafish causes mislocalisation of outer segment proteins, F-actin disruption and cone-rod dystrophy. *Sci Rep*; **7**: 46098.
9. Yu M, Liu Y, Li J, Natale BN, Cao S, Wang D, Amack JD, Hu H. (2016) Eyes shut homolog is required for maintaining the ciliary pocket and survival of photoreceptors in zebrafish. *Biol Open*; **5**: 1662-1673.
10. Collin RW, den Hollander AI, van der Velde-Visser SD, Bennicelli J, Bennett J, Cremers FP. (2012) Antisense Oligonucleotide (AON)-based Therapy for Leber Congenital Amaurosis Caused by a Frequent Mutation in CEP290. *Mol Ther Nucleic Acids*; **1**: e14.
11. Duijkers L, van den Born LI, Neidhardt J, Bax NM, Pierrache LHM, Klevering BJ, Collin RWJ, Garanto A. (2018) Antisense Oligonucleotide-Based Splicing Correction in Individuals with Leber Congenital Amaurosis due to Compound Heterozygosity for the c.2991+1655A>G Mutation in CEP290. *Int J Mol Sci*; **19**.
12. Garanto A, Chung DC, Duijkers L, Corral-Serrano JC, Messchaert M, Xiao R, Bennett J, Vandenberghe LH, Collin RW. (2016) In vitro and in vivo rescue of aberrant splicing in CEP290-associated LCA by antisense oligonucleotide delivery. *Hum Mol Genet*; **25**: 2552-2563.
13. Parfitt DA, Lane A, Ramsden CM, Carr AJ, Munro PM, Jovanovic K, Schwarz N, Kanuga N, Muthiah MN, Hull S, et al. (2016) Identification and Correction of Mechanisms Underlying Inherited Blindness in Human iPSC-Derived Optic Cups. *Cell Stem Cell*; **18**: 769-781.

14. Gerard X, Perrault I, Hanein S, Silva E, Bigot K, Defoort-Delhemmes S, Rio M, Munnich A, Scherman D, Kaplan J, et al. (2012) AON-mediated Exon Skipping Restores Ciliation in Fibroblasts Harboring the Common Leber Congenital Amaurosis CEP290 Mutation. *Mol Ther Nucleic Acids*; **1**: e29.
15. Dulla K, Aguila M, Lane A, Jovanovic K, Parfitt DA, Schulkens I, Chan HL, Schmidt I, Beumer W, Vorthoren L, et al. (2018) Splice-Modulating Oligonucleotide QR-110 Restores CEP290 mRNA and Function in Human c.2991+1655A>G LCA10 Models. *Mol Ther Nucleic Acids*; **12**: 730-740.
16. Albert S, Garanto A, Sangermano R, Khan M, Bax NM, Hoyng CB, Zernant J, Lee W, Allikmets R, Collin RWJ, et al. (2018) Identification and Rescue of Splice Defects Caused by Two Neighboring Deep-Intronic ABCA4 Mutations Underlying Stargardt Disease. *Am J Hum Genet*; **102**: 517-527.
17. Slijkerman RW, Vache C, Dona M, Garcia-Garcia G, Claustres M, Hetterschijt L, Peters TA, Hartel BP, Pennings RJ, Millan JM, et al. (2016) Antisense Oligonucleotide-based Splice Correction for USH2A-associated Retinal Degeneration Caused by a Frequent Deep-intronic Mutation. *Mol Ther Nucleic Acids*; **5**: e381.
18. Bonifert T, Gonzalez Menendez I, Battke F, Theurer Y, Synofzik M, Schols L, Wissinger B. (2016) Antisense Oligonucleotide Mediated Splice Correction of a Deep Intronic Mutation in OPA1. *Mol Ther Nucleic Acids*; **5**: e390.
19. Hammond SM, Wood MJ. (2011) Genetic therapies for RNA mis-splicing diseases. *Trends Genet*; **27**: 196-205.
20. Aartsma-Rus A, van Ommen GJ. (2007) Antisense-mediated exon skipping: a versatile tool with therapeutic and research applications. *RNA*; **13**: 1609-1624.
21. Kinali M, Arechavala-Gomez V, Feng L, Cirak S, Hunt D, Adkin C, Guglieri M, Ashton E, Abbs S, Nihoyannopoulos P, et al. (2009) Local restoration of dystrophin expression with the morpholino oligomer AVI-4658 in Duchenne muscular dystrophy: a single-blind, placebo-controlled, dose-escalation, proof-of-concept study. *Lancet Neurol*; **8**: 918-928.
22. van Deutekom JC, Janson AA, Ginjaar IB, Frankhuizen WS, Aartsma-Rus A, Bremmer-Bout M, den Dunnen JT, Koop K, van der Kooi AJ, Goemans NM, et al. (2007) Local dystrophin restoration with antisense oligonucleotide PRO051. *N Engl J Med*; **357**: 2677-2686.
23. Aartsma-Rus A, Fokkema I, Verschuuren J, Ginjaar I, van Deutekom J, van Ommen GJ, den Dunnen JT. (2009) Theoretic applicability of antisense-mediated exon skipping for Duchenne muscular dystrophy mutations. *Hum Mutat*; **30**: 293-299.
24. Takahashi K, Yamanaka S. (2006) Induction of pluripotent stem cells from mouse embryonic and adult fibroblast cultures by defined factors. *Cell*; **126**: 663-676.
25. Wiley LA, Burnight ER, Songstad AE, Drack AV, Mullins RF, Stone EM, Tucker BA. (2015) Patient-specific induced pluripotent stem cells (iPSCs) for the study and treatment of retinal degenerative diseases. *Prog Retin Eye Res*; **44**: 15-35.
26. Nakano T, Ando S, Takata N, Kawada M, Muguruma K, Sekiguchi K, Saito K, Yonemura S, Eiraku M, Sasai Y. (2012) Self-formation of optic cups and storable stratified neural retina from human ESCs. *Cell Stem Cell*; **10**: 771-785.

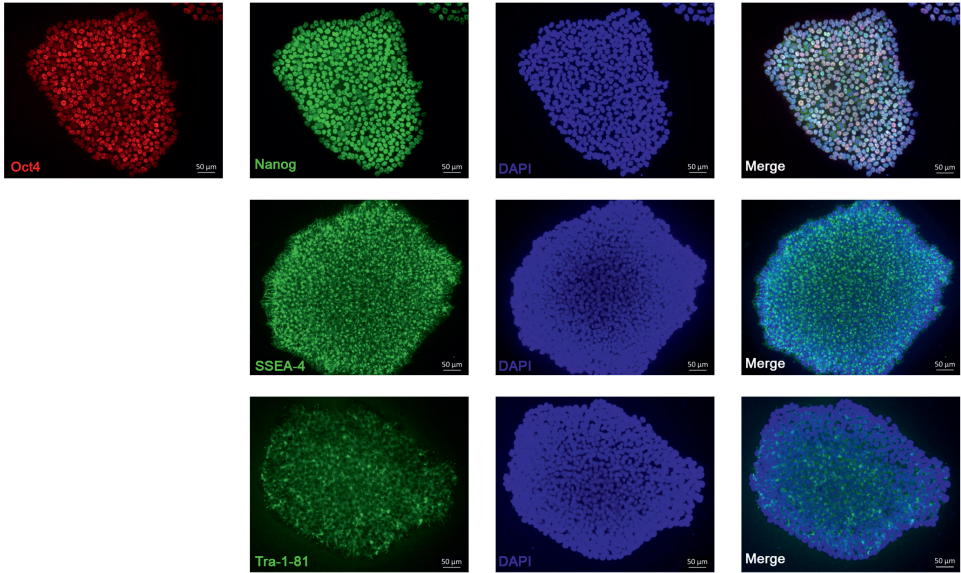


27. Zhong X, Gutierrez C, Xue T, Hampton C, Vergara MN, Cao LH, Peters A, Park TS, Zambidis ET, Meyer JS, et al. (2014) Generation of three-dimensional retinal tissue with functional photoreceptors from human iPSCs. *Nat Commun*; **5**: 4047.
28. Gonzalez-Cordero A, Kruczek K, Naeem A, Fernando M, Kloc M, Ribeiro J, Goh D, Duran Y, Blackford SJ, Abelleira-Hervas L, et al. (2017) Recapitulation of Human Retinal Development from Human Pluripotent Stem Cells Generates Transplantable Populations of Cone Photoreceptors. *Stem Cell Reports*; **9**: 820-837.
29. Garanto A, Collin RWJ. (2018) Design and In Vitro Use of Antisense Oligonucleotides to Correct Pre-mRNA Splicing Defects in Inherited Retinal Dystrophies. *Methods Mol Biol*; **1715**: 61-78.
30. Messchaert M, Haer-Wigman L, Khan MI, Cremers FPM, Collin RWJ. (2018) EYS mutation update: In silico assessment of 271 reported and 26 novel variants in patients with retinitis pigmentosa. *Hum Mutat*; **39**: 177-186.
31. Aartsma-Rus A, van Vliet L, Hirschi M, Janson AA, Heemskerk H, de Winter CL, de Kimpe S, van Deutekom JC, t Hoen PA, van Ommen GJ. (2009) Guidelines for antisense oligonucleotide design and insight into splice-modulating mechanisms. *Mol Ther*; **17**: 548-553.
32. Crone M, Mah JK. (2018) Current and Emerging Therapies for Duchenne Muscular Dystrophy. *Curr Treat Options Neurol*; **20**: 31.
33. Aartsma-Rus A, Janson AA, Kaman WE, Bremmer-Bout M, van Ommen GJ, den Dunnen JT, van Deutekom JC. (2004) Antisense-induced multiexon skipping for Duchenne muscular dystrophy makes more sense. *Am J Hum Genet*; **74**: 83-92.
34. Rutten JW, Dauwerse HG, Peters DJ, Goldfarb A, Venselaar H, Haffner C, van Ommen GJ, Aartsma-Rus AM, Lesnik Oberstein SA. (2016) Therapeutic NOTCH3 cysteine correction in CADASIL using exon skipping: in vitro proof of concept. *Brain*; **139**: 1123-1135.
35. den Hollander AI, Koenekoop RK, Mohamed MD, Arts HH, Boldt K, Towns KV, Sedmak T, Beer M, Nagel-Wolfrum K, McKibbin M, et al. (2007) Mutations in LCA5, encoding the ciliary protein lebercilin, cause Leber congenital amaurosis. *Nat Genet*; **39**: 889-895.
36. Koehler KR, Tropel P, Theile JW, Kondo T, Cummins TR, Viville S, Hashino E. (2011) Extended passaging increases the efficiency of neural differentiation from induced pluripotent stem cells. *BMC Neurosci*; **12**: 82.
37. Meyer JS, Shearer RL, Capowski EE, Wright LS, Wallace KA, McMillan EL, Zhang SC, Gamm DM. (2009) Modeling early retinal development with human embryonic and induced pluripotent stem cells. *Proc Natl Acad Sci U S A*; **106**: 16698-16703.
38. Tucker BA, Anfinson KR, Mullins RF, Stone EM, Young MJ. (2013) Use of a synthetic xeno-free culture substrate for induced pluripotent stem cell induction and retinal differentiation. *Stem Cells Transl Med*; **2**: 16-24.
39. Chin MH, Mason MJ, Xie W, Volinia S, Singer M, Peterson C, Ambartsumyan G, Aimiwu O, Richter L, Zhang J, et al. (2009) Induced pluripotent stem cells and embryonic stem cells are distinguished by gene expression signatures. *Cell Stem Cell*; **5**: 111-123.

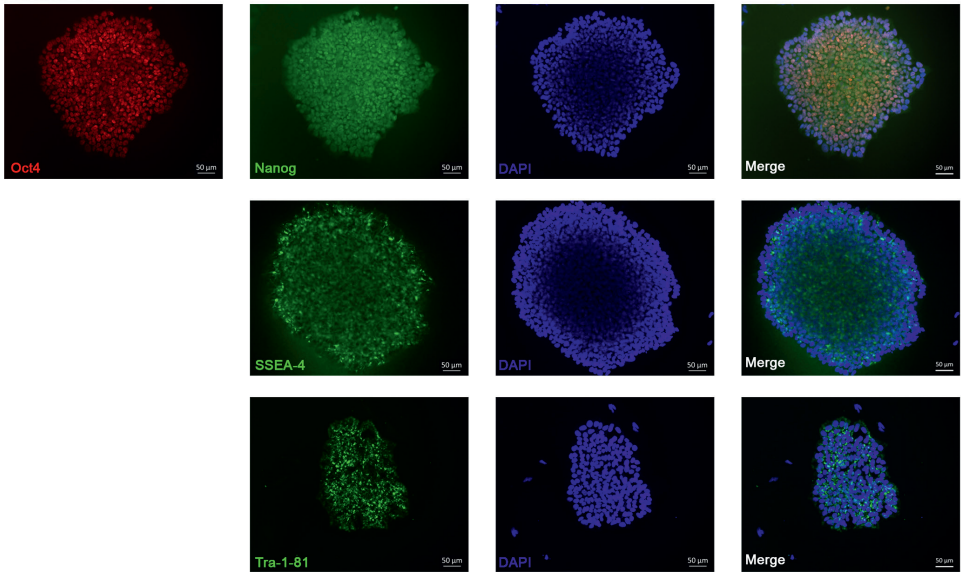
40. Bar-Nur O, Russ HA, Efrat S, Benvenisty N. (2011) Epigenetic memory and preferential lineage-specific differentiation in induced pluripotent stem cells derived from human pancreatic islet beta cells. *Cell Stem Cell*; **9**: 17-23.
41. Bilic J, Izpisua Belmonte JC. (2012) Concise review: Induced pluripotent stem cells versus embryonic stem cells: close enough or yet too far apart? *Stem Cells*; **30**: 33-41.
42. Weed LS, Mills JA. (2017) Strategies for retinal cell generation from human pluripotent stem cells. *Stem Cell Investig*; **4**: 65.
43. Kruczek K, Gonzalez-Cordero A, Goh D, Naeem A, Jonikas M, Blackford SJI, Kloc M, Duran Y, Georgiadis A, Sampson RD, et al. (2017) Differentiation and Transplantation of Embryonic Stem Cell-Derived Cone Photoreceptors into a Mouse Model of End-Stage Retinal Degeneration. *Stem Cell Reports*; **8**: 1659-1674.
44. Alter J, Lou F, Rabinowitz A, Yin H, Rosenfeld J, Wilton SD, Partridge TA, Lu QL. (2006) Systemic delivery of morpholino oligonucleotide restores dystrophin expression bodywide and improves dystrophic pathology. *Nat Med*; **12**: 175-177.

## 6.6 Supplemental information

### A Control iPSC

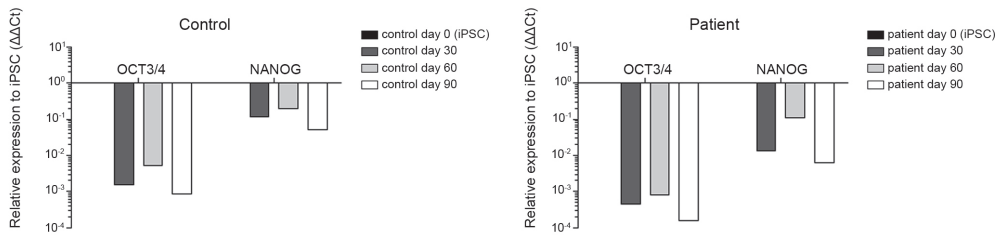


### B Patient iPSC



### Supplementary Figure S1. Expression of stem cell markers in iPSCs.

Undifferentiated iPSCs derived from (A) control and (B) patient stained for the nuclear markers NANOG and OCT4 and surface antigens SSEA4 and TRA-1-81.



**Supplementary Figure S2. Gene expression of pluripotency markers during differentiation.**

Relative gene expression of pluripotency markers *OCT3/4* and *NANOG* to iPSCs in patient and control cells. Normalized to *GUSB*.

**Supplementary Table S1.**

Primers used for qPCR.

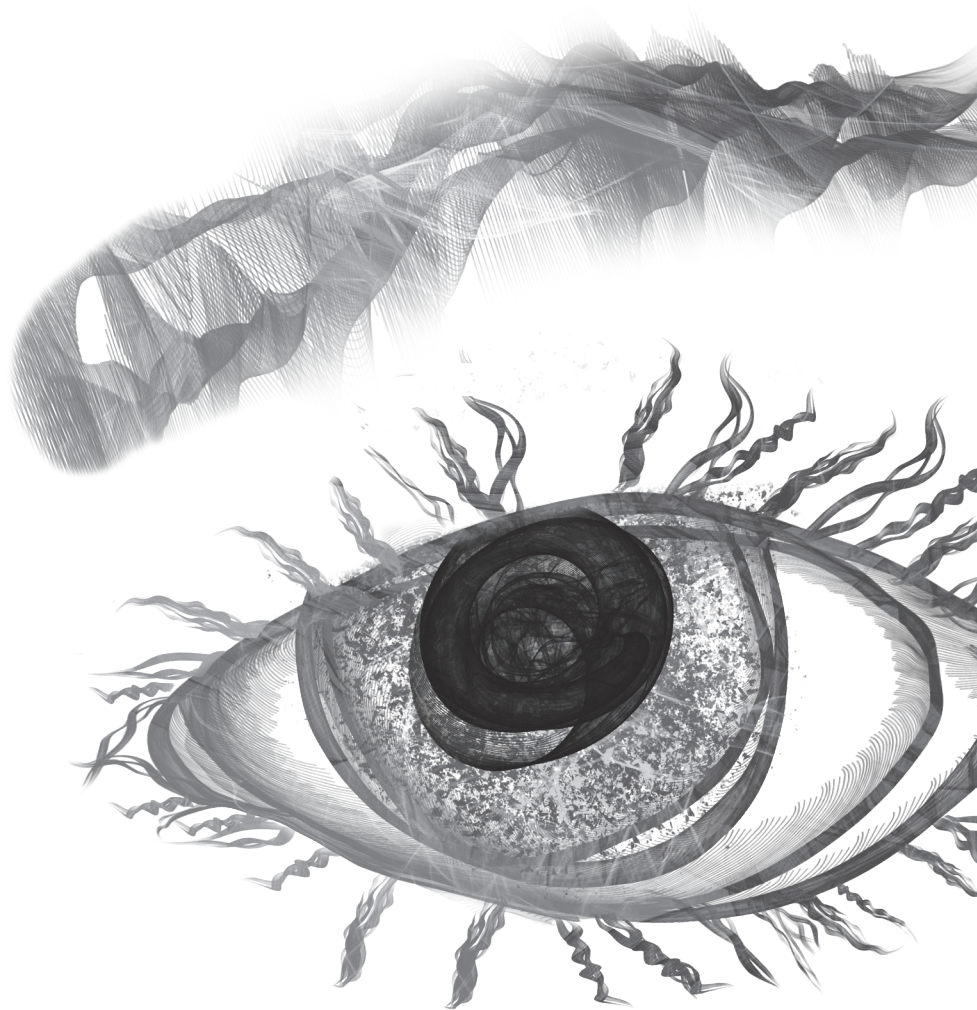
Gene name	Forward primer (5' > 3')	Reverse primer (5' > 3')
<i>SIX6</i>	CCAGGCAACCGGACTGAC	TGTGACAGGACCTGCTGCT
<i>CRX</i>	ATGATGGCGTATATGAACCC	TCTTGAACCAAACCTGAACC
<i>OPN1SW</i>	GCTTCATTGTGCTCTCTCC	TTCAGCCTTCTGGGTCGTAG
<i>ARR3</i>	GGTGTGTGCTCTGGTTGATCC	GTCACAGAACAGGGCAGGTT
<i>PDE6H</i>	CTCCCAAGTTCAAGCAGAGG	ATCTGTTCCTAGCCCCCTCCA
<i>PDE6C</i>	TTGGGAACAAGGAGATCTGG	AACAAAATCAATAAATCCAACCTGA
<i>EYS</i>	TGTGGCAATTGGGATTGCA	GGATCGTTCACATAGGTTGCA
<i>OCT3/4</i>	GTTCTTCATCACTAAGGAAGG	CAAGAGCATCATTGAACTTCAC
<i>NANOG</i>	TTCTCCACCAGTCCCAAAG	TTGCTCCACATTGGAAGGTT
<i>PAX6</i>	TCTAATCGAAGGGCCAAATG	TGTGAGGGCTGTGCTGTTC
<i>NRL</i>	GTTTAGGTGC CGCAGCGG	ACAGACATCGAGACCAGCG
<i>RHO</i>	CAACTACATCCTGCTCAACCTAGC	GTGTAGTAGTCGATTCCACAGAG
<i>RPE65</i>	CGTGAGAAC TGGGAAGAGGT	AATCTTGCCTGTGTCAGCC
<i>GUSB</i>	AGAGTGGTGCTGAGGATTGG	CCCTCATGCTCTAGCGTGTC

**Supplemental Table S2.**

Primers used for RT-PCR analysis.

Fragment name	Forward primer (5' > 3')	Reverse primer (5' > 3')
<i>EYS</i> exon 25-27 PCR 1	TGCTCCATTGGGCTTCTTTG	GCTTGACATACAGCAGAAGTCC
<i>EYS</i> exon 25-27 nested PCR	ACTTTGGTCAGCAGCTTCC	GCTGAAGGTCTGAAATCTAGGG
<i>Actin</i>	ACTGGGACGACATGGAGAAG	TCTCAGCTGTGGTGGTGAAG

# Chapter 7



# **General discussion**

Mutations in *EYS* are responsible for approximately 5-10% of all the autosomal recessive RP cases. In addition, there are also macular dystrophy and CRD patients described who harbor causative *EYS* mutations. Currently, there is no treatment for *EYS*-associated retinal dystrophy available and still very little is known about the underlying pathogenic mechanism. In this doctoral thesis, I have aimed to unravel the function of *EYS* and the pathogenic mechanism underlying *EYS*-associated retinal dystrophy, and to take the first steps towards a therapy for this disease. This chapter reviews our main discoveries and discusses future directions and challenges for the development of therapeutic approaches for retinal dystrophy caused by mutations in *EYS*.

### 7.1 The role of *EYS* in photoreceptors

Since the discovery of *EYS* in 2008 by two independent groups,<sup>1,2</sup> many groups have reported on RP patients carrying mutations in *EYS*. However, limited data were, and still are, available about the function of *EYS* protein and its role in the development of retinal dystrophy. Therefore, I have aimed to unravel the function of *EYS*, in order to be able to get a better understanding of the pathogenic mechanism underlying *EYS*-associated retinal dystrophy.

When looking at the domain structure of the *EYS* protein, many epidermal growth factor (EGF)-like domains, mainly N-terminal, and five laminin A G-like (LamG) domains are predicted at the C-terminus (**Chapter 1, section 1.5**).<sup>1,2</sup> The EGF domains are around 30-40 amino acids long and are found in a large variety of, predominantly, animal proteins. These domains are mainly found in the extracellular parts of membrane-bound proteins or in proteins that are secreted.<sup>3</sup> It has been described that EGF domains might be involved in cell signaling and adhesion, although the exact function of the EGF domain is not fully clear.<sup>4</sup> The LamG domain is around 180 amino acids long and is found in one to six copies in various proteins of the laminin family as well as in a large number of other extracellular proteins. Laminin A G-like domains can vary in their function, and a variety of binding functions has been described for different LamG modules. Proteins containing LamG domains appear to have roles in a wide variety of processes, such as cell adhesion, cell signaling, migration, adhesion and differentiation.<sup>5</sup> Another retinal protein described to have both EGF and LamG domains is CRB1. The CRB1 protein contains a short intracellular domain, a trans-membrane domain, and a large extracellular portion that includes EGF and LamG domains.<sup>6</sup> Human CRB1 is expressed in the fetal brain, Müller cells and inner segments of photoreceptors and is considered to be crucial for photoreceptor morphogenesis.<sup>7-10</sup> Furthermore, CRB1 has been described to play a role in mechanisms that control cell adhesion, polarity and intracellular communication.<sup>11</sup> In addition to the EGF and LamG domains, a signal peptide is predicted to be present at the N-terminal end of the *EYS* protein. This might indicate that the protein is translocated to the (cellular) membrane, where it can be potentially cleaved and excreted. All together, this suggests that *EYS* is a protein with extracellular domains or a protein that is secreted.

In *Drosophila*, the ortholog of EYS, also known as spam or spacemaker, is located in the inter-rhabdomere space of the compound eye of the fly. Here, it is shown to play a major role in proper formation of the inter-rhabdomere lumen, since in *ey*s deficient flies the inter-rhabdomeral space was closed or collapsed.<sup>12</sup> In **Chapter 4**, we describe the generation of an *ey*s knock-out zebrafish line using CRISPR/Cas9 technology that allowed us to study EYS function in zebrafish. We showed that EYS localizes near the connecting cilium in wild-type zebrafish, whereas in *ey*s mutant fish no EYS protein was observed. This was in line with the observation of Yu et al., who reported the localization of EYS in the region of the connecting cilium/transition zone in zebrafish. In the primate retina, EYS was not only located near the connecting cilium but also in the outer segments of rods and cones, and cone terminals.<sup>13</sup> Another study by Alfano et al. reported localization of EYS in the ciliary axoneme in Y79 cells, and in macaque retinal sections, EYS was located in the photoreceptor ciliary axoneme of both rods and cones.<sup>14</sup> Together, these results indicate that, in photoreceptor cells, EYS could be a protein involved in structural organization of the outer segments and/or maintaining the stability of the ciliary axoneme.

In *Drosophila*, *Eys* localizes extracellular in the inter-rhabdomere space, whereas in zebrafish and human it appears to be intracellular. This might suggest that the signal peptide is not cleaved in zebrafish and human. However, differences in localization between *Drosophila* and vertebrates might also be due to the morphological differences between the rhabdomeres and photoreceptors. Yu et al. suggest that EYS, like in *Drosophila*, is secreted into the lumen of the ciliary pocket, because they observed that in EYS deficient photoreceptors the ciliary pocket is collapsed or filled with vesicles.<sup>13</sup> Despite these morphological and localization differences, *Drosophila* and human EYS could possibly still have similar roles in the maintenance of photoreceptors, since their domain structures are very similar.

It will be essential to determine the precise location of the EYS protein with respect to the connecting cilium in order to explore the function of EYS, for example, by employing electron microscopy studies. In addition, co-localization with other ciliary proteins can be investigated, as well as the effect of the absence of EYS protein on ciliary trafficking of other ciliary proteins. Furthermore, it will be interesting to investigate whether EYS interacts with other ciliary proteins, in order to get more insights into its function. Techniques that can be used to study protein-protein interactions are the yeast two-hybrid system and protein complex affinity purification followed by mass spectrometry.<sup>15,16</sup> With the yeast two-hybrid system, direct, binary interactions between two proteins that are ectopically expressed in a yeast cell can be identified, whereas with mass-spectrometry entire interacting protein complexes can be mapped without detailed information on their direct interactions.

Remarkably, *Eys* is not present in rodent species, such as mouse and rat. When looking at the morphology of photoreceptors, an important difference between rodents and other species is the absence of calyceal processes in rodents.<sup>17,18</sup> These are axially oriented microvilli-like structures, near the connecting cilium, which form a collar around the base



of the outer segment in rods and cones. Calyceal processes have been suggested to play a role in the shaping and growing of the rod outer segments.<sup>17</sup> It has also been predicted that calcium within the calyceal processes controls mechanical tension by regulating plus-directed motor myosin VIIa.<sup>19,20</sup> Possibly, in humans, EYS function might be somehow related to these calyceal processes.

## 7.2 Spectrum of EYS-associated retinal dystrophy

In **Chapter 2**, we collected all reported *EYS* variants present in 377 arRP index cases published before June 2017. We also described 36 additional index cases, carrying 26 novel variants. In the meantime, as expected since the discovery of *EYS* was only 10 years ago, several additional papers were published to report on retinal dystrophy patients that carry *EYS* variants.<sup>21-25</sup> Novel *EYS* variants that were not included in **Chapter 2** or **Chapter 3** are listed in Table 7.1.

In **Chapter 3**, we describe the phenotypic data in a cohort of 30 patients with *EYS* mutations. In addition to RP, there was one patient with cone-rod dystrophy (CRD) and two siblings with macular dystrophy. Cone-rod dystrophy patients with *EYS* mutations were also reported previously (Chapter 2),<sup>1,26</sup> whereas *EYS* mutations in macular dystrophy patients were not reported before. Recently, Sun et al. reported an Usher syndrome patient with *EYS* mutations (p.(Asn773Lysfs\*2) and p.(Gly2186Glu)). The patient complained about hearing loss since his middle age, but pure-tone audiometry examination showed normal results after his molecular testing.<sup>24</sup> So it is not completely clear whether this patient has indeed Usher syndrome or just RP. Screening patients diagnosed with other IRDs than RP, such as macular dystrophy or CRD, for *EYS* variants might increase the diagnostic yield in currently unsolved cases.

Sengillo et al. described that variants occurring in positions closer to the C-terminus of *EYS* are more common in patients presenting with hyperautofluorescent rings on fundus autofluorescence imaging.<sup>23</sup> In both **Chapter 2** and **Chapter 3**, we were not able to draw any conclusions regarding the relationship between *EYS* variants and disease phenotype, nor could we identify obvious indications that individuals with protein-truncated variants had a more severe phenotype compared to patients with missense variants. The main reason for this is probably the small sample size in both studies. For example, in the cohort used in **Chapter 3**, many variants were observed only once. Furthermore, sometimes phenotypic data were not always clearly reported or not available. In addition, there is a lack of consistency in reporting disease manifestation and methods used for diagnosis between different clinical centers.

In **Chapter 2**, we described that many variants had to be classified as of uncertain significance, mainly because there was not enough evidence to meet one of the four pathogenicity criteria. This group consisted mainly of missense variants, but also some intronic variants and variants at the 5'-UTR were reported as of uncertain significance. One of the things that will help by the classification of these variants, but is not yet available, is

**Table 7.1.**

*EYS* (NM\_001142800.1) variants not described previously in this thesis.

Exon/ intron	DNA change	Protein effect	ACMG classification	Reference
Exon 6	c.963_979del	p.(Pro321Profs*4)	Pathogenic	Sengillo <sup>23</sup>
Exon 7	c.1155T>A	p.(Cys385*)	Pathogenic	McGuigan, <sup>21</sup> Sengillo <sup>23</sup>
Intron 7	c.1184+1G>A	p.?	Pathogenic	Mucciolo <sup>25</sup>
Exon 9	c.1308C>A	p.(Cys436*)	Pathogenic	Sengillo <sup>23</sup>
Exon 11	c.1641_1644del	p.(Ser547Argfs*62)	Pathogenic	Sengillo <sup>23</sup>
Exon 11	c.1645G>T	p.(Glu549*)	Pathogenic	Sengillo <sup>23</sup>
Exon 11	c.1682_1686del	p.(Asn561Ilefs*7)	Pathogenic	Mucciolo <sup>25</sup>
Exon 12	c.1961dup	p.(Asn654Lysfs*5)	Pathogenic	Sengillo <sup>23</sup>
Intron 13	c.2137+1G>A	p.?	Pathogenic	McGuigan <sup>21</sup>
Intron 14-18	c.2260-1437_2847- 6134del	p.(Ser754Ilefs*4)	Pathogenic	McGuigan <sup>21</sup>
Exon 15	c.2318dup	p.(Asn773Lysfs*2)	Pathogenic	Sun <sup>24</sup>
Exon 16	c.2542C>T	p.(Gln848*)	Pathogenic	Mucciolo <sup>25</sup>
Exon 19	c.2889T>A	p.(Cys963*)	Pathogenic	McGuigan <sup>21</sup>
Intron 19	c.2992+1G>A	p.?	Pathogenic	Sengillo <sup>23</sup>
Exon 23	c.3555C>G	p.(Cys1185Trp)	US	Sengillo <sup>23</sup>
Exon 26	c.4152del	p.(Pro1385Leufs*14)	Pathogenic	Mucciolo <sup>25</sup>
Exon 29	c.5928del	p.(Arg1976Serfs*11)	Pathogenic	Sengillo <sup>23</sup>
Exon 29	c.5976T>A	p.(Asn1992Lys)	US	Mucciolo <sup>25</sup>
Exon 31	c.6198_6201del	p.(Gln2066Hisfs*16)	Pathogenic	Mucciolo <sup>25</sup>
Exon 32	c.6528C>A	p.(Tyr2176*)	Pathogenic	McGuigan <sup>21</sup>
Intron 32	c.6571+5G>A	p.?	US	Sengillo <sup>23</sup>
Intron 38	c.7578+1G>A	p.?	Pathogenic	Sengillo <sup>23</sup>
Exon 42	c.8133_8137del	p.(Phe2712Cysfs*33)	Pathogenic	Mucciolo <sup>25</sup>
Exon 42	c.8111T>G	p.(Leu2704*)	Pathogenic	Sengillo <sup>23</sup>
Exon 43	c.8338_8342delins <sup>a</sup>	p.(Gly2780_Ser2781delinsTyrLysLeu*)	Pathogenic	McGuigan <sup>21</sup>
Exon 43	c.8411_8412insTT	p.(Thr2805*)	Pathogenic	McGuigan <sup>21</sup>
Exon 43	c.8413dup	p.(Thr2805Asnfs*7)	Pathogenic	Sengillo <sup>23</sup>
Exon 43	c.9178A>C	p.(Ile3060Leu)	US	Mucciolo <sup>25</sup>
Exon 43	c.9317_9336del	p.(Thr3106Lysfs*13)	Pathogenic	Sengillo <sup>23</sup>
Exon 43	c.9383_9387del	p.(Lys3128Argfs*7)	Pathogenic	Sengillo, <sup>23</sup> Mucciolo <sup>25</sup>

<sup>a</sup>inserted sequence: TATAAACTATAAACTATAAACTATAAACTATAAACTATAAACTATAAACTATAAACTATAAACTATA  
US: uncertain significance.

experimental evidence. In **Chapter 3**, we showed how the effect of a variant on *EYS* pre-mRNA splicing could be determined by using an *in vitro* minigene splice assay. This is a manageable method that also has been shown useful by others.<sup>27,28</sup> Ideally, one would like to make use of patient-derived cells, from which RNA can be extracted to subsequently investigate *EYS* mRNA composition and levels. However, since *EYS* is predominantly expressed in the photoreceptor cells of the retina, alternative *in vitro* or *in vivo* systems that have sufficient *EYS* expression are needed. These models will be discussed in **section 7.3**.

### 7.3 Disease models for *EYS*-associated retinal dystrophy

The use of disease models can also help to give more insights into the function of *EYS* and its role in the pathogenesis of RP. One can either make use of *in vivo* models or cellular models. In **Chapter 4**, we described the generation of a zebrafish *ey*s knock-out line using CRISPR/Cas9 technology, which allowed us to investigate *EYS* function in zebrafish. We showed that in *ey*s deficient fish, the photoreceptor outer segments were highly disorganized. In addition, photoreceptor specific proteins such as rhodopsin and cone transducin, were mislocalized in *ey*s<sup>-/-</sup> fish. Furthermore, these fish were visually impaired, showing a decreased ERG b-wave amplitude and a diminished VMR response. Two other groups reported on the generation of a zebrafish model for *EYS*-associated retinal dystrophy.<sup>13,29</sup> The study by Yu et al. also generated mutations in the zebrafish using CRISPR/Cas9 technology, and demonstrated a progressive loss of rod and cone photoreceptors, and disruption of the ciliary pocket of cones.<sup>13</sup> Lu et al. used TALEN technology to create their *ey*s knock-out line. Using ERG recordings, they showed that these fish were visually impaired. Furthermore, they reported F-actin disruption and mislocalization of retinal proteins in the absence of *Eys*.<sup>29</sup> So far, these and our own zebrafish model are the only *in vivo* disease models reported for *EYS*-related retinal dystrophy. Since *Eys* is not present in mouse and rat, they are excluded from being used as a model.<sup>1,2</sup> Alternative animal models could be for instance dog or pig (**Chapter 1**), which both do express *Eys*. The porcine retina is cone-rich, has an area centralis dorsal to the optic nerve,<sup>30</sup> and lacks a tapetal zone,<sup>31</sup> which makes it a good model to study IRDs, although the *EYS* gene is not completely annotated yet in pig. The dog retina is rod-dominated in most parts, but it does have a central area with a high density of cones.<sup>32</sup> Drawbacks of the use of pig or dog as a model for retinal dystrophy are the ethical aspects, long regeneration time and housing.<sup>33</sup>

Since the discovery of reprogramming factors by the groups of Yamanaka and Thomson,<sup>34,35</sup> the use of iPSCs for the differentiation into any cell type of interest became booming, leading to the rapid generation of disease-specific cellular models. We aimed to differentiate human-derived iPSCs into 3D optic cups using the differentiation protocol adapted from Nakano et al.,<sup>36</sup> as described in **Chapter 6**. Using qRT-PCR analysis, we showed the expression of some retinal markers, indicating differentiation towards a retinal

fate. However, expression levels were very low. In addition, we observed the presence of pigmented cells, suggesting the development of RPE cells, although also other cells, like melanocytes, do form pigments. By using the experience we have from this differentiation together with protocols published by other groups, lessons can be learned to improve the differentiation in the future. Playing with the differentiation factors or extending differentiation time are examples of how the differentiation can be optimized (**Chapter 6**). Besides the use of patient-derived iPSCs, it is also possible to use wild-type iPSCs and introduce a mutation manually by the use of CRISPR/Cas9 technology. In this way, variability between lines could be reduced.

In general, differentiation of iPSCs into retinal organoids is not easy and the challenges are manifold. The generation of retinal organoids takes at least several months and is largely dependent on manual manipulation and subjective selection criteria at initial stages. In addition, there is high variability among different human-derived iPSC lines<sup>37</sup> and between iPSCs and ESCs.<sup>38</sup> Hence, this results in variability in differentiation efficiency, structural features and expression of cell specific markers at a particular stage. Photoreceptors generated via iPSC differentiation reported so far, do not show fully mature outer segments. This could be due to the fact that the photoreceptors are not in direct contact with RPE cells, as in the human retina. It has been shown that aberrant RPE could affect photoreceptors by lack of outer segment morphogenesis.<sup>39</sup> Further research is required to lead to the generation of better retinal organoids, including contact between photoreceptor cells and RPE cells and interactions between cell populations. Another challenge will be to include vascularisation in the retinal organoids. In this way, a more humanized model is created that can be used to study molecular mechanism underlying retinal dystrophy. Finally, it might be useful to introduce standardized, robust differentiation protocols, thereby increasing translational impact. In addition, there is a need for quantitative methods for the analysis of the retinal organoids.

The above mentioned disease models can also be used to study the effect of missense mutations. Since most of the missense variants described in **Chapter 2** had to be classified as of uncertain significance, experimental evidence might help by their classification. Human-derived iPSCs can be used to determine the effect of missense mutations on the development and morphology of photoreceptors. Differentiated iPSCs derived from a patient can be compared to iPSCs derived from a healthy control. A huge drawback of the differentiation of human-derived iPSC is that this will be very time-consuming and labour-intensive. In addition, there is lot of variation in protocols currently used for the differentiation, leading to high variation in differentiation outcome. To be able to implement these techniques in clinical diagnostics, protocols have to be standardized. Moreover, robust quantitative methods are required for the analysis of these differentiated cells. We (**Chapter 4**) and others,<sup>13,29,40</sup> previously reported on the disruption of *eyes* in zebrafish using CRISPR/Cas9 or TALEN, leading to a retinal phenotype. In a similar way, missense mutations can be introduced and the effect of these mutations can be studied by

a variety of assays, such as immunohistochemistry, ERG and VMR measurement. However, due to differences between human *EYS* and its ortholog in zebrafish, not all variants can be tested. For instance, zebrafish *eys* is lacking an equivalent of exon 26 of human *EYS*, therefore mutations located in this exon are excluded from analysis. Similar as for iPSC, the use of *in vivo* models for the screening of *EYS* mutations will be expensive, labour intensive and time-consuming. Taken together, experimental evaluation of *EYS* variants for diagnostic purposes remains to be very challenging.

#### 7.4 Potential therapies for *EYS*-associated retinal dystrophy

The retina is an accessible and immune-privileged structure, which makes it suitable for therapeutic intervention, including gene augmentation therapy. Previous studies already have shown that gene therapy for retinal disease can be effective and safe, both in animal models and clinical trials.<sup>41-44</sup> In addition, the first gene therapy for retinal disease caused by mutations in *RPE65*, named Luxturna™, is recently approved by the US Food and Drug Administration (FDA). Most of the successful examples of gene therapy for retinal disease make use of AAV-mediated gene delivery into the retina.<sup>44,45</sup> However, the limited cargo capacity of an AAV makes it unsuitable for delivery of the large *EYS* cDNA. Therefore, as described in **Chapter 5**, we generated *EYS* microgenes encoding proteins that will fit into an AAV. We have shown that at least two out of three *EYS* microgenes encode stable proteins. However, many different aspects of the *EYS* microgenes need to be evaluated in order to decide whether the microgenes are functional, and thus can be used for therapeutic purposes. First, localization studies need to be performed to assess whether the *EYS* microgene proteins are hosted at the right location in the cell. Unfortunately, we were not able to draw any conclusions on the localization of the microgenes based on our localization studies in hTERT-RPE1 cells. This was probably due to the low transfection efficiency of the cells. The use of other cell types that also contain cilia, such as COS-1 cells, might circumvent this problem. Second, it needs to be evaluated whether the *EYS* microgenes encode for functional proteins. To study this in a cellular model, one can make use of patient-derived iPSCs. To study the functionality of the microgenes *in vivo*, a zebrafish *eys* knock-out model with a clear retinal phenotype (as described in **Chapter 4**) will be a suitable model. Third, a suitable delivery strategy for the *EYS* microgenes needs to be developed. Microgene A can, together with a retinal specific promoter, be packaged into a single AAV vector. However, for the packaging of microgene B, two AAV vectors will be required. A dual-AAV vector approach was reported by Trapani et al., in which the gene was divided in two parts, and simultaneously delivered in separate AAV vectors.<sup>46</sup> To be able to deliver larger genes, such as full length *EYS*, a triple AAV approach would be required. Additionally, lentiviral and nanoparticle-based delivery strategies for large genes, including *ABCA4* and genes mutated in Usher syndrome, are also being investigated.<sup>47,48</sup> However, for the full length *EYS* cDNA, a lentivirus will also not be sufficient, and a disadvantage of the use of lentiviruses is that they integrate

into the genome of the host cell, thereby running the risk of insertional mutagenesis. In addition, they do not efficiently target photoreceptor cells which are the primary target for *EYS* gene augmentation therapy. Another challenge of the use of gene augmentation therapy is that expression levels of the protein cannot be regulated, thereby risking that expression levels exceed those of endogenous protein, which in turn can lead to toxicity. Besides gene therapy, the use of AONs as a therapeutic strategy for IRDs has also emerged over the last years. An advantage of the use of AONs over gene augmentation therapy is that they can be more easily delivered, since the small sequences fit in an AAV or can be delivered as naked AONs. In addition, AONs target the endogenous mRNA and therefore the maximum expression levels of the protein will never exceed that of the endogenous protein. The successful use of AONs for IRD has been shown for a deep-intronic variant in *CEP290* (c.2991+1655A>G),<sup>49-51</sup> and proof-of-concept studies for the use of AONs to correct splicing were published for deep-intronic variants in *USH2A* (c.7595-2144A>G) and *OPA* (c.610+364G>A).<sup>52,53</sup> Recently, a study by Albert et al. showed AON-mediated splice correction of two neighboring deep-intronic mutations in *ABCA4* causing Stargardt disease using iPSC technology.<sup>54</sup> The use of AONs is proven not only to be effective for correction of intronic mutations, it also can be used for the skipping or inclusion of regular exons. AON-mediated exon skipping is currently one of the most promising therapeutic tools for DMD and promising results have also been reported for the treatment of CADASIL caused by mutations in *NOTCH3*.<sup>55,56</sup> As a therapy for spinal muscular atrophy, AONs are used for the inclusion of exon 7 in *SMN2* leading to the production of a functional protein.<sup>57</sup> In **Chapter 6**, we aimed to investigate whether this AON-mediated exon skipping approach might also work as a therapy for *EYS*-related retinal dystrophy. We designed AONs for the skipping of *EYS* exon 26, a large exon which does not encode any functional domains. Skipping of this exon will not disrupt the reading frame. In addition, many protein truncated variants are located in this exon, including the most frequently reported p.(Ser1653Lysfs\*2) variant in the Japanese population as described in **Chapter 2**. We showed that *EYS* lacking exon 26 is translated into a stable protein by western blot analysis. As for the microgenes, patient-derived iPSCs can be used to investigate whether *EYS* protein lacking exon 26 ( $\Delta 26EYS$ ) is functional. Since there is no corresponding exon of human *EYS* exon 26 in zebrafish *eyes*, functionality of the  $\Delta 26EYS$  protein cannot be studied in this animal model. As discussed in **Chapter 4**, the low complexity region encoded by exon 26 is also missing from chicken *EYS*. This might suggest that this region is not of great importance for the functionality of the *EYS* protein, at least not in vertebrate species. A blast search with the amino acid sequence of the low complexity region only gave hits of the human *EYS* protein and a small number of *EYS* orthologs, such as gorilla, macaque, pig and dog. We tested different AONs in hTERT-RPE1 cells and in iPSCs. The outcome of the two experiments was not consistent. In both experiments we worked at the limit of detection, since nested PCR was necessary to detect the *EYS* transcripts. An alternative for testing AONs is to make use of a so-called minigene, which contains at

least exon 26 and parts of the flanking introns. HEK293T cells can be transfected with the minigene and then treated with the AONs. The effect on splicing can then be evaluated by RT-PCR analysis. Eventually, the AONs need to be tested in an *in vivo* model before they can be applied to human subjects. Unfortunately, there is no equivalent of human *EYS* exon 26 present in the zebrafish, which makes it unsuitable to test the AON approach in zebrafish. As mentioned before, dog and pig do show a low complexity region as seen in human *EYS*, which might be alternatives for the testing of AONs *in vivo*.

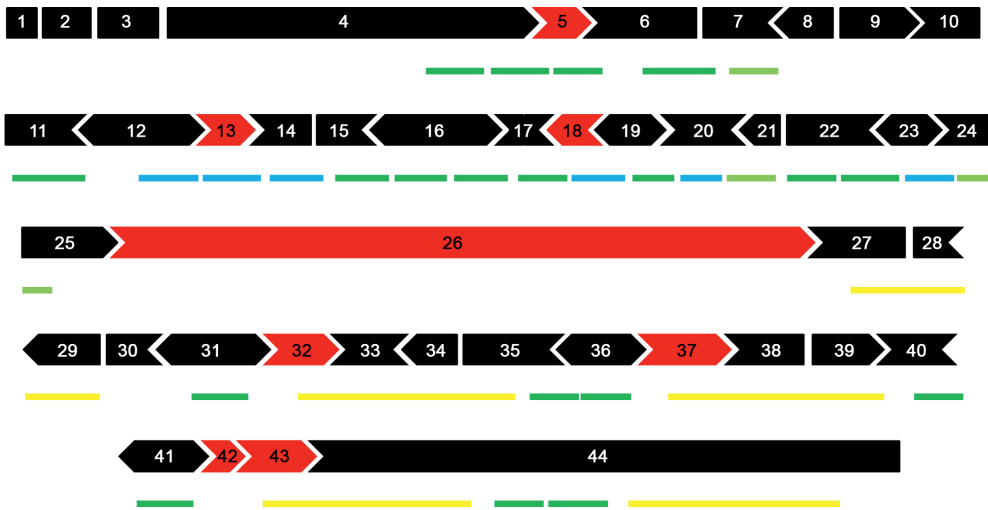


**Figure 7.1. Schematic representation of candidate exons of *EYS* for AON-mediated skipping.**

Candidate exons for AON-mediated exon skipping are depicted in red. Colored lines underneath the exons represent functional domains. Dark green: epidermal growth factor (EGF) domain; light green: EGF-like domain; blue line: EGF calcium; yellow line: laminin A G-like domain.

In **Chapter 6**, we selected exon 26 of *EYS* as a target exon for AON-mediated exon skipping. In addition, there are several other candidate exons for AON-mediated exon skipping. In total, there are seven other *EYS* exons that, when skipped, do not lead to a frameshift (Figure 7.1). Besides the skipping of single exons, skipping of two or more exons, could also be a possible strategy. For instance, skipping of exon 7 or exon 8 alone will lead to disruption of the reading frame, whereas skipping of both exons together will leave the reading frame intact (Figure 7.1). The same holds true for exon 9 and exon 10, and even skipping of exons 7 until 10 could be a possibility. The fact that exons 8, 9 and 10 do not encode for any functional domains, makes this region even more interesting to target. In **Chapter 2**, we found eleven patients reported with retinal dystrophy carrying a protein truncating variant (eight unique variants) in one of these four exons of *EYS*. In papers

published after June 2017, an additional five patients were described to carry *EYS* variants (4 novel variants) in one of those exons (Table 7.1).

It has been recently discovered that prokaryotic immune components known as clustered regularly interspaced short palindromic repeats (CRISPR) and CRISPR-associated nucleases, such as Cas9, are able to mediate genome editing in mammalian cells.<sup>58-60</sup> This CRISPR/Cas9 technology can be used to correct disease-causing mutations while leaving the gene under control of its endogenous regulation. The Cas9 nuclease cleaves double-stranded DNA at a specific target in the genome. These double-strand breaks are repaired by either the non-homologous end joining (NHEJ) pathway, introducing insertions and/or deletions at the target locus, or by the homology-directed repair (HDR) pathway, which allows precise genome editing using a donor DNA template for repair. For the treatment of retinal diseases, direct silencing of dominant negative mutations via the NHEJ pathway is most commonly used. For example, Bakondi et al. showed the allele specific disruption of Rhodopsin containing the p.(Ser334\*) mutation in rats using CRISPR/Cas9.<sup>61</sup> Next to inactivation of mutations, it is also possible to insert DNA to restore wild-type function of a gene using the HDR pathway.<sup>62,63</sup> Preferably, therapeutic targets using CRISPR/Cas9 and the HDR pathway are selected based on the frequency of the variant. In this way, many patients can be treated with the same therapy, which makes it more cost-effective. Although *EYS* variants are found to be located across the entire gene, and no real mutational hotspot can be identified, there are some variants reported in quite some patients. As mentioned before, the p.(Ser1653Lysfs\*2) variant is reported in 79 index patients, and thereby the most frequently reported variant in the Japanese population. In addition, the p.(Tyr2935\*), p.(Tyr3135\*) and p.(Ile2239Serfs\*17) variants are reported in 38, 12, and 9 patients, respectively (**Chapter 2**). Interestingly, 21 patients with the p.(Tyr2935\*) variant carried the p.(Ser1653Lysfs\*2) variant on the other allele. When in the future a therapy will be developed using CRISPR/Cas9 in combination with HDR, these variants would be interesting candidates to target.

Although the results of using CRISPR/Cas9 as a therapeutic strategy are promising, still quite some challenges have to be overcome before it can be applied in the clinic, such as reduction of off-target effects and increasing the efficiency of gene editing and the rates of HDR in the eye.<sup>64,65</sup> Besides the use on CRISPR/Cas9 technology on its own, it can also be combined with iPSCs to create a powerful therapeutic strategy for IRDs which can be used regardless of the disease state. Using CRISPR/Cas9, mutations can be corrected in patient-derived iPSCs, which in turn can be differentiated into retinal cells and re-implanted into the eye.

Most of the above mentioned potential therapeutic strategies are only effective if they are applied in early stages of disease, when there is still retinal activity left. In later stages of disease, alternative treatment options such as retinal prosthesis, optogenetics and cell transplantation (as described in **Chapter 1**) can be the solution.



### 7.5 Concluding remarks

Since the discovery of *EYS* in 2008, many retinal dystrophy patients have been reported to carry mutations in *EYS*, however, little was known about its exact function. With this thesis we provided more insights into *EYS*-related retinal dystrophy in relation to disease spectrum and development of a genetic therapy. There is still a lot to discover about *EYS*, especially about its exact localization, protein function and interactions with other proteins. Further studies may lead to a better understanding of the role of *EYS* in the pathogenesis underlying retinal dystrophy and photoreceptor degeneration and will progress the development of therapies for *EYS*-related retinal dystrophies. Gene therapy and other genetic therapeutic approaches are focused on the treatment of one specific disease. As a consequence, these therapies are only applicable to a small proportion of the IRD patients and thereby making it not very cost-effective. In the future, more effort should be made on the development of therapies that target a broader range of IRDs.

## 7.6 References

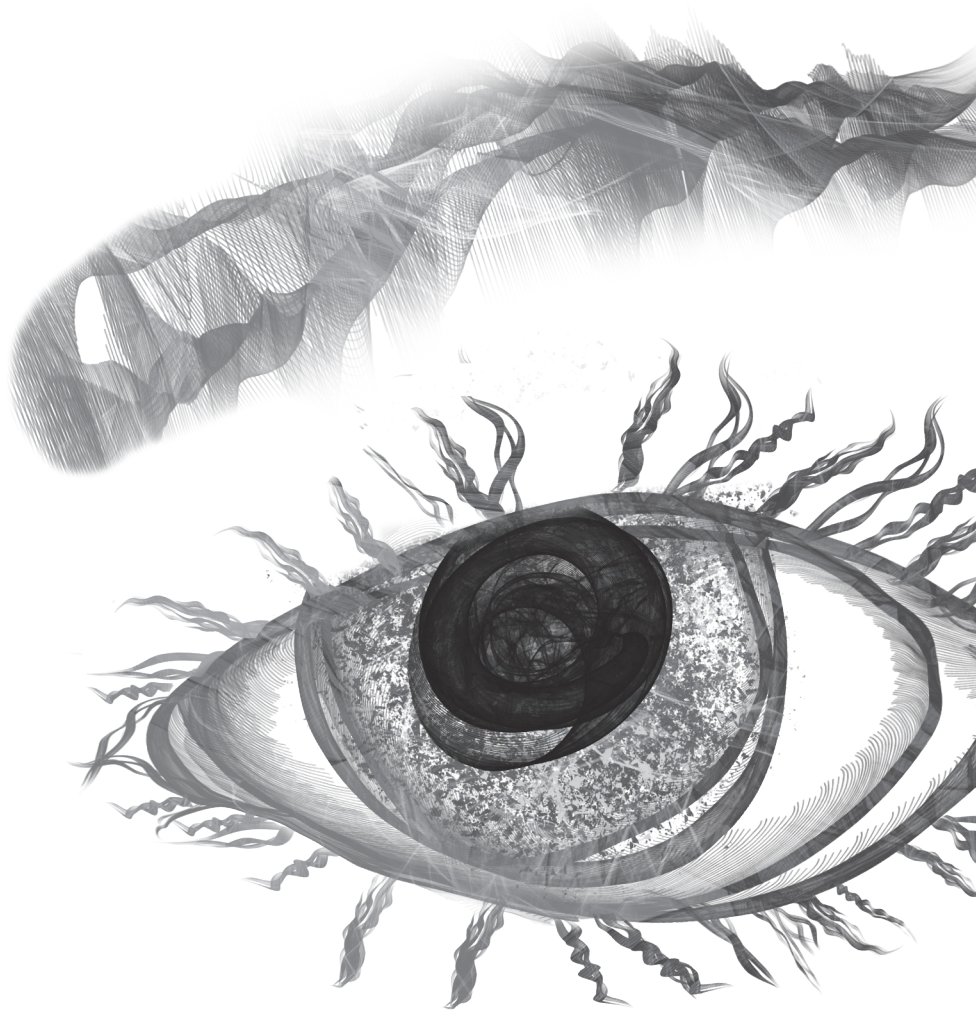
1. Collin RW, Littink KW, Klevering BJ, van den Born LI, Koenekoop RK, Zonneveld MN, Blokland EA, Strom TM, Hoyng CB, den Hollander AI, et al. (2008) Identification of a 2 Mb human ortholog of *Drosophila* eyes shut/spacemaker that is mutated in patients with retinitis pigmentosa. *Am J Hum Genet*; **83**: 594-603.
2. Abd El-Aziz MM, Barragan I, O'Driscoll CA, Goodstadt L, Prigmore E, Borrego S, Mena M, Pieras JI, El-Ashry MF, Safieh LA, et al. (2008) EYS, encoding an ortholog of *Drosophila* spacemaker, is mutated in autosomal recessive retinitis pigmentosa. *Nat Genet*; **40**: 1285-1287.
3. Engel J. (1989) EGF-like domains in extracellular matrix proteins: localized signals for growth and differentiation? *FEBS Lett*; **251**: 1-7.
4. Wouters MA, Rigoutsos I, Chu CK, Feng LL, Sparrow DB, Dunwoodie SL. (2005) Evolution of distinct EGF domains with specific functions. *Protein Sci*; **14**: 1091-1103.
5. Tisi D, Talts JF, Timpl R, Hohenester E. (2000) Structure of the C-terminal laminin G-like domain pair of the laminin alpha2 chain harbouring binding sites for alpha-dystroglycan and heparin. *EMBO J*; **19**: 1432-1440.
6. Richard M, Roepman R, Aartsen WM, van Rossum AG, den Hollander AI, Knust E, Wijnholds J, Cremers FP. (2006) Towards understanding CRUMBS function in retinal dystrophies. *Hum Mol Genet*; **15 Spec No 2**: R235-243.
7. den Hollander AI, Ghiani M, de Kok YJ, Wijnholds J, Ballabio A, Cremers FP, Broccoli V. (2002) Isolation of *Crb1*, a mouse homologue of *Drosophila* crumbs, and analysis of its expression pattern in eye and brain. *Mech Dev*; **110**: 203-207.
8. Alves CH, Pellissier LP, Wijnholds J. (2014) The CRB1 and adherens junction complex proteins in retinal development and maintenance. *Prog Retin Eye Res*; **40**: 35-52.
9. van de Pavert SA, Kantardzhieva A, Malysheva A, Meuleman J, Versteeg I, Levelt C, Klooster J, Geiger S, Seeliger MW, Rashbass P, et al. (2004) Crumbs homologue 1 is required for maintenance of photoreceptor cell polarization and adhesion during light exposure. *J Cell Sci*; **117**: 4169-4177.
10. van Rossum AG, Aartsen WM, Meuleman J, Klooster J, Malysheva A, Versteeg I, Arsanto JP, Le Bivic A, Wijnholds J. (2006) Pals1/Mpp5 is required for correct localization of *Crb1* at the subapical region in polarized Muller glia cells. *Hum Mol Genet*; **15**: 2659-2672.
11. Khan KN, Robson A, Mahroo OAR, Arno G, Inglehearn CF, Armengol M, Waseem N, Holder GE, Carss KJ, Raymond LF, et al. (2018) A clinical and molecular characterisation of CRB1-associated maculopathy. *Eur J Hum Genet*; **26**: 687-694.
12. Husain N, Pellikka M, Hong H, Klimentova T, Choe KM, Clandinin TR, Tepass U. (2006) The agrin/perlecan-related protein eyes shut is essential for epithelial lumen formation in the *Drosophila* retina. *Dev Cell*; **11**: 483-493.
13. Yu M, Liu Y, Li J, Natale BN, Cao S, Wang D, Amack JD, Hu H. (2016) Eyes shut homolog is required for maintaining the ciliary pocket and survival of photoreceptors in zebrafish. *Biol Open*; **5**: 1662-1673.

14. Alfano G, Kruczek PM, Shah AZ, Kramarz B, Jeffery G, Zelhof AC, Bhattacharya SS. (2016) EYS Is a Protein Associated with the Ciliary Axoneme in Rods and Cones. *PLoS One*; **11**: e0166397.
15. Fields S, Song O. (1989) A novel genetic system to detect protein-protein interactions. *Nature*; **340**: 245-246.
16. Puig O, Caspary F, Rigaut G, Rutz B, Bouveret E, Bragado-Nilsson E, Wilm M, Seraphin B. (2001) The tandem affinity purification (TAP) method: a general procedure of protein complex purification. *Methods*; **24**: 218-229.
17. Sahly I, Dufour E, Schietroma C, Michel V, Bahloul A, Perfettini I, Pepermans E, Estivalet A, Carette D, Aghaie A, et al. (2012) Localization of Usher 1 proteins to the photoreceptor calyceal processes, which are absent from mice. *J Cell Biol*; **199**: 381-399.
18. Wheway G, Parry DA, Johnson CA. (2014) The role of primary cilia in the development and disease of the retina. *Organogenesis*; **10**: 69-85.
19. Inoue A, Ikebe M. (2003) Characterization of the motor activity of mammalian myosin VIIA. *J Biol Chem*; **278**: 5478-5487.
20. Caride AJ, Penheiter AR, Filoteo AG, Bajzer Z, Enyedi A, Penniston JT. (2001) The plasma membrane calcium pump displays memory of past calcium spikes. Differences between isoforms 2b and 4b. *J Biol Chem*; **276**: 39797-39804.
21. McGuigan DB, Heon E, Cideciyan AV, Ratnapriya R, Lu M, Sumaroka A, Roman AJ, Batmanabane V, Garafalo AV, Stone EM, et al. (2017) EYS Mutations Causing Autosomal Recessive Retinitis Pigmentosa: Changes of Retinal Structure and Function with Disease Progression. *Genes (Basel)*; **8**.
22. Hirashima T, Miyata M, Ishihara K, Hasegawa T, Sugahara M, Ogino K, Yoshikawa M, Hata M, Kuroda Y, Muraoka Y, et al. (2017) Choroidal Vasculature in Bietti Crystalline Dystrophy With CYP4V2 Mutations and in Retinitis Pigmentosa With EYS Mutations. *Invest Ophthalmol Vis Sci*; **58**: 3871-3878.
23. Sengillo JD, Lee W, Nagasaki T, Schuerch K, Yannuzzi LA, Freund KB, Sparrow JR, Allikmets R, Tsang SH. (2018) A Distinct Phenotype of Eyes Shut Homolog (EYS)-Retinitis Pigmentosa Is Associated With Variants Near the C-Terminus. *Am J Ophthalmol*; **190**: 99-112.
24. Sun T, Xu K, Ren Y, Xie Y, Zhang X, Tian L, Li Y. (2018) Comprehensive Molecular Screening in Chinese Usher Syndrome Patients. *Invest Ophthalmol Vis Sci*; **59**: 1229-1237.
25. Mucciolo DP, Sodi A, Passerini I, Murro V, Cipollini F, Borg I, Pelo E, Contini E, Virgili G, Rizzo S. (2018) Fundus phenotype in retinitis pigmentosa associated with EYS mutations. *Ophthalmic Genet*: 1-14.
26. Iwanami M, Oshikawa M, Nishida T, Nakadomari S, Kato S. (2012) High prevalence of mutations in the EYS gene in Japanese patients with autosomal recessive retinitis pigmentosa. *Invest Ophthalmol Vis Sci*; **53**: 1033-1040.
27. Sangermano R, Bax NM, Bauwens M, van den Born LI, De Baere E, Garanto A, Collin RW, Goercharn-Ramlal AS, den Engelsman-van Dijk AH, Rohrschneider K, et al. (2016) Photoreceptor Progenitor mRNA Analysis Reveals Exon Skipping Resulting from the ABCA4 c.5461-10T-->C Mutation in Stargardt Disease. *Ophthalmology*; **123**: 1375-1385.

28. Sangermano R, Khan M, Cornelis SS, Richelle V, Albert S, Garanto A, Elmelik D, Qamar R, Lugtenberg D, van den Born LI, et al. (2018) ABCA4 midgenes reveal the full splice spectrum of all reported noncanonical splice site variants in Stargardt disease. *Genome Res*; **28**: 100-110.
29. Lu Z, Hu X, Liu F, Soares DC, Liu X, Yu S, Gao M, Han S, Qin Y, Li C, et al. (2017) Ablation of EYS in zebrafish causes mislocalisation of outer segment proteins, F-actin disruption and cone-rod dystrophy. *Sci Rep*; **7**: 46098.
30. Chandler MJ, Smith PJ, Samuelson DA, MacKay EO. (1999) Photoreceptor density of the domestic pig retina. *Vet Ophthalmol*; **2**: 179-184.
31. Ollivier FJ, Samuelson DA, Brooks DE, Lewis PA, Kallberg ME, Komaromy AM. (2004) Comparative morphology of the tapetum lucidum (among selected species). *Vet Ophthalmol*; **7**: 11-22.
32. Mowat FM, Petersen-Jones SM, Williamson H, Williams DL, Luthert PJ, Ali RR, Bainbridge JW. (2008) Topographical characterization of cone photoreceptors and the area centralis of the canine retina. *Mol Vis*; **14**: 2518-2527.
33. Slijkerman RW, Song F, Astuti GD, Huynen MA, van Wijk E, Stieger K, Collin RW. (2015) The pros and cons of vertebrate animal models for functional and therapeutic research on inherited retinal dystrophies. *Prog Retin Eye Res*; **48**: 137-159.
34. Takahashi K, Tanabe K, Ohnuki M, Narita M, Ichisaka T, Tomoda K, Yamanaka S. (2007) Induction of pluripotent stem cells from adult human fibroblasts by defined factors. *Cell*; **131**: 861-872.
35. Yu J, Vodyanik MA, Smuga-Otto K, Antosiewicz-Bourget J, Frane JL, Tian S, Nie J, Jonsdottir GA, Ruotti V, Stewart R, et al. (2007) Induced pluripotent stem cell lines derived from human somatic cells. *Science*; **318**: 1917-1920.
36. Nakano T, Ando S, Takata N, Kawada M, Muguruma K, Sekiguchi K, Saito K, Yonemura S, Eiraku M, Sasai Y. (2012) Self-formation of optic cups and storable stratified neural retina from human ESCs. *Cell Stem Cell*; **10**: 771-785.
37. Kytälä A, Moraghebi R, Valensisi C, Kettunen J, Andrus C, Pasumarthy KK, Nakanishi M, Nishimura K, Ohtaka M, Weltner J, et al. (2016) Genetic Variability Overrides the Impact of Parental Cell Type and Determines iPSC Differentiation Potential. *Stem Cell Reports*; **6**: 200-212.
38. Cahan P, Daley GQ. (2013) Origins and implications of pluripotent stem cell variability and heterogeneity. *Nat Rev Mol Cell Biol*; **14**: 357-368.
39. Nasonkin IO, Merbs SL, Lazo K, Oliver VF, Brooks M, Patel K, Enke RA, Nellissery J, Jamrich M, Le YZ, et al. (2013) Conditional knockdown of DNA methyltransferase 1 reveals a key role of retinal pigment epithelium integrity in photoreceptor outer segment morphogenesis. *Development*; **140**: 1330-1341.
40. Messchaert M, Dona M, Broekman S, Peters TA, Corral-Serrano JC, Slijkerman RWN, van Wijk E, Collin RWJ. (2018) Eyes shut homolog is important for the maintenance of photoreceptor morphology and visual function in zebrafish. *PLoS One*; **13**: e0200789.
41. Bennett J, Wellman J, Marshall KA, McCague S, Ashtari M, DiStefano-Pappas J, Elci OU, Chung DC, Sun J, Wright JF, et al. (2016) Safety and durability of effect of contralateral-eye administration of AAV2 gene therapy in patients with childhood-onset blindness caused by RPE65 mutations: a follow-on phase 1 trial. *Lancet*; **388**: 661-672.

42. MacLaren RE, Groppe M, Barnard AR, Cottrill CL, Tolmachova T, Seymour L, Clark KR, During MJ, Cremers FP, Black GC, et al. (2014) Retinal gene therapy in patients with choroideremia: initial findings from a phase 1/2 clinical trial. *Lancet*; **383**: 1129-1137.
43. Acland GM, Aguirre GD, Ray J, Zhang Q, Aleman TS, Cideciyan AV, Pearce-Kelling SE, Anand V, Zeng Y, Maguire AM, et al. (2001) Gene therapy restores vision in a canine model of childhood blindness. *Nat Genet*; **28**: 92-95.
44. Dias MF, Joo K, Kemp JA, Fialho SL, da Silva Cunha A, Jr., Woo SJ, Kwon YJ. (2018) Molecular genetics and emerging therapies for retinitis pigmentosa: Basic research and clinical perspectives. *Prog Retin Eye Res*; **63**: 107-131.
45. Deng WT, Dyka FM, Dinculescu A, Li J, Zhu P, Chiodo VA, Boye SL, Conlon TJ, Erger K, Cossette T, et al. (2015) Stability and Safety of an AAV Vector for Treating RPGR-ORF15 X-Linked Retinitis Pigmentosa. *Hum Gene Ther*; **26**: 593-602.
46. Trapani I, Colella P, Sommella A, Iodice C, Cesi G, de Simone S, Marrocco E, Rossi S, Giunti M, Palfi A, et al. (2014) Effective delivery of large genes to the retina by dual AAV vectors. *EMBO Mol Med*; **6**: 194-211.
47. Han Z, Conley SM, Makkia RS, Cooper MJ, Naash MI. (2012) DNA nanoparticle-mediated ABCA4 delivery rescues Stargardt dystrophy in mice. *J Clin Invest*; **122**: 3221-3226.
48. Hashimoto T, Gibbs D, Lillo C, Azarian SM, Legacki E, Zhang XM, Yang XJ, Williams DS. (2007) Lentiviral gene replacement therapy of retinas in a mouse model for Usher syndrome type 1B. *Gene Ther*; **14**: 584-594.
49. Collin RW, den Hollander AI, van der Velde-Visser SD, Bennicelli J, Bennett J, Cremers FP. (2012) Antisense Oligonucleotide (AON)-based Therapy for Leber Congenital Amaurosis Caused by a Frequent Mutation in CEP290. *Mol Ther Nucleic Acids*; **1**: e14.
50. Garanto A, Chung DC, Duijkers L, Corral-Serrano JC, Messchaert M, Xiao R, Bennett J, Vandenberghe LH, Collin RW. (2016) In vitro and in vivo rescue of aberrant splicing in CEP290-associated LCA by antisense oligonucleotide delivery. *Hum Mol Genet*; **25**: 2552-2563.
51. Gerard X, Perrault I, Hanein S, Silva E, Bigot K, Defoort-Delhemmes S, Rio M, Munnich A, Scherman D, Kaplan J, et al. (2012) AON-mediated Exon Skipping Restores Ciliation in Fibroblasts Harboring the Common Leber Congenital Amaurosis CEP290 Mutation. *Mol Ther Nucleic Acids*; **1**: e29.
52. Slijkerman RW, Vache C, Dona M, Garcia-Garcia G, Claustres M, Hetterschijt L, Peters TA, Hartel BP, Pennings RJ, Millan JM, et al. (2016) Antisense Oligonucleotide-based Splice Correction for USH2A-associated Retinal Degeneration Caused by a Frequent Deep-intronic Mutation. *Mol Ther Nucleic Acids*; **5**: e381.
53. Bonifert T, Gonzalez Menendez I, Battke F, Theurer Y, Synofzik M, Schols L, Wissinger B. (2016) Antisense Oligonucleotide Mediated Splice Correction of a Deep Intronic Mutation in OPA1. *Mol Ther Nucleic Acids*; **5**: e390.
54. Albert S, Garanto A, Sangermano R, Khan M, Bax NM, Hoyng CB, Zernant J, Lee W, Allikmets R, Collin RWJ, et al. (2018) Identification and Rescue of Splice Defects Caused by Two Neighboring Deep-Intronic ABCA4 Mutations Underlying Stargardt Disease. *Am J Hum Genet*; **102**: 517-527.

55. Aartsma-Rus A, van Ommen GJ. (2007) Antisense-mediated exon skipping: a versatile tool with therapeutic and research applications. *RNA*; **13**: 1609-1624.
56. Rutten JW, Dauwerse HG, Peters DJ, Goldfarb A, Venselaar H, Haffner C, van Ommen GJ, Aartsma-Rus AM, Lesnik Oberstein SA. (2016) Therapeutic NOTCH3 cysteine correction in CADASIL using exon skipping: in vitro proof of concept. *Brain*; **139**: 1123-1135.
57. Wood MJA, Talbot K, Bowerman M. (2017) Spinal muscular atrophy: antisense oligonucleotide therapy opens the door to an integrated therapeutic landscape. *Hum Mol Genet*; **26**: R151-R159.
58. Jinek M, East A, Cheng A, Lin S, Ma E, Doudna J. (2013) RNA-programmed genome editing in human cells. *Elife*; **2**: e00471.
59. Mali P, Yang L, Esvelt KM, Aach J, Guell M, DiCarlo JE, Norville JE, Church GM. (2013) RNA-guided human genome engineering via Cas9. *Science*; **339**: 823-826.
60. Cong L, Ran FA, Cox D, Lin S, Barretto R, Habib N, Hsu PD, Wu X, Jiang W, Marraffini LA, et al. (2013) Multiplex genome engineering using CRISPR/Cas systems. *Science*; **339**: 819-823.
61. Bakondi B, Lv W, Lu B, Jones MK, Tsai Y, Kim KJ, Levy R, Akhtar AA, Breunig JJ, Svendsen CN, et al. (2016) In Vivo CRISPR/Cas9 Gene Editing Corrects Retinal Dystrophy in the S334ter-3 Rat Model of Autosomal Dominant Retinitis Pigmentosa. *Mol Ther*; **24**: 556-563.
62. Wang B, Li K, Wang A, Reiser M, Saunders T, Lockey RF, Wang JW. (2015) Highly efficient CRISPR/HDR-mediated knock-in for mouse embryonic stem cells and zygotes. *Biotechniques*; **59**: 201-202, 204, 206-208.
63. Zhang JP, Li XL, Li GH, Chen W, Arakaki C, Botimer GD, Baylink D, Zhang L, Wen W, Fu YW, et al. (2017) Efficient precise knockin with a double cut HDR donor after CRISPR/Cas9-mediated double-stranded DNA cleavage. *Genome Biol*; **18**: 35.
64. Peddle CF, MacLaren RE. (2017) The Application of CRISPR/Cas9 for the Treatment of Retinal Diseases. *Yale J Biol Med*; **90**: 533-541.
65. Burnight ER, Giacalone JC, Cooke JA, Thompson JR, Bohrer LR, Chirco KR, Drack AV, Fingert JH, Worthington KS, Wiley LA, et al. (2018) CRISPR-Cas9 genome engineering: Treating inherited retinal degeneration. *Prog Retin Eye Res*; **65**: 28-49.



# Summary



## Summary

Inherited retinal diseases (IRDs) are a heterogeneous group of blinding disorders characterized by progressive degeneration of retinal cells (**Chapter 1, section 1.4**). Mutations in *Eyes shut homolog (EYS)* are one of the most common causes of autosomal recessive (ar) retinitis pigmentosa (RP), an IRD characterized by the degeneration of photoreceptors (**section 1.5**). Since the discovery of *EYS* in 2008, numerous *EYS* variants have been found in patients with retinal dystrophy. However, there is a lack of studies that investigate the function of the gene and the *EYS* protein. Furthermore, there is no treatment available for *EYS*-related retinal dystrophy. With this thesis, we aimed to unravel the pathogenic mechanism underlying *EYS*-associated retinal dystrophy, which can serve as the basis for the development of therapeutic approaches for the disease.

**Chapter 2** gives an overview of all 271 reported and 26 novel *EYS* variants reported in patients with retinal dystrophy. All these patients and their variants, together with phenotypic information (when available) were uploaded to the Leiden Open Variation Database ([www.LOVD.nl/EYS](http://www.LOVD.nl/EYS)). In addition, *in silico* assessment of all *EYS* variants was performed, as well as classification of all the variants according to their pathogenicity following the American College of Medical Genetics and Genomics (ACMG) guidelines. The variants covered the complete pathogenicity spectrum from likely benign to likely pathogenic, although the majority of the missense variants had to be classified as of uncertain significance. In this chapter, we highlight the need of functional assays to assess the pathogenicity of *EYS* variants, in order to improve molecular diagnostics and counseling of patients with *EYS*-related retinal dystrophy.

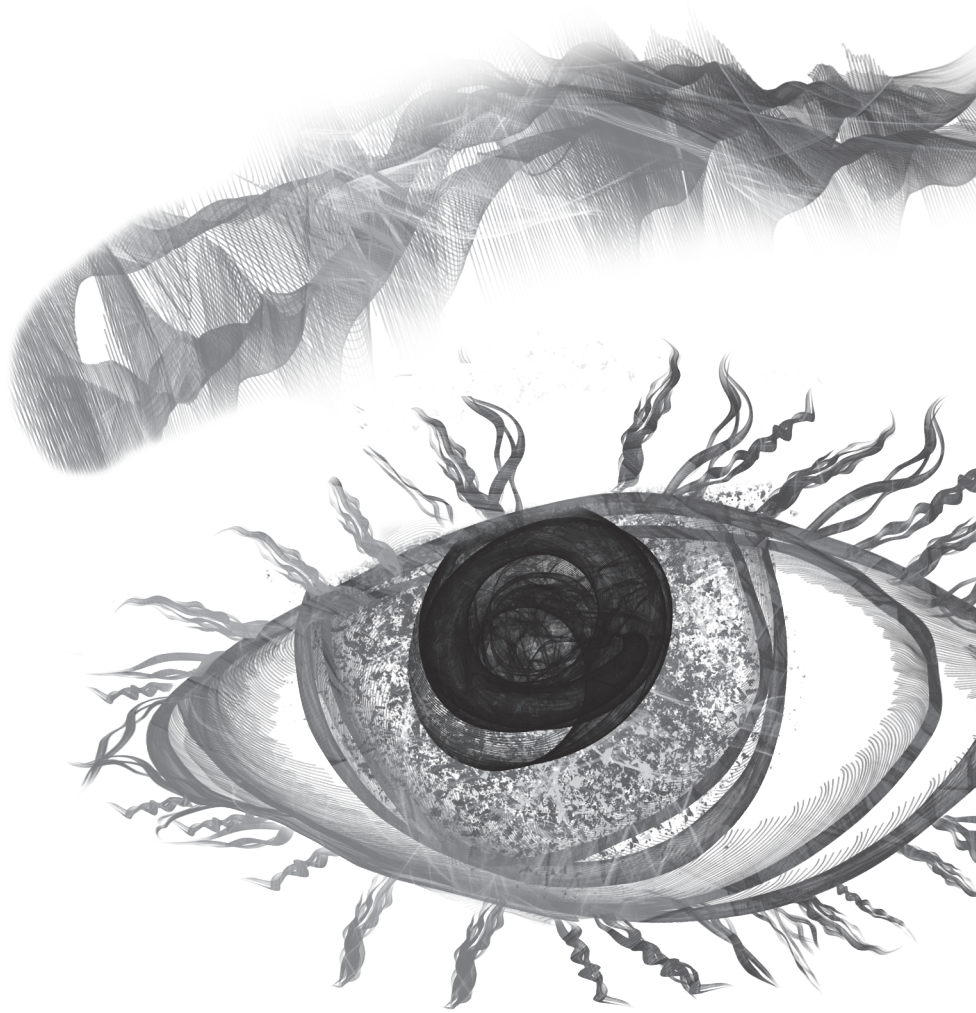
In **Chapter 3**, we describe the spectrum of retinal dystrophy and the course of visual function in a cohort of 30 patients carrying bi-allelic *EYS* variants. The majority of the patients were diagnosed with RP, and one patient had cone-rod dystrophy (CRD). In addition, two siblings diagnosed with macular dystrophy carried heterozygous *EYS* variants: c.1299+5\_1299+8del and c.6050G>T (p.(Gly2017Val)). We showed that the c.1299+5\_1299+8del mutation affects splicing using an *in vitro* minigene splice assay. This study indicates that screening of CRD and macular dystrophy patients for *EYS* variants might increase diagnostic yield in previously unsolved cases.

**Chapter 4** describes the generation of an *ey*s knock-out zebrafish line using CRISPR/Cas9 technology to allow us to study *Eys* function in zebrafish. We showed that *Eys* localizes at the region of the connecting cilium. In the absence of *Eys*, photoreceptor architecture was disorganized and photoreceptor specific protein rhodopsin and cone transducin were mislocalized. Furthermore, electroretinogram (ERG) recordings showed diminished b-wave amplitudes in *ey*s deficient zebrafish (5 dpf) compared to wild-type zebrafish. In addition, a decrease in visual motor response (VMR) was observed in the *ey*s mutant fish. In conclusion, this chapter showed that *Eys* is important for maintenance of the photoreceptor architecture and visual function in zebrafish.

**Chapter 5** describes the generation of three *EYS* microgenes that can be used as a potential therapeutic approach for the treatment of *EYS*-associated retinal dystrophy. Based on conservation analysis of the *EYS* domains, we selected the most conserved regions of *EYS* to be part of one or more microgenes. Western blot analysis showed that at least two out of three microgenes are stable. Further research is necessary to investigate whether the *EYS* microgenes localize properly in the cell, whether the microgenes are functional, and how they can be delivered to the photoreceptors.

In **Chapter 6**, we describe the design of AONs for skipping of *EYS* exon 26 as a therapeutic approach for retinal dystrophy cause by mutations in this exon. Western blot analysis revealed that *EYS* lacking exon 26 ( $\Delta 26EYS$ ) encodes a stable protein. AON efficacy was tested in hTERT-RPE1 cells. Transcriptional analysis of cells treated with AONs showed that a combination of two AONs resulted in skipping of exon 26, whereas the use of one of the AONs alone had no effect. In order to investigate the potential of AON-mediated exon skipping in patients, we differentiated patient-derived iPSCs into 3D optic cups. Treatment of these 3D cups with the AONs did not show any effect on *EYS* transcripts except in control cells treated with AON6. Sanger sequencing confirmed partial skipping of exon 25 and exon 26 in those samples, in contrast to what was observed in hTERT-RPE1 cells. This chapter is a first attempt towards the development of AON-mediated exon skipping therapy for retinal dystrophy patients with mutations in *EYS* exon 26.

In **Chapter 7**, the main findings of this thesis are discussed. The role of *EYS* in the photoreceptor and the future prospects on how to get more insight in its exact function are discussed in **section 7.1**. We analyze the spectrum of *EYS*-associated retinal dystrophy in **section 7.2** and discuss how the pathogenicity of variants can be experimentally assessed in the future. In **section 7.3**, we discuss the available animal and cellular disease models to study *EYS*-associated retinal dystrophy. Finally, potential therapies for *EYS*-associated retinal dystrophy, such as AON-mediated therapy, (micro)gene therapy, and CRISPR/Cas9 technology, are discussed in **section 7.4**.



# Samenvatting

## Samenvatting

Erfelijke netvliesaanandoeningen vormen een heterogene groep van blindheid die gekenmerkt wordt door progressieve degeneratie van cellen in het netvlies (**Hoofdstuk 1, paragraaf 1.4**). Retinitis pigmentosa (RP) is een vorm van erfelijke blindheid waarin de fotoreceptorcellen afsterven. Mutaties in het gen *Eyes shut homolog* (*EYS*) zijn één van de meest voorkomende oorzaken van autosomaal recessief overervende RP (**paragraaf 1.5**). Het *EYS* gen is ontdekt in 2008 en sindsdien zijn er veel RP patiënten gevonden met mutaties in dit gen. Er is echter nog maar weinig bekend over de daadwerkelijke functie van het gen en het gecodeerde *EYS* eiwit. Op dit moment is er nog geen therapie beschikbaar voor patiënten met netvliesaanandoeningen die veroorzaakt zijn door *EYS* mutaties. Het doel van dit proefschrift was om meer inzicht te verkrijgen in de rol die *EYS* speelt bij het ontstaan van netvliesdegeneratie en om een eerste stap te zetten richting het ontwikkelen van mogelijke therapieën.

In **Hoofdstuk 2** geven we een overzicht van alle 271 *EYS* varianten die zijn gerapporteerd in patiënten met netvliesdegeneratie. Daarnaast bespreken we ook 26 nieuwe varianten die nog niet eerder gerapporteerd waren. Alle beschikbare informatie over het ziektebeeld van deze patiënten met hun varianten zijn opgenomen in de Leiden Open Variation Database ([www.LOVD.nl/EYS](http://www.LOVD.nl/EYS)). Alle varianten zijn geclassificeerd op basis van hun pathogeniciteit met behulp van de richtlijnen van de American College of Medical Genetics and Genomics (ACMG). De varianten bekleedden alle mogelijke klassen van oorzakelijk tot niet oorzakelijk. Een groot deel van de (met name) missense varianten kon niet met zekerheid worden ingedeeld in een van de pathogeniciteitsklassen. Om deze varianten toch goed te kunnen classificeren zijn er functionele experimenten nodig. Een beter inzicht in de ernst van de *EYS* varianten zorgt ervoor dat een betere diagnose gesteld kan worden bij patiënten, waardoor ze beter geholpen kunnen worden.

Het complete ziektebeeld van 30 patiënten met bi-allelische *EYS* varianten wordt beschreven in **Hoofdstuk 3**. Het merendeel van de patiënten was gediagnosticeerd met RP en er was één patiënt met kegel-staaf dystrophy. Daarnaast waren er twee broers met macula degeneratie die drager waren van twee heterozygote *EYS* varianten, namelijk c.1299+5\_1299+8del en c.6050C>T (p.(Gly2017Val)). Met behulp van een *in vitro* minigen splice assay hebben we aangetoond dat de c.1299+5\_1299+8del variant een effect heeft op mRNA splicing. Screening van patiënten met macula degeneratie of kegel-staaf dystrophy voor *EYS* varianten zou kunnen helpen bij het stellen van de juiste diagnose.

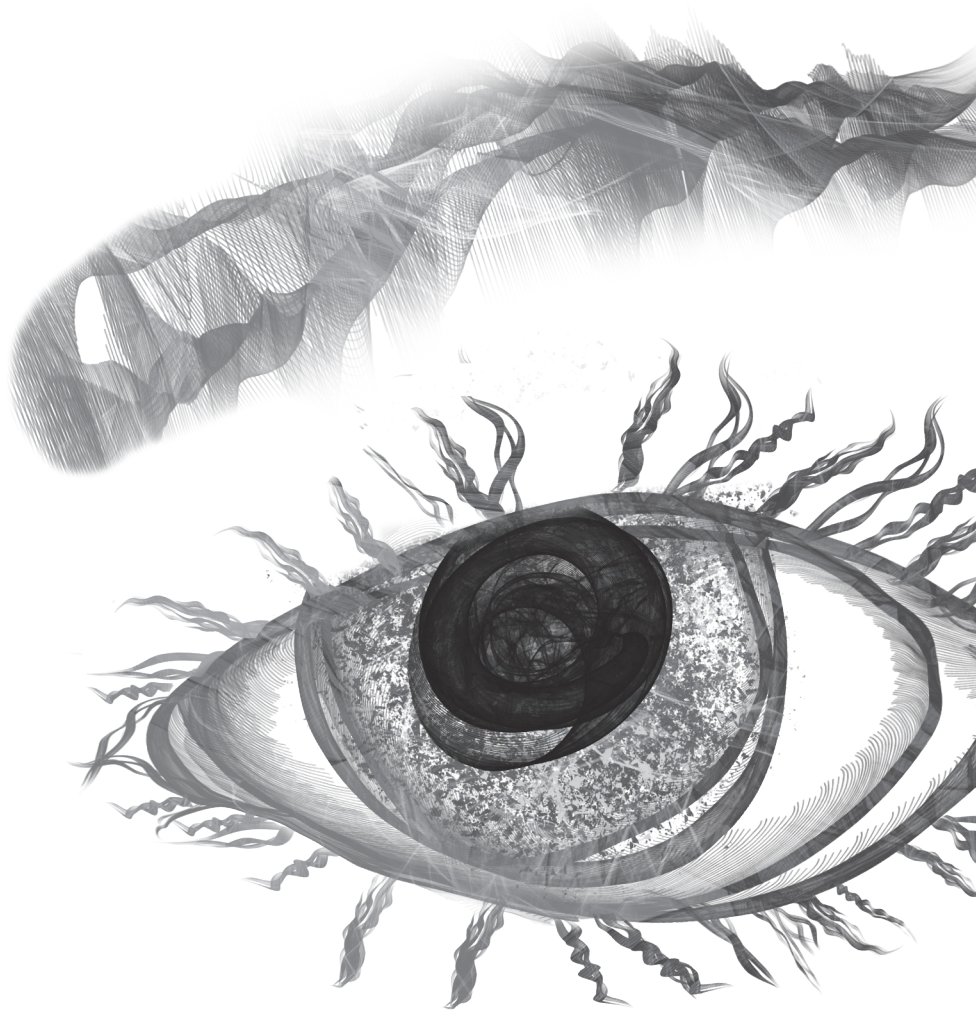
Om de functie van *EYS* te kunnen bestuderen in de zebravis hebben we een zebravis *eyes* knock-out model gemaakt met behulp van CRISPR/Cas9 technologie. Dit staat beschreven in **Hoofdstuk 4**. Lokalisatie studies lieten zien dat *Eys* zich bevindt in de regio van het connecting cilium. De morfologie van fotoreceptorcellen was afwijkend in de afwezigheid van *Eys*. Ook hebben we aangetoond dat de fotoreceptor specifieke eiwitten rhodopsin en cone transducin niet goed gelokaliseerd worden in *eyes* mutanten. Verder lieten ERG opnames een kleinere b-golf amplitude zien in mutanten in vergelijking met wild-type

larves. Tenslotte zagen we ook dat de visuele motor respons in *ey*s knock-out zebrafissen was afgenomen. Hieruit kunnen we concluderen dat *Eys* belangrijk is voor de morfologie van fotoreceptorcellen en de visuele functie in zebrafissen.

In **Hoofdstuk 5** hebben we een eerste stap gezet in de richting van het ontwikkelen van een microgentherapie voor patiënten met netvliesdegeneratie veroorzaakt door *EYS* mutaties. We hebben hiervoor drie verschillende *EYS* microgenen ontworpen die zijn opgebouwd uit de belangrijkste geconserveerde domeinen van het *EYS* eiwit. Met behulp van western blot hebben we aangetoond dat twee van de drie microgenen stabiele eiwitten kunnen vormen. Verder onderzoek is nodig om te bepalen of de microgenen op de juiste plek in de cel lokaliseren, of ze ook daadwerkelijk functioneel zijn en hoe ze de fotoreceptoren het beste kunnen bereiken.

Het doel van **Hoofdstuk 6** was om exon 26 van *EYS* te excluseren van het mRNA met behulp van antisense oligonucleotiden (AONs), zodat we een potentiële therapie kunnen ontwikkelen voor patiënten met *EYS* mutaties die gelegen zijn in dit exon. Met behulp van western blot hebben we aangetoond dat *EYS* zonder exon 26 ( $\Delta 26EYS$ ) codeert voor een stabiel eiwit. De werkzaamheid van de AONs werd eerst getest in hTERT-RPE1 cellen. Analyse van *EYS* transcripten van behandelde cellen liet zien dat behandeling met een combinatie van twee AONs kan leiden tot skipping van exon 26. Om te onderzoeken of we exon 26 ook kunnen uitsluiten in patiënten cellen hebben we pluripotente stamcellen afkomstig van een patiënt met een mutatie in exon 26 gedifferentieerd in netvlies cellen. In het merendeel van de cellen zagen we geen effect van de AON behandeling op de *EYS* transcripten. Een uitzondering hierop waren controle cellen die behandeld waren met AON-6. Sanger sequencing bevestigde dat in deze cellen een deel van exon 25 en het grootste deel van exon 26 afwezig waren. Dit in tegenstelling tot wat we eerder zagen in de hTERT-RPE1 cellen. Dit hoofdstuk beschrijft een eerste poging tot het ontwikkelen van exon exclusie therapie met behulp van AONs voor netvliesdegeneratie patiënten met mutaties in exon 26 van *EYS*.

De meest belangrijke bevindingen van dit proefschrift werden bediscussieerd in **Hoofdstuk 7**. In **paragraaf 7.1** bediscussieren we de mogelijke rol van *EYS* in de fotoreceptorcellen, alsmede hoe verder onderzoek kan zorgen dat de exacte functie van *EYS* beter in kaart kan worden gebracht. Het ziektebeeld van patiënten met netvliesdegeneratie dat veroorzaakt wordt door *EYS* mutaties wordt besproken in **paragraaf 7.2**. Ook gaan we hier dieper in op de mogelijke experimenten die uitgevoerd kunnen worden, zodat er meer duidelijkheid komt over de ernst van de varianten. In **paragraaf 7.3** beschrijven we welke dier- en celmodellen er beschikbaar zijn om *EYS*-gerelateerde netvliesdegeneratie te bestuderen. Als laatste bespreken we in **paragraaf 7.4** hoe AONs, (micro)gentherapie en CRISPR/Cas9 technologie mogelijk kunnen worden ingezet als therapie voor patiënten met netvliesdegeneratie en *EYS* mutaties.



# Curriculum vitae



### **About the author**

Muriël Messchaert was born on Thursday June 15th 1989 in Delden, The Netherlands. After finishing high school in 2007, she started her studies in Biomedical Sciences at the Radboud University Nijmegen. After obtaining her Bachelor's degree in 2011, she continued studying at the Radboud University to obtain her Master's degree in Biomedical Sciences as well. During this period, she performed two internships of six months, one at the department of Laboratory of Paediatric Infectious Diseases at the Radboudumc, and a second internship at the department of Pharmacology and Toxicology at the Radboud Institute for Molecular Life Sciences in Nijmegen, The Netherlands. In 2014, Muriël Messchaert started her career as a PhD student in the Blindness Genetic Therapy group led by dr. Rob Collin at the Department of Human Genetics at the Radboudumc in Nijmegen, The Netherlands. After finishing her thesis manuscript in October 2018, she started as a trainee to become clinical chemist at Gelre ziekenhuizen in Apeldoorn and at the St. Antonius hospital in Nieuwegein, The Netherlands.

## List of publications

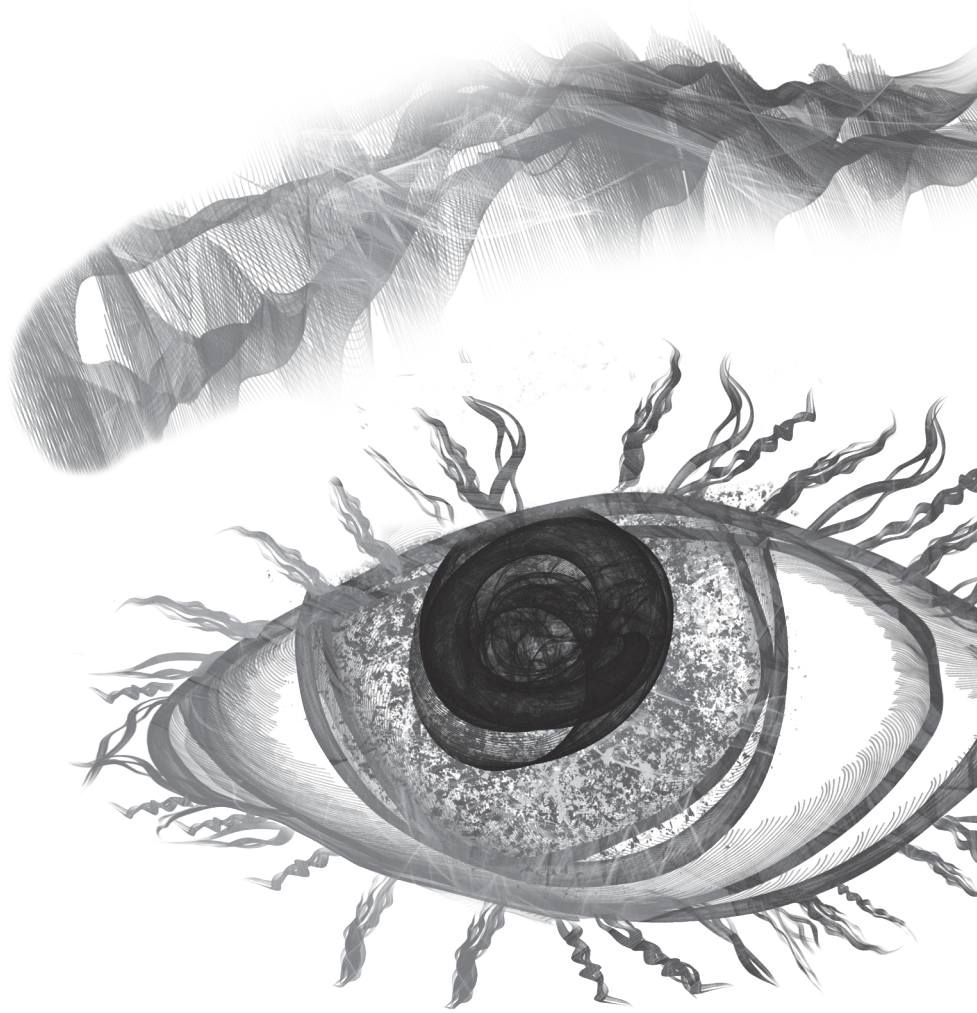
**Messchaert M**, Dona M, Broekman S, Peters TA, Corral-Serrano JC, Slijkerman RWN, van Wijk E, Collin RWJ. (2018) Eyes shut homolog is important for the maintenance of photoreceptor morphology and visual function in zebrafish. *PLoS One*; **13**: e0200789.

Corral-Serrano JC, **Messchaert M**, Dona M, Peters TA, Kamminga LM, van Wijk E, Collin RWJ. (2018) C2orf71a/pcare1 is important for photoreceptor outer segment morphogenesis and visual function in zebrafish. *Sci Rep*; **8**: 9675.

**Messchaert M**, Haer-Wigman L, Khan MI, Cremers FPM, Collin RWJ. (2018) EYS mutation update: In silico assessment of 271 reported and 26 novel variants in patients with retinitis pigmentosa. *Hum Mutat*; **39**: 177-186.

Garanto A, Chung DC, Duijkers L, Corral-Serrano JC, **Messchaert M**, Xiao R, Bennett J, Vandenberghe LH, Collin RW. (2016) In vitro and in vivo rescue of aberrant splicing in CEP290-associated LCA by antisense oligonucleotide delivery. *Hum Mol Genet*; **25**: 2552-2563.

Weigand KM, **Messchaert M**, Swarts HG, Russel FG, Koenderink JB. (2014) Alternating Hemiplegia of Childhood mutations have a differential effect on Na(+),K(+)-ATPase activity and ouabain binding. *Biochim Biophys Acta*. **1842**: 1010-1016.



# Dankwoord

## Dankwoord

Het tot stand komen van dit proefschrift was natuurlijk niet gelukt zonder de hulp van vele anderen. Een aantal mensen wil ik hier in het bijzonder bedanken.

Allereerst wil ik mijn promotoren bedanken. **Rob**, bedankt voor je begeleiding gedurende het gehele traject. Je betrokkenheid en optimisme waren voor mijn project en zijn voor de gehele onderzoeksgroep erg van waarde. Het EYS-project was niet het makkelijkste project, maar ondanks de hobbels op de weg wisten we dat het uiteindelijk allemaal goed zou komen. Het resultaat in de vorm van dit proefschrift is nu eindelijk daar!

**Frans**, je bent met name in de afrondende fase van mijn proefschrift erg betrokken geweest. Je ervaring, kennis en snelle feedback waren daarbij erg waardevol. Dank daarvoor. Ik heb de samenwerking als erg prettig ervaren.

De BGT groep: **Alex, Anita, Dyah, Galuh, Julio, Lonneke, Matthijs, Tamara, Tess**. Alex, thank you for the answers on all the ask-Alex-questions and your support during my PhD. Dyah, we spent a lot of time together at the zebrafish facility. It was nice working with you. Also, thanks for the great time during our trip to ARVO, Washington and NYC. Anita, bedankt voor alle experimentele ondersteuning in de laatste maanden van mijn promotieonderzoek. Zonder die extra paar handen was het allemaal niet (zo snel) gelukt.

**Marieke** en **Laura**, dat het werken aan *EYS* niet makkelijk was hebben jullie tijdens je stage zeker ook gezien. Ik hoop dat jullie er veel van hebben geleerd. Bedankt voor jullie inzet en de fijne samenwerking. Heel veel succes met jullie verdere loopbaan.

Overige collega's van het ZAT-lab: **Erik, Lisette, Margo, Ralph, Sanne** en **Theo**. Fijn dat ik met jullie kon sparren en kon meevaren op jullie ervaring op zebravisgebied, zodat het wiel niet steeds opnieuw uitgevonden hoefde te worden. Ook wat betreft het experimentele werk heb ik regelmatig op jullie kunnen terug vallen: coupes snijden, kleuringen, danio vision, ERGs. Thanks allen voor de fijne samenwerking en goede sfeer op het lab.

**Tom** en **Antoon**, bedankt voor het verzorgen van de zebravissen en voor jullie tips en tricks om te zorgen dat de vissen genoeg eitjes zouden leggen.

To my office mates: **Daniel, Gido, Julio, Mubeen** and **Riccardo**. Thank you for selecting me out of all the candidates as your new office member ;p. We had a great time together. I wish you all good luck with finishing your thesis and/or your next steps in your career. We keep in touch!

**Lonneke** en **Michael** (the Kwint one) super gaaf dat jullie mij op deze bijzondere dag bij willen staan als paranimfen. Het klikte van begin af aan. Met plezier kijk ik terug op de vele leuke momenten die we samen hebben meegemaakt tijdens werk maar ook zeker daarbuiten, zoals carnaval in Venlo en natuurlijk onze trip naar Barcelona. Ik zal de koffiemomentjes zeker missen!

Als laatste wil ik ook graag mijn familie en vrienden bedanken. **Francette**, wat ben ik blij dat we van onze moeders vanaf dat we in de wieg lagen vriendinnen moesten zijn. Superfijn dat ik regelmatig gebruik kon maken van mijn (logeer)kamer bij jullie in Nijmegen. **Kjell**, jou moet ik hier natuurlijk ook voor bedanken.

Lieve **pap** en **mam**, bedankt voor alles dat jullie me hebben gegeven en voor jullie steun in alles wat ik doe. Niks is voor jullie te gek als het om jullie dochters gaat. **Melanie** en **Daisy**, love you!

Allerliefste **Michael**, wat moet ik toch zonder jou. Bedankt voor alles. We did it! ♥

## **Donders Graduate School for Cognitive Neuroscience**

For a successful research Institute, it is vital to train the next generation of young scientists. To achieve this goal, the Donders Institute for Brain, Cognition and Behaviour established the Donders Graduate School for Cognitive Neuroscience (DGCN), which was officially recognized as a national graduate school in 2009. The Graduate School covers training at both Master's and PhD level and provides an excellent educational context fully aligned with the research programme of the Donders Institute.

The school successfully attracts highly talented national and international students in biology, physics, psycholinguistics, psychology, behavioral science, medicine and related disciplines. Selective admission and assessment centers guarantee the enrolment of the best and most motivated students.

The DGCN tracks the career of PhD graduates carefully. More than 50% of PhD alumni show a continuation in academia with postdoc positions at top institutes worldwide, e.g. Stanford University, University of Oxford, University of Cambridge, UCL London, MPI Leipzig, Hanyang University in South Korea, NTNU Norway, University of Illinois, North Western University, Northeastern University in Boston, ETH Zürich, University of Vienna etc.. Positions outside academia spread among the following sectors: specialists in a medical environment, mainly in genetics, geriatrics, psychiatry and neurology. Specialists in a psychological environment, e.g. as specialist in neuropsychology, psychological diagnostics or therapy. Positions in higher education as coordinators or lecturers. A smaller percentage enters business as research consultants, analysts or head of research and development. Fewer graduates stay in a research environment as lab coordinators, technical support or policy advisors. Upcoming possibilities are positions in the IT sector and management position in pharmaceutical industry. In general, the PhDs graduates almost invariably continue with high-quality positions that play an important role in our knowledge economy.

For more information on the DGCN as well as past and upcoming defenses please visit:  
<http://www.ru.nl/donders/graduate-school/phd/>

## Data management

Type of data	Subject to privacy (yes/no)	Way of anonymization	Storage
<b>Antibodies</b>	No	n.a.	Antibodies were registered in the antibody database from the Department of Human Genetics in Labguru: <a href="https://radboudumc.labguru.com/biollections/antibodies">https://radboudumc.labguru.com/biollections/antibodies</a> . Antibodies were stored with a traceable number in the assigned freezer/fridge at the Department of Human Genetics, according to the manufacturer's instructions.
<b>Fluorescence images</b>	No	n.a.	Fluorescence imaging data was stored on the private network of the Blindness Genetics Therapy group at the Department of Human Genetics: T:\PIgroup-Rob-Collin\02 Microscopy images\09 Muriel Messchaert.
<b>Plasmids</b>	No	n.a.	Plasmids were registered in the Blindness Genetics Therapy database and assigned to a pGT-number. H:\GR Theme groups\10 PI Group Rob Collin\05 Vector_AAV_AON Database. Plasmids were stored in the assigned freezer at -80°C at the Department of Human Genetics.
<b>Patient-derived cell lines</b>	Yes	All patients received an untraceable number, the identity of the patient is only known by the treating physician.	Cell lines received a traceable number and were registered at the cell culture facility of the Department of Human Genetics. Cell lines were frozen in liquid nitrogen and stored in the assigned freezer at -80°C at the Department of Human Genetics. The number of the cell lines used can be found in the labjournal of Muriël Messchaert, stored at the Department of Human Genetics or in Labguru in the EYS project: <a href="https://radboudumc.labguru.com/knowledge/projects/701">https://radboudumc.labguru.com/knowledge/projects/701</a> . Contact person to find the cell lines in the assigned freezer: Saskia van der Velde-Visser.



---

<b>Other cell lines</b>	No	n.a.	Cell lines were stored with a traceable number at the cell culture facility at the Department of Human Genetics, according to the manufacturer's instructions. The number of the cell lines used can be found in the labjournal of Muriël Messchaert, stored at the Department of Human Genetics or in Labguru in the EYS project: <a href="https://radboudumc.labguru.com/knowledge/projects/701">https://radboudumc.labguru.com/knowledge/projects/701</a> . Contact person to find the cell lines in the assigned freezer: Saskia van der Velde-Visser.
-------------------------	----	------	--

---

n.a.: not applicable.



